Mitochondrial Metabolism and Redox Homeostasis in Health and Disease

By

Rebecca Louise Westbrook

A thesis submitted to
the University of Birmingham
for the degree of
Doctor of Philosophy

Institute of Metabolism and Systems Research
College of Medical and Dental Sciences
University of Birmingham
September 2022

ABSTRACT

In order to maintain essential cellular metabolic pathways, the availability of required redox co-factors must remain favourable. For example, several reactions in the oxidative direction of the tricarboxylic acid (TCA) cycle, such as α-ketoglutarate conversion to succinyl-CoA, require nicotinamide adenine dinucleotide (NAD^+) as an oxidising agent. The redox balance of the cell can be challenged by outside influences, such as the tumour microenvironment and oxygen availability. It can also be influenced by cell intrinsic factors, such as genetic loss or alteration of enzymes involved in redox-heavy pathways.

Hypoxia presents a significant challenge to redox homeostasis and leads to a marked rewiring of the metabolic network. This thesis will begin by exploring the metabolism of the non essential amino acid, proline, in cancer cells under low oxygen conditions. Proline metabolism is closely linked to redox state due to the requirement of NAD(P)H in multiple reactions. Use of stable isotope tracing reveals that the synthesis of proline from glutamine through pyrroline-5-carboxylate reductase 1 (PYCR1) is increased in hypoxia. The implications of loss of this isozyme, particularly the impact on the cellular redox balance, on the phenotype of breast cancer cells in 2D culture is then investigated. This reveals a reduced NAD^+:NADH ratio, reduced oxidative incorporation of glutamine carbons into the TCA cycle and a slowed proliferative rate.

Leading on from these observations, a spheroid culture model is employed to more closely recapitulate the oxygen and nutrient gradients present in solid tumours. Again, stable isotope tracing suggests dysregulated redox balance with PYCR1 loss, leading to apoptosis and expression of hypoxic markers. Finally, this is explored *in vivo*, using a doxycyline-inducible shPYCR1 xenograft model. Under these conditions, chronic knockdown of PYCR1 results in slowed tumour growth, while acute knockdown results in increased hypoxia, apoptosis and necrosis.

Additionally, a suspected inborn error of metabolism is investigated, initially hypothesised to be caused by a mutation in decaprenyl phosphate synthase subunit 1 (PDSS1), a key step in the synthesis of coenzyme Q10. The mRNA and protein expression of this enzyme are not found to be altered, but a change in function cannot be ruled out. The metabolism of primary fibroblasts from this patient is investigated, and phenotype consistent with a dysregulated redox balance is discovered.

ACKNOWLEDGMENTS

I would first, of course, like to thank Professor Daniel Tennant for his supervision. Thank you for quietly but firmly believing in me until finally we published and this thing got finished. I'm leaving the lab with a good sense of who I am as a scientist, and (not to be dramatic!) as a person.

I would also like to thank all of our collaborators. It has been a privilege to be able to work with so many brilliant scientists and clinicians. Thank you to Dr Ester Bridges and Professor Adrian Harris for the very exciting *in vivo* work. Thank you to Colin Nixon for the spheroid sectioning and staining. Thank you to Dr Abeer Shabaam for the core needle biopsy samples, and for being a brilliant and patient teacher of pathology.

I would like to thank all of the people who have been a part of the Tennant lab throughout my PhD. I have loved working with everyone, and I've learnt so much from all of you. Many valuable skills, including: pottery, crazy golf, houseplant parenthood, wine tasting, how to choose the right teapot.. Of course, special thanks to Kat, my unofficial third supervisor. The absolute highlight of my PhD has to be drinking margaritas in Cali with you and Himani - I'm not sure I'll ever quite believe we did that?!

I also have to mention the pub/lunch group of pre-covid times - it's been a pleasure, but if I never play coup again I really won't mind. Special thank you's to Claire, Kat, Chloe, Justine and Belinda for being so much fun - time went so fast, I blinked and I missed it!

Thank you to my family, for being so endlessly supportive of anything I decide to do. Thank you to my parents for always saying "I'm not sure, lets find out". I'm happy I ended up in a lab coat like Mum (minus the silly badges). And finally; to Wes, for moving to *Birmingham*, in a *pandemic*, to live with me in the *final year* of my PhD.

Contents

List of Figures

List of Tables

Acronyms

$2HG$ (R)-2-hydroxyglutarate. 30

$4E-BP1$ Eukaryotic translation initiation factor 4E-binding protein 1. 30

BSA Bovine serum albumin. 116

$CA9$ Carbonic anhydrase 9. 75

DAB Diaminobenzidine. 71

$DCIS$ Ductal carcinoma in situ. 91

$DMEM$ Dulbecco's Modified Eagle's medium. 71

ECM Extracellular matrix. 30

ER Endoplasmic reticulum. 30

FBS Foetal bovine serum. 71

GCS Glycine cleavage system. 30

GSH Reduced glutathione. 30

$HBRC$ Human Biomaterials Resource Centre. 75

HIF Hypoxia inducible factor. 30

HRE Hypoxia-responsive element. 30

IDH Isocitrate dehydrogenase. 30

IEM Inborn errors of metabolism. 30

KO Knockout. 71

$LCMS$ Liquid chromatography mass spectroscopy. 116

LDH Lactate dehydrogenase. 30

$MAPK$ Mitogen-activated protein kinase. 30

$NADP$ Nicotinamide adenine dinucleotide phosphate. 30

NAD^+ Nicotinamide adenine dinucleotide. 30

$NEAA$ Non-essential amino acids. 71

NNT Nicotinamide nucleotide transhydrogenase. 30

NO Nitric oxide. 30

NOX NADH oxidase. 116

NT Non-target. 71

OAT Ornithine aminotransferase. 30

$P5CS$ Pyrroline-5-carboxylate synthase. 30

PBS Phosphate buffered saline. 71

$PBS-T$ Phosphate buffered saline with 0.1% Tween. 71

PC Pyruvate carboxylase. 30

$PDAC$ Pancreatic ductal carcinoma. 30

PDH Pyruvate dehydrogenase. 30

$PDSS1$ Decaprenyl diphosphate synthase subunit 1. 30

PHD HIF prolyl hydroxlyase. 30

$PPAR\gamma$ Peroxisome proliferator-activated receptor γ. 30

$PRODH$ Proline dehydrogenase. 30

$PYCR1$ Pyrroline-5-carboxylate reductase 1. 30

$PYCR2$ Pyrroline-5-carboxylate reductase 2. 30

$PYCRL$ Pyrroline-5-carboxylate reductase 3/L. 30

ROS Reactive oxygen species. 30

$RPMI$ Roswell Park Memorial Institute. 71

RT Room temperature. 71

SDS Sodium dodecyl sulfate. 71

TCA Tricarboxylic acid. ii

TRX Thioredoxin. 30

$TRXR$ Thioredoxin reductase. 30

UCP Uncoupling proteins. 116

$UHPLC$ High performance liquid chromatography. 116

$VEGF$ Vascular endothelial growth factor. 116

$mPTP$ Mitochondrial permeability transition pore. 116

Chapter One

Introduction

1.1 Metabolism

Metabolism encompasses the complex network of biochemical reactions which occur within cells to produce the energy needed for survival and growth. Broadly, metabolic reactions can be categorised as the breakdown and synthesis of macromolecules, described as catabolism and anabolism respectively, and the elimination of waste products. Catabolic reactions involve the degradation of molecules to produce simpler molecules, such as water and carbon dioxide. Conversely, anabolism produces complex molecules including proteins, nucleic acids and lipids. Catabolic reactions will often yield energy, whilst anabolic reactions require energy to progress. The metabolic network is dynamic, and the balance of anabolism and catabolism is responsive to factors such as nutrient availability and the energy requirements of cellular processes. Many metabolic reactions are reversible; the direction and rate of these reactions is dependent on many factors, including concentrations of substrates, co-factors and products, enzyme kinetics and energy availability. Metabolic pathways are also often coupled to other pathways, forming a complex network of reactions which depend on the outputs of other reactions.

All cellular processes are intrinsically linked to metabolism, whether they require energy, anabolic products or influence the availability of substrates and co-factors. In this way, most disease phenotypes have an associated cellular metabolic phenotype as this network adapts. This also means that changes to metabolism caused by genetic alterations to key enzymes can cause a wide array of diseases. When these occur in the germline, such disor-

ders are known as inborn errors of metabolism (IEM), after Archibald Garrod introduced the term in 1908[1], to describe alkaptonuria, albinism, cystinuria and pentosuria which he had observed had a pattern of heritability. There are now over 400 known IEMs[2], involving a huge number of metabolic pathways. The care of patients who have an IEM, the study of their clinical presentation and discovery of treatment options has contributed hugely to the understanding of many aspects of metabolism[3].

Investigation into the metabolic consequences and causes of disease aims to discover new targets for disease treatment, which may have been overlooked when studying the cellular processes which define the disease phenotype alone.

1.1.1 Cancer Metabolism

Reprogrammed energy metabolism was included as a hallmark of cancer for the first time in 2011[4], based on an increasing body of evidence that metabolic alterations are a fundamental part of the cancer cell phenotype. The first studies showing a distinct metabolic switch in cancer cells were performed almost 90 years prior to this by Otto Warburg[5]. Warburg found that tumour slices consumed more glucose and produced more lactate than normal tissue, showing an alteration in glucose usage which became known as the Warburg effect[6].

Since this observation, many other metabolic changes have been associated with transformed cells. Most frequently, cancer cells metabolise glutamine[7] and synthesise fatty acids[8] at higher rates than normal cells. These metabolic changes are necessary to support an increased proliferative rate, but are also required in order to survive under conditions of increased stress often experienced by cancer cells. As a result, somatic mutations in metabolic enzymes which support these processes may be selected for during tumour formation. Additionally, some key metabolic pathways are under the regulation of well-defined oncogenes or tumour suppressors[9]. For example, the tumour suppressor p53 acts in a number of ways, including downregulation of the glucose transporters GLUT1 and GLUT4[10], to reduce glycolysis[11].

As well as alterations to the fuel preferences of transformed cells, the rate and route of usage is also changed, compared to healthy tissues. Tumour cells have been shown to be dependent on the activity of the TCA cycle, in order to maintain an NAD^+:NADH ratio

which is favourable for the production of aspartate[12][13] (which will be discussed in more detail). However, recent data from *in vivo* stable isotope tracing experiments shows that the flux of carbons through the TCA cycle is lower than in healthy tissues[14], findings which agree with Warburgs original hypothesis. The published work suggests that this may be due to either a reduction in fuel availability, or in ATP demand, as they also demonstrate that dedifferentiation leads to loss of specialist cell functions.

Additionally, there are situations in which transformation is driven by mutations in metabolic enzymes. Under these circumstances, the metabolic phenotype which results from a loss or change of expression or function of certain enzymes drives tumourigenesis. For example, germline heterozygous loss-of-function mutations in succinate dehydrogenase (SDH) subunits predispose to hereditary paraganglioma, if the functional gene copy is also lost[15]. In cells lacking SDH activity, succinate accumulates, interfering with pleiotropic cellular processes. Notably it can prevent c-Jun dependant apoptosis, which relies on the activity of prolyl-hydroxylase 3 (PHD3) an enzyme which is significantly product inhibited by succinate[16]. Inhibition of PHDs in this way also leads to constitutive hypoxia inducible factor (HIF) stabilisation, and related transcriptional activity regardless of oxygen tension[17] - a phenotype described as pseudohypoxia. Somatic change-of-function mutations in isocitrate dehydrogenase (IDH) 1 and 2 have been identified in a subset of glioma, thought to occur after formation of a low-grade glioma, and drive progression[18]. Wild type IDH1 and 2 isozymes catalyse the conversion of isocitrate to α-ketoglutarate, reducing $NADP^+$. Mutations can lead to loss of this activity, with the enzyme instead producing the oncometabolite 2-hydroxyglutarate (2HG) and oxidising NADPH[19].

The aim of studying metabolism in cancer is to find opportunities for targeted treatment strategies which exploit metabolic vulnerabilities in cancer cells. Whether these are the result of mutations in metabolic enzymes, sustained high proliferative rate, or adaptations to a stressful environment. Metabolic vulnerabilities may include reliance on a particular nutrient source. One of the most successful examples of targeting metabolism is the use of asparaginase to treat paediatric acute lymphoblastic leukaemia. Leukaemic cells lose the ability to synthesis asparagine and rely on extracellular sources, which can be therapeutically limited through the use of asparaginase[20]. Metabolic vulnerabilities may also include an increased reliance on a particular pathway. For example, loss of the tumour suppressor fumarate hydratase which causes hereditary leiomyomatosis and renal-cell cancer, leads to reliance on the heme synthesis pathway through haem oxygenase[21]. It is hoped that in-

vestigation of metabolic changes such as these will guide treatment strategies which may selectively target cancer cells, or may synergise with current chemotherapy, to improve patient outcomes.

1.2 Redox Co-factors

Nicotinamide adenine dinucleotide (NAD^+/NADH) and nicotinamide adenine dinucleotide phosphate (NADP/NADPH), are the two forms of nicotinamide-based co-enzymes required for biochemical reactions involving the loss or gain of electrons. These reduction and oxidation (redox) reactions require small molecules to receive or donate electrons, in turn becoming reduced or oxidised themselves. NAD^+ most commonly accepts two electrons and a proton from an oxidation reaction to produce NADH. It is important for cells to maintain a stable pool of redox co-factors, and for the redox state of these available co-factors to be balanced, in order for central metabolic reactions to remain favourable.

NAD^+ can be synthesised *de novo* from dietary tryptophan or from nicotinic acid. Additionally, cells can replenish the pool through recycling of other precursors, termed the salvage pathway. There are 3 precursors available for this pathway: nicotinamide (produced through NAD^+ consuming enzymes), nicotinamide riboside (vitamin B3 derivative) and nicotinamide mononucleotide. Finally, phosphorylation of NAD^+ via the NAD^+ kinases, either in the cytosol or in the mitochondria, produces NADP. However, these are not necessarily static pools, as interconversion is possible through NAM nucleotide transhydrogenase, which utilises the inner mitochondrial membrane proton gradient to catalyse the reaction: $NADH + NADP^+ \leftrightarrow NAD^+ + NADPH$.

In addition to maintaining the amounts of redox co-factors, the ratios of reduced to oxidised forms must also be tightly controlled. This work will focus on redox balance; factors which challenge this balance, the consequences of loss of redox homeostasis and mechanisms to maintain it.

1.2.1 NAD^+:NADH

NAD^+ is required as an electron acceptor for the oxidation of carbon sources such as glucose, lipid and amino acids. As previously discussed, these catabolic reactions are central to growth and viability, providing energy to drive ATP production and supplying building blocks for anabolic reactions[22]. The ratio of NAD^+:NADH is often higher in more proliferative cells, and lowered in quiescence[23]. In fact, alteration of the NAD^+:NADH balance has been shown to regulate senescence in mesenchymal stem cells[24]. Regeneration of the oxidised co-factor is critical for continued proliferation which means that cells must rely on metabolic pathways which oxidise NADH to produce NAD^+ to support their proliferative drive. One example of this is through lactate dehydrogenase (LDH), which converts pyruvate to lactate in the cytosol. High levels of lactate production have been associated with a highly proliferative phenotype for many years, named the Warburg effect[25,26]. Amongst other factors, this activity regenerates cytosolic NAD^+ which is then available for catabolic reactions, such as glycolysis.

Cells are dependent on NAD^+ regeneration through other sources, to support further metabolic processes. Mitochondrial sources of NAD^+ are vital; certain cancer cells have been shown to become dependent on extracellular pyruvate to increase the NADH oxidising activity of LDH, when they don't have functional mitochondria[13].

In circumstances where electron acceptors are limited, such as in hypoxia, cells can develop a reliance on metabolic pathways which oxidise NADH, increasing flux through these pathways - even when the end product is in excess. This is demonstrated by the excretion of lactate into the microenvironment under hypoxic conditions.

1.2.2 NADP:NADPH

Although very similar, the $NADP^+$:NADPH and NAD^+:NADH redox couples have distinct cellular roles. NADPH is the electron donor for many anabolic reactions, and is important in antioxidant pathways. The amount of $NADP^+$(H) varies between cell types, however unlike NAD(H), the $NADP^+$:NADPH ratio is relatively consistent[27]. The NADP:NADPH couple is maintained in a more reduced state that the NAD^+:NADH couple, due to the activity of the mitochondrial NAM nucleotide transhydrogenase. The reaction catalysed by this enzyme

($NADH + NADP^+ \leftrightarrow NAD^+ + NADPH$), is primarily in the forward direction[27].

Biosynthetic reactions requiring NADPH include: DNA synthesis, *de novo* fatty acid synthesis, amino acid synthesis and purine synthesis[28]. It is also required for cytochrome P450 reductase activity, which is involved in metabolism of steroid hormones and drugs[29]. Additionally, NADPH is a substrate for NADPH oxidases, which generate reactive oxygen species (ROS), and can transfer electrons out of the cytosol[28].

NADPH is an essential part of the cellular antioxidant system, required to protect the cell against the effects of excessive ROS and oxidative stress. Glutathione is an essential part of this system. In its reduced form (GSH), it acts as a substrate for GSH peroxidase to reduce peroxides to water or alcohol. NADPH acts as a cofactor for glutathione reductase to regenerate the pool of reduced glutathione, available for this reaction[30]. NADPH is also the electron donor for thioredoxin reductases (TRXR) which reduce thioredoxins (TRX). TRX are able to scavenge H_2O_2 and maintain DNA synthesis by reducing ribonucleotide reductase[31]. In a further antioxidant role, NADPH also binds catalases, which can directly convert H_2O_2 to oxygen and water. Bound NADPH protects catalases from inactivation by H_2O_2[32]. An altered NADP:NADPH ratio can therefore result in an altered GSH:GSSG ratio, and an increased sensitivity to oxidative stress.

1.3 Redox homeostasis

1.3.1 Overview

There is a high degree of compartmentalisation of redox cofactors, facilitating the differing redox requirements of cellular compartments. Neither dinucleotide is able to cross the mitochondrial inner membrane[33], meaning organelle-specific regulatory mechanisms must exist within the cell. In HEK293 cells, the majority of the intracellular NAD pool has been shown to be within the mitochondria[34]. There is also evidence to suggest that the mitochondrial NAD(H) pool is more tightly regulated, as it shows a decreased sensitivity to challenges such as nutrient availability, when compared to the cytoplasmic and nuclear pools[35].

Mechanisms exist to facilitate the indirect transfer of reducing potential from NADH

between the cytosol and the mitochondria; a key transfer system being the malate-aspartate shuttle. The shuttle depends on the activity of the cytosolic and mitochondrial forms of malate dehydrogenase (MDH) and glutamic-oxaloacetate transaminase (GOT). In the cytosol, MDH catalyses the reduction of malate to oxaloacetate, driven by NADH oxidation. The malate-α-ketoglutarate antiporter transports malate into the mitochondria, against the export of α-ketoglutarate into the cytosol. In the mitochondria, malate is oxidised to oxaloacetate, to drive reduction of NAD^+. Oxaloacetate cannot be transported back into the cytosol and is aminated to form aspartate by GOT, with glutamate as the amino group donor. The aspartate-glutamate antiporter brings glutamate for this reaction into the mitochondria, and exports aspartate into the cytosol (Figure 1.1).

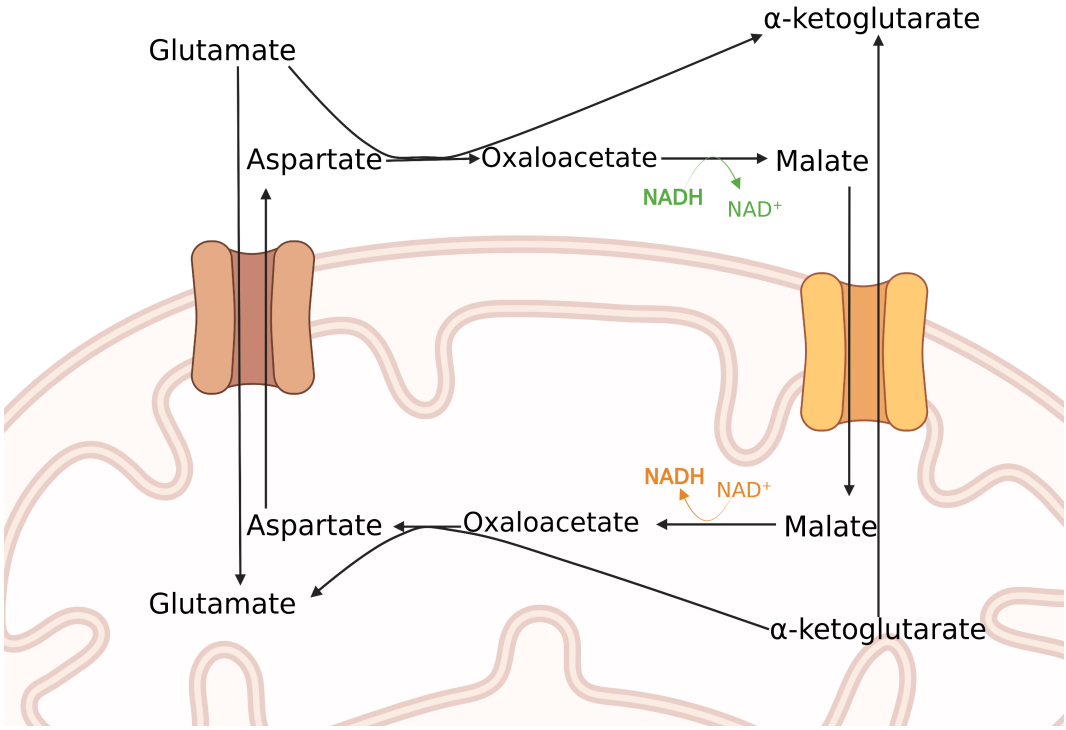

Figure 1.1: The Malate-Aspartate Shuttle

The function of the ETC has also been shown to be crucial in the maintenance of a favourable redox balance in proliferating cells. Two studies using similar, but differing techniques concluded that one of the central function of the ETC, aside from ATP generation is to direct electrons to oxygen, thereby maintaining a pool of electron acceptors (NAD) for other reactions; in particular, the synthesis of aspartate[36,12].

As discussed, cellular redox balance must be maintained to ensure reactions involved

in nutrient catabolism and biosynthesis are favourable and to protect against oxidative stress. This work will focus on the NAD:NADH balance and the importance of this in TCA cycle activity. Several of the most important NAD(H) reducing and oxidising reactions which are crucial to central carbon metabolism are outlined in Figure 1.2.

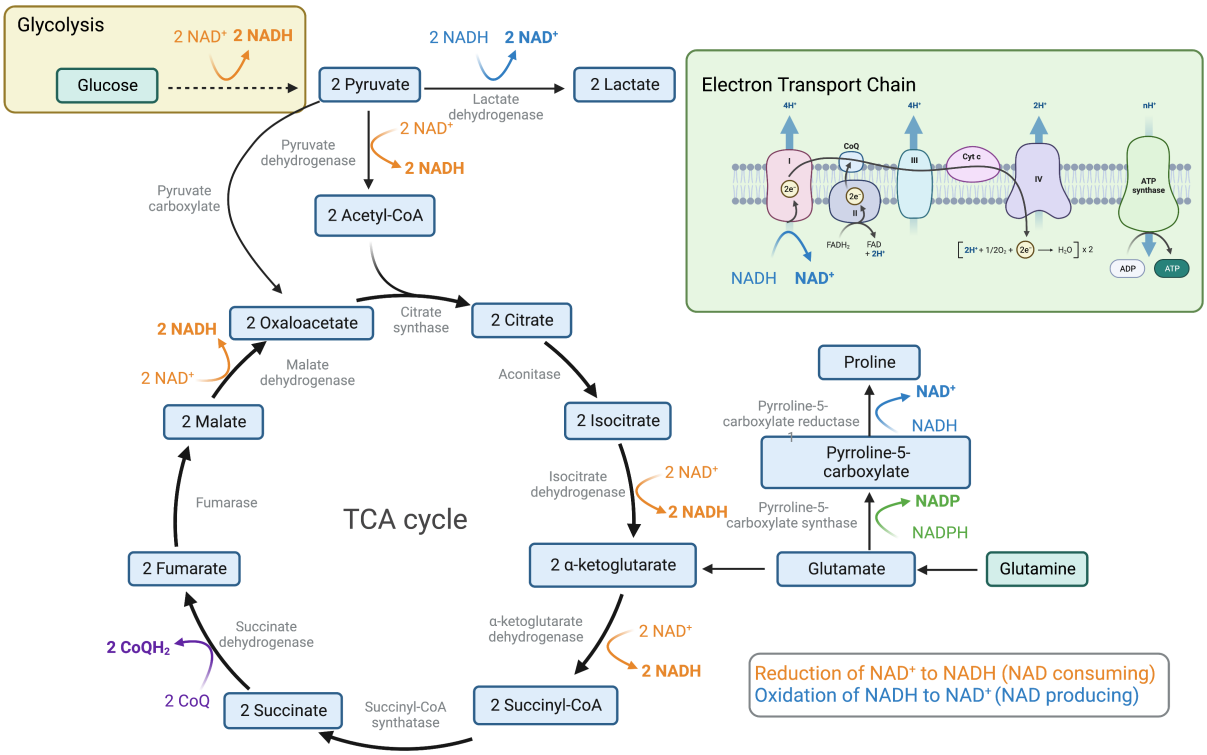

Figure 1.2: Schematic demonstrating several NAD(H) reducing and oxidising reactions in central carbon metabolism.

1.3.2 Redox homeostasis in cancer

Cancer cells face challenges to their redox balance as a result of an increased rate of proliferation, changes to the microenvironment, and from cell intrinsic factors such as genetic alterations. This section will explore several of these circumstances in detail.

Isocitrate dehydrogenase 1 mutation

Mutations in two of the three isocitrate dehydrogenase (IDH) isoforms (IDH1 and IDH2), are prevalent in cancer[37]. In particular, a common mutation in IDH1 - substitution of arginine 132 (R132X) - causes a redox imbalance[38]. This mutation results in a loss of isocitrate oxidation activity, but the enzyme retains the ability to reduce α-ketoglutarate, to the alternative product, (R)-2-hydroxyglutarate (2HG). As a result, instead of oxidising $NADP^+$, IDH1R132X activity reduces NADPH[19]. This disrupts the $NADP^+$:NADPH ratio, causing a dysregulated GSH:GSSG ratio, thereby making these cells more sensitive to oxidative damage[39]. IDH1R132-mutated cells therefore have to adapt their metabolism to try to correct this redox imbalance.

Hypoxia

Cells in solid tumours are often in an environment with a low oxygen tension. This occurs as a result of the high proliferative rate of cancer cell populations - whose demand is in excess of the available oxygen supply. Tumours can undergo a pro-angiogenic switch, upregulating signalling factors which induce new blood vessel formation. However, while normal neovascularisation is a closely regulated process, the continued presence of pro-angiogenic factors in the tumour microenvironment does not allow normal maturation of the newly formed vessels. This leads to a tumour vasculature which is poorly organised and hyperpermeable resulting in areas of continued or intermittent hypoxia[40].

The extent of hypoxia in tumours has been measured both directly and indirectly using a range of techniques. Needle electrodes, which can directly record the partial pressure of oxygen in tissue were used to demonstrate a link between hypoxia and poor treatment responses in the first instance[41]. Methods have since been developed which can be used to study hypoxia in inaccessible tumours. Pimonidazole, which forms adducts in hypoxic cells *in vivo* that can be detected in samples *ex vivo* using antibody staining[42], has been used extensively. This method has been used to validate the hypoxic expression of several proteins, including GLUT-1 and CA9[43]. Imaging of hypoxic tumour areas is an alternative method, which allows regions to be studied *in situ* and in a non-invasive way. One widely used method for this is positron emission tomography (PET) imaging using radiotracers which are retained only in hypoxic cells. This is most useful for establishing the area of a

tumour which is hypoxic, rather than a measurement of the extent of the hypoxia in a given area[41].

Hypoxia induces phenotypic changes in cells due to hypoxic signalling pathways, direct effects of insufficient oxygen and damage by ROS. Much of the hypoxic signalling is mediated through the activity of the hypoxia inducible factors (HIFs) - heterodimer transcription factors. Under normoxic conditions the oxygen-labile subunits of HIFs (either HIF1α or HIF 2α) are hydroxylated by HIF prolyl hydroxylases (PHDs), targeting them for binding and ubiquitylation by pVHL[44,45]. PHD activity is dependent on α-ketoglutarate, iron, ascorbate and oxygen availability. Therefore, under hypoxic conditions HIF subunits are unable to be targeted for degradation, HIFα is stabilised and can translocate to the nucleus where it dimerises with HIFβ and functions as a transcription factor[46]. Through their regulation of the expression of genes containing a hypoxia-responsive element (HRE)[46] HIFs regulate pathways involved in a range of cellular processes, including metabolism, angiogenesis, migration and cell survival[47,48,49 ,50].

Hypoxia presents a significant challenge to cellular redox balance, which cancer cells have to respond to in order to survive in the hypoxic niche. Activity of the ETC has been found to slow in hypoxia; there are several explanations for this phenomenon. It has been suggested that this is due to hypoxic cells decreasing their ATP consumption, as a result of downregulated protein synthesis[51] and suppression of ATP dependent plasma membrane sodium-potassium pumps[52,53]. This may also be due to inhibition of complex IV by nitric oxide (NO). Under normoxic conditions, the available oxygen is sufficient to compete with the NO, but when oxygen is limiting, NO inhibition reduces the function of complex IV[54,55,56]. Further to this, HIF mediates complex switching in complex IV, inducing the degradation of the COX-4-1 subunit, and increasing expression of the COX-4-2 subunit. This switch is considered to be an adaptation which reduces ROS generation due to inefficient electron transfer[57].

The impact of hypoxia on ROS formation and the impact of this on metabolism is still not completely clear. Recently, the role of ROS in signalling and regulation of cellular processes has become more recognised - they are no longer regarded as just a byproduct of inefficient electron transfer. Production of ROS, however, must be tightly regulated to avoid toxic levels of oxidative damage[58]. Mitochondrial ROS are involved in hypoxic signalling processes, one of which is the stabilisation of HIF1[59], which is thought to rely on an increase

in mitochondrial ROS and their release into the cytosol for full activation[60]. However, hypoxic cells need to regulate this ROS production to prevent damage. The more reduced mitochondrial NAD^+:NADH ratio may aid this as the mitochondrial NNT can generate NADPH from NADH that increases regeneration of the mitochondrial antioxidant systems[61].

Slowed ETC activity leads to a decrease in the NAD^+:NADH ratio, as less NADH is oxidised by complex IV. This shift means that several reactions through the TCA cycle become less favourable. Not only does this affect production of biosynthetic intermediates, reduced mitochondrial NAD^+:NADH also reduces the efficiency of the malate-aspartate shuttle in regenerating NAD^+ in the cytosol. In order to maintain a cytosolic NAD^+:NADH ratio which is favourable for glycolysis, pyruvate is reduced to lactate, oxidising NADH. This lactate is then excreted through monocarboxylate transporters, the expression of which are also under HIF regulation[62]. This slowing of ETC activity and altered NAD^+:NADH ratio may also render aspartate a limiting metabolite in hypoxia[36,12].

In order to maintain some proton pumping activity of complex I, and the activity of reactions which require CoQ_{10} in the mitochondrial membrane as an electron acceptor, the ETC can be reversed in response to low oxygen conditions. The lack of oxygen as a terminal electron acceptor for the ETC causes the pool of CoQ_{10} to become more reduced, and therefore less able to transfer electrons to complex III. This drives the reversal of succinate dehydrogenase (SDH) activity, so that it reduces succinate to fumarate. In this way, fumarate acts as a terminal electron acceptor, allowing continued activity of complex I when oxygen is lacking[63].

Metastasis

Cancer cells which survive metastatic transformation and break away from the primary tumour have to contend with several significant challenges to their redox balance. Detachment from the extracellular matrix (ECM) causes redox dysregulation, through signalling pathway activation and metabolic change, which lead to cell death in the majority of cells[64]. Anchorage independent survival relies on the ability of cancer cells to bring the redox balance under control, or the availability of antioxidants to support this[65]. It is likely that invading cells also downregulate anabolism; it has been suggested that cells either infiltrate or proliferate, but not at the same time (so called "grow or go")[66,67], due to the redox implications of trying

to support both phenotypes.

Cells are exposed to further oxidative stress on entry to the vasculature. The blood is an oxidative environment, with high levels of oxygen and iron[68,69]. Once cells have reached the metastatic niche, they must again restructure their metabolic network to increase their anabolism. This is another metabolic switch which challenges redox homeostasis. Indeed, it has been hypothesised that an inability to overcome redox stress could be a cause of dormancy in some metastatic nodules[70].

ROS levels are increased in metastatic cells[71], which may in part be due to increased ETC activity, compared to the primary tumour cells. Genes associated with oxidative phosphorylation are upregulated in melanoma metastases[71] and *in vitro* melanoma cells with a higher metastatic potential consume more oxygen, linked to ATP production[72]. Additionally, there is now direct, *in vivo*, evidence that metastatic nodules have a higher flux through the TCA cycle than primary tumours, as shown by an increased rate of m+2 glutamate production after infusion of [U_{13}C]-lactate. It is as yet unclear why this is the case. It could be hypothesised that this is an adaptation to the metastatic niche, or that this is a necessary adjustment to meet the ATP requirements of the metastatic process. Alternatively, the increased ROS production as a result of ETC activity, likely in the context of reduced oxygen availability, may contribute to a metastatic phenotype.

The redox requirements of cells are highly dynamic and dependent on a multitude of concurrent factors. Transformed cells experience further challenges to their redox homeostasis, which must be overcome in order for the cells to survive and the cancer to progress. The mechanisms by which cancer cells prevail under such conditions are important to study, as they may expose vulnerabilities and dependencies which could be exploited for therapy.

1.4 Amino acid metabolism and redox in cancer

1.4.1 Overview

The amino acid requirements of highly proliferative cancer cells are significant, in order to fulfil increased energetic and biosynthetic demands. In addition to an increase in overall

demand, cancer cells may also have specific amino acid dependencies, due to previously discussed changes to the metabolic network and redox regulation. One such example is the dependance on exogenous asparagine seen in several cancer types, due to dysfunction of the major synthetic enzymes for this amino acids[73,74]. This dependence has been successfully exploited in treatment using bacterial asparaginase to reduce the availability of extracellular asparagine. This is now a routine treatment and cure for paediatric acute lymphoblastic leukaemia, demonstrating the potential efficacy of targeting amino acid metabolism[75].

Cancer cells are often auxotrophic for glutamine. This may be due to cell intrinsic factors such as downregulation or loss of glutamine synthatase[76,77]. Additionally, increased glucose flux through glycolysis and away from the TCA cycle[78], increases reliance of cancer cells on glutamine to fuel production of anabolic precursors and fatty acid synthesis through the TCA cycle[79]. The tumour microenvironment can also contribute to this dependence, particularly under hypoxic conditions, where reductive carboxylation of glutamine is increased[80]. Glutamine is also required for the synthesis of glutathione, providing carbons directly after its conversion to glutamate and indirectly through enhancing the uptake of cysteine. Reduced glutathione is an antioxidant, required for protection against high levels of oxidative stress in transformed and highly proliferative cells[81]. It therefore follows that components of glutamine metabolism are under the regulation of oncogenes and tumour suppressors. c-MYC transcriptionally upregulates the expression of several glutamine transporters[82] while p53 can directly bind glutaminase (GLS2)[83] and Retinoblastoma (Rb) downregulates expression of the glutamine transporter SLC1A[84].

In addition to glutamate, the synthesis of glutathione requires cysteine and glycine. Cysteine can be produced through the uptake and NADPH-dependant reduction of cystine from the microenvironment. Cells can also produce cysteine via *de novo* synthesis through the transsulfuration pathway from homocysteine derived from the methionine cycle[85]. Cystine uptake is via the cystine/glutamate antiporter (xCT), so influx of cystine occurs alongside a reduction in the size of the intracellular glutamate pool. Cancer cells may have limited access to exogenous cystine[86], and also have more difficulties utilising the import mechanism, due to the redox implication of glutamate loss and NADP utilisation[87,88], making them more dependent on the transsulfuration pathway. This raises the possibility of targeting this pathway as a therapeutic strategy. However, the *in vitro* data is as yet unclear, as a range of cell lines respond differently to cystine starvation[85]. It may be that this process is context specific, and more work is necessary to unpick this.

Serine is important for the maintenance of the glutathione pool, both through its role in the transsulfuration pathway, and in the synthesis of glycine. Serine metabolism is also important for nucleotide synthesis, DNA methylation and protein synthesis, through one carbon metabolism[89]. Some tumours have been found to be dependent on extracellular serine, and noteably, serine starvation *in vivo* reduces the growth of colorectal tumours[90].

Increased serine synthesis has been identified as a cancer-associated metabolic change in several studies[91]. Serine is synthesised *de novo* from the glycolytic intermediate 3-phosphoglycerate (3-PG), in a pathway which requires NAD^+. Expression levels of one of the key enzymes of the serine synthesis pathway, phosphoglycerate dehydrogenase (PHGDH), appear to determine whether a cancer cell is likely to be dependant on extracellular serine[92], and whether tumours will respond to knockdown of small molecule targeting of this protein[93,94]. It may be that serine dependence and expression levels of the associated enzymes change at different stages of tumourigenesis, or in different microenvironments.

One carbon metabolism encompasses both the folate and the methionine cycles. The single carbon unit is supplied either from the conversion of serine to glycine, or through the glycine cleavage system. This carbon is transferred to tetrahydrofolate (THF), which is converted to 5, 10-methylenetetrahydrofolate (meTHF), reduction of meTHF produces 5-methyltetrahydrofolate (mTHF). Demethylation of mTHF donates carbon units to homocysteine, which can then be converted to methionine, linking the folate and methionine cycles[95]. Downstream, one carbon units are important for the biosynthesis of purine and pyrimidine nucleotides[96] and S-adenosylmethionine (SAM) from the methionine cycle is a methyl donor, notably important in DNA methylation. Additionally, these cycles are redox-linked. The conversion of methylene-THF to formyl-THF (for purine biosynthesis) reduces NAD^+ or NADP in the mitochondria, and NAD^+ only in the cytosol. Mitochondrial NADPH is also produced by the activity of ALDH1L2 which catalyses the oxidation of formyl-THF to THF and CO_2[97].

Glycine has been linked to growth in cancer cells, with upregulation and reliance on expression of enzymes of the glycine cleavage system (GCS) shown in lung tumour initiating cells[98] and in glioblastoma[99]. Conversely, glycine in excess can be detrimental to cancer cell proliferation. High glycine levels in the context of lower serine levels can reverse the activity of SHMTs, thereby pulling carbon units away from entry into the folate cycle[100]. Additionally, in glioblastoma cells with elevated glycine production, the GCS has been shown

to be necessary to prevent accumulation of aldehydes and associated toxicity[99]. Regulation of intracellular levels of glycine, and the ratio of serine to glycine is important to continued proliferation.

Other potential sources of carbon for one-carbon metabolism include histidine, which can decrease the size of the pool of available THF, sensitising cancer cells to anti-folate treatment[101]. The essential amino acid tryptophan can also donate a carbon, via the kynurenine pathway. Tryptophan is converted to formyl-kynurenine, which spontaneously releases formate to form kynurenine. In PDAC cells, tryptophan can be used as an alternative source of carbon when serine levels are low[102].

Another amino acid which has recently gained more attention in the context of tumour metabolism is aspartate, which has been shown to be a limiting metabolite in hypoxia, where *de novo* synthesis is impaired due to reduced ETC activity. Under these conditions, aspartate supplementation can restore growth and is primarily used for synthesis of purines[12]. In fact, one of the main functions of the ETC may be to produce aspartate. Blockade of the ETC can be rescued by addition of aspartate or exogenous electron acceptors[103,104], but whether this rescue is only through the anabolic potential of aspartate, or the redox implications of its insufficiency is still a matter of debate.

Additionally, the local redox balance; availability of oxidative or reductive cofactors, within cellular compartments can influence the directionality of amino acid metabolic reactions. An example being the synthesis of proline from glutamine or ornithine, which will be discussed in depth below.

Proline Metabolism

Proline is a non-essential, proteinogenic amino acid. It has a unique structure, formed of a pyrrolidine ring with a side chain connected to the amino group, forming a secondary amine[105]. It has an important structural role in proteins, notably making up 25% of the residues of collagen, including hydroxyproline[106]. Cellular availability of proline is determined by the rates of proteinolysis, the rate of proline biosynthesis and breakdown and extracellular availability. Importantly, the synthesis and breakdown of proline are both redox-active processes, linking the metabolism of proline to the wider redox-state of the cell.

Proline can be synthesised *de novo* via the intermediate, pyrroline-5-carboxylate (P5C) from glutamate or from ornithine. P5C is synthesised from glutamate by pyrroline-5-carboxylate synthase (P5CS), an ATP-dependant reaction which oxdises NADPH. Ornithine is first converted to glutamate-5-semialdehyde (GSA) by ornithine amino transferase (OAT), which then spontaneously cyclises to P5C. The turnover of P5C is rapid, and it is very unstable, making it technically challenging to measure directly in cells[107]. The synthesis of proline from P5C is catalysed by the pyrroline-5-carboxylate reductases (PYCRs) (Figure 1.3).

There are 3 PYCR isoforms; PYCR1, PYCR2 and PYCRL. PYCR1 and 2 are the most similar (84% sequence similarity) and are both mitochondrial, with PYCR1 associated with the mitochondrial membrane and PYCR2 in the matrix[108]. PYCRL is 40 amino acids shorter and shares only 45% of its sequences with the other isoforms, it is also spatially separate from the two other isoforms as it is located in the cytosol[108].

The isoforms also have differing substrate preferences, established using stable isotope tracing techniques in combination with siRNA-mediated knockdown of each of the isozymes. PYCRL appears to catalyses proline production primarily from P5C which is derived from ornithine, whilst PYCR2 preferentially produces proline from glutamate-derived P5C. PYCR1 has also been observed to produce proline mainly from P5C derived from glutamate, but in conditions of high ornithine and low glutamate it has been shown to use ornithine-derived P5C as well[108].

Additionally, the isozymes have differing affinities for the co-factors NAD and NADP. Continual monitoring of NAD(P) by absorbance measurement during the conversion of P5C to proline by recombinant PYCR1, 2 or L suggests that PYCR1 and PYCR2 preferentially use NADH as an electron acceptor, whilst PYCRL uses NADPH[108]. These specific roles and locations imply that there is a separation between P5C formed from glutamate and from ornithine, and that P5C from ornithine is channelled to the cytosol for proline production. OAT is a mitochondrial enzyme, which implies there is a mechanism for specific transport into the cytosol for ornithine-derived P5C. Finally, PYCR2 shows a high levels of product inhibition (Ki_app = 0.1mM), with PYCR1 also strongly regulated (Ki_app = 0.6mM), both inhibited by a proline concentration within the physiological range. PYCRL on the other hand is relatively insensitive to proline concentrations (Ki_app = 8mM).

The first step of proline catabolism is the conversion of proline to P5C, catalysed by proline dehydrogenase (PRODH). This enzymes is also referred to elsewhere as proline oxidase (POX). This reaction also reduces a molecule of FAD to $FADH_2$, which can transfer electrons to the ETC, contributing to ATP generation. P5C generated through this reaction is then converted to glutamate by pyrroline-5-carboxylate dehydrogenase (P5CDH)[109,110].

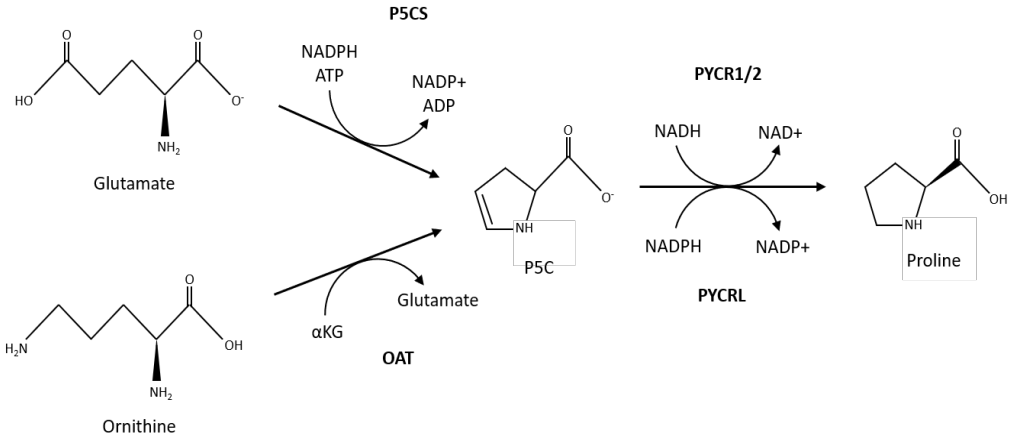

Figure 1.3: Proline synthesis from glutamate and from ornithine through the PYCR isoforms.

1.4.2 Proline metabolism as a stress response

Proline metabolism has long been associated with stress in plants, bacteria, protozoa and algae. In plants, proline is known to accumulate under stress conditions, such as altered osmotic pressure, drought, low temperature, heavy metal exposure and UV radiation[111]. In these conditions, increased proline levels impart stress tolerance via three mechanisms; as a signalling molecule, metal chelator and oxidative stress protection[111].

The role of proline metabolism in stress and links to oxidative stress protection have been increasingly investigated in mammalian cells, particularly in the context of cancer. Proline is known to be able to scavenge ROS[112,113,114,113]. This was demonstrated using a graft co-polymerisation assay technique, which measures the extent of free radical-dependant grafting of two materials. Proline addition reduces the grafting in a dose-dependent manner, suggesting it is able to reduce the availability of reactive species[113]. It has been further shown in a system using ascorbate, hydrogen peroxide and iron to generate free radicals, and measurement of salicylic acid hydroxylation as a surrogate for the amount of radicals present. The ability of compounds to compete with salicylic acid can therefore be determined,

and is assumed in this model to suggest free radical scavenging. In this system, proline was found to reduce salicylic acid hydroxylation, again in a dose-dependant manner[114].

In the context of myocardial infarction, proline supplementation is sufficient to reduce oxidative damage and apoptosis. This affect appears to be transcriptional, increasing expression of Glutathione peroxidase 1, and decreasing the expression of Thioredoxin-interacting protein - which acts on thioredoxin to inhibit the antioxidant system[115].

The effects of proline itself and the effects of its metabolism appear to be distinct. For instance, pre-treatment with proline was found to be protective against oxidative stress induced by H_2O_2 in a melanoma cell line. However, the protective effects are dependent on the metabolism of proline, as rescue was lost with siRNA mediated knockdown or inhibition of PRODH[116].

Components of the proline metabolic pathways are downstream of stress-induced signalling pathways. The expression of PRODH is induced by the tumour suppressor, p53[117]. p53 is activated in response to multiple stressors, including; DNA damage, oncogene activation, hypoxia and ribosomal stress[118]. Additionally, components of the proline synthetic pathway are downstream of mTOR signalling pathways[119].

PRODH is also regulated by mammalian target of rapamycin (mTOR) signalling, in response to nutrient stress. Indeed, treatment with rapamycin has been shown to induce PRODH expression[109]. ATP levels after rapamycin treatment show a slight initial decline, and stabilise thereafter. ATP levels are unable to maintained after rapamycin treatment with siRNA knockdown of PRODH[109]. PRODH can contribute to ATP generation by direct transfer of electrons from proline to the ETC via cytochrome C[120]. ATP generation through PRODH activity may also be through increased flux through the pentose phosphate pathway, as blockade of this reverses the PRODH dependant maintenance of ATP after rapamycin treatment[109]. It has been suggested that this is driven by $NADP^+$ produced through proline cycling, although the evidence for this is not yet strong.

Interestingly, it has been suggested that there is a direct interaction between the mitochondrial isoforms of PYCR and the RRMB2 subunit of ribonucleotide reductase (RR)[121]. RR catalyses the rate limiting step of deoxyribonucleotide synthesis, essential for DNA synthesis and repair. The RRMB2 subunit is induced by oxidative stress and DNA damage. Notably, in hypoxia, subunit switching to RRMB2 is essential for hypoxic cell viability[122]

Overexpression can reduce ROS accumulation in cancer cells and provide protection against hydrogen peroxide treatment. Indeed, RRMB2 can catalyse the conversion of hydrogen peroxide to water and oxygen[123], suggesting it may also have a direct catalase-like function. Knockdown of PYCR1 and 2 decreases cell survival under oxidative stress and expression of both isoforms has been shown as important in the maintenance of mitochondrial structure[121]. Cells overexpressing RRMB2 lose resistance to oxidative stress when PYCR1 and 2 are silenced, indicating that the oxidative protection of RRMB2 requires expression of the mitochondrial PYCRs[121]. It is not clear whether this coordination requires interaction between the proteins, or whether downstream effects of the PYCRs can modulate RRMB2 activity.

PYCR1 is further implicated in cellular stress responses due to the phenotype associated with germline mutations of this isoform. Fibroblasts from affected individuals have abnormal mitochondrial morphology, exhibiting altered cristae and a smaller size; a phenotype that is exacerbated upon treatment with H_20_2. These cells are more sensitive to H_20_2 than controls, resulting in 5-fold higher rates of cell death after treatment[124].

1.4.3 Proline metabolism and redox

The proline metabolic network, or proline cycle[110] is closely linked to the redox state of the cell, or cellular compartment, due to the electron transfer requirements at multiple steps. Flux through these steps is therefore responsive to the availability of these co-factors. In this way, it may also act to buffer perturbations in the redox balance.

The close link between proline metabolism and redox co-factor availability is clearly demonstrated with deletion of NADK2, the enzyme responsible for the mitochondrial phosphorylation of NAD to produce NADP. When NADK2 is lost, cells become auxotrophic for proline for their continued growth and proliferation. As a result of the loss of NADP production in the mitochondria, cells do not have sufficient levels of mitochondrial NADPH to maintain production of P5C from glutamate through P5CS activity[125].

Conversely, proline synthesis can also be responsive to increased availability of co-factors. Upon stimulation with growth factor cells increase uptake of nutrients, often exceeding their metabolic capacity. High levels of oxidation of substrates through the TCA cycle yields excessive NADH and FADH2. These levels can exceed the electron transfer ca-

pacity of the ETC, leading to ROS formation[126].After treatment with transforming growth factor beta (TGFβ), glutamine is directed away from the TCA cycle and into proline synthesis. Levels of proline increase in response to the observed increase in mitochondrial oxidative activity. Additionally, high levels of incorporation of proline into collagen were seen in this context. Deletion of P5CS results in loss of these responses[127].

Proline metabolism has also been identified, alongside lipogenesis, as a mechanism for maintaining electron transfer when the ETC is limited, using a model of cellular electron balance. *In vitro* this translated to an increase in glutamine-derived proline export in response to ETC inhibition or hypoxia and an increase in glutamine incorporation into fatty acids. This was shown to be in response to NADH accumulation. Knockdown of P5CS, which completely ablates glutamine-derived proline synthesis, was seen to be synergistic with inhibition of lipogenesis in a xenograft model[128].

Proline metabolism has been referred to as a "redox valve"[129] and a "redox vent"[127], in references to its close links to the redox state of the cell. These terms focus on the loss of NADH and possibly understate the importance of the regeneration of NAD. Therefore, it may be more apt to refer to the network as "redox modulating".

1.4.4 Proline metabolism in cancer

Throughout the development and progression of cancer, the metabolic requirements of the cell change. The catabolism of proline appears to be particularly important in the process of metastasis, through PRODH activity. In a comparison of cells grown in 2D vs 3D, a switch from proline excretion to consumption is seen, with a corresponding increase in expression of PRODH. Accordingly, knockdown of PRODH reduces spheroid size, suggesting that PRODH activity is required for maintenance of cell viability when nutrients are restricted. Inhibition of PRODH in this model caused a marked decrease in ATP levels, supporting the idea that PRODH activity supports 3D growth by maintaining ATP production. This translates into a striking effect of PRODH inhibition *in vivo*, where the weight of the primary breast tumour remains the same between conditions, but the number of lung metastases is halved[130]. Interestingly, in this study the removal of proline from the media of cells grown in 3D did not affect spheroid size, unless in conjunction with knockdown of PYCR1[130]. This further supports the hypothesis that proline itself is not supportive of growth in stress conditions, and

that both its breakdown and synthesis are required. Interestingly, this is another study which identifies a role for PYCR1, but does not find any effect of PYCR2 in their model. It also serves as a reminder of the dynamic nature of metabolism, and that metabolic vulnerabilities of cancer cells are often context dependant.

Further work has also identified a subset of cancer cell lines which are dependent on exogenous proline in order to form colonies in culture. These cell lines showed relatively higher expression of genes associated with oxidative ER (endoplasmic reticulum) stress, compared with cell lines which are not dependent on exogenous proline. These cells also had altered expression of signalling pathways downstream of mTOR, and were more sensitive to its inhibition. Knockdown of PYCRL or c-myc (in order to reduce expression of P5CS) was able to reduce the clonogenic potential of cell lines which were proline-independent, although it is not clear if this phenotype can be rescued with the addition of proline. This work again implicates proline metabolism in the cellular response to stress, further linking it to mTOR signalling. *In vivo* this translates into a sensitivity of proline-dependent cell lines to proline starvation, with a significant reduction in tumour formation in mice on a proline-free diet[119].

Proline metabolism and the tumour microenvironment

Proline metabolism is adapted in response to a changing tumour microenvironment and the metabolic implications of this. It can also be linked more directly to the physical microenvironment and the ECM.

Collagen is one of the major components of the ECM, and is strongly linked to proline metabolism. A significant proportion of the amino acids which make up collagen are proline and hydroxyproline; only glycine is more abundant.[131]. Accordingly, collagen can also act as an extracellular proline reserve alongside its more widely recognised role in ECM structure. Under nutrient limited conditions, pancreatic ductal adenocarcinoma (PDAC) cells have been shown to take up collagen fragments and metabolise the proline derived from this through PRODH[132].

Proline synthesis in response to TGFβ stimulation, can also support enhanced collagen production in fibroblasts[127]. It seems likely that increased proline synthesis in response to redox stress in cancer cells could contribute to collagen synthesis in a similar way. Interestingly, in lung cancer, proline synthesis has been seen to be increased in response to

ECM stiffness. This occurs through an interaction between Kindlin-2, involved in integrin-mediated cell-ECM interaction, and PYCR1 in the mitochondria. Loss of kindlin-2 resulted in decreased proline synthesis and fibrosis[133].

PYCR1 in cancer

Use of differential ribosomal codon profiling to screen for tumour-specific amino acid vulnerabilities identified proline as limiting in ccRCC, due to decreased availability of proline-tRNA for protein synthesis. Analysis of the proline metabolic enzymes in this context showed an increase in PYCR1 expression. Intriguingly, the expression of PYCR1 was found to be increased in response to glutamine deprivation, but not in response to proline depletion[134]. This study further showed that proline appears to be limiting in tumourigenesis, and that loss of PYCR1 in this context is detrimental to tumour growth. This suggests a role for proline synthesis in the early stages of tumour development, to support protein synthesis.

PYCR1 has been increasingly studied in the context of cancer in the last few years. Increased expression has been linked to poor prognosis, through publicly available dataset analysis in bladder[135], colorectal[136] and gastric cancer[137], small cell lung carcinoma[138], hepatocellular carcinoma[139] and lung adenocarcinoma[140]. Analysis using microarray gene expression datasets in conjunction with tissue-array data from breast cancer patients also showed a significant association between higher PYCR1 mRNA and protein levels and poorer outcomes in multiple molecular subtypes[141].

Recently, a number of papers have investigated the effects of siRNA mediated knockdown, or small molecule inhibition of PYCR1[135,136,137,138,139,140]. These have shown it to reduce proliferation, invasion and migration in several cell lines. So far, the majority of these investigations have associated PYCR1 expression with downstream processes and pathways without elucidating a mechanism, and often without consideration of the metabolic implications of PYCR1 loss. PYCR1 has, for example, been associated with Akt phosphorylation and activation of the Akt signalling pathway[142,135]. In this way, increased expression of PYCR1 in cancer cells is directly linked to signalling leading to increased proliferation, invasion and migration. This, without a mechanism or proven interaction, seems likely to be an oversimplification, given the likely effects of loss of a source of proline synthesis and NADH oxidation. Given the body of evidence to suggest that the proline metabolic network

is involved in oxidative stress, alterations to proliferative and apoptotic signalling pathways are likely to be in response to metabolic dysregulation.

One study does show a direct interaction via co-immunoprecipitation of PYCR1 with STAT3, which can mediate p38 mitogen-activated protein kinase (MAPK) and nuclear factor kappa B signalling[136]. However, while this may point to an as yet undescribed extramitochondrial pool of PYCR1, this interaction has yet to be shown *in cellulo*.

PYCR1 in IDH1R132 Glioma

As previously discussed, glioma cells with an IDH1R132X mutation have an increased $NADP^+$:NADPH ratio, altering the GSH:GSSG ratio with implications for their oxidative stress response. In these cells, proline synthesis from glutamine has been shown to increase. Knockdown of each of the PYCR isoforms showed that this increase is through the activity of PYCR1. Further to this, the expression of this enzyme was also found to be higher in patient IDH1R132X tumour samples, compared to IDH1WT. The levels of 2HG in tumours were also found to correlate with levels of proline[143], suggesting that the degree of 2HG synthesis is correlated with proline synthesis, further suggesting that proline synthesis is required to counteract the effects of this reaction. In this system, the loss of PYCR1 was also shown to increase the cellular oxygen consumption, suggesting that the activity of PYCR1 is oxygen sparing. This may be due to the NAD^+ produced through the reaction allowing bypass of complex I of the ETC, requiring less oxygen as a terminal electron acceptor. Based on this observation, it can be hypothesised that this may be a useful mechanism in hypoxia, where oxygen for the ETC is limited, and the NAD^+:NADH ratio is lowered.

1.5 Methods and Models

1.5.1 Inborn Errors of Metabolism

As previously mentioned, IEM encompass a wide range of disorders resulting from genetic alteration to components of metabolic pathways. IEM have been described as collectively common, but individually very rare, given the huge diversity of pathways which can be

impacted and the ways these can be affected. IEM can be due to increased or decreased activity of a metabolic enzyme, deficiency in a co-factor, or accumulation of metabolites due to issue with transport or degradation[144]. Early discovery and intervention is crucial in patients with IEM as symptoms tend to progress with development. This has led to the development of widespread screening programs including, most famously, phenylketouria (PKU) for which newborn babies have been routinely tested in the UK since 1969. Advances in metabolomic testing and medical genetics have led also to an increase in adult diagnosis, with 23% of diagnoses in a case study in the UK occurring in adults[145].

The study of metabolism, and cancer metabolism in particular, has been hugely influenced by insights gained from the treatment of individuals with IEM. Once such example was the finding that L-2-hydroxyglutaric aciduria, caused by a mutation in the L-2-hydroxyglutarate dehydrogenase gene, was associated with the development of CNS tumours[146]. In combination with studies which uncovered the role of IDH1 mutations, 2-hydroxyglutarate was designated an oncometabolite[147]. The effects of alterations to a pathway or an enzyme can inform our understanding of how these pathways function physiologically, and also in the context of other diseases.

Understanding the physiological role of proline metabolism has been furthered by research involving individuals with germline mutations in the proline biosynthetic enzymes, PYCR1[124] and PYCR2[148]. Mutations resulting in loss of PYCR1 result in a spectrum of disorders, with similar features, including: wrinkly skin (cutis laxa), generalised connective tissue weakness, hernias, ostopenia, hypoplasia of the jaw and intellectual disability. Serum proline levels in these individuals are in the lower region of the normal range.

Because the organ most affected in these patients is the skin, fibroblasts were isolated for *in vitro* analysis. In culture, these cells do not require supplementary proline in the media, and have an intracellular proline level comparable to that of controls[124]. This implies that synthesis of proline through the other PYCR isoforms is sufficient to maintain proline levels, and cells do not become auxotrophic for proline. No differences were seen in the oxygen consumption rates, nor in the production of ROS. These cells were, however, much more sensitive to treatment with hydrogen peroxide[124]. As ROS production is unchanged, this sensitivity is not due to a higher burden oxidative stress, but rather a decreased ability to deal with H_2O_2. These observation of both the patient symptoms, and corresponding molecular analysis can inform treatment and further investigations into fundamental metabolism.

1.5.2 Metabolic tracing

The field of cancer metabolism has rapidly grown in the last few years, and the techniques and methods have evolved extensively. There are several methods available to measure specific metabolites, for example lactate and glucose assay kits and meters. These provide a readout of the concentration of these metabolites, most often only in the media. They are useful to give an indication of the overall activity of a pathway, or consumption of a nutrient. For example, increased consumption of glucose and secretion of lactate would suggest increased glycolysis, although lactate measurement alone is likely an underestimate of glycolytic activity. In a similar way, but on a larger scale, metabolomics methods give a read out of levels of a large number of metabolites. This usually uses gas or liquid chromatography (GC or LC), coupled to a mass spectrometer (MS), which can separate and detect a panel of metabolites, to give a snapshot of the overall metabolic network. However, from this information, regulation of pathways can be inferred and not necessarily concluded. For example, an increase in a TCA cycle metabolite may indicate result from a decrease in breakdown or increase in synthesis. It also does not provide any information on the nutrient source used to produce the metabolite, or whether it was produced oxidatively or reductively.

Stable isotope tracing is a technique which can be used to answer these questions, and to interrogate nutrient usage in more detail. This method uses nutrients which contain stable isotopes that are most often heavier than those most commonly found naturally[149]. For example, carbon 13 in place of carbon 12, nitrogen 15 in place of 14 and deuterium in place of hydrogen. For this work, glucose or glutamine with all carbons replaced with $_{13}$C ([U$_{13}$C]) was used. These nutrients are metabolised with the same kinetics as their lighter counterparts, allowing the heavy atoms to be incorporated into downstream metabolites. Incorporation of a heavy isotope results in an increase in the fragment mass of that compound. For example, where the fragment detected by the mass spectrometer of proline has a mass of 286 (n), if that proline contains one heavy carbon isotope ($_{13}$C), the detected mass will be 287 (n+1). This is the same for any number of heavy carbons the metabolite contains, so proline which is fully comprised of $_{13}$C ([U$_{13}$C]-) has a fragment mass of 291 (n+6).

Using this technique, coupled to GCMS or LCMS, it is possible to determine how many of the carbons in a metabolite are derived from the labelled nutrient. With this information, the pathways utilised by the cell can be determined. For example, the majority of citrate m+2 is produced through the activity of pyruvate dehydrogenase (PDH), while

citrate m+3 indicates pyruvate carboxylate (PC) activity (Figure 1.4)[150]. Similarly, tracing using fully labelled glutamine into citrate can indicate the directionality of the TCA cycle. M+4 citrate from glutamine is indicative of oxidative TCA cycle activity, as a carbon is lost in the conversion of α-ketoglutarate to succinyl-CoA. M+5 citrate is a result of reductive TCA cycle activity, in which all of the carbons are retained (Figure 1.5).

1.5.3 Modelling the Tumour Microenvironment

As previously discussed, the microenvironment; particularly the hypoxic nature of this, affects redox regulation. Several methods have been employed in this work which aim to recapitulate aspects of this microevironment more closely than standard 2D cell culture. The study also uses methods to image tumours which generate data relating to the conditions the cancer cells inhabit, as well as the cells themselves. These methods will be discussed in detail below.

Hypoxia

Hypoxia Chambers

Cells grown in standard cell culture are maintained in incubators at atmospheric oxygen tensions (21%). In order to study the effect of hypoxia on cells in culture, cells can be cultured and experiments carried out in hypoxia chambers. The temperature, humidity and percentage CO2 are kept the same for the purpose of these experiments, but the percentage of oxygen is altered. For this work, two oxygen tensions are used, and referred to as hypoxia: 1% and 0.3%. These percentages were chosen to reflect a low oxygen environment, where cellular oxygen availability is sufficiently low to stabilise HIF1α, and lower than physoxic measurements for most tissues[41]. 1% is regarded as a mild hypoxia, and 0.3% as more severe.

Spheroid Culture

Spheroid cell culture is another technique which can be used to subject cells to hypoxic conditions. Spheroids develop a hypoxic core, due to the diffusion gradient of oxygen through

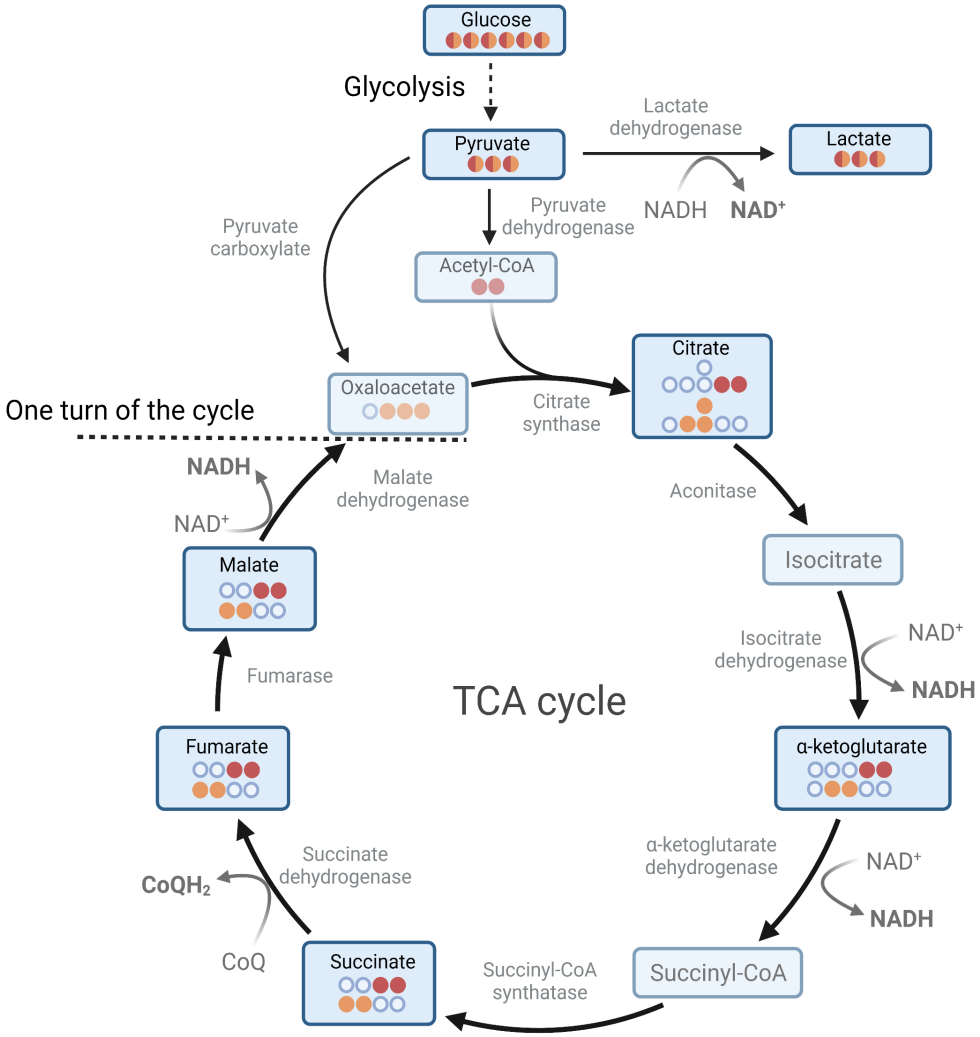

Figure 1.4: Incorporation of $_{13}$C Carbons from glucose into the TCA cycle

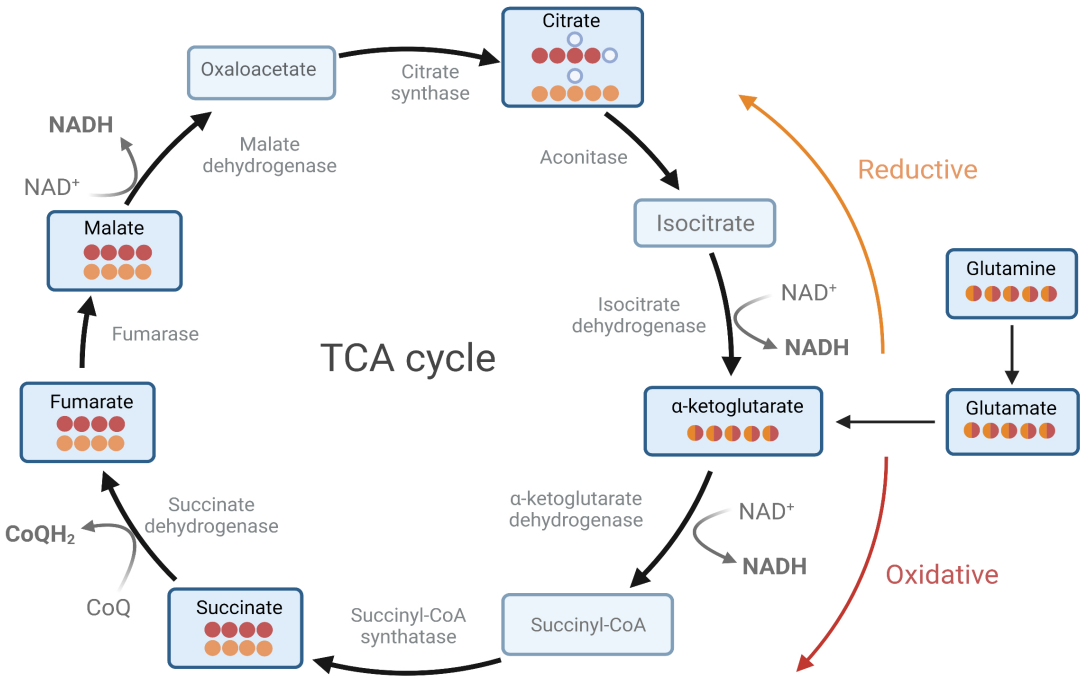

Figure 1.5: Incorporation of $_{13}$C Carbons from glutamine into the TCA cycle

the mass of cells (Figure 1.6). This level of hypoxia is also sufficient to induce HIF1α stabilisation. Cells in spheroids are exposed to a range of oxygen tensions, as they would *in vivo*. In this model the degree of hypoxia can't be defined in the same way as using a hypoxia chamber, so the use of both techniques gives a more thorough picture.

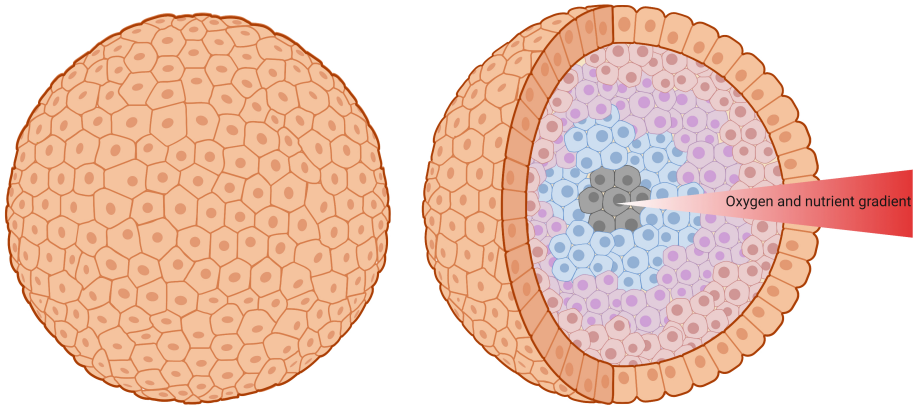

Figure 1.6: Cells grown in spheroid models are subject to an oxygen and nutrient diffusion gradient, which aims to more closely represent the conditions in a solid tumour.

Histology

Staining of sections taken from a tumour allows a snapshot of the cancer cells and the microenvironment in which they are growing. Staining of proteins not only in cells, but in the stroma provides information on conditions such as hypoxia.

Hypoxia in solid tissues can be studied both directly and indirectly. Staining for proteins which are upregulated by HIF1α can show when cells have been subject to a low enough oxygen tension to cause stabilisation. CA9 is commonly used as a marker for hypoxia for this reason[151].

Detection of hypoxia in tissues through the use of pimonidazole gives a more direct read out of oxygen availability. Pimonidazole is a 2-nitroimidazole, shown to form adducts with thiol groups in amino acids, peptides and proteins in cells with a pO2 $<$ 10 mmHg. Adduct formation is not affected by variations in NADH or NADPH levels. Antibodies have been raised against pimonidazole protein adducts, allowing immunodetection in samples. Pimonidazole is administered intravenously, tissues are snap frozen and prepared for analysis.

The use of pimonidazole for hypoxia detection has been extensively validated[152,153], and immunodetection has been shown to correlate with oxygen electrode measurements[42] and distance from blood vessels. This method also allows visualisation of hypoxic gradients in tissues and tumours.

1.6 Thesis Aims

This work aims to investigate the role of proline biosynthesis through PYCR1 in hypoxia. It aims to address the hypothesis that flux through this pathway is increased in low oxygen conditions, in order to regulate the NAD^+:NADH ratio. The impact of loss of PYCR1 in breast cancer cells in normoxia and hypoxia will be investigated, using a range of molecular biology techniques. In particular, the metabolism of these cells will be studied using stable isotope tracing methods. Further to this, it will explore the effect of PYCR1 loss in tumour cells *in vivo*, using a xenograft model.

Taking the PYCR1 investigation further, using a bank of slides from breast needle biopsy samples, the expression of PYCR1, the hypoxia marker, CA9, and collagen will be studied in biopsy sample from triple negative breast cancer tumours. Using spatial image analysis software, interactions and associations between these markers will be investigated.

Finally, using the the molecular methods previously discussed, this thesis will characterise dermal fibroblasts from a patient with an inborn error of metabolism, hypothesised to be caused by a mutation in decaprenyl diphosphate synthase subunit (PDSS-1). This enzyme catalyses a step of the coenzyme Q synthesis pathway. The mutation will be investigated, to establish whether it is likely to be causative.

Chapter Two

Proline Biosynthesis Through PYCR1 Supports Hypoxic Cancer Cell Survival

2.1 Introduction

Cancer cells undergo extensive metabolic reprogramming in order to support uncontrolled proliferation and to promote cell survival in an often challenging microenvironment. Identification of metabolic changes which occur in these cells will hopefully lead to the discovery of new targets for therapy. In particular pathways or nutrients upon which cancer cells become more reliant, either chronically (often due to (epi)genetic modification/mutation), in specific microenvironments, or at different stages of progression, may present metabolic vulnerabilities.

The metabolism of non-essential amino acids (NEAA) is often altered in cancer, with increased glutamine consumption, sometimes even characterised as glutamine 'addiction', being one of the most well-documented metabolic phenotypes[154]. NEAAs have been in implicated in numerous mechanisms in cancer, including lipid and nucleotide synthesis, epigenetic regulation and redox homeostasis[155]. One of the most successful examples of a metabolism-targeting treatment, asparaginase, targets leukaemic cells that are unable to synthesis the NEAA asparagine[20].

Proline has been studied in this context, with steps of its metabolism now linked to cancer cell survival and metastasis[110]. In addition to its role as a proteinogenic amino acid, both proline synthesis and catabolism are metabolically important processes. Several steps

of the proline metabolic network are redox-linked and ATP producing/consuming.

2.1.1 Proline biosynthesis

Proline is synthesised from the unstable intermediate, P5C, by the PYCR family of enzymes (PYCR1, 2 and L). The PYCR1 and PYCR2 isoforms preferentially use P5C derived from glutamate as a substrate, while PYCRL uses ornithine-derived P5C[108]. P5C is formed spontaneously from glutamate-5-semialdehyde (GSA), which is produced either through ornithine aminotransferase (OAT) from ornithine or through pyrroline-5-carboxylate synthase (P5CS) from glutamate. P5CS activity is ATP-dependent and oxidises NADH.

The synthesis of proline is redox-linked, with both routes requiring reducing equivalents. The different isoforms preferentially use different co-factors, with PYCRL mostly oxidising NADPH, and PYCR1 and 2 mostly oxidising NADH in their respective reactions[108](Figure 2.1).

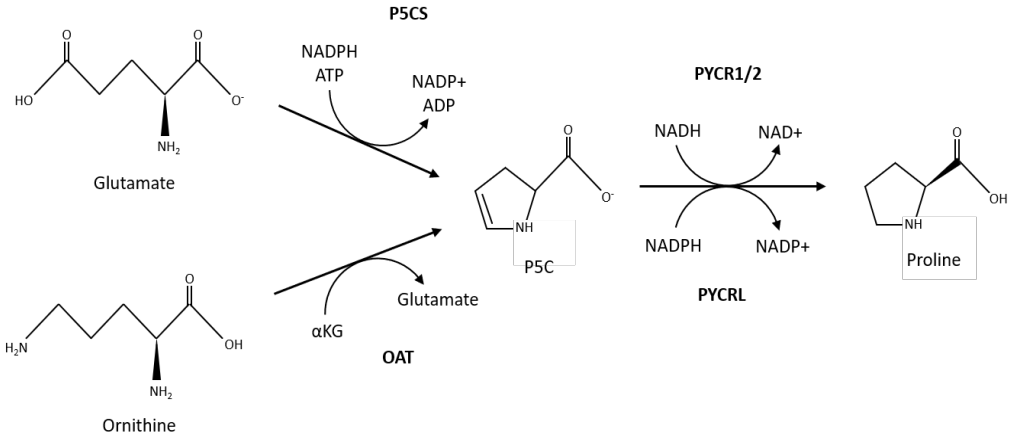

Figure 2.1: Diagram to show the possible routes of proline synthesis from glutamate or ornithine and the co-factors required for this reaction.

2.1.2 Tumour Hypoxia

Cells in solid tumours often have reduced and unreliable access to sufficient oxygen. Uncontrolled cancer cell proliferation often results in a dense mass in which competition for oxygen in increased, and in which cells are pushed further from the physiological blood supply. Tumour neoangiogenesis is able to compensate to some degree, but the vessels produced in this way are often disordered and inefficient[50,156]. Cancer cells must therefore be able to survive a hypoxia microenvironment, and overcome the metabolic and oxidative stress associated with this.

There are several clear metabolic changes which occur when cells are in hypoxia. Glucose metabolism is significantly altered, with increased consumption due to an increased reliance on glycolysis for ATP production. This is accompanied by an increase in lactate production and excretion, in response to a change in the NAD^+:NADH ratio. This results from slowed ETC activity[157], as the rate of oxidation of NADH is reduced. TCA cycle reactions are impacted by the lack of NAD^+, meaning the malate-aspartate shuttle is less capable of moving NADH produced though glycolysis out of the cytosol and into the mitochondria. The conversion of pyruvate to lactate is increased as this oxidises some of this NADH, and ensures glycolytic reactions are still favourable[61]. This overall glucose consumption increase and lactate excretion phenocopy the classic observations in cancer metabolic research. In this way, adaptation to hypoxia may not only be a means of survival, but may contribute to the malignant phenotype.

In hypoxia, the fate of glutamine is also changed. When levels are sufficient, glutamine is primarily oxidised through TCA cycle reactions, to ultimately produce anabolic precursors, as well as reduce NAD^+ to donate high energy electrons to the ETC to generate the proton gradient required for ATP generation through OXPHOS. In hypoxia however, the rate of oxidation of glutamine is reduced, and reductive metabolism plays a greater role. This involves its conversion to citrate through the activity of IDH1/2 and aconitase, using NADPH[61].

Hypoxic cancer cells are associated with a more aggressive and invasive phenotype, and hypoxic areas are known to be more resistant to chemo- and radiotherapy[158]. For these reasons, finding novel ways to target these cells is an important area of research focus. Additionally, the metabolic alterations which are required for cells to survive in hypoxic

conditions may present therapeutic targets.

2.1.3 PYCR1 in hypoxia

In light of the evidence demonstrating that PYCR1 activity is oxygen sparing in IDH1 mutated glioma cells[143], it was hypothesised that cells could use this pathway when oxygen is limiting. The NAD^+ generated through PYCR1 could allow by-pass of complex 1 of the ETC, permitting continued oxidative TCA cycle activity, and partially uncoupling these two processes. If this hypothesis is correct, proline biosynthesis through PYCR1 could represent a specific metabolic vulnerability in hypoxic cells.

2.1.4 Aims

The aim of this chapter is to investigate proline metabolism in hypoxia, to establish whether this pathway is altered with decreased oxygen availability, and the impact of its disruption on cell phenotype. Further to this, the system will be investigated *in vivo*, using a xenograft model, to establish whether any vulnerabilities can be translated into reduced tumour cell viability.

The key findings of this chapter have been published[159], and the paper is attached in Appendix .1.

2.2 Results

2.2.1 Proline Biosynthesis in Hypoxia

There is now a body of evidence that suggests proline metabolism is altered in response to redox challenge[127,143]. Hypoxia represents a significant challenge to redox homeostasis, therefore it was hypothesised that proline metabolism would be altered under these conditions. This was initially investigated by incubating SUM159PT cells in normoxia (21% O_2) and in two lower oxygen tensions, regarded as hypoxia (1% O_2 and 0.3% O_2). Both intracellular and extracellular proline were measured via GCMS. Extracellular ion counts are first normalised to a sample of cell-free medium to establish, before normalisation in the same way. This means we can infer whether a metabolite is taken up from, or released into the medium. In the cells, proline levels were increased consistently at 1% O_2 but were lower again at the lowest oxygen tension (Figure 2.2A). There was a step-wise increase in proline in the medium with decreasing oxygen tension (Figure 2.2B). This suggests that proline biosynthesis is increased in response to hypoxia, particularly proline export into the medium at 0.3% O_2.

Stable isotope tracing was then used to determine the route of synthesis for this excess proline. Based on the observation that synthesis from glutamine was increased in IDH1 R123H cells[143], glutamine contribution to proline was investigated. SUM159PT cells were incubated in normoxia or hypoxia with [U_{13}-C]-glutamine for 24 hours, before GCMS analysis. No carbons are lost in the conversion of glutamine to proline, meaning that the m+5 isotopologue of proline is glutamine-derived. This value is normalised to an internal standard and to a measurement of protein to account for any alterations in cell number. The normalised ion count of this isotopologue was seen to increase in 1% O_2 intracellularly (Figure 2.2C). The extracellular m+5 proline was significantly increased in 0.3% (Figure 2.2D).

The protein expression of PYCR1 and PYCR1, the two isoforms which are known to catalyse the synthesis of proline from glutamine, was investigated by western blotting. No change in expression in either isoform was seen in either 1% or 0.3% O_2. Induction of HIF1α was seen in hypoxia, as expected (Figure 2.3).

These findings were investigated in 3 more cell lines: HCC1806, ONS-76 and HS5. The HCC1806 cell line is epithelial in origin, derived from an acantholytic squamous cell carcinoma. The ONS-76 cell line is derived from a paediatric medulloblastoma. The HS5 cell line is a fibroblast-like line, derived from the bone marrow stroma.

The extracellular level of proline was significantly increased in 0.3% O_2 in each of the cell lines. The extracellular m+5 proline levels were also increased with hypoxia - in the HCC1806 cells this was significant in 1% O_2 (Figure 2.3), in the ONS-76 and HS5 cells this was significant at 0.3% O_2 (Figure 2.3 B-D). The expression of PYCR1 and PYCR2 was also checked in these three cell lines and was again found to be unchanged with hypoxia, representative blots are shown in figures 2.3 E, G, and I. This was also confirmed with densitometry of n=3 blots, shown in figures 2.3 F, H, and J.

Taken together, these results suggest that proline synthesis from glutamine is indeed increased in hypoxia and that the proline produced through this reaction is released into the medium. This increase in synthesis also occurs without an increase in either PYCR1 or PYCR2.

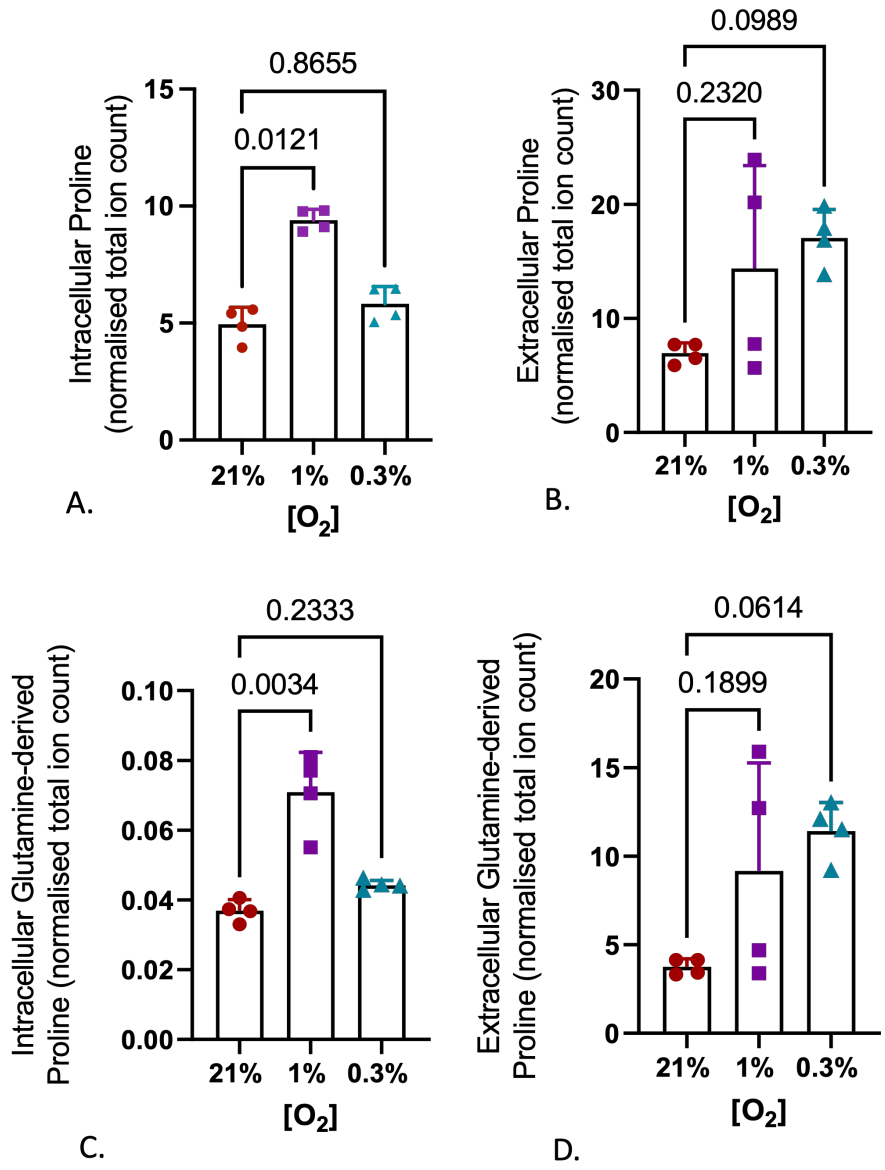

Figure 2.2: A. In SUM159PT cells, the total normalised ion count of intracellular proline is increased significantly in 1% O_2, and the levels at 21% and 0.3% are similar. B. Extracellular proline ion counts are variable at 1% O_2, and significantly increased at 0.3%. C. Using [U_{13}]C-glutamine, and measuring [U_{13}]C-proline, shows glutamine-derived proline is increased intracellularly at 1% O_2, and remains the same at 0.3%. D. Total glutamine-derived extracellular proline is again, variable at 1% O_2, and significantly increased at 0.3%. (n=4 technical replicates, representative of n=3 biological replicates)

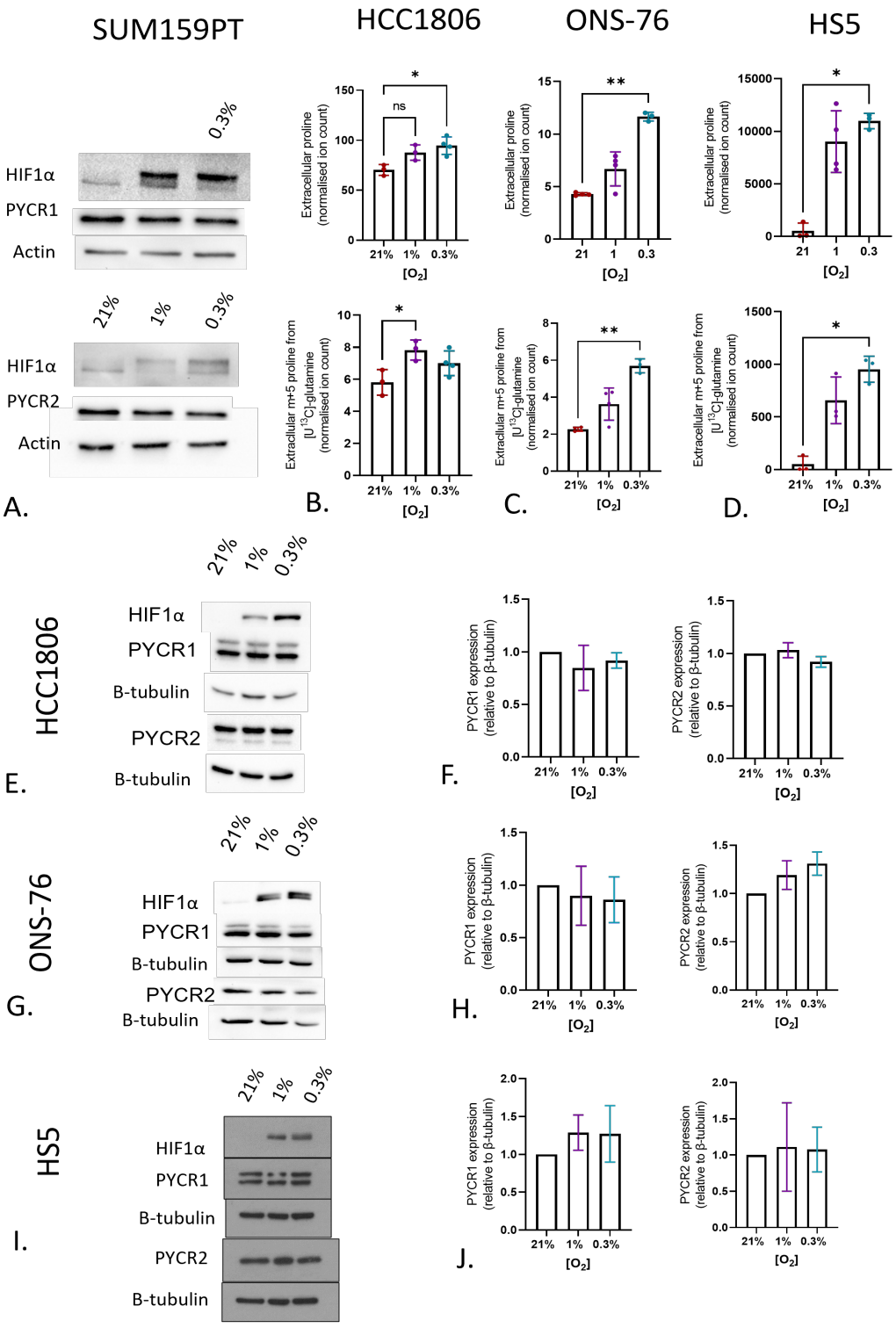

Figure 2.3: A. Western blot of PYCR1 and PYCR2 in 21%, 1% ad 0.3% oxygen in the SUM159PT cell line, levels of the 2 isoforms remain consistent B-D. Extracellular proline ion count and total extracellular glutamine-derived proline ion counts are increased with hypoxia in the HCC1806, ONS-76, and HS5 cell lines.

Figure 2.3: (n=3-4 technical replicates, representative of n=3 biological replicates) E-J. Western blots and associated quantification of PYCR1 and PYCR2 in 21%, 1%, and 0.3% oxygen show no significant alteration in expression. (n=3)

2.2.2 Proline Biosynthesis in Hypoxia is through PYCR1 activity

Proline can be synthesised from glutamine by PYCR1 and PYCR2. Although no changes were seen in the expression of either of these isoforms, changes in flux through a pathway can occur independently of protein expression changes[160]. siRNA-mediated knockdown of these isoforms was used to investigate which contributed to the observed hypoxia-induced increase in glutamine-derived proline synthesis. Knockdown of PYCR1 significantly decreased the intracellular glutamine-derived proline levels (Figure 2.4A), and the increase in glutamine-derived proline in hypoxia was lost (Figure 2.4B). PYCR2 knockdown did not show a similar effect, and intracellularly, even seemed to increase the level of glutamine-derived proline at 1% O_2 (Figure 2.4A and B). The knockdown was confirmed by western blotting, with densitometry of n=3 blots and a representative blot shown in figure 2.4 C. This also shows that knockdown of either isoform does not induce any compensatory increase in the other. It also confirms the specificity of the siRNA construct, which is particularly important given the significant sequence similarity.

The results of the siRNA-mediated knockdown experiments were recapitulated in a SUM159PT PYCR1 knockout (KO) cell line, previously described in[134]. In the PYCR1 KO cells, proline synthesis from glutamine was significantly reduced, and the previously described hypoxic response was lost (Figure 2.4D and E). The loss of PYCR1 in this model was confirmed by western blotting, as well as confirmation that PYCR2 expression remained consistent between the non targeting (NT) and PYCR1 KO (Figure 2.4).

This suggests that PYCR1 mediates the increase in proline synthesis from glutamine. It also seems the proline produced through this activity is in excess of cellular demand, as the increase (which is lost with PYCR1 loss) is seen most consistently in the medium.

Briefly, this similarity of sequence and structure was explored using BLAST alignment tool and PyMol software to overlay the structure of the two isoforms. This reveals that the amino acids which differ between the isoforms are not located in substrate binding regions. Overlay of the structure shows striking similarity, with the differing amino acids dispersed throughout the structure, this returns a root means squared deviation of 0.846Å (Figure

2.5).

Additionally, the tissue expression of both of the isozymes was investigated, using publicly available relative RNA tissue expression data from the Human Protein Atlas (Figure 2.5D and E). PYCR1 RNA expression is highest in the salivary glands and stomach, with relative expression levels approximately twice that of the next highest level. Relative expression of PYCR1 RNA is lowest in haematological tissues, namely: T-cells, NK-cells, monocytes, neutrophils and basophils. PYCR2 RNA expression is more consistent across tissue types, although expression was highest in naive CD4 T-cells, the adrenal glands and the spinal cord.

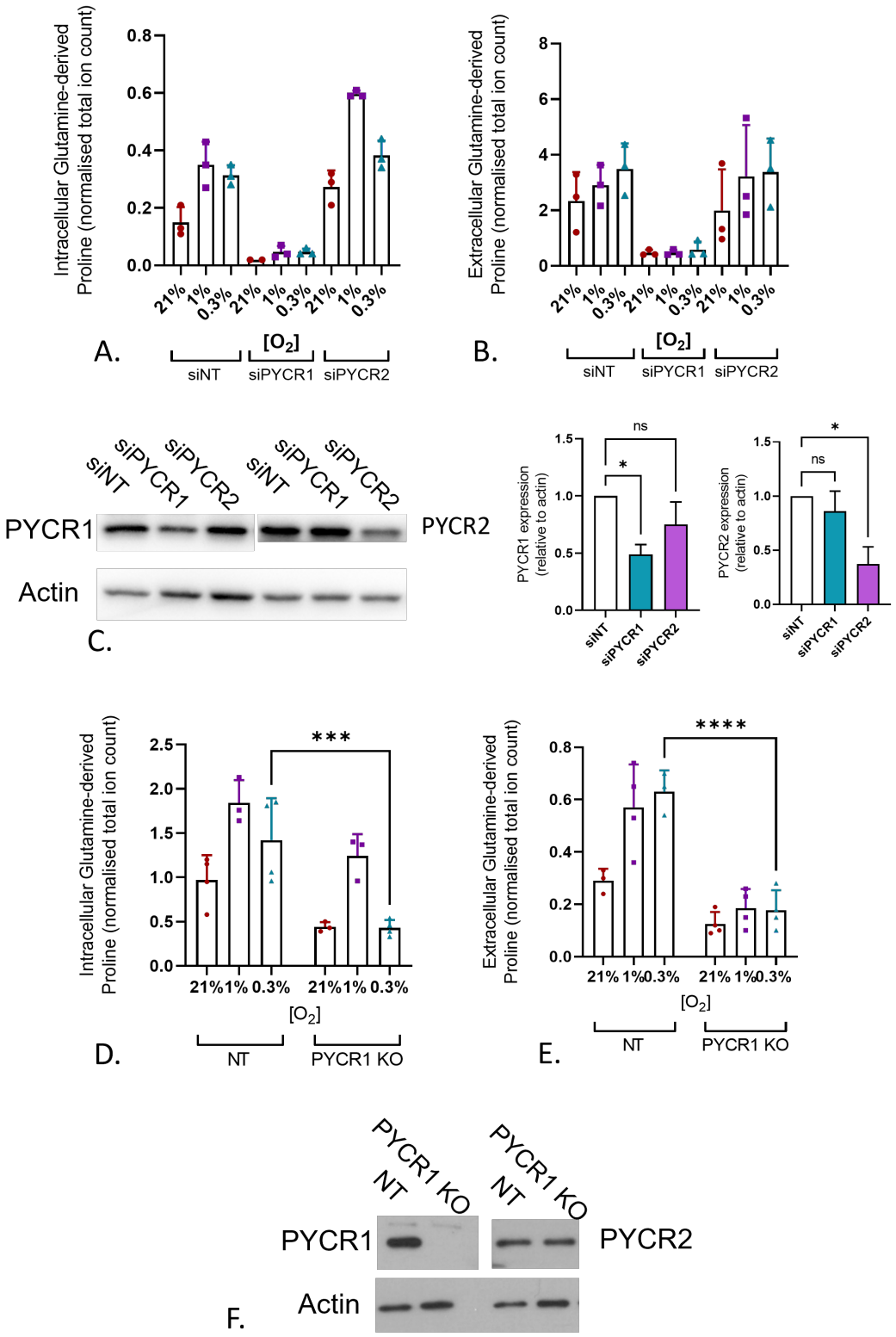

Figure 2.4: A. Intracellular glutamine-derived proline is increased in response to hypoxia in cells treated with an NT siRNA construct, and not with siPYCR1. siPYCR2 does not result in loss of glutamine-derived proline production, and this is still responsive to oxygen tension.

Figure 2.4: B. Extracellular glutamine-derived proline production shows a similar trend to intracellular levels. (n=3-4 technical replicates, representative of n=3 biological replicates) C. Western blot to show siRNA mediated knockdown of each isoform, with actin as a loading control, and densitometry of 3 blots. D. In the PYCR1 KO SUM159PT cell line, intracellular glutamine-derived proline is decreased. E. Extracellular proline is also decreased in this system. F. Western blot to show the expression of PYCR1 and PYCR2 in the NT and PYCR1 KO 159PT cell lines, with actin as a loading control.

2.2.3 PYCR1 activity is redox modulating

As previously discussed, proline metabolism is redox-linked[143,127,105]. Proline synthesis through PYCR1 uses NADH as an electron donor, regenerating NAD^+. The impact of loss of PYCR1, and therefore loss of a source of NAD^+ on the whole cell NAD^+:NADH ratio was measured in the PYCR1 KO cell line. In this model, PYCR1 loss reduces the NAD^+:NADH ratio (Figure 2.6A). A trend towards a reduction was also seen with siRNA-mediated knockdown, but this does not reach significance (Figure 2.6B). The GSH:GSSG ratio was also measured, as a surrogate for the $NADP^+$:NADPH ratio. This was unchanged between conditions (Figure 2.6D), indicating the $NADP^+$:NADPH ratio is maintained. This was again measured in the siRNA knockdown model, and was unchanged (Figure 2.6E).

A change in the ratio of NAD^+:NADH is expected to affect the conversion of pyruvate to lactate as the overall direction of the flux is determined by the cytosolic NAD^+:NADH ratio. When the NAD^+:NADH ratio is low, production of lactate is often increased[161]. This was measured in PYCR1 KO and NT cells, in normoxia and hypoxia. This showed a trend towards an increase with hypoxia, as expected, although this did not reach significance. PYCR1 loss exacerbated this effect (Figure 2.6 C).

The effect of a loss of a mitochondrial source of NADH oxidising ability, large enough to alter the whole cell redox balance, was hypothesised to affect oxidative TCA cycle activity. Stable isotope tracing was again used to investigate this. The incorporation of glutamine into glutamate was unchanged between conditions suggesting no difference in the activity of glutaminase (Figure 2.6F).

Glutamate carbons are incorporated into the TCA by conversion to α-ketoglutarate. α-ketoglutarate can then be converted to succinyl Co-A by α-ketoglutarate dehydrogenase, in a reaction which requires NAD^+. 4 carbons from glutamate are taken through into the TCA cycle in this way, termed oxidative TCA cycle activity. Alternatively, α-ketoglutarate

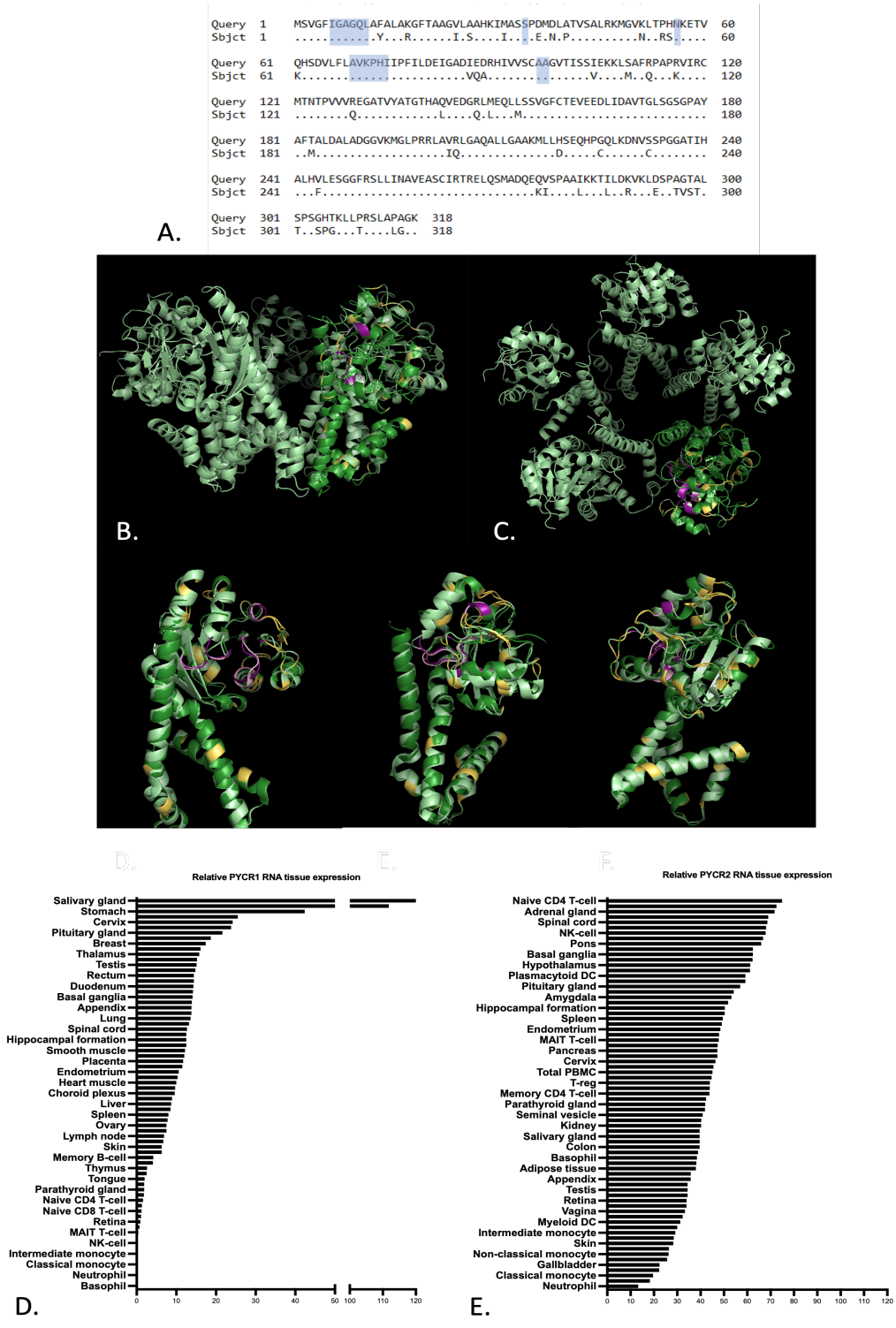

Figure 2.5: A. BLAST alignment of amino acid sequences for PYCR1 (Query) and PYCR2 (Sbjct). Highlighted areas denote binding regions, as defined by UniProt. B. Full structure of the PYCR1 complex in pale green, with PYCR2 structure in dark green overlayed on one subunit. Regions flagged as forming part of the binding site are shown in pink. Differences in amino acid sequence between PYCR1 and PYCR2 are highlighted in yellow.

Figure 2.5: C. Alignment of PYCR1 and PYCR2 structures in PyMol returns a root means squared deviation (RMSD) of 0.846 Å. D. Relative RNA tissue expression of PYCR1. E. Relative RNA tissue expression of PYCR2. Data taken from Human Protein Atlas.

can be converted to isocitrate via isocitrate dehydrogenase. This reaction takes 5 carbons from glutamine into the TCA cycle, and is the first reaction in the reductive (or reverse) TCA cycle[162].

Incorporation of glutamine carbons into succinate is almost entirely into the m+4 isotopologue, and is reduced in response to hypoxia, and with PYCR1 KO (Figure 2.6G). The percentage m+4 was significantly lower in 0.3% compared to 21% in the PYCR1 KO cells (Figure 2.8D). m+4 and m+3 isotopologues are seen in fumarate. A switch between the two is seen with hypoxia, with a higher percentage of m+3, and less m+4 at lower oxygen tensions. With PYCR1 loss there is more m+3 than the NT in normoxia, with reduced overall incorporation (Figure 2.6H). In malate, total incorporation of glutamine carbons is similar between conditions (Figure 2.6I). m+4 labelling is reduced with hypoxia, and is reduced even further with PYCR1 KO in all oxygen tensions (Figure 2.6I, Figure 2.8F). Aspartate shows the same trend, with the effect more pronounced (Figure 2.6J, Figure 2.8G). Total incorporation into citrate is lower in 0.3% oxygen in the NT cells. There is also a reduction in percentage labelling into m+4 (Figure 2.8H), while the m+5 incorporation is increased at 1% O_2. The PYCR1 KO cells show less incorporation into citrate in all conditions, with the majority of label being m+5, even in normoxia (Figure 2.6K). Glucose incorporation into citrate is also decreased with PYCR1 KO (Figure 2.8I).

The ratio of m+4:m+5 citrate from glutamine can be used as a read-out of the relative contribution of oxidative TCA cycle activity versus reductive carboxylation of glutamine. This is reduced with hypoxia, as previously reported[61]. PYCR1 KO appears to reduce this further, and in 0.3% O_2 this is undetectable (Figure 2.8A). The inverse ratio was increased in 1% O_2 compared 21% O_2 to the NT cells, while in 0.3% there was too little m+4 to calculate a ratio for the PYCR1 KO cells (Figure 2.8B).

Overall, these data suggest that PYCR1 loss decreases the NAD^+:NADH ratio, resulting in more reductive TCA cycle activity and less oxidative activity than the NT cells. This is the case in normoxia, and exacerbates a switch which occurs normally in hypoxia. Reduced incorporation of glutamine into citrate, and into succinate and fumarate, suggest the TCA cycle is impaired, which is likely to affect production of anabolic precursors.

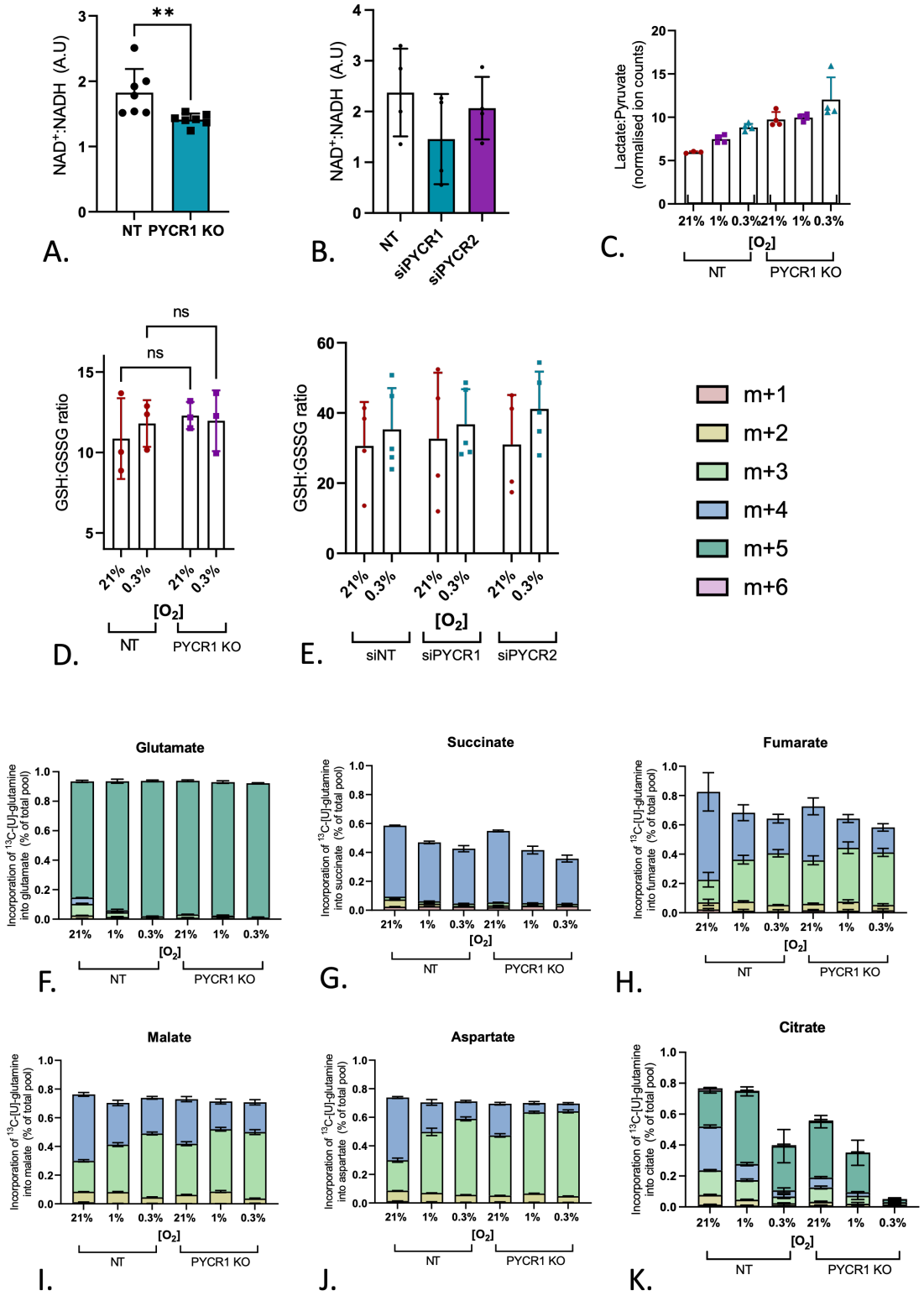

Figure 2.6: A. The whole cell NAD^+:NADH ratio is lower in the PYCR1 KO SUM159PT cells, compared to the NT cells. B. siRNA-mediated knockdown of PYCR1 nor PYCR2 significantly reduces the NAD:NADH ratio. C. The ratio of lactate to pyruvate is increased with hypoxia in both conditions.

Figure 2.6: D. The GSH:GSSG ratio is not significantly altered with PYCR1 KO. E. The GSH:GSSG ratio is not significantly altered with siRNA knockdown of PYCR1 or PYCR2. F. Incorporation of carbons from [U_{13}C]-glutamine into glutamate is not significantly altered between conditions. G. Incorporation of glutamine carbons into succinate is reduced with hypoxia. H. Incorporation of carbons from glutamine is also reduced with hypoxia, with reduction in m+4 labelling, and increase in m+3 labelling. Loss of PYCR1 induces this change in normoxia, and it is exaggerated in these cells in hypoxia. I. Total carbon incorporation into malate is not altered between conditions. The percentage incorporation into m+3 malate is increased with hypoxia, while m+4 malate is reduced. This is exaggerated with PYCR1 KO. J. Aspartate shows a similar trend to malate. K. In hypoxia, fewer carbons are incorporated into citrate, with the majority of label switching from m+5 to m+4. This is also true of the PYCR1 KO cells. In 0.3% oxygen, there is almost no label into citrate in the PYCR1 KO cells.

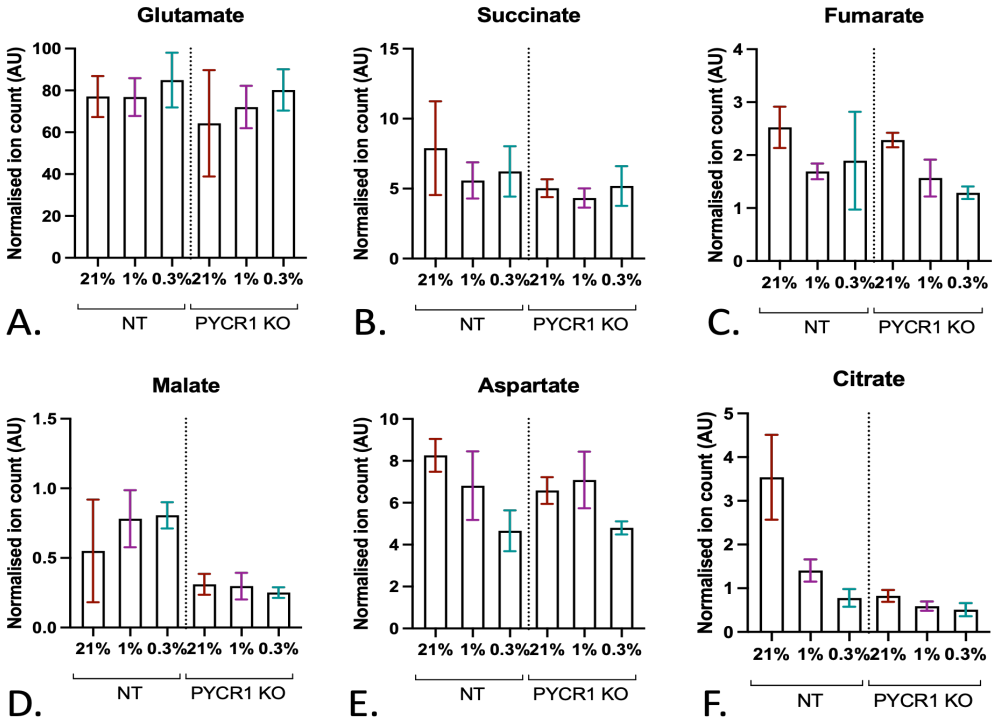

Figure 2.7: Ion counts, normalised to total protein (ug) for A. Glutamate B. Succinate C.Fumarate D. Malate E. Aspartate and F. Citrate. (n=4 biological replicates, representative of 3 technical replicates)

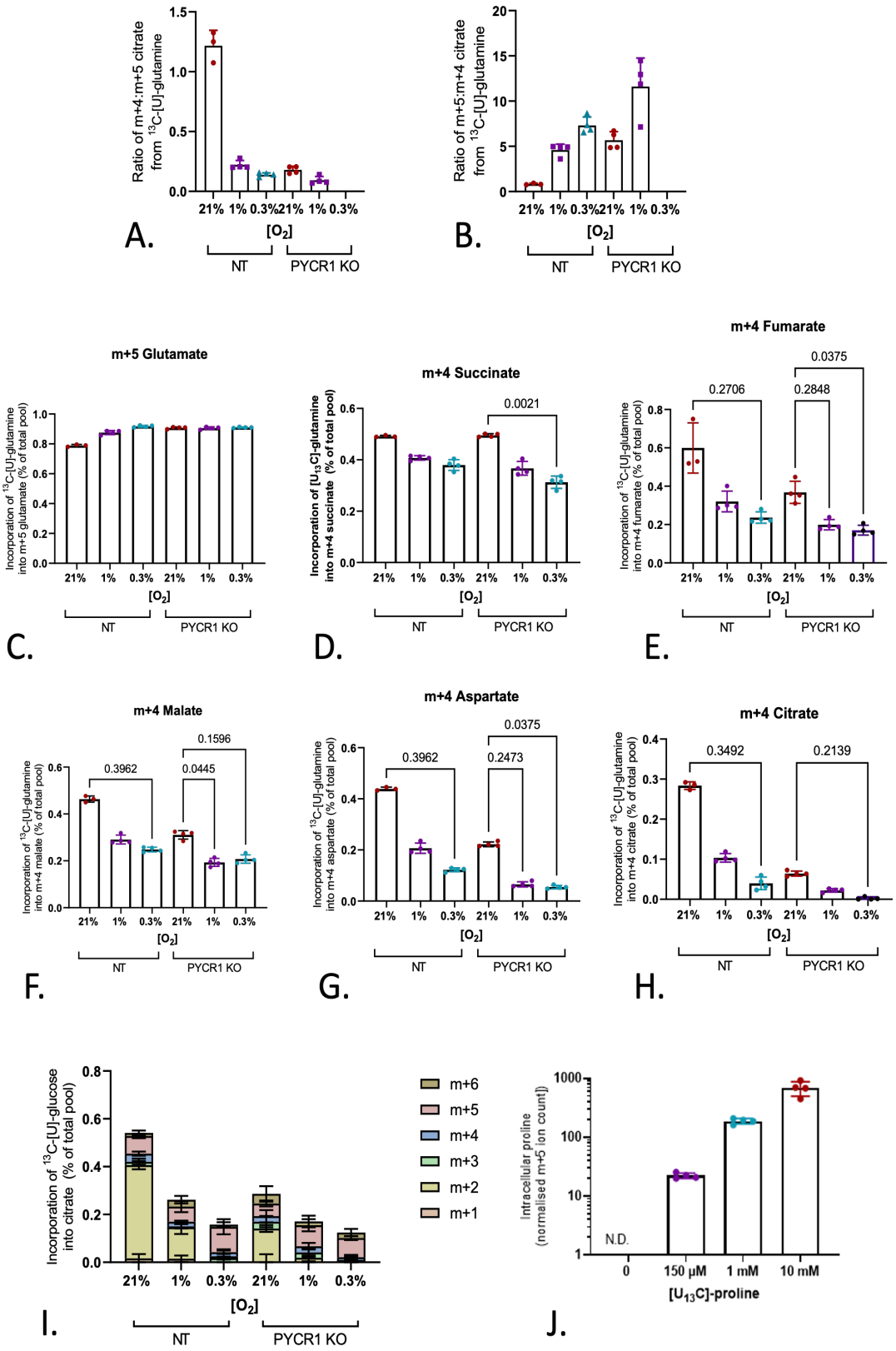

Figure 2.8: A. The ratio of m+4:m+5 citrate from [U$_{13}$C]-glutamine is reduced with decreasing oxygen tension and PYCR1 KO.

Figure 2.8: B. The ratio of m+5:m+4 citrate from [$U_{13}C$]-glutamine is increased with hypoxia and PYCR1 KO. C. Incorporation of glutamine carbons into the glutamate m+5 isotopologue is unchanged with PYCR1 loss or hypoxia. D-H. Incorporation of glutamine carbons into the m+4 isotopologues of succinate, fumarate, malate, aspartate and citrate is reduced with PYCR1 loss in normoxia, and this is compounded by hypoxia. I. The total incorporation of glucose carbons into citrate is reduced with PYCR1 loss, with the largest change seen in the m+2 isotopologue. This is compounded by hypoxia. J. The intracellular m+5 ion count of proline increases with the concentration of extracellular [$U_{13}C$]-proline.

2.2.4 Effects of PYCR1 Loss on Cell Phenotype *in vitro*

Impaired TCA cycle activity is expected to impact cell proliferation, due to reduced anabolism. Proliferation was measured in the PYCR1 KO cells, in both hypoxia and normoxia by SRB assay. This showed that the proliferative rate was reduced in both conditions, with a larger difference seen with lower oxygen tension (Figure 2.9A-C). As proline is an important proteinogenic amino acid, PYCR1 loss may affect the total cellular protein levels. A comparison was made between SRB and cell count as a method of assessing growth in this model. No significant difference was found between the growth defect seen in PYCR1 KO cells compared to NT cells using SRB or cell count, validating the use of SRB as an experimental approach (Figure 2.9 D).

SUM159PT cells are cultured in DMEM/Hams F12, which contains 150μM proline. In order to assess whether this affects the growth rate of PYCR1 KO cells, growth was assessed in proline-free conditions. The PYCR1 KO cells were still capable of proliferating, although the proliferative defect remained compared to the NT cells (Figure 2.9E). The addition of exogenous proline was unable to rescue the growth defect, in either condition (Figure 2.9A-C and E). [U-$_{13}$C]-proline was used to check the additional proline was taken up by the cells (Figure 2.8J). Labelled proline allowed specific measurement of proline imported from the medium. This shows that with increasing concentrations of supplemental proline, the intracellular proline ion count increases, validating the experimental design. This, therefore, suggests that the PYCR1 KO cells have sufficient intracellular proline, likely due to the continued activity of PYCR2 and PYCRL.

This may suggest that PYCR1 is not the main enzyme involved in proline production for proteinogenesis and that one of the other isoforms serves this function. It may also suggest that the rate of cellular proline synthesis may exceed the proline requirements of the

cell, in a manner similar to the excretion of lactate under aerobic conditions in the Warberg Effect.

As PYCR1 cells were observed to synthesise lactate, likely as a result of an imbalanced NAD^+:NADH ratio, it was hypothesised that pyruvate supplementation may rescue the growth phenotype by increasing flux through this pathway. SUM159PT cells were supplemented with 2mM sodium pyruvate. The presence of pyruvate led to a moderate increase in growth in the NT cells, whilst it doubled the growth of the PYCR1 KO cells, rescuing growth to the same level as the NT cells. In hypoxia, pyruvate did not affect the NT cells, but significantly increased the growth of PYCR1 KO cells in 0.3% O_2 (Figure 2.9F).

Additionally, as PYCR1 activity was shown to be oxygen sparing in IDH1-mutant cells[143], the effect of PYCR1 loss in SUM159PT cells on HIF1α stabilisation and oxygen consumption. HIF1α was stabilised later in PYCR1 KO cells, seen as a reduced band at 1 hour and 2 hours. At the 4 hour time point, HIF1α is stabilised to the same extent (Figure 2.9G). No difference in basal oxygen consumption was seen in normoxic conditions, as shown by measurements on intact cells by Oxygraph (experiments carried out by Cristina Escribano Gonzalez). PYCR1 KO cells show a decreased maximal respiration in response to FCCP (Figure 2.9H). Due to the alteration in HIF stabilisation, the basal oxygen consumption was also measured in hypoxia, at 1.7% and 0.3%, where no difference was observed between the NT and PYCR1 KO cells (experiments carried out by Dr Kattri-Liis Eskla) (Figure 2.9I and J).

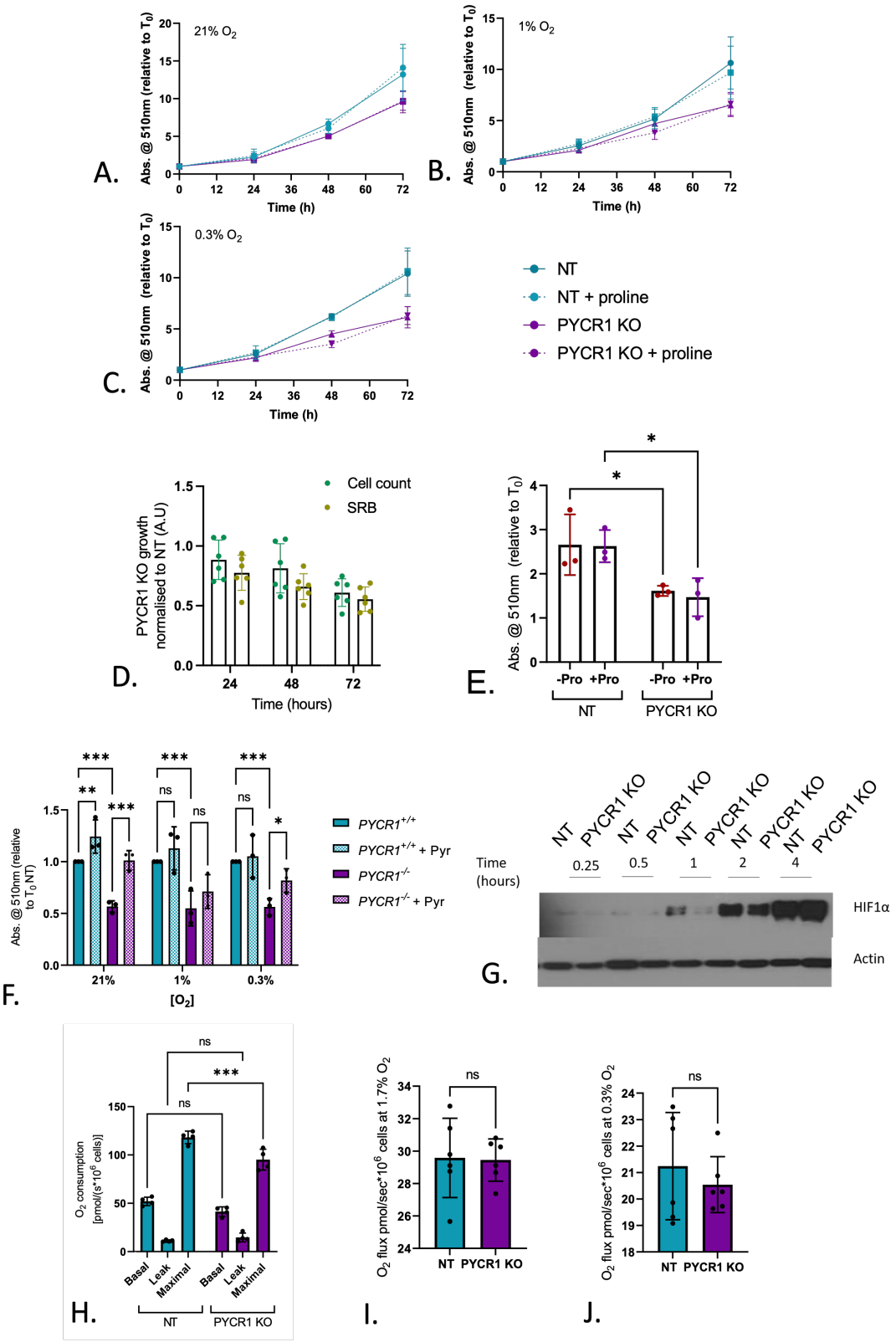

Figure 2.9: A-C. Growth, as measured by SRB assay, is reduced with PYCR1 loss, in 21%, 1% and 0.3% O_2. Supplementation with 1mM proline does not rescue this phenotype. (n=3 biological replicates presented as mean +/- SD.)

Figure 2.9: D. The growth rate of PYCR1 KO cells, compared to NT cells is reduced and the effect size is the same when growth is measured by cell count or SRB protein quantification. E. In media with no proline (DMEM flux) PYCR1 KO cells are still able to proliferate, and the growth defect remains. (n=3 biological replicates , +/- SD.) E. 2mM sodium pyruvate supplementation was able to rescue the growth of these cells, with the largest effect in normoxia. Data shown relative to NT time=0. (n=3 biological replicates, +/- SD). F. HIF1α stabilisation in the NT and PYCR1 KO cells, over a 4 hour time course. Actin as a loading control. G. Basal, leak and maximal oxygen consumption of intact NT and PYCR1 KO cells, measured by Oxygraph (n=3 biological replicates, +/- SD). H-I. Basal oxygen consumption of NT and PYCR1 KO cells in normoxia and at 0.3% oxygen. (n=6 biological replicates, +/- SD)

2.2.5 PYCR1 activity supports growth in spheroid culture

When cells are grown as spheroids (often referred to as 3D cell culture), as opposed to as a monolayer (2D), more elements of the tumour microenvironment are recapitulated. Cells form attachments to one another and to extracellular proteins, creating a 3D structure, which in turn creates diffusion gradients for both nutrients and oxygen. Cells in the centre of these structures are in a hypoxic environment, which more closely mimics hypoxic tumour regions than 2D cell culture in a hypoxia station. Due to the reduced proliferation rate of PYCR1 KO cells, the spheroid generation method required consideration. A standard way of forming spheroids involves seeding cells in agar-coated 6 well plates, and allowing the cells to clump together over 10 days. In this model, the size of PYCR1 spheroids is markedly reduced, but this may be exaggerated by the growth rate of these cells. Therefore, an alternative method was used, in which cells are seeded in U-bottom, ultra low adherence 96 well plates, followed by centrifugation. This forces the cells to form a single mass per well (Figure 2.10A), allowing the assessment of the resulting phenotype over much shorter time points[163]. The extent of hypoxia in this model was assessed by GLUT1 and pimonidazole staining (Figure 2.10B and C).

The most striking difference between NT and PYCR1 KO spheroids is the altered morphology of the PYCR1 KO, most clearly seen in the H&E staining (Figure 2.11A). This was accompanied by a stronger and more diffuse pattern of staining of CA9 (Figure 2.11B). The PYCR1 KO cells were observed to form spheroids which are less compact than then NT cells, with significant numbers of cell-free regions.

The size of the spheroids formed was similar, as expected by use of the 96 well plate

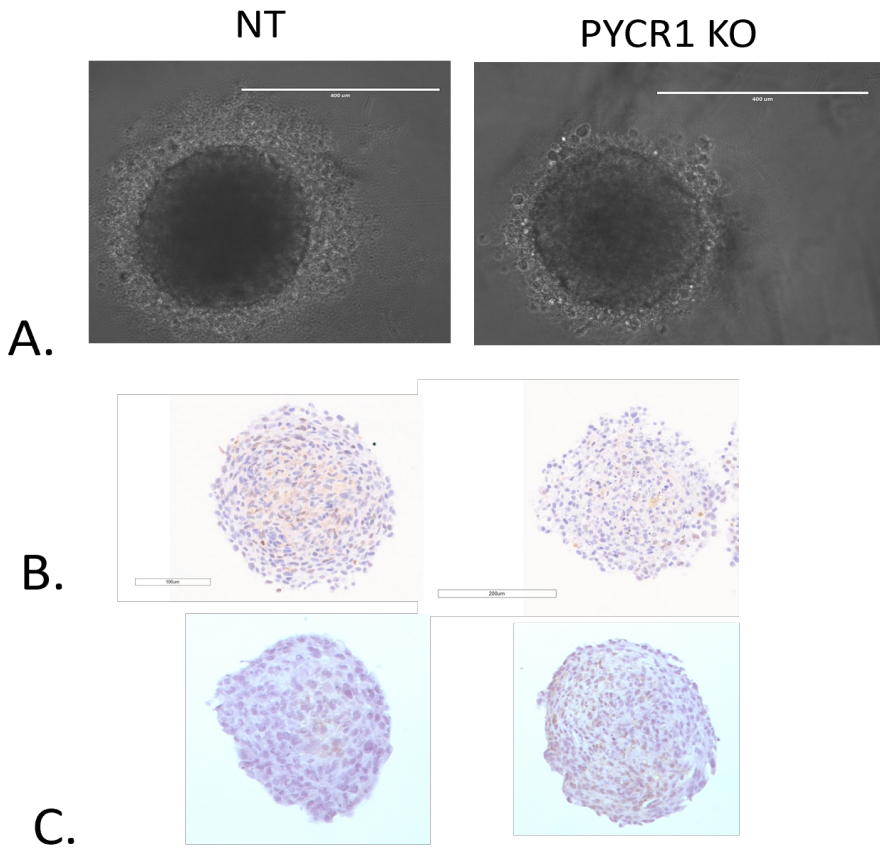

Figure 2.10: A. Representative light microscopy images of spheroids formed from NT and PYCR1 KO cells (scale bar=400μm). B. CA9 staining in NT and PYCR1 KO spheroids. C. Pimonidazole staining in NT and PYCR1 KO spheroids.

method, allowing experimental comparison at early time points. At 72 hours after spheroid formation, the PYCR1 KO spheroids were smaller than the NT(Figure 2.11C). Consistent with the data in 2D growth conditions, the addition of proline to the medium did not affect the size of spheroids, indicating that proline is not limiting with PYCR1 loss (Figure 2.11C).

The metabolism of these cells in 3D was investigated, again using stable isotope tracing. This showed the decrease in glutamine-derived proline in the PYCR1 KO cells was consistent in 3D culture (Figure 2.11D). The increased lactate:pyruvate ratio was also maintained (Figure 2.11E). Additionally, glutamine labelling into citrate was investigated, which again showed an overall decrease with PYCR1 KO and a particular loss of m+4 labelling (Figure 2.11F). The ratio of m+4:m+5 citrate was indeed reduced in the PYCR1 KO spheroids (Figure 2.11G).

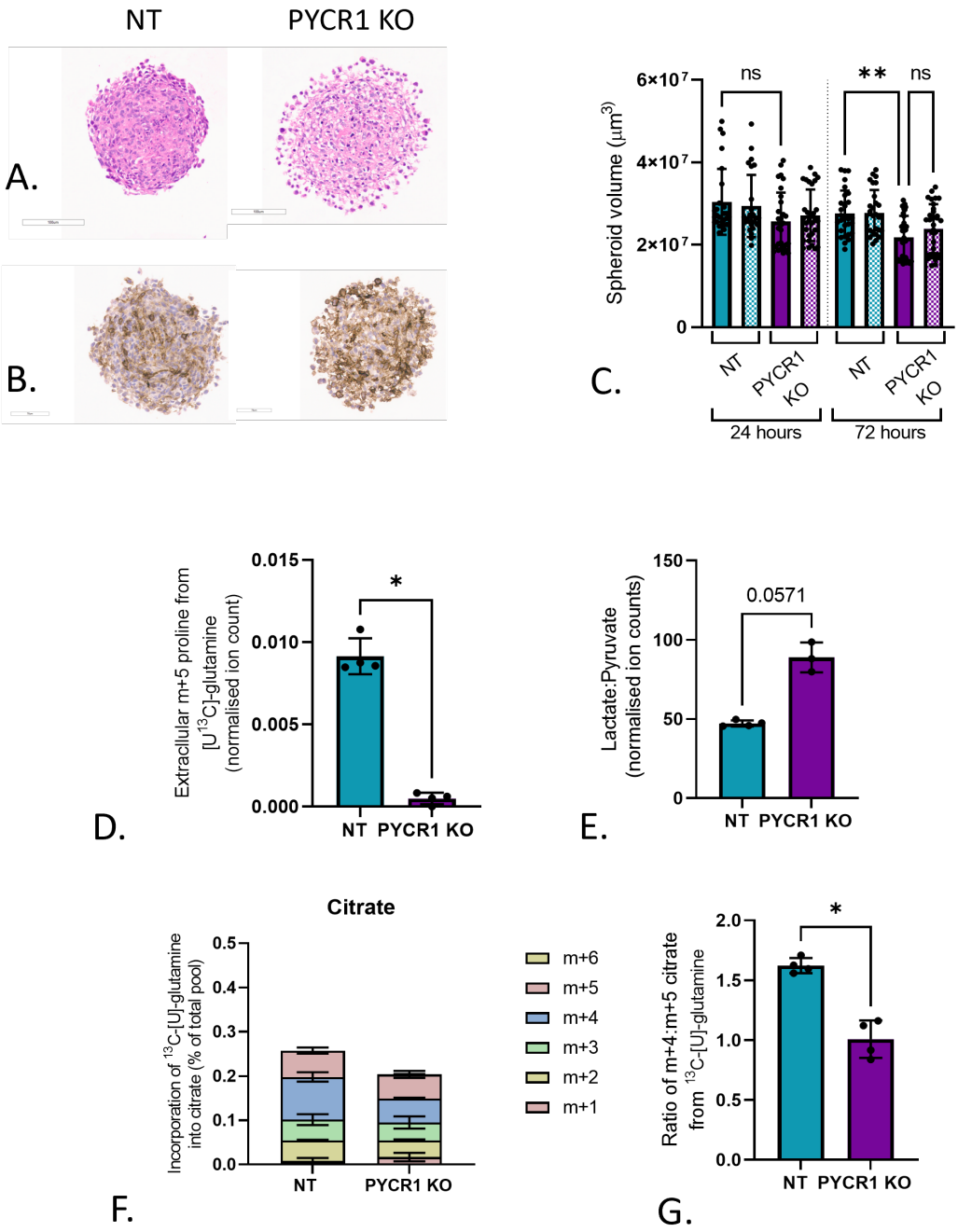

Figure 2.11: A. Haematoxylin and eosin staining of NT and PYCR1 KO spheroids shows a less dense morphology in PYCR1 KO spheroids. B. Cleaved caspase-3 staining. D. Spheroid volume (μm^3) is not significantly altered in any condition at 24 hours. At 72 hours, PYCR1 spheroids have a significantly reduced volume compared to NT spheroids. Proline supplementation does not rescue this phenotype. (n=26-40 technical repliactes, across 3 biological replicates.) E. Extracellular glutamine-derived proline is reduced in PYCR1 KO spheroids. (n=4 biological replicates) F. The ratio of lactate:pyruvate is increased in PYCR1 KO spheroids.(n=3 biological replicates) G. Incorporation of glutamine carbons into citrate is reduced in PYCR1 KO spheroids. H. The ratio of m+4:m+5 citrate is reduced in PYCR1 KO spheroids. (n=3 biological replicates)

2.2.6 *in vivo*

To to assess the effect of PYCR1 loss in a model of breast cancer *in vivo*, a doxycycline (DOX) inducible short hairpin RNA knockdown cell line model was developed. This cell model was established in the lab by Cristina Escribano Gonzalez. The inducible knockdown was validated after selection and cell sorting (Figure 2.12A). This shows a significant reduction in PYCR1 expression after DOX treatment.

All *in vivo* work was carried out by Dr Esther Bridges, in the lab of Professor Adrian Harris (University of Oxford). Mice were treated with one dose of DOX once xenografts were established. The knockdown of PYCR1 was confirmed by IHC (Figure 2.13A), using an antibody specific for the human protein (Figure 2.12B).

In this model, knockdown of PYCR1 significantly increased the expression of the hypoxia-responsive protein CA9. In response to hypoxia, angiogenic signalling is upregulated, as the cells attempt to restore the blood supply. CD31, also known as platelet endothelial cell adhesion molecule, is a marker of endothelial cells[164] and can be used to identify and quantify the vasculature[165]. This would be expected to increase in response to hypoxic signalling. However, a decrease in CD31-positive cells was seen in the PYCR1 knockdown xenografts. This could suggest that the angiogenic signalling in these cells is impaired, or that the process of angiogenesis itself is impacted. Despite this, no difference between conditions was seen in perfusion, as measured by total radiant efficiency (Figure 2.13D).

In addition to hypoxic changes in the xenografts, the effect of reduced PYCR1 expression on the tumour phenotype. Ki67 expression is seen in cells during all active phases of the cell cycle (G_1, S, G_2 and mitosis), but is not seen during G_0[166]. In response to DOX-induced knockdown of PYCR1, expression of Ki67 was decreased, suggesting a reduced number of actively proliferating cells (Figure 2.14A). There was also an increase in apoptotic cell death, as measured by staining of cleaved caspase-3 (Figure 2.14B). Caspase-3 is an executioner caspase, which in its active state is a protease involved in apoptotic pathways. Caspase-3 is itself activated by cleavage, allowing a conformational change to bring together two active sites[167]. The presence of cleaved caspase-3 is therefore indicative of a cell in which apoptosis pathways have been initiated. Furthermore, large areas of histological necrosis are visible in the H&E stained images, after induction of the PYCR1 knockdown (Figure 2.14C). Taken

together, these results suggest that as a result of loss of PYCR1, proliferation is impaired, apoptosis is increased and large scale cell death occurs.

Mice were injected with [$U_{13}C$]-glutamine, and xenografts were extracted for GCMS analysis. This shows similar incorporation of labelled carbon of 40-60% into the total pool of glutamine in both conditions (Supplementary figure 2.12C). Incorporation into glutamate was significantly increased in shPYCR1 + DOX samples, suggested increased activity of glutaminase *in vivo* (Supplementary figure 2.12D). Given this would impact the proportion of labelled carbons into proline, the ratio of m+5 glutamate to m+5 proline was calculated to account for this difference between conditions. This is lowered in the shPYCR1 + DOX samples (Supplementary figure 2.12E), suggesting the loss of PYCR1 is functional. The ratio of lactate to pyruvate was also calculated, as previous *in vitro* data showed this was increased with PYCR1 loss. However, this does not appear to be affected *in vivo* (Supplementary figure 2.12F).

A different experimental setup was also used, in which mice were chronically dosed with DOX to induce knockdown of PYCR1 over an extended period of time, to assess the effect of long-term loss of the protein. In this model, tumour volume was measured daily, until all tumours in a group reached an average of 500mm^3 and mice were culled (Figure 2.15A). At day 29, shPYCR1 dox-treated xenografts were significantly smaller than shNT and shNT treated with DOX (Figure 2.15B). Non-linear regression analysis was then used to fit data to an exponential (Malthusian) growth curve. R values, denoting goodness of fit were recorded (Figure 2.15C). From this, the k value (rate constant) for each curve was determined, from which the doubling time could be calculated (Figure 2.15D). This shows a longer doubling time for the shPYCR1 + DOX treatment group, with a 95% confidence interval which shows no overlap with the other groups.

Taken together, the *in vivo* data suggest that PYCR1 loss in xenografts causes an increase in hypoxia and hypoxia-responsive protein expression. Cell proliferation is decreased, while apoptosis is increased, leading to significant cell death, seen as large areas of tumour necrosis. Chronically, PYCR1 knockdown slows tumour growth.

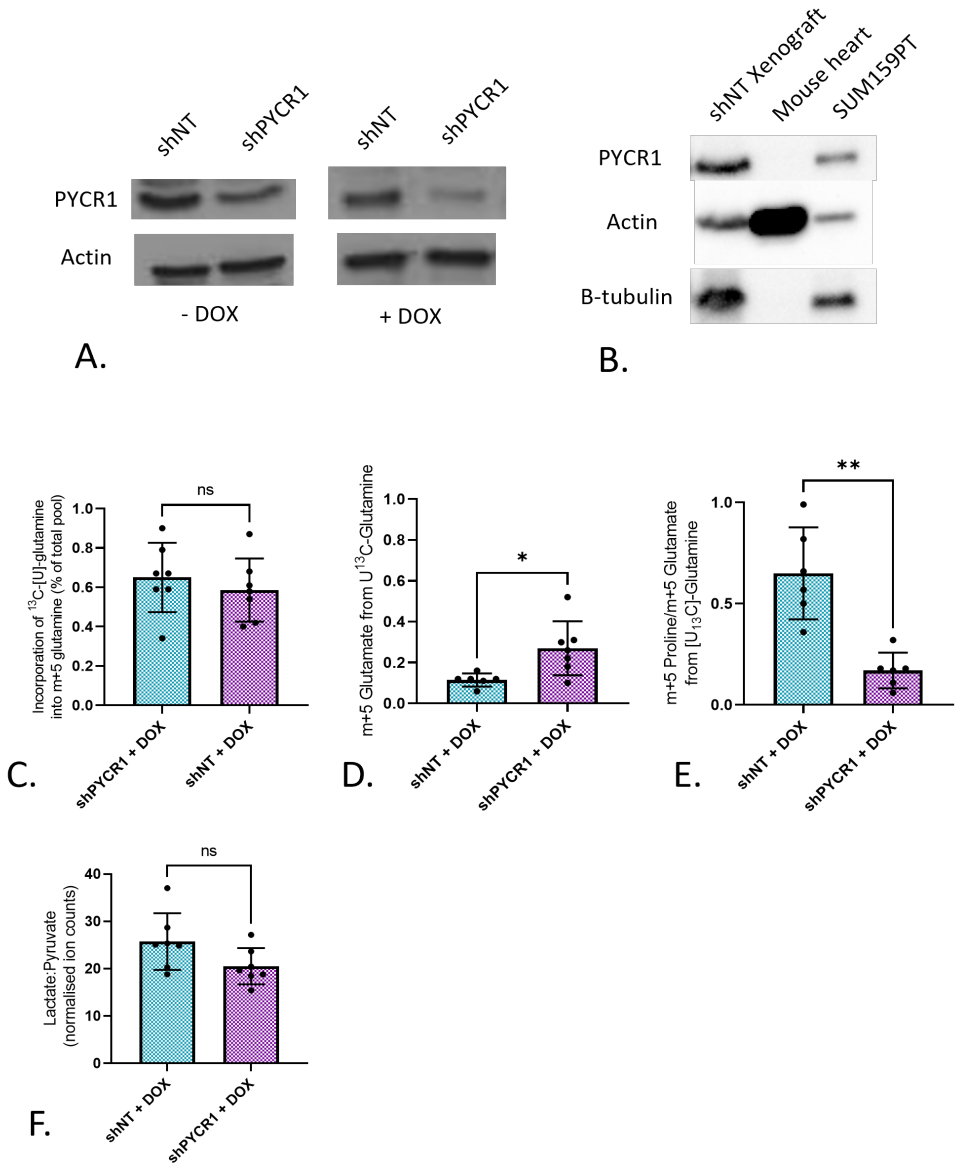

Figure 2.12: A. Western blot showing knockdown of PYCR1 when inducible shPYCR1 expressing cells are treated with DOX for 24 hours. B. Western blot showing reactivity of the PYCR1 antibody with the xenograft samples, and the SUM159PT cell line, but not with the mouse heart sample. Actin is used as a loading control which reacts with both human and mouse, while B-tubulin is a loading control which reacts only with the human protein. C. The percentage of glutamine which is fully labelled in xenografts after *in vivo* glutamine tracing is unchanged by PYCR1 loss. D. The incorporation of glutamine into m+5 glutamate is increased with PYCR1 loss in xenografts. E. The ratio of fully labelled proline to fully labelled glutamine is decreased in xenografts after PYCR1 knockdown. F. The ratio or lactate to pyruvate is not significantly different with PYCR1 knockdown in xenografts. (n=7 xenografts per conditions for all tracing data).

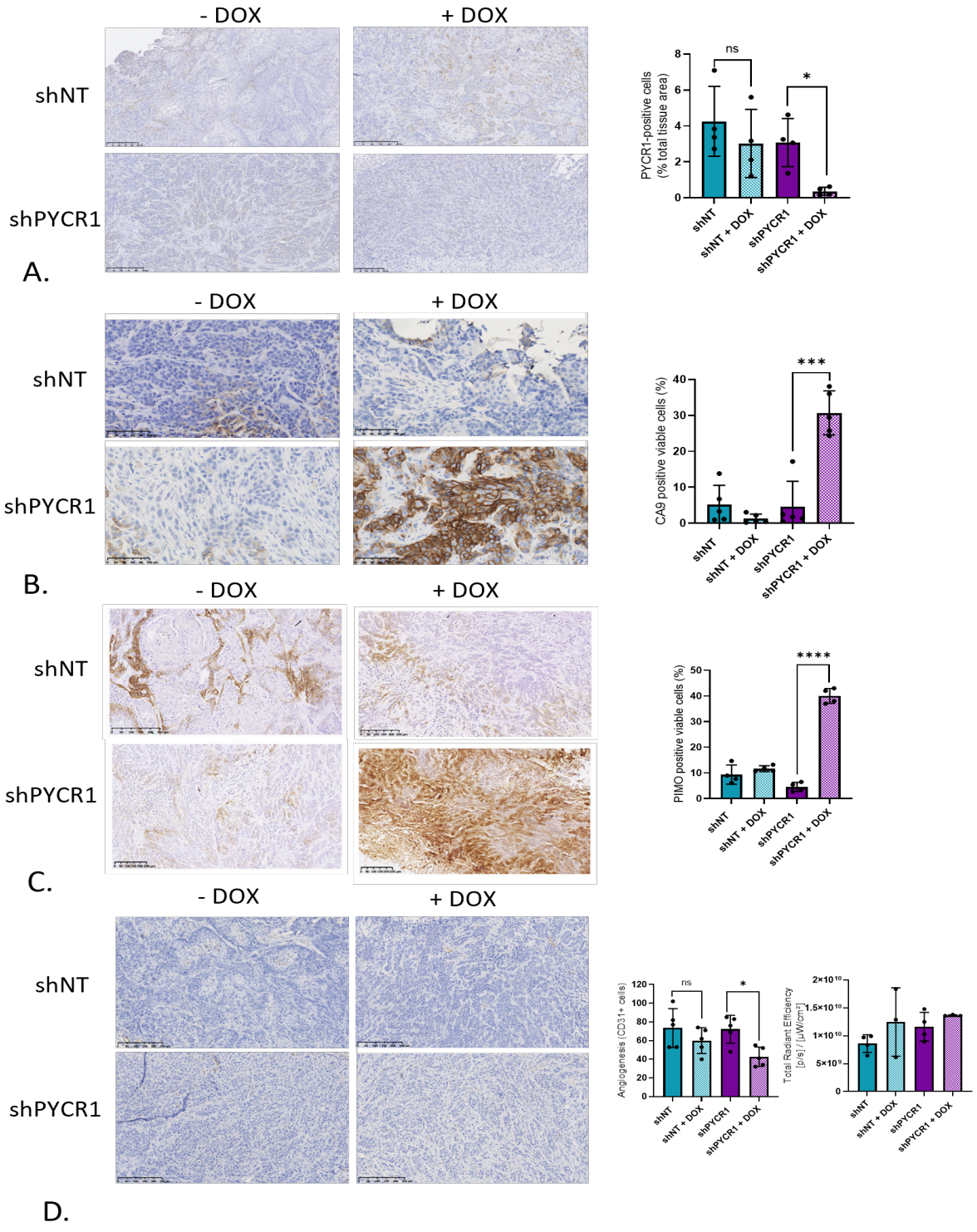

Figure 2.13: A. Representative images showing staining in xenografts, with quantification as percentage positive cells A. PYCR1 B. CA9 C. Pimonidazole D. Representative images showing CD31 staining in xenografts, with quantification of CD31+ cells and total radiant efficiency. Data presented as mean ± SD. $*$, $p < 0.05$ p; $***$, $p < 0.001$; $****$, $p< 0.000.1$. All scale bars represent 250μm. n=5 biological replicates, 3 technical for all experiments.

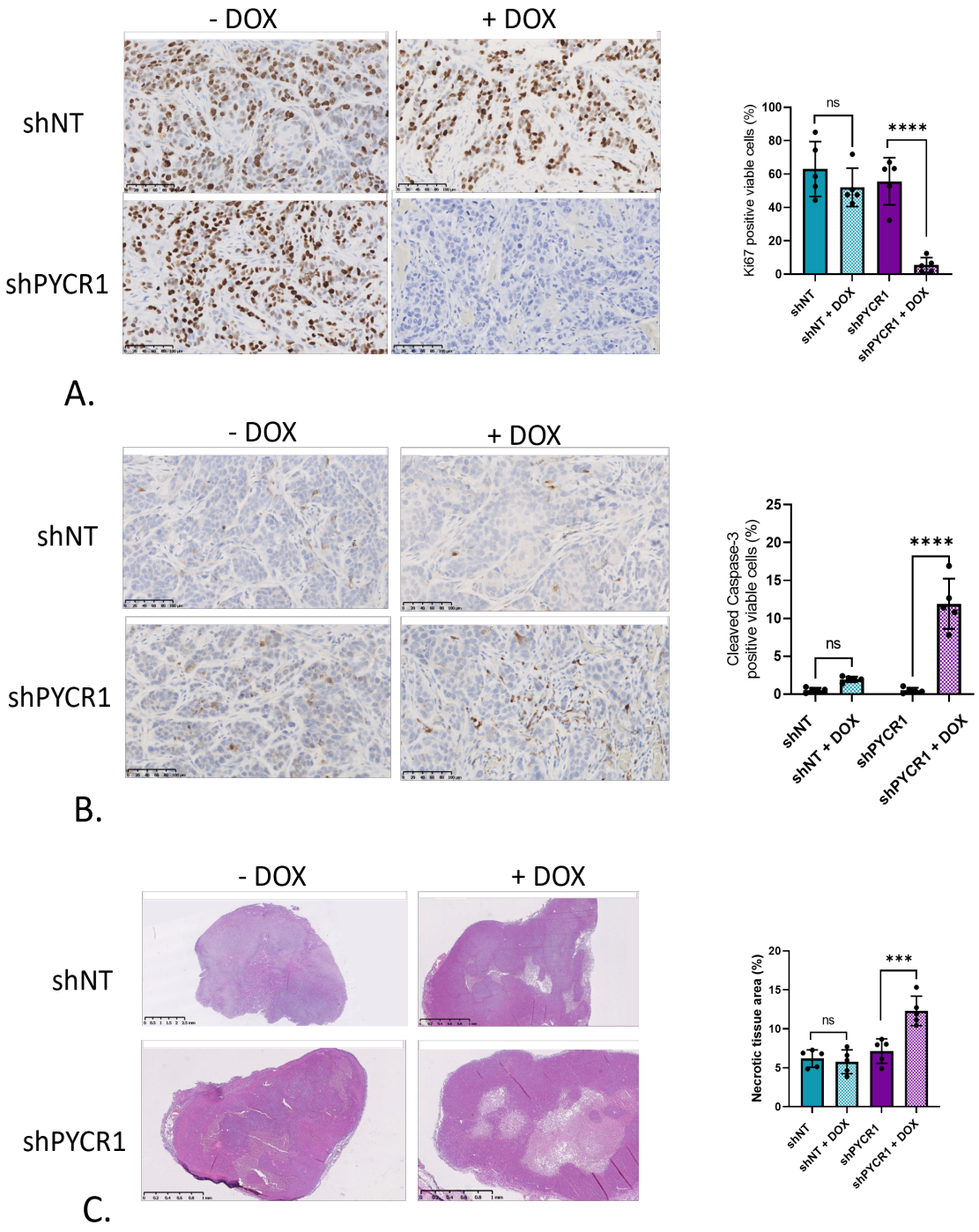

Figure 2.14: A. Representative images showing Ki67 staining in xenografts, with quantification as percentage positive cells. B. Representative images showing cleaved caspase staining in xenografts, with quantification as percentage positive cells. C. Representative images showing H&E staining in xenografts to show necrotic tissue area, with quantification as percentage necrotic area. Data presented as mean ± SD. $***$, $p < 0.001$; $****$, $p< 0.0001$. All scale bars represent 250μm. n=5 biological replicates, 3 technical for all experiments.

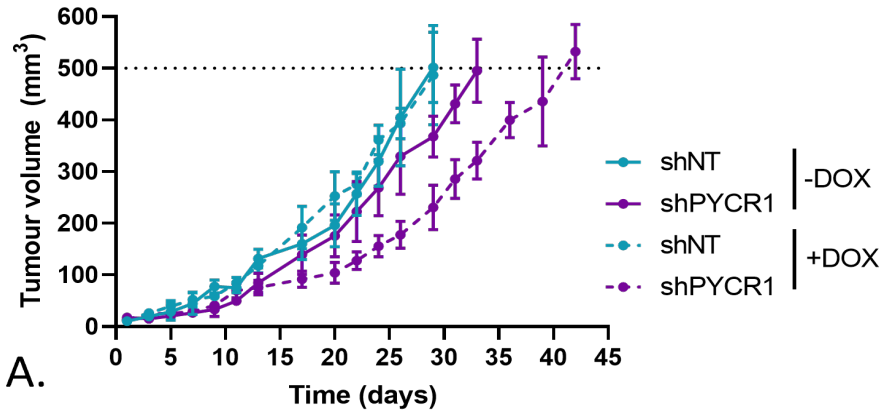

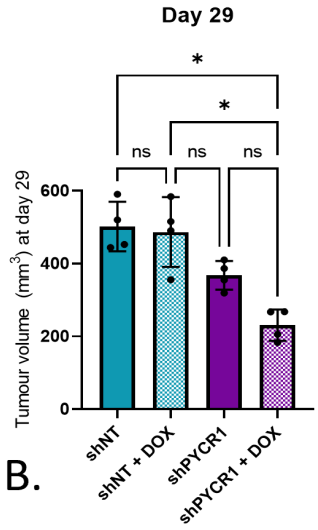

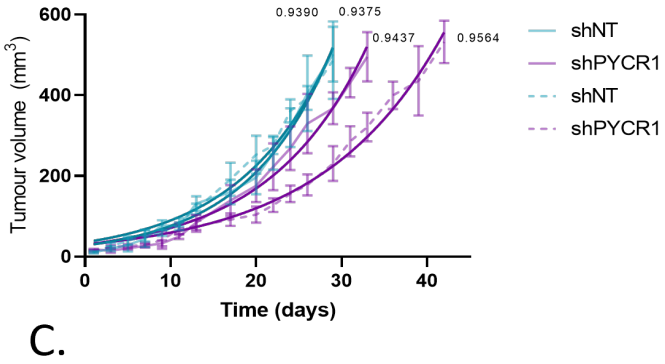

D.

	shNT	shNT + DOX	shPYCR1	shPYCR1 + DOX
k	0.1009	0.0866	0.09209	0.0672
k 95% CI	0.09144 to 0.1112	0.07909 to 0.09483	0.08413 to 0.1006	0.06532 to 0.07435
Doubling Time	6.869	7.999	7.527	9.941
Doubling Time 95% CI	6.233 to 7.580	7.310 to 8.764	6.888 to 8.239	9.323 to 10.61

Figure 2.15: A. Tumour volume over time; shPYCR1 + DOX xenografts take longer to reach 500mm^3 (endpoint) (n=7 biological replicates, presented as mean ± SD). B. Tumour volume at day 29, shows shPYCR1 + DOx xenografts are significantly smaller than shNT and shNT + DOX. (n=7 biological replicates, presented as mean ± SD) $*$, $p < 0.05$. C. Tumour volume over time fitted to an exponential (Malthusian) growth curve. R^2 values shown on curves.

Figure 2.15: (n=7 biological replicates, presented as mean ± SD) D. Table to show k values and corresponding 95% CI and doubling time with corresponding 95% CI from non-linear regression analysis.)

2.3 Discussion

Proline metabolism has been implicated in the regulation of cellular redox state under certain conditions[143,127], data presented here suggest that hypoxia is one such condition.

Increased proline synthesis in hypoxia was found to be dependent on PYCR1 (Figure 2.4A and B, figure 2.4D and E), although there was no increase in expression of this isoform seen with decreasing oxygen tension (Figure 2.3). This suggests that there is functional capacity in the normoxic expression of PYCR1 to increase flux sufficiently in response to acute challenge to mitochondrial redox homeostasis without a compensatory increase in expression. Specifically, it also confirms that this system is able to respond very rapidly to a change in redox balance and that the control of flux is likely through another mechanism, potentially through modulation of substrate availability or product inhibition.

Knockdown experiments lead to the conclusion that PYCR1 is the isozyme responsible for the majority of glutamine-derived proline (Figure 2.4). As the isozymes are so similar in sequence, some redundancy in the system might be expected, therefore the expression of both isoforms was monitored in experiments using siRNA to target each one. Accordingly, the use of a SMARTpool system was ruled out, as there was seen to be an effect on PYCR2 expression with PYCR1 knockdown. A single siRNA construct was instead used. In this model, no change in either isoform was seen with knockdown of the other (Figure 2.4C). This suggests that there is no compensatory increase in expression when one is lost. This is particularly interesting given the proportion of glutamine-derived proline production which is lost with PYCR1 knockdown. PYCR1 KO cells also show PYCR2 expression which is comparable to the NT cells. These cells are capable of proliferating normally in media that lacks proline, suggesting that these cells do not need to upregulate PYCR2 to compensate.

The similarity between PYCR1 and PYCR2 is especially interesting given the distinct role for PYCR1 shown in this work and that of others, and the very distinct phenotypes associated with germline mutations in each of these isozymes[124,168]. Again, a brief investigation into the structure and sequence, shows the small differences in sequence do not alter

the structures to any great extent (Figure 2.5). The different co-factor affinities between the isoforms, with PYCR1 having a higher affinity for NADH, and PYCR2 preferentially using NADPH[108] may be the reason behind the distinct functions, although the small difference in their localisation (mitochondrial inner membrane-associated versus matrix soluble) could also be a factor. The co-regulation of the three PYCR isoforms warrants further investigation. One explanation for the differing mutational phenotypes may be tissue-specific expression. PYCR2 mRNA is more highly expressed in neuronal tissues[169], while PYCR1 has not been reported to have any distinct tissue expression profile.

The proline synthesised in response to hypoxia appears to be in excess of cellular demand as seen in the export of glutamine-derived proline into the media (Figure 2.2B and D). As PYCR1 is highly product inhibited[108], proline export may be necessary to allow continued flux through this pathway. The intracellular proline levels increase at 1% oxygen but fall to normoxic levels at lower oxygen tension. Extracellular levels, on the other hand, are consistently highest at the lowest oxygen tension. This suggests that the export of proline is upregulated as the oxygen tension is lower, maybe in response to the increased proline or directly in response to hypoxia. This mechanism is likely to include the upregulation of a mitochondrial proline transporter, which as yet has not been identified. This is worthy of further investigation, as a potential therapeutic target. If increased proline export in hypoxia could be blocked, it could be hypothesised that intracellular proline would accumulate and activity of PYCR1 would decrease due to product inhibition. This may allow modulation of PYCR1 activity specifically under circumstances where proline production is in excess, such as hypoxia.

Loss of PYCR1 *in vitro* increased the synthesis and export of lactate from pyruvate, which suggests that PYCR1 activity may support the activity of mitochondrial redox shuttles. Increased lactate production suggests that the cytosolic NAD^+:NADH ratio is decreased, making the forward reaction more favourable. When PYCR1 is present, the NAD^+ availability in the mitochondria supports the reactions of the malate-aspartate shuttle. Supplying cells with additional pyruvate could rescue the phenotype by allowing more activity of this reaction, however, in hypoxia the rescue effect was blunted. It is likely that the combined effect of hypoxia and PYCR1 would require more available LDH in order to sufficiently upregulate the activity of the pathway. This could be investigated using overexpression of LDH, or expression of lbNOX (Complementation of mitochondrial electron transport chain by manipulation of the NAD+/NADH ratio). However, the use of the LbNOX enzyme to

support NAD^+ regeneration in hypoxia would have confounding effects due to its consumption of oxygen.

The effect of PYCR1 loss was shown to be specific to the NAD^+/NADH pool, with no effect on the GSH:GSSG ratio which is a surrogate for the $NADP^+$:NADPH ratio. This is despite the requirement for NADPH in the generation of P5C from glutamate, which makes proline synthesis dependent on $NADP^+$ availability and renders NADK2 null cells auxotrophic for proline[125]. PYCR1 loss increased reductive TCA cycle flux, and thus the activity of IDH, which consumes NADPH. This may go some way to explaining the apparent lack of change in this ratio.

In IDHR132H cells, proline synthesis through PYCR1 was shown to partially uncouple the TCA cycle from the ETC through the oxidation of NADH. In this model, loss of PYCR1 lead to an increase in oxygen consumption[143]. This observation led to the hypothesis that PYCR1 would be important in hypoxia in the same way, allowing a higher rate of oxidative TCA cycle activity per oxygen molecule. However, in the PYCR1 KO cells, basal oxygen consumption is unchanged compared to the NT in both normoxia and hypoxia (Figure 2.6G and H). This may be explained by the fact that IDH1R132H cells are dependent on the oxidative TCA cycle, as they have an impaired ability to use the reductive pathway and are particularly sensitive to inhibition of oxidative TCA[170]. In the PYCR1 KO SUM159PT cells, when NAD^+ is lacking, reductive carboxylation of glutamine could be used to maintain proliferation, with no need to increase their oxygen consumption. IDH1R132H rely on increased ETC flux to generate NAD^+ when PYCR1 is lost. The reduced maximal respiratory capacity seen with PYCR1 KO may be a result of altered mitochondrial organisation and membrane potential, as seen in fibroblasts from patients with PYCR1 mutations[124]. It may also result from the shuttling of pyruvate into lactate, resulting in reduced incorporation into the TCA cycle which is known to decrease the maximal respiratory capacity in hypoxic cells[171]. This is likely the case in PYCR1 KO cells, where lactate synthesis is increased (Figure 2.6C), and glucose entry into the TCA cycle is reduced (as seen in labelling from glucose into citrate (Figure 2.8I)).

In a spheroid model diffusion gradients of oxygen are generated which more closely mimic the tumour microenvironment than 2D cell culture. In this model, PYCR1 loss was again associated with decreased glutamine-derived proline synthesis and export. The ratio of lactate to pyruvate was also altered to suggest a decreased NAD^+:NADH ratio, and

glutamine tracing into citrate suggests a more reductive phenotype (Figure 2.11E and F). This affects spheroid morphology; PYCR1 KO spheroids are less dense and, if left for over 72 hours, have a reduced size. This is consistent with the theory that PYCR1 activity supports growth, particularly when oxygen is limited. Other work has suggested that PYCR1 activity is important in producing proline for degradation by PRODH in this context, in order to produce ATP. This study identified a dependency on PYCR1 expression in spheroid growth, showing a 73% reduction in size, even when proline is available in the media. Notably, they also show an increase in intracellular proline content with PYCR1 knockdown, which is unexpected[130]. Whilst there is undoubted a role for PRODH in spheroid growth, it can be argued that the role of PYCR1 extends beyond the supply of proline to cycle through PRODH. Supplementation with proline was not sufficient to rescue spheroid size in this model (Figure 2.11C), even though it was supplied before spheroid formation, so uptake was not limited by diffusion gradients. Proline was also shown to be taken up in these cells (Figure 2.8J).

The *in vivo* data support the hypothesis that PYCR1 is necessary to support tumour cell growth, with reduced markers of proliferation, increased apoptosis, and necrosis (Figure 2.14). Chronic loss of this isozyme decreases the growth rate of these xenografts (Figure 2.15). A decrease in proline synthesis from glutamate is seen in PYCR1 loss. Although the NAD^+:NADH ratio could not be measured directly, the lactate to pyruvate was measured, although it trended towards a decrease with PYCR1 loss, this did not reach significance (Figure 2.12F), likely due to the influence of infiltrating PYCR1 wild-type cells. Interestingly, one of the most striking findings was the increase in hypoxia and in hypoxic signalling (Figure 2.13B and C) in the shPYCR1+DOX condition. This decreased oxygen availability does not appear to be a result of poorer vascularisation, as there is no difference in the total radiant efficiency. This increasing hypoxia, in combination with the cells reduced ability to survive under these conditions, leads to tumour cell death.

This suggests that cells in xenografts without PYCR1 consume more oxygen, despite no change in oxygen consumption seen *in vitro*. As increased CA9 staining was also seen in spheroids, it seems that PYCR1 loss increases hypoxia, most likely through increased consumption of the available oxygen when cells are in 3D or in solid tumours. Under these conditions, cells are also subject reduced nutrient availability. It may be that in 2D cell culture, cells are able to use another pathway to compensate for loss of PYCR1 activity, in order to preserve oxygen, which they are unable to use when other nutrients are limited.

In order to understand this, nutrient deprivation experiments should be carried out in 2D culture.

The suitability of PYCR1 as a therapy target is unclear from this work. Several studies have begun to explore the possibility of PYCR1 inhibition[172,173], although the likely effects on PYCR2 should be investigated, given the similarity in structure (Figure 2.5). Work presented here shows that PYCR1 loss *in vivo* can lead to tumour necrosis, but that tumour hypoxia is increased alongside this. The effect of increased hypoxia on the remaining tumour cells may lead to therapy resistance, increased invasion, and other phenotypes associated with hypoxic tumour cells. This warrants further investigation before PYCR1 can be considered a treatment target.

Overall, these data support the hypothesis that proline synthesis through PYCR1 can modulate the cellular redox balance, and that flux through this pathway is particularly important in hypoxia for this reason. The NAD^+ reduced through the activity of PYCR1 is available to support oxidative TCA cycle activity, which supports proliferation. In low oxygen conditions, where redox homeostasis is challenged and NAD^+ availability is reduced, the activity of this pathway is increased (Figure 2.16).

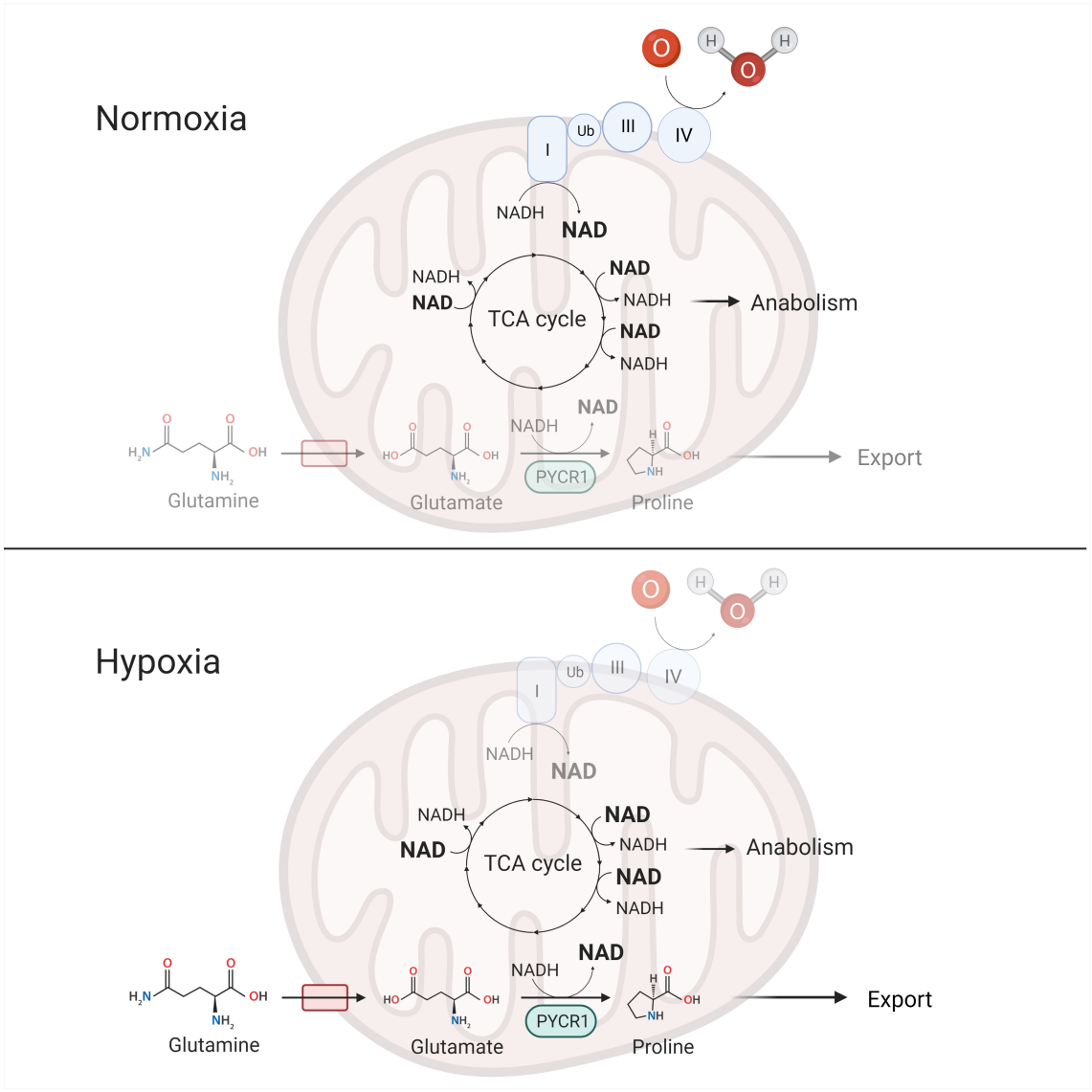

Figure 2.16: Proline synthesis through PYCR1 is increased in hypoxia to support TCA activity through oxidation of NADH. Creating using BioRender.

2.4 Materials and Methods

2.4.1 Cell Culture

For routine cell culture, flasks were maintained at 37°C in 5% CO_2 and passaged when they reached 70-80% confluency, using 0.05% Trypsin (Gibco, 15400-054). SUM159PT cells were grown in DMEM/Hams F12 (Sigma, D8062) with 5% FBS, 5μg/ml hydrocortisone (Sigma, H0888) and 5mg/ml insulin (Sigma, I6634). ONS-76 cells were also grown in DMEM Hams F-12 (Sigma, D8062) with 10% FBS. MDA-MB231 and HCC1806 cells were cultured in RPMI (Sigma-Aldrich, R8758) with 10% FBS. For hypoxia experiments plates were moved to and maintained in a Don Whitley H35 Hypoxystation. For metabolic tracing experiments, media was changed to flux (basic formulation with no glucose, glutamine or phenol read) DMEM or flux RPMI, depending on the cell line.

2.4.2 Inducible shPYCR1 cell line

HCC1806 cells were transfected with shERWOOD UltraMiR Lentiviral inducible pZip target gene set for PYCR1 (Transomic, TLHSU2300-5831) by Cristina Escribano-Gonzales. For validation, cells were treated with 1μg/ml doxycyclin for 24 hours.

2.4.3 Spheroid culture

Cells were plated in low-adherence U-bottom 96 well plates and centrifuged for 5 minutes at 500xg to form a single cell clump in each well. Spheroids were allowed to form for 48 hours before experimentation. For supplementation experiments, cells were instead seeded in DMEM flux media, as previously described, with or without 1mM proline.

For sectioning and staining, spheroids were first plated and allowed to form. For pimonidazole staining, spheroids were incubated overnight. Spheroids were collected, media removed, and washed with 1x PBS. They were then fixed overnight in neutral buffered formalin, and transferred to 70% ethanol for storage. These prepared spheroids were then sent for sectioning and staining, carried out by Colin Nixon, at the Beatson Institute in

Glasgow.

Here, spheroids were transferred to biopsy paper (CellPath, UK), before processing. Staining was performed on 4μm paraffin-embedded sections. H&E staining was carried out using a Leica ST5020 autostainer, while all antibodies were stained on a Leica Bond Rx autostainer. Sections were first loaded and underwent dewaxing (Leica, AR9222) and epitope retrieval at 95°C for 20 minutes. Sections were then rinsed with wash buffer, before antibody incubation for 30 minutes, before another wash step and incubation with the appropriate secondary antibodies for 30 minutes. This was followed by a final wash step and visualisation using DAB with the Intense R kit. Counterstaining with haematoxylin was carried out before coverslipping with DPX mountant (CellPath, SEA-1300-00A). Slides were imaged with a Leica Aperio AT2 slide scanner.

2.4.4 Western Blotting

Cells were plated to be 70-80% confluent for protein collection. After media removal and washing with PBS (phosphate buffered saline), cells were scraped into Laemmli buffer with a rubber scraper. Samples were boiled at 100°C for 10 minutes, then briefly centrifuged and vortexed. Proteins were separated by running samples through a 10 or a 12% SDS (sodium dodecyl sulfate)-polyacrylamide gel, depending on the target protein, at 120V for 1 hour. The protein was then transferred to a nitrocellulose membrane using an iBlot 2 dry transfer system (Thermo Fisher). After blocking in 5% milk for 1 hour, the membrane was incubated in the primary antibody overnight. The membrane was briefly washed with PBS-T (PBS with 0.1% Tween), then incubated with the secondary antibody at room temperature (RT) for 1 hour. Details of antibodies used are included in Table 2.1. After another washing step, ECL Western Blotting substrate was added to the membrane for imaging using a BioRad ChemiDoc imaging system.

2.4.5 Oxygen Consumption Measurements

Oxygen consumption measurements in normoxia were carried out by Cristina Escribano-Gonzales. Measurements were carried out in an Oxygraph-2k (Oroboros instruments) chamber. Basal respiration was recorded, followed by addition of oligomycin (2.5μM). Uncoupled

ETC activity was measured by stepwise titration of carbonyl cyanide 4-(trifluoromethoxy)phenylhydrazo (FCCP). Respiration was then inhibited by addition of antimysin A (2.5μM) and rotenone (0.5μM). Oxygen consumption measurements in hypoxia were carried out by Kattris-Liis Eskla (University of Tartu). Cells were plated on 100mm dishes on a sterile glass disc (Pilkington Microwhite) 24 hours before experimentation. Media was removed and discs washed with 1x PBS before being placed in the respiration chamber. 0.5ml medium was added on top of the cells. Oxygen consumption was recorded at each oxygen tension for 25 minutes or until recordings stabilised. Values were normalised to cell number.

2.4.6 Sulforhodamine B assay

100μl 20% trichloracetic acid was added to the medium and incubated at 4°C for 30 minutes. This was then removed and wells were washed 3 x with tap water and left to dry. Once dry, wells were covered with 0.4% sulforhodamine B (Sigma, 230162) and incubated at 10°C at RT. This was removed and wells were washed with 1% acetic acid and wells were allowed to dry again. The stain was dissolved using 50mM pH8.8 Tris, and samples were transferred to a 96 well plate, to be read on a platereader at 510nm.

2.4.7 GSH:GSSG

Cells were plated for transfection in 6 well plates. siRNA was used at 50nM, using Dharmafect 1 (Dharmacon, T-2001-03). Contructs and sequences are detailed in Table 2.2. 24 hours after transfection, cells were trypsinised and transferred to clear bottom, white 96 well plates (Corning, 3903), and moved to hypoxia as required. After 24 hours the Promega GSH:GSSG Glo assay kit (Promega, V6612) was used according to the manufacturer's protocol.

2.4.8 NAD^+:NADH assay

Transfection was carried out as detailed above. Cells were plated in 6 well plates to be 70% confluent, assay was carried out according to the manufacturers protocol (Biovision kit K337).

2.4.9 Metabolite Extraction for GCMS

Cells were plated 24 hours prior to the addition of tracing medium, to be 80% confluent at the time of extraction. Plating medium was removed and wells washed with sterile PBS. DMEM or RPMI (depending on the cell line) with no glucose, no glutamine or phenol red was used as a base medium. To this, 5 or 10% (again, depending on the cell line) dialysed FBS was added, with 10mM glucose and 2mM glutamine, using fully heavy isotope labelled where required. Branched chain amino acids were also added to RPMI: (CONC) leucine, (CONC) isoleucine and (CONC) valine.

Metabolite extraction was carried out on ice throughout. Media was removed before washing twice with 0.9% saline. 500μl pre-chilled methanol was added, with 200μl pentanedioic-d6 acid (CDN isotopes, D-5227) in LCMS grade water. This was scraped and collected, before addition of 500μl pre-cooled chloroform. Tubes were vortexed for 10 seconds and centrifuged at 13,000 rpm for 10 minutes. The top (polar) layer was transferred to a fresh tube and dried in a vacuum centrifuge.

Spheroids were established in normal growth medium, before collection, washing and transfer to flux medium with [U_{13}C]-glutamine in agarose-coated 12 well plates, and incubated for 48 hours. These were collected again, washed with ice cold saline, transferred to MeOH and homogenised (2 x 30 seconds) with a Precellys 24 tissue homogeniser (Bertin Instuments). Extraction was performed from this point forwards in the same way as the cell samples. Data were normalised to total ion count.

Samples were derivitised by reconstitution in 40μl 2% methoxamine in pyridine, followed by vortexing and heating at 60°C for 1 hour, addition of 50μl N-tert-Butyldimethylsilyl-N-methyltrifluoroacetamide with 1% tert-Butyldimethylchlorosilane, and another hour at 60°C. 80μl of each sample was then transferred to glass GCMC vials.

2.4.10 Gas Chromatography Mass Spectroscopy

1μl of sample was injected in splitless mode, using helium as a carrier gas at a rate of 1ml/minute. The GC oven temperature was 100°C for 1 minute, before ramping to 160°C at 10°C/minute, then to 200°C at 5°C/minute and finally to 320 °C at 10°C/minute and a

5 minute hold. Detection was carried out in scan mode. D^6-Glutaric acid was used as an internal standard. Data was analysed using a MatLab script, kindly shared by the Fendt Lab.

2.4.11 *in vivo* work

All mouse work and associated immunohistochemistry was carried out by Dr Esther Bridges, in the lab of Professor Adrian Harris at the Weatherall Institute of Molecular Medicine in Oxford. According to UK Animal law (Scientific Procedures Act 1986), with local ethics and Home Office approval.

Xenografts were induced by injection of 100μl matrigel containing 2 x 10^6 DOX-inducible shNT or shPYCR1 HCC1806 cell into the mammary fat pad of 5-6 week old CD1 nude female mice. For single dose experiments, DOX was administered when tumours reached an average of 50mm^3. At this point, mice were given 25mg/kg DOX by oral gavage. Adverse effects on animal welfare were seen in the shPYCR1 group, with 1 mortality. The other animals in the group showed significantly reduced mobility and decreased body temperature. Mice were culled the day after dosing. Xenografts were resected and processed for both flash freezing and fixation. For chronic dosing, DOX was administered once tumours reached an average of 75mm^3, and given every two days at 10mg/kg. No adverse effects on welfare were observed. When tumours reached a size of 500mm^3, mice were injected with [U_{13}C]-glutamine (3 x 200μl 36.3mg/ml stock solution at 15 minute intervals), 45 minutes before cull. Pimonidazole (2 mg/kg) and a 647-Tomato lectin (1 mg/kg) and Hoescht (2 mg/kg) mixture was administered intravenously 5 minutes before visualisation on IVIS system for imaging of tumour perfusion. Blood samples were also collected by cardiac puncture when mice were culled.

2.4.12 Immunohistochemistry

Slides were dewaxed in histoclear, and rehydrated. H&E staining was carried out according to a standard protocol. Antigen retrieval was performed in pH 6 and staining was carried out using the FLEX staining protocol (Agilent). Peroxidase activity was blocked before the addition of primary antibodies and incubation for 2 hours at RT. Slides were then washed

with Flex buffer, before incubation with Flex secondary antibodies for 30 minutes at RT and another washing step. Sections were then incubated in diaminobenzidine (Flex-DAB) for 10 minutes and counterstained with Flex-hematoxylin for 5 minutes before mounting with mounting medium (Sigma). The Visiopharm Integrator system was used to quantify the expression of markers and necrotic area. HDAB-DAB colour deconvolution band was used to detect positive cells. Thresholds were set by checking against control xenografts. Quantification was based on: intensity of staining (calculated from DAB pixilation, corresponding to stain intensity) and percentage of coverage (calculated from DAB positive total area relative to the total area of tissue).

2.4.13 Data analysis

Data from GCMS experiments were analysed using Agilent Mass Hunter software, to check data quality. Files were then converted to .CDF format and analysed using in-house MATLAB scripts for integration and natural abundance corrections. Graphs were plotted and statistical analysis was carried out with GraphPad Prism 9. Non-parametric tests were used throughout, Mann-Whitney tests were used for 2-way analysis, while Kruskal-Wallis tests with Dunn's multiple comparison post hoc tests were used where there were more than 2 conditions. Sample numbers and statistical significance is shown in figure legends.

Target Protein	Molecular Weight	Host	Dilution	Catalogue number
Actin	52kDa	Mouse	1:5000	Sigma A4700
HIF1α	120kDa	Mouse	1:500	BD Biosciences 610959
PYCR1	30kD	Rabbit	1:2000	Proteintech 13108-1-AP
PYCR2	34kD	Rabbit	1:2000	Proteintech 17146-1-AP
Anti-Mouse-HRP	N/A	Goat	1:5000	Cell Signalling 7076S
Anti-Rabbit-HRP	N/A	Goat	1:5000	Cell Signalling 7074S
Carbonic Anhydrase IX	N/A	Mouse	1:500	Absolute Antibody M75
Ki67	N/A	Mouse	1:1000	Agilent M7240
PYCR1 (Mouse)	30kDa	Rabbit	1:1000	Cell Signalling 37635
CD31	N/A	Mouse	1:250	Agilent M082301/2
GLUT1	N/A	Rabbit	1:500	Abcam ab652

Table 2.1: Antibody Information

Target Protein	Catalogue number
PYCR1 siRNA	Dharmacon J-012349-06-0005
PYCR2 siRNA	Dharmacon J-016646-06-0005
Non-targeting siRNA	Dharmacon D-001810-10-05
PYCR1 inducible shRNA	Transomic TLHSU2300-5831

Table 2.2: Oligonucleotide Information

Chapter Three

PYCR1 in Multiplex Image Analysis of Breast Cancer Needle Biopsy Samples

3.1 Introduction

Proline biosynthesis has been linked to multiple aspects of cancer cell biology[112,110]. The expression of PYCR1, in particular has been linked to a poorer prognosis in multiple cancer types, including lung adenocarcinoma[140], hepatocellular carcinoma[174], gastric cancer[142] and colorectal cancer[136]. Recently, a role for proline synthesis through PYCR1 in regulation of cellular redox homeostasis has been proposed, in several models[143,127]. Cancer cells experience challenges to their redox balance due to many factors, including a sustained high proliferative rate, signalling pathway activation, and environmental stresses. One such stress is hypoxia, which occurs frequently in solid tumours, due to the rapid proliferation of cells and inadequate blood supply. The effect of hypoxia on cellular metabolism is profound, and involves a substantial decrease in the NAD^+:NADH ratio[61].

Data outlined in Chapter 1 suggest that under these circumstances, PYCR1 activity may regenerate the NAD^+ pool, thereby allowing continued oxidative activity of the TCA cycle and supporting cell survival. This increased PYCR1 activity produces proline, the majority of which appears to be exported into the medium. *In vivo*, loss of PYCR1 lead to cell death, associated with an increase in both pimonidazole and CA9 staining. This suggests that PYCR1 loss leads to an increase in tumour hypoxia, and hypoxic cell death.

In light of this, the relationship between PYCR1 expression and hypoxia was investi-

gated in human triple negative breast cancer samples. Breast tumours have been shown to have a high level of variation in the extent of hypoxia between patients[175]. It was hoped that this variation would lead to a diverse sample set in terms of expression of hypoxic markers.

Further to this, the proline which is generated through PYCR1 in hypoxia appears to be in excess of the cellular needs as it is exported into the cell culture medium. *In vivo*, this increased extracellular proline is likely to influence the tumour microenvironment. Collagen deposition is an important factor in breast tumour development, making this tumour type a good model to investigate the potential effects of exported proline.

3.1.1 Samples

Samples were kindly given to us by Dr Abeer Shabaam at the Queen Elizabeth Hospital Birmingham. Slides were collected over a number of years from a large cohort of patients with triple negative breast cancer. The samples are core needle biopsies: small, cylindrical sections taken from the breast using a needle. One or more cores are taken and mounted on slides for analysis by a pathologist, and used for diagnosis of a new primary breast tumour.

These slides were stained with antibodies for PYCR1, CA9 and collagen, along with DAPI.

3.1.2 Collagen

Collagens are the most abundant protein in the extracellular matrix (ECM) and are the main contributor to the structure[176]. Collagen plays a central role in the remodelling of the ECM which occurs during tumour progression. In breast cancer, in particular, an association between tissue density and cancer risk is well established. As a breast tumour develops, collagen thickens and stiffens, which assists cell migration, thereby promoting metastasis[177]. The importance of collagen and the ECM in breast cancer progression make this a good model system in which to study this interaction.

Proline and hydroxyproline make up a significant proportion of collagen residues, with only glycine being more abundant[131]. The increased activity of PYCR1 produces more proline, which is exported from cancer cells. The slides were stained with a collagen antibody

to assess whether there is any relationship between PYCR1 expression patterns and collagen deposition in tumours. If the proline produced through PYCR1 activity is in excess, as is predicted to be the case in hypoxia, it would be expected to be exported from the cell into the matrix. Here it would be available as a substrate for collagen production.

3.1.3 CA9

Carbonic anhydrase 9 is involved in regulation of extracellular pH. At the cell surface it catalyses the conversion of cellular CO_2 to HCO_3- and H^+, promoting a more acidic microenvironment[178].CA9 expression is induced in hypoxia by HIF1α stabilisation, it is one of the most uniformly and strongly induced hypoxic genes. This, and its plasma membrane localisation make it a good histological marker for hypoxia[151]. Although the *in vitro* work in Chapter 2 does not suggest an increase in PYCR1 expression in response to hypoxia, it does suggest that the expression of PYCR1 promotes survival in these regions. Therefore, CA9 was used as a marker of hypoxic cells to investigate whether there is an relationship in this model between PYCR1 expression and hypoxia.

3.1.4 Chapter Aims

This chapter aims to explore the expression of PYCR1, CA9 and collagen in a set of breast cancer core needle biopsy samples from 41 patients with a diagnosis of triple negative breast cancer. Analysis will be carried out using spacial image analysis software, which uses machine learning methods to analyse images based on algorithms developed from a training data set. This will be used to assess whether there are any associations between PYCR1 expression, hypoxia and collagen deposition.

3.2 Methods

3.3 Sample collection, staining and imaging

Samples were collected over several years by Dr Abeer Shabaam, at the point of diagnosis, in collaboration with the Human Biomaterials Resource Centre (HBRC). Patients consented to the use of their clinical biopsy in further research at the point of consent for the procedure. Staining for this study, and imaging of the slides were carried out at the HBRC.

3.3.1 Region selection

After scanning, images were analysed using Phenochart visualisation software. Regions were selected for further analysis, using the stamp tool. Regions were selected if they were determined to contain malignant tissue, with no areas of healthy tissue. Areas were excluded if they contained regions of ductal carcinoma *in situ* (DCIS), or any areas of sample folding or ripping. Training for identification of tumour, DCIS and normal tissue regions was provided by Dr Abeer Shabaam. A selection of these regions, comprising at least 20% of the total, was reviewed by Dr Shabaam, and she also advised on regions which were unclear. All regions of each sample which could be used were taken forward. This resulted in at least 10 stamps per sample. Examples are shown in Figure 3.1.

A set of stamps were also selected to be used as a training data set. At least two stamps per sample were used for this set. Records were kept of the number of stamps for each slide, and which of these were included in the training set.

3.3.2 Training

Tissue segmentation

For training of the tissue segmentation algorithm, sections were selected that represented 'tumour', 'stroma' and 'other'. These regions were selected by eye, using the H&E view. Dr Shabaam again advised on this, and example slides were reviewed by her after the tissue

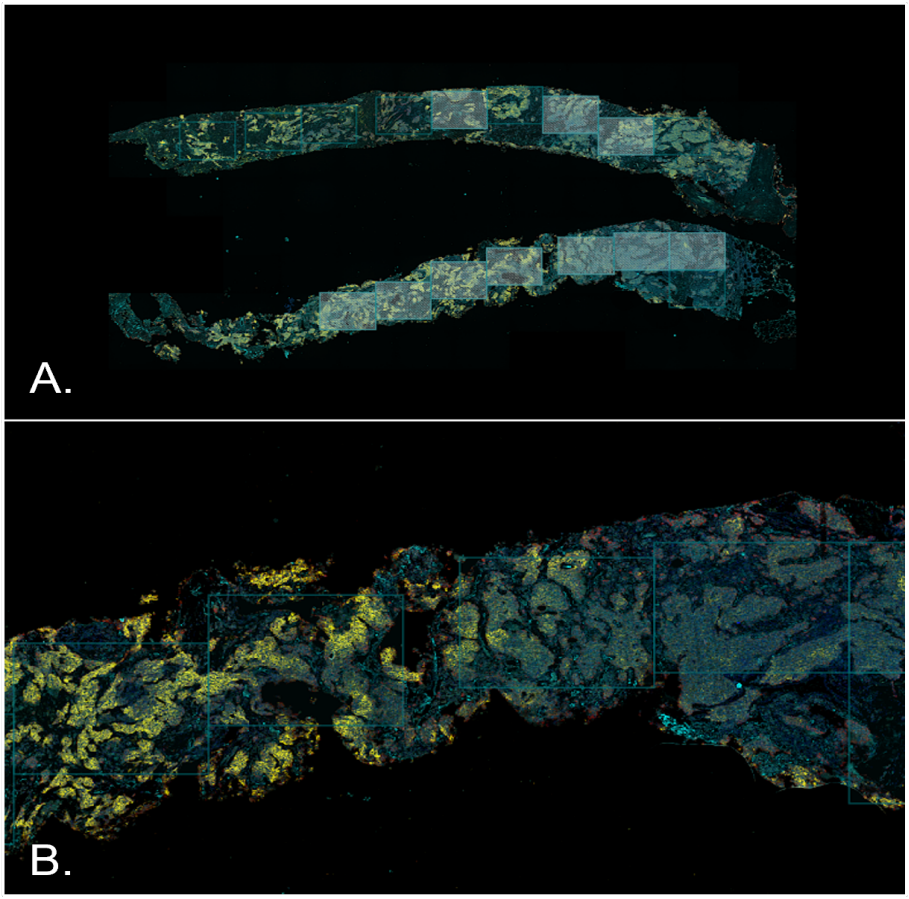

Figure 3.1: A. Example slide showing two core biopsy samples, with stamp selections. B. Higher magnification example image.

segmentation algorithm was applied.

Tumour regions were defined as areas clearly recognisable as tumour. This identification was carried out considering increased nuclear size, high cell density, and disordered architecture. Stroma regions were identified as anything in the core samples which was not defined as tumour, but that associated with tumour regions and was not defined as healthy or DCIS, and that contained cells and matrix. Regions defined as other contained no staining. This included areas outside of the core, and any regions which were missing. Example segmentation is shown in Figure 3.2.

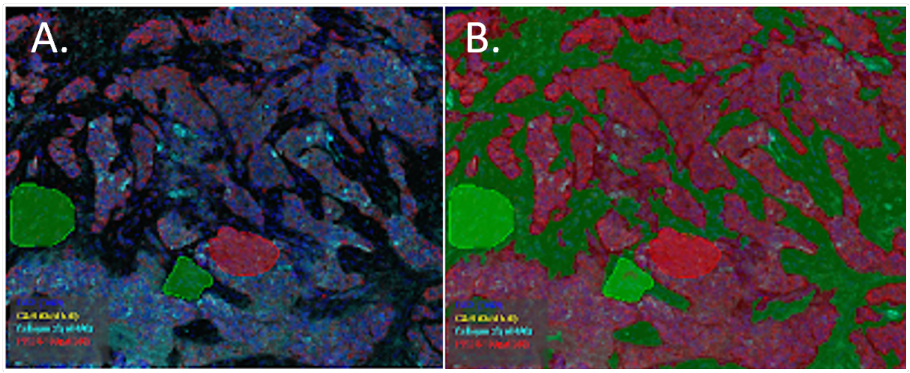

Figure 3.2: A. Example of regions selected for tissue category training. Tumour shown in red, stroma in green. B. Example of tissue segmentation algorithm. Tumour in red, stroma in green.

The training parameters used were as follows:

- Only DAPI included - in order to avoid bias.
- Pattern scale: medium
- Segment resolution: fine
- Minimum segment size: 1000 pixels

With these parameters and at least 10 training regions per category, tissue training efficiency was 96%. Several stamps with the tissue training applied were reviewed by Dr Shabaam.

Cell segmentation

For cell segmentation algorithm training, stamps were viewed using the DAPI fluorescence view. The DAPI component was used to determine cell nuclei. The final parameters were as follows:

- Splitting sensitivity: 0.59
- Minimum nuclear size: 30 pixels
- Fill nuclear holes smaller than: 5

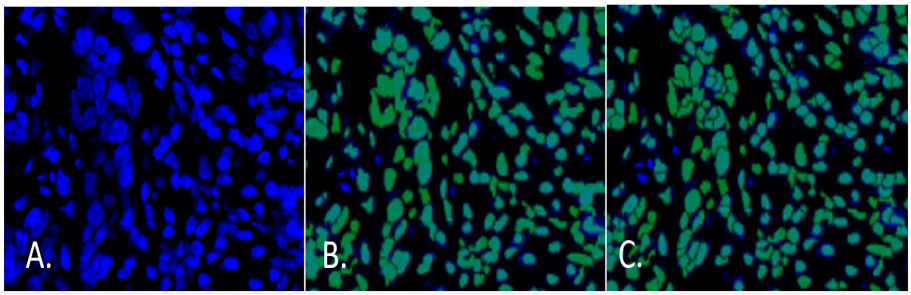

Figure 3.3: A. Example slide section with DAPI staining shown. B. Example cell segmentation with low splitting sensitivity. C. Example cell segmentation with optimised parameters.

Phenotyping

At this stage, the tissue and cell segmentation algorithm was cloned, and separate cell phenotyping branches were created. This meant these could be run in parallel, with consistent cell and tissue segmentation, but monitoring multiple phenotypes. In each algorithm, two phenotypes were defined: the phenotype of interest (CA9 or PYCR1), and 'other'. At least ten cells of each phenotype, with different staining intensities were used for training.

3.3.3 Data analysis

Running the algorithms in InForm produces a series of image files showing tissue, cell and phenotyping maps for each stamp. The tissue segmentation maps were reviewed to rule out any stamps where the identification had not worked. The following steps were carried out using the phenoptrReports R add-in package in RStudio, which uses the functionalities from phenoptr, developed and maintained by Akoya Biosciences. First, the text files were merged using the 'merge cel seg files' function. Files from separate algorithms were then combined, at this step a third condition was added which collated data from the two algorithms to find cells which were positive for both PYCR1 and CA9, using the 'Consolidate and summarize' function. The final reports were collated into an excel file, using 'Analyze consolidated data'.

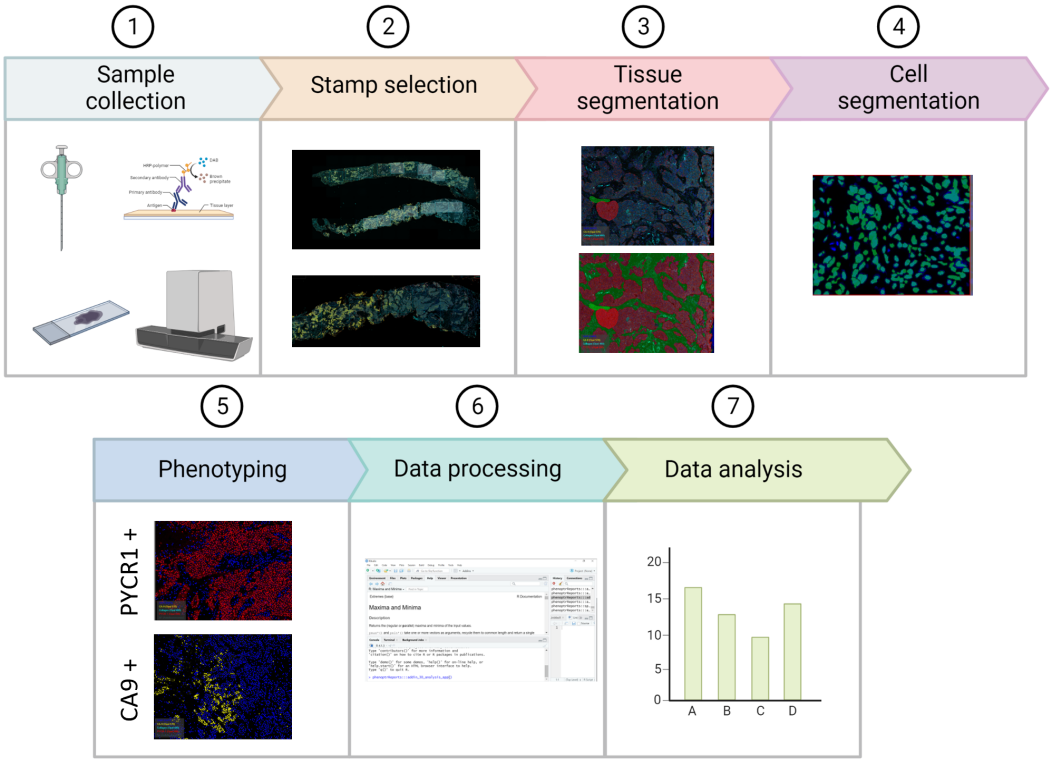

Figure 3.4: Summary of workflow. Sample collection, staining and imaging (step 1) were carried out by Dr Abeer Shabaan and the Human Biomaterials Resource Centre. Created using BioRender.

3.4 Results

3.4.1 Localisation of phenotypes

The localisation of the three phenotypes was first investigated. The percentages of cell of each phenotype which were identified as being in either the tumour or the stroma are shown in Figure 3.5A. The majority of cells identified as expressing PYCR1 are located in tumour regions (mean = 93%). CA9 expressing cells were also more likely to be located in tumour regions (mean = 84%), as were collagen-expressing cells (mean = 77%). This suggests that most of the PYCR1 expressing cells in these samples were located in the tumour cells, and not in the stroma. The same is true of CA9 and collagen. However, the variability in these two markers is much more pronounced than PYCR1.

The percentage of cells from each region which expressed each of the markers was also investigated (Figure 3.5B). This shows that the majority of tumour cells in these samples express PYCR1, while it is expressed in a a very small percentage of stromal cells. CA9 is expressed in a higher percentage of tumour cells than stromal cells. A smaller proportion of tumour cells were found to express CA9 than PYCR1, with a mean of 10%. This suggests than in these samples, around 10% of the tumour cells are in regions where the oxygen tension is low enough to induce a hypoxic signalling response. There is a large amount of variation in the percentage of tumour cells which associate with collagen staining, with some samples showing up to 90% of cells, with others having as low as 2%.

These data also suggest that PYCR1 expression is highly linked to tumour cell, rather than stromal cell identity.

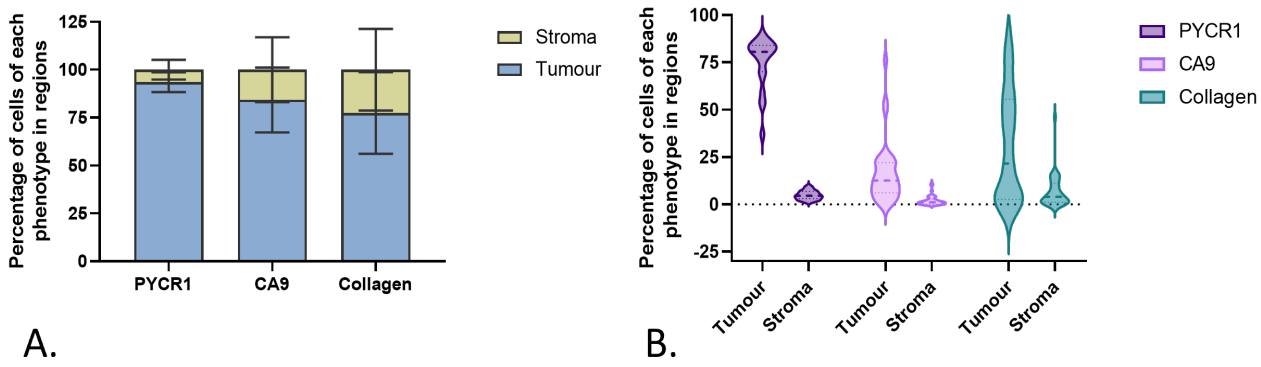

Figure 3.5: A. Percentage of cells of each phenotype which are located in the tumour or stroma regions. B. Percentages of cells in each region which are assigned to each phenotype. (n=36)

3.4.2 Correlation of target protein expression

Due to the association between the expression of target proteins, in particular PYCR1, and tumour regions, any correlations must be stratified by region. Analysis which does not take into account the different regions finds weak correlations between PYCR1 and CA9, and PYCR1 and collagen (Figure 3.6), as the majority of tumour cells express these markers. Slides which contain more tumour regions will therefore show higher numbers of cells expressing these targets.

Correlations are not found between any of the target proteins when the analysis stratified, in the tumour (Figure **??**A-C), or in the stroma (Figure **??**D-F). Previously published data has shown a correlation between these two markers in the stroma of triple negative breast tumours, using an available gene expression dataset of microdissected stroma and epithelium from samples of invasive ductal carcinoma[179]. In this study, the association between PYCR1 and collagen in the stroma comes the closest of those investigated, with an R squared value of 0.3, but this does not reach significance.

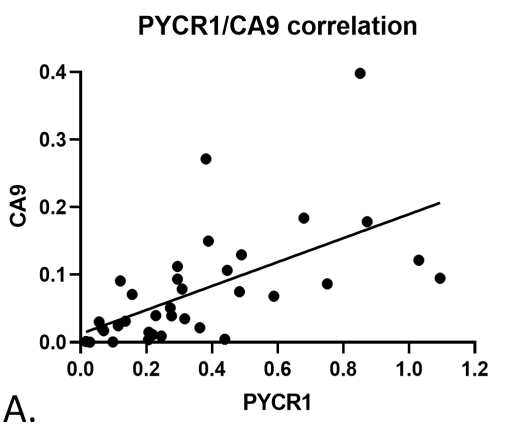

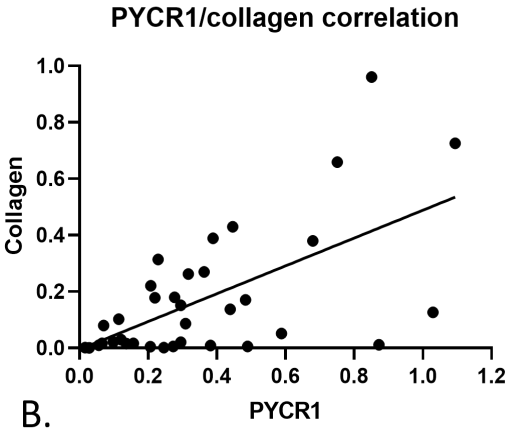

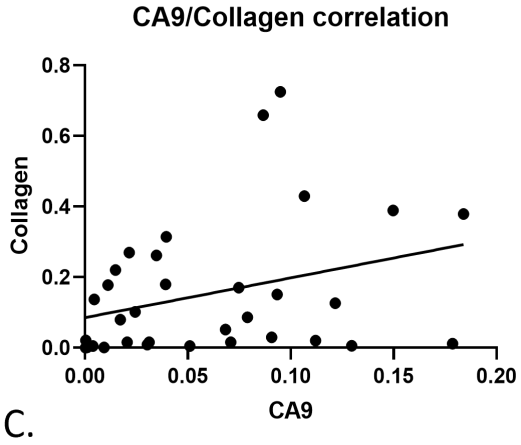

Correlation	R squared	P value
PYCR1/CA9	0.3603	0.001
PYCR1/Collagen	0.3718	0.0001
CA9/Collagen	0.0997	0.07733

D.

Figure 3.6: A. Graph to show the correlation between PYCR1 and CA9 expression across all cells. B. Graph to show the correlation between PYCR1 and collagen expression across all cells. C. Graph to show the correlation between collagen and CA9 expression across all cells. D. R squared and P values for A, B and C. (n=36)

3.4.3 Double positive phenotypes

The InForm software assigns each cell in each stamp a phenotype and an x and y coordinate, meaning that the data generated from multiple algorithms can be consolidated, allowing double phenotypes to be defined. These phenotypes are shown here as a percentage of the total cells of one of the single phenotypes, in order to assess the likelihood of a cell which expresses one of the proteins of interest to express another.

The percentage of PYCR1 expressing cells in the tumour which also express collagen is highly variable, with a mean of 16.63% and a range of 0-70.92%. This is significantly higher than the percentage of PYCR1 expressing cells which also express CA9 in the tumour (Figure 3.7A). However, both of these suggest that PYCR1 expressing cells are more likely not to express these proteins than to express them, in the tumour as a whole. In the stroma, again collagen co-expression is very variable. The percentage of PYCR1 positive cells expressing both of the proteins is lower than in the tumour, and CA9 is again lower than collagen (Figure 3.7B).

CA9 expression is indicative of a cell experiencing hypoxia. The percentage of cells expressing CA9, which also express PYCR1 and collagen was therefore assessed to determine whether either of these markers are associated with hypoxic regions. In the tumour, CA9 expressing cells were very likely to also express PYCR1, with a mean percentage expression of PYCR1 of 87.78% and a range of 46.72-100%. Although from the violin plot it is clear that the data points are clustered around the top end of the range (Figure 3.7C). The percentage of CA9 expressing cells which also express collagen is much lower and much more variable, with a mean of 50.8% and a range of 2.4-98%. However, given the data which shows that the majority of tumour cells express PYCR1 (Figure 3.5B), it is likely that this association is artificially inflated.

Therefore, the percentage of CA9 expressing tumour cells which express PYCR1 was compared to the percentage of non-CA9 expression tumour cells which express PYCR1. This was calculated as: ((PYCR1)-(PYCR1 and CA9))/((Total cells)-(CA9)). This shows that hypoxic tumour cells are significantly more likely to express PYCR1 than non-hypoxic tumour cells (Figure 3.7D).

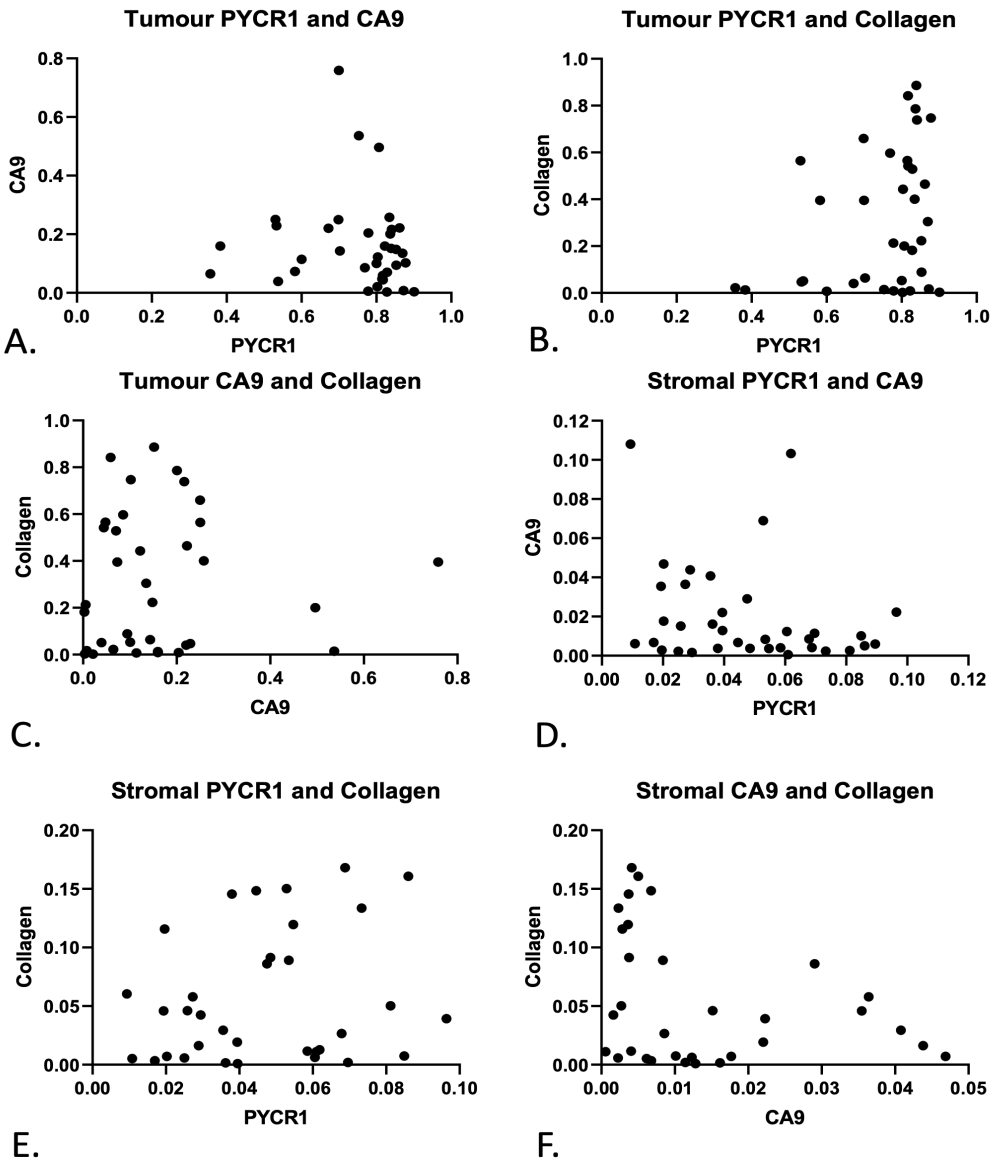

G.

Correlation	R squared	P value
Tumour PYCR1/CA9	0.007	0.627
Tumour PYCR1/Collagen	0.096	0.065
Tumour CA9/Collagen	0.001	0.836
Stromal PYCR1/CA9	0.061	0.146
Stromal PYCR1/Collagen	0.064	0.160
Stromal CA9/Collagen	0.095	0.0854

Figure 3.7: There is no correlation between expression of A. PYCR1 and CA9 in tumour regions, B. PYCR1 and collagen in tumour regions, C. CA9 and collagen in tumour regions, D. PYCR1 and CA9 in stromal regions, E. PYCR1 and collagen in stromal regions, F. CA9 and collagen in stromal regions. (n=36) G. R squared and p values for A, B, C, D, E and F.

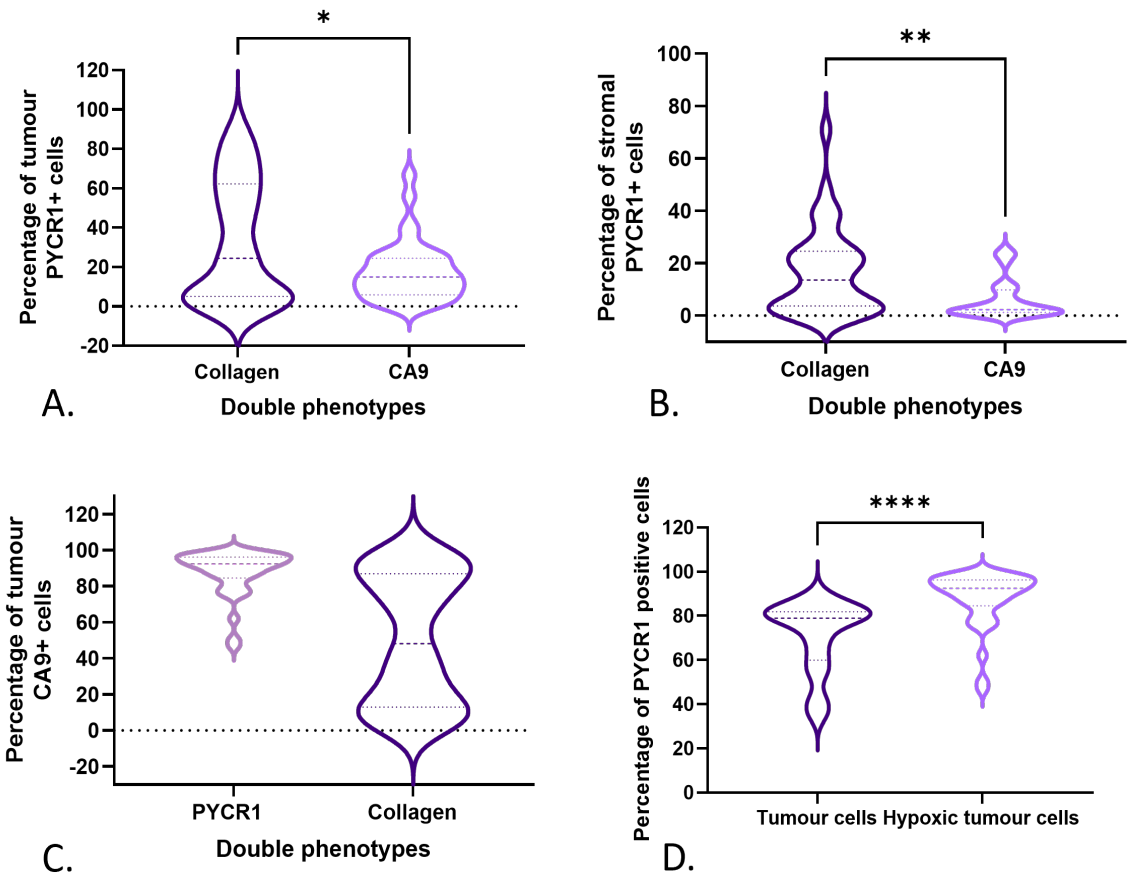

Figure 3.8: A. The percentage of PYCR1 positive cells in the tumour, which also express collagen is very variable, and significantly higher than the percentage of PYCR1 expressing cells which also express CA9. B. The same trend can be seen in the stromal cells. C. The percentage of CA9 expressing cells in the tumour which also express PYCR1 is very high and does not show much variation. The percentage which also express collagen is very variable. D. The percentage of hypoxic tumour cells expressing PYCR1 is higher than that of normal tumour cells. (n=36)

3.5 Discussion

The use of these core needle biopsy samples, taken from patients at the time of diagnosis, in combination with high resolution slide scanning and the image analysis software, allows an in-depth analysis into protein expression in the context of the tumour microenvironment. Additionally, the ability to train an algorithm using InForm allows for the analysis of multiple stamps across multiple slides, separated by region, and phenotyping of individual cells in those regions. This data collection would not be possible manually. In this study, it allows investigation into the localisation of the three proteins of interest; PYCR1, collagen and CA9, in the tumour and stroma.

This analysis reveals, firstly, that the majority of tumour cells express PYCR1, while the majority of cells in the stroma do not (Figure 3.5). This is in agreement with several studies which have suggested that PYCR1 expression (at the mRNA level) is associated with the tumour cell phenotype in multiple cancers[142,180]. However, in this study, the expression in healthy tissue could not be compared to that of the tumour, given the nature of the biopsy samples. Therefore, it may be that PYCR1 expression is associated with the cell type of origin, which in a breast tumour is likely to be epithelial. This is worthy of further investigation, to establish whether there is a role for PYCR1 in cancer cell transformation.

The low percentage of stromal cells which express PYCR1 suggests that few of the cells which make up the stroma express PYCR1 (Figure 3.5). This appears to contradict the findings of a recent publication which shows that cancer associated fibroblasts utilise PYCR1 activity to produce proline for collagen production, for deposition of pro-tumourigenic extracellular matrix. The study showed PYCR1 expression in the stroma of breast tumours is increased with tumour progression, and was weakly correlated with collagen expression[179]. These observations were made using publicly available gene expression data-sets from micro-dissected stroma and tumour samples[181], these quantify mRNA levels, whereas this work used protein expression. Additionally, the difference in observation may result from the sampling used to define the stroma. The publicly available dataset used micro-dissection to separate "tumor-associated and adjacent normal stromal components", whereas this work defined any cellular region taken as part of the biopsy, but not identified as tumour as the stroma. Given the often heterogeneous nature of the stroma[182] it was not determined to be feasible to differentiate any further in these samples. This may mean that presented

here incorporates more stromal regions which may have been considered "normal stromal components" in the previously published work.

No correlations were found between any combination of PYCR1, collagen and CA9 in this work, when phenotypes were stratified by region. Given the observation that the majority of tumour cells express PYCR1, and to a lesser extent CA9 and collagen, any stamps which contain more tumour regions are likely to have more cells of each phenotype, thereby artificially creating positive correlations between phenotypes. This is demonstrated in Supplementary figure 3.8, where positive correlations are found between all three phenotypes. This demonstrates the importance of spacial resolution in analysis of protein expression.

This analysis also allowed for the quantification of double phenotypes - cells expressing two of the proteins of interest. Calculating the percentage of cells of one phenotype which also express another allows co-expression of proteins to be investigated. Most notably, this allows the association of protein expression to regions of tumour hypoxia to be explored, as CA9 is expressed in hypoxic cells. This finds that the majority (mean = 87.78%) of CA9 expressing cells in the tumour also express PYCR1 (Figure 3.7C). However, as previously described, as the majority of tumour cells express PYCR1 this may not be due to an association with CA9. In order to assess this, the percentage of PYCR1 expressing cells in the tumour cells expressing CA9 (hypoxic) and tumour cells not expressing CA9 (normoxic) was calculated. This shows that a significantly higher percentage of hypoxic tumour cells express PYCR1.

In the context of the data in Chapter 2, which suggests that cells in hypoxia rely on PYCR1 expression and activity to regulate their redox homeostasis, this observation seems to support the hypothesis that PYCR1 promotes survival in regions of tumour hypoxia. Data in Chapter 2 also show that loss of PYCR1 *in vitro*, in a xenograft model, leads to a rapid increase in hypoxia, leading to cell death and necrosis. Taken together, these two studies suggest that cells in hypoxic regions may benefit from PYCR1 expression, and that cells which do not express this protein may be less likely to survive in hypoxic regions. Further work is required to establish whether there is an association between the degree of hypoxia and the level of PYCR1 expression.

Further work is also needed to establish whether collagen deposition is associated with PYCR1 expression, or with tumour hypoxia. This work does not find any association between collagen deposition and PYCR1 or CA9 expression.

3.5.1 Future directions

To further this work, it would first be important to work with Akoya to establish a means by which areas of high collagen expression which were not associated with cells could be defined. The ability to assign regions and assess the expression of a marker, independently of cellularity would benefit this work greatly. With this capability, it would be possible to define areas of high/low collagen deposition, and stratify the microenvironment further.

This work would also benefit from the analysis of healthy breast tissue. Core needle biopsies are very small samples taken directly from the site of a suspected tumour. Therefore, by design, comprised of mostly tumour tissue, with very few samples containing areas of healthy tissue. This means that paired comparisons between tumour and healthy tissue are not possible. This study could be expanded to include biopsy samples which are not diagnosed as invasive ductal carcinoma. Biopsies are only carried out if there is a high level of suspicion that a tumour is present, after examination and ultrasound. This means that the likelihood of samples containing tissue which is not healthy is high. Inclusion of more samples could be used to correlate these markers with tumour stage, including pre-cancerous regions of DCIS.

The analysis of patient outcomes alongside the spacial protein expression data would make these observations more clinically relevant. This could be used to investigate several questions which are raised by the work. Firstly, does expression of CA9 correlate with survival parameters or metastatic progression in these patients? Secondly, does an increased expression of PYCR1, and particularly PYCR1 in hypoxic regions correlate with prognosis? This has been investigated using mRNA data from unstratified samples, but there is an opportunity here to investigate this using protein expression in a more targeted way. Thirdly, does the extent of collagen deposition correlate with any survival parameters or metastatic progression? The make-up of the tumour associated stroma is a developing area of research, particularly in the context of breast tumours where there may be an association between breast density and the probability of tumour development[183].

Finally, it would be important to establish whether the findings from this work translate into other tumour types. In particular, tumours which are known to have a particularly hypoxic signature; including squamous cell carcinomas of the head and neck (notably glioma and glioblastoma[184]), cervical cancers and lung adenocarcinoma[175]. Comparisons of PYCR1,

collagen and CA9 expression between tumour types would be beneficial in understanding the relationship between the markers in the context of different tissue types.

Chapter Four

Investigation of a Potential Inborn Error of Ubiquinone Synthesis via PDSS-1

4.1 Introduction

Inborn errors of metabolism (IEM) are a wide range of inherited disorders that mainly arise from germline monogenic mutations, often resulting in pathogenic alterations to metabolic pathways. These are often diagnosed in early childhood, with a diverse range of symptoms and signs that make them difficult to diagnose due to their overlap with other conditions. The more common IEMs have a defined clinical or biochemical profile. However, given the number of potentially affected pathways, many IEMs are rare or novel. If a patient is suspected of having an IEM, for example, if no other definitive diagnosis can be made, genetic testing can be carried out, although this is based on a panel of selected (and more commonly mutated) genes, rather than whole genome sequencing. This aims to identify the cause of the symptoms and guide the management of symptoms.

This chapter will investigate a suspected IEM, the cause of which could not be definitively determined through panel-based sequencing alone. Several potential mutations were identified, and the aim of this work is to establish whether the top sequencing hit may be the cause of the patient's phenotype.

4.1.1 Clinical Presentation

Patient M is under the care of the Queen Elizabeth hospital, Birmingham. He first presented shortly after birth with faltering growth, vomiting and a repaired intestinal malrotation. At 5 months old, he was experiencing episodes of hypoglycaemia, with blood glucose concentrations as low as 2.5mM. Under controlled fasting conditions, his blood glucose fell to <3mM after 4 hours, with poor lipolytic and ketotic responses. He was not found to be hyperinsulinaemic, as insulin was undetectable throughout. He had plasma lactate levels slightly above the normal range, at 0.9-1.2mmol/L. Due to this fasting intolerance, testing for glycogen storage disease was carried out which showed no abnormalities in any known glycogen storage genes. He also had slight hepatomegaly, and raised TCA cycle metabolites.

A family history of NDUFA10 deficiency was also recorded. The NDUFA10 gene encodes a subunit of complex I, loss of which leads to a deficiency of this electron transport chain complex. As a result, oxidative phosporylation (OXPHOS) is impaired. Reduced efficiency of OXPHOS can lead to a wide range of clinical presentation, primarily affecting organs with the most significant energies demands, including the heart, skeletal muscle, liver and the brain (https://www.ncbi.nlm.nih.gov/pmc/articles/PMC3061993/).

4.1.2 Genetic Sequencing

Next generation sequencing was performed, at the University of Birmingham, under the supervision of Professor Andrew Beggs, which identified a point deletion mutation in the splice acceptor site within intron 2 of PDSS1. This also found no likely mutation in NDUFA10.

The sequence from which the thymidine is lost in this mutation forms a part of the poly-pyrimidine tract preceding exon 3. The poly-pyrimidine tract is important for the binding of the U2AF65 subunit of the spliceosome and alterations to its compositions and length have been shown to influence splicing[185,186]. Several previously identified mutations in the poly-pyrimidine tract of other genes have been shown to lead to mis-splicing, leading to inherited disease; affecting Factor IX and mitochondrial acetoacetyl-CoA thiolase[187,188]. The single base loss observed in this patient could therefore potentially affect the splicing efficiency, which could lead to splicing out of exon 3. This could result in the truncation of the protein product, or nonsense-mediated decay of the whole mRNA. As the active enzyme is a

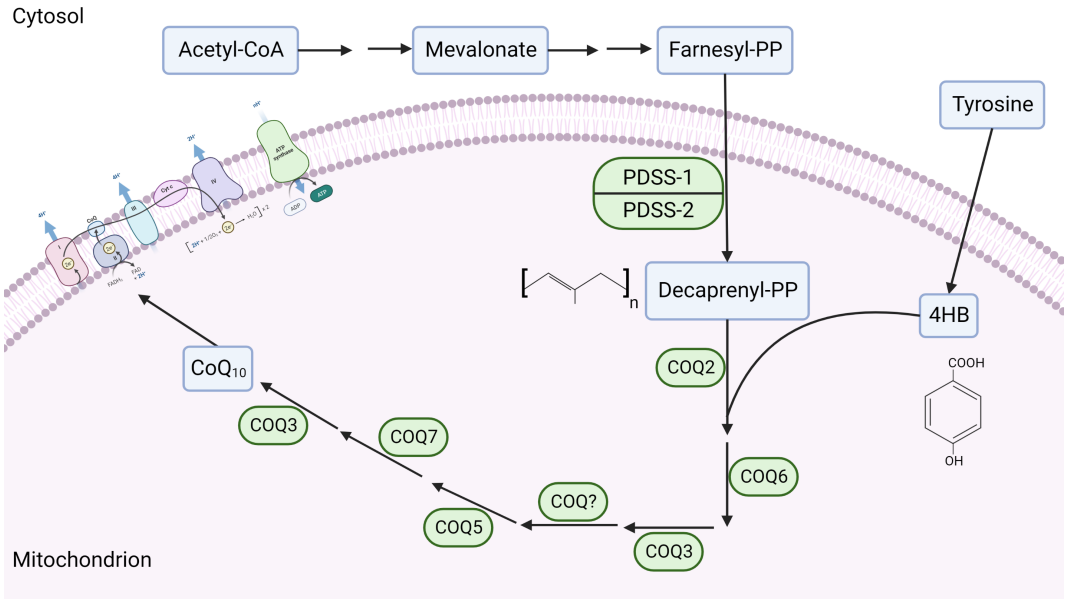

Figure 4.1: Schematic to show the synthesis pathway of CoQ_{10}. Creating using BioRender.

heterotetramer, comprising 2 subunits of PDSS1 and PDSS2, any alteration to the subunit which influences complex formation would likely affect function.

Based on identification through sequencing and downstream analysis, and based on previously identified mutations in similar regions leading to inherited disease, it was hypothesised that this mutation in PDSS1 could be the cause of Patient M's symptoms.

4.1.3 PDSS1 Structure and Function

As previously mentioned, PDSS1 forms a part of a heterotetramer comprising 2 PDSS1 and 2 PDSS2 subunits. The active complex is known as COQ1 and is involved in the synthesis of CoQ (also referred to as ubiquinone or Q), in the mitochondria[189]. CoQ is comprised of a benzoquinone, derived from tyrosine or phenylalanine. In the mitochondria, this is conjugated to an isoprenoid side chain, formed from farnesyl disphosphate derived from the mevalonate pathway, elongated by the addition of isopentenyl diphosphate molecules. CoQ_{10} is the most abundant form of CoQ, the '10' denoting the number of isopentenyl diphosphate units forming the side chain[190]. The COQ1 complex catalyses the elongation of this side chain, before condensation to the benzoquinone unit. This is then methylated, decarboxylated and hydroxylated to form CoQ_{10} (Figure 4.1).

CoQ_{10}

The most well-documented role of CoQ_{10} is as a central part of the mitochondrial electron transport chain. Here, CoQ_{10} transfers electrons from complex I (NADH ubiquinone oxidoreductase) and II (succinate dehydrogenase) to complex III. It is commonly denoted as "Q" in diagrams of the ETC. Electron transfer is coupled to the movement of protons across the membrane and into the intermembrane space, generating a proton gradient which fuels ATP synthesis through ATP synthase. Succinate dehydrogenase, (SDH), which reduces CoQ_{10} during the oxidation of succinate to fumarate[191], therefore directly couples TCA cycle activity to CoQ_{10} and the ETC.

It has been hypothesised that there are two physically distinct pools of CoQ_{10} in the mitochondria. One is associated with the membrane, as a part of super-complexes in the ETC, which serves to transfer electrons from complex I only. The second pool is unbound and is available to transfer electrons from complex II, or from several other mitochondrial oxidising enzymes, including: choline dehydrogenase, electron transfer flavoprotein dehydrogenase, sulfide:quinone oxidoreductase, proline dehydrogenase, glycerol phosphate dehydrogenase and dihydroorotate dehydrogenase[192]. This implicates CoQ_{10} in serine and glycine metabolism, fatty acid oxidation, sulphide detoxification, proline catabolism and pyrimidine synthesis, as an electron acceptor. It is also hypothesised that CoQ_{10} can be transferred between these two spatially separated pools if necessary. For example, when the free pool is over-reduced - which may occur when fatty acids are used as the main fuel source. This leads to the reversal of electron flux, reducing NADH via the super-complex associated pool. Reversal of electron transport increases the possibility of electron escape, which leads to localised ROS accumulation, resulting in degradation of complex I and the release of complex II and CoQ from super-complexes[193]. This CoQ is then available to restore the free pool.

CoQ_{10} is also essential for the activity of plasma membrane-bound NADH oxidase (NOX). This is a part of a system at the plasma membrane, comprised of NADH cytochrome b reductase on the inner membrane, CoQ in the membrane, and a CoQ oxidase on the outer membrane, as the terminal oxidase. This system can transfer electrons from NADH in the cytosol, to CoQ in the membrane and finally to an extracellular electron acceptor. The activity of this complex is regulated by hormones and growth factors[194]. There are several suggested functions for this activity, including: control of cell growth[194] and regulation of the cytoplasmic NAD^+:NADH ratio[195,196]. It has also been suggested that lysosomes may also

contain a NADH-dependant CoQ reductase which could transfer protons into the lysosomal lumen[197].

In its reduced state, $CoQH_2$, it plays an important role in the protection of membrane lipids from peroxidation. The pool of CoQ in the mitochondrial membrane is maintained in a highly reduced state[198]. $CoQH_2$ can prevent the formation of lipid peroxyl radicals, by reduction of the initiating perferryl radical. In this way, $CoQH_2$ is a highly effective antioxidant, important in the protection of the mitochondrial membrane[199]. The redox state of the pool varies between tissue types, ranging from 20-25% in the brain and lung to 90-100% in the intestine, liver, and pancreas[198]. It seems likely that the redox state of the pool may reflect the need for protection from oxidative stress in different cell types.

Additionally, CoQ is a cofactor for uncoupling proteins (UCPs). UCPs are located in the inner mitochondrial membrane, and are able to transport H^+ into the mitochondria. This activity uncouples the proton gradient from oxidative phosphorylation. This produces heat instead of energy[200]. This reaction requires the presence of oxidised CoQ[201].

Finally, another documented role of CoQ in the mitochondria is modulation of the activity of the mitochondrial permeability transition pore (mPTP). The mPTP is a regulator of cell death, shown to be responsive to high concentration of mitochondrial $Ca^(2+)$, and to oxidative stress[202]. Opening of the mPTP increases the permeability of the mitochondrial membrane, allowing larger macromolecules to cross, thus disrupting the proton gradient, hydrolysis of ATP, and osmotic shock. Altogether, this leads to a loss of iron regulation, and cellular integrity, leading to necrotic cell death[203,204]. This mitochondrial permeability also results in the release of cytochrome C, an initiator of apoptotic pathways[205].

CoQ_9

The composition of the CoQ pool, in regards to side chain length, is known to vary between species and between tissue types. In humans, the main species is CoQ_{10}, with CoQ_9 making up 2-7% of the pool. However, in rats this figure is 80-90% for most tissues, falling to 60-70% in the brain, spleen and intestine[198]. It was initially thought that different chain lengths might impart specialisation, and mean that different CoQ species might be responsible for performing the various functions associated with CoQ. Although, further observations in rat brain showed no specificity in brain region or in subcellular compartment[206], which suggest

that there is no separation of the two pools.

There are differences in the ability of membrane-associated ubiquinols to inhibit lipid peroxidation, with differing chain length. Shorter chains are more potent inhibitors than those with longer chains, although this difference becomes less and less pronounced between longer-chain length ubiquinols. The difference between CoQ9 and CoQ10 is therefore very small[207]. Any significant difference in the ability of these ubiquinones to oxidise NADH is also unlikely. Although again, the shorter chain uiquinones exhibit a lower Vmax than longer chains, the difference between longer chains (CoQ6-10) is minimal[208].

4.1.4 PDSS1 in Cancer

There is an emerging role for PDSS1 in cancer, which has yet to be very well understood or explored. Recently, an association between higher PDSS1 expression and decreased overall and progression-free survival time was identified in hepatocellular carcinoma (HCC). This study also linked the expression of PDSS1 to decreased abundance of $CD8^+$ T cells and increased activity of WNT, TGFβ, VEGF signaling pathways[209].

Additionally, it was separately identified as part of a screen for hypoxia-related deferentially expressed genes in HCC[210]. No other mechanistic relationship between PDSS1 and hypoxia has yet been described. It seems counterintuitive that expression of PDSS1 would be increased in response to hypoxia, as under these conditions electron transport is slowed. Although, as previously discussed there is a role for CoQ in cytosolic NAD^+:NADH regulation through its contribution to the activity of the plasma membrane NADH oxidoreductase. Inhibition of CoQ biosynthesis has also been shown to induce HIF1/*apha* stabilisation, whilst also leading to an increase in cholesterol levels[211]. Finally, treatment with oxidised CoQ_{10} increased ROS levels and leads to apoptotic cell death in pancreatic cancer organoids[212].

Given the many roles of CoQ_{10} throughout the cell, and the key role in the ETC, its role in metabolic rewiring in cancer remains to be elucidated.

4.1.5 PDSS1 Mutation Phenotype

There are several papers outlining case studies of patients with CoQ_{10} deficiencies and different mutations in the PDSS1 gene. The key phenotypic changes will be outlined below, and discussed in the context of the patient described in this study.

A novel missense mutation; substitution of the guanine at position 735 for thymidine, resulting in a single amino acid alteration in a highly conserved region, was described in two sisters. Both siblings presented with mild intellectual disability, sensorineural deafness, optic atrophy and muscle weakness[213]. Inherited optic neuropathies are known to be most commonly caused by mitochondrial dysfunction, and involvement of the visual system has been previously reported in alterations in the early steps of CoQ_{10} synthesis[214,215,216]. This study does not report any metabolic alterations.

Mollet et al[217] identify another patient with a mutation in the PDSS1 gene, this time a T to G substitution at nucleotide 977 in exon 10. Again, this resulted in a single amino acid alteration in a highly conserved region. The CoQ_{10} synthesis pathway was investigated as cultured skin fibroblasts showed normal activity of complexes II, III and IV, although the ratios of respiratory complex activity (CIV/CII+CIII, CII+CIII/G3PDH+CIII) revealed alterations compared to controls, which suggested a deficiency in CoQ. CoQ_{10} levels were measured by LCMS, and found to be lower than controls, while CoQ_9 levels were unaffected.

The patient presented with deafness, livedo reticularis, and optic atrophy by 3 years old. With age he also developed valvulopathy and was seen to have mild intellectual disability. This phenotype is consistent with the patient reported by Nardecchia et al, above. The patient was also found to have a slightly elevated plasma lactate level and increased lactate/pyruvate ratio.

Interestingly, this study reports two other patients who were found to have mutations in CoQ_{10} synthetic genes, and associated low CoQ_{10} levels in cultured cells, who both died within days of birth. It is not clear what influences survival of patients with CoQ_{10} deficiency, as the other patient in this study was 14 years old.

The phenotype of Patient M does not involve deafness or optical atrophy, although due to his young age these cannot yet be ruled out. Faltering growth and intestinal issues have not previously been reported in patients with PDSS1 mutations. Additionally, neither

study reported any alterations to glucose metabolism and fasting tolerance, as is seen in Patient M. Raised plasma lactate levels were seen across several patients, and are associated with other mutations in early CoQ_{10} synthetic enzymes[215,190]. It is clear from previous studies that there are many phenotypes and symptoms associated with alterations in the CoQ_{10} synthesis pathway.

4.1.6 CoQ_{10} Deficiency

The study of patients with of CoQ_{10} deficiencies, caused by alterations to parts of the synthetic pathway besides PDSS1, is also relevant in this context. As very few patients with PDSS1 mutations have been identified, there is as yet very limited in vitro data. As PDSS1 dysfunction reduces CoQ_{10} abundance, there is likely overlap in the phenotypes of these disorders.

Clinically, CoQ_{10} deficiency is associated with a diverse range of symptoms, which can be categorised into 5 distinct phenotypes: infantile multisystemic disease, nephropathy, cerebrallar ataxia atrophy, encephalopathy and myopathy[218].

As expected, fibroblasts from several patients with inborn errors resulting in a lack of CoQ_{10} *in vitro* show less efficient OXPHOS, and they become more reliant on glycolysis for ATP generation. Transcriptome analysis shows that these cells upregulated pyruvate metabolism alongside glycolysis, and show increased lactate dehydrogenase expression. Interestingly, they also show a decrease in the expression of proteins involved in cholesterol and fatty acid metabolism[219].

4.1.7 Chapter Aims

The chapter will investigate this PDSS1 mutation, with the aim of determining whether it may be the causative in this case. First, any effects on the product of transcription will be investigated, followed by the expression of the PDSS1 protein. The downstream products of PDSS1 activity will also be measured using LCMS, to assess the function of the protein. Finally, the effects of this on the metabolic and growth phenotypes will be assessed.

4.2 Results

4.2.1 mRNA and Protein Expression

For the purposes of this investigation, 'normal human dermal fibroblasts' purchased from Promocell will be used as a control model. These cells are derived from a healthy sample of the dermis, in the same way as the patient cells, taken from a donor.

The mutation identified through Next Generation Sequencing in Patient M, is a single base pair deletion of a thymidine. This is located in intron 2 of PDSS1, within the slice acceptor site preceding exon 3 (Figure 4.2A). It was hypothesised that this mutation would affect the splicing efficiency at intro 2, potentially resulting in loss of exon 3, or nonsense-mediated decay of the mRNA. As a first step, total mRNA was collected and extracted from both the fibroblasts from Patient M (hereafter referred to as ?PDSS1), and normal human dermal fibroblasts (NHDF). A PCR reaction was carried out and the products run on a gel. The primers were designed to target regions before and after the mutation. Primary pair 1 targeted exon 1, pair 2 targeted exon 2, while pair 3 targeted exon 7 (Figure 4.2A-D). These reactions showed no difference in any of the products when comparing the NHDF and ?PDSS1 cells. This strongly suggests that there is unlikely to be nonsense mediated decay of the mRNA in the ?PDSS1 cells. However, loss of exon 3 cannot be ruled out at this stage.

As the mRNA is expressed in ?PDSS1 cells, the expression of the protein was investigated (Figure 4.2F). There was a trend towards a lower expression of PDSS1, but this does not reach significance when multiple blots were analysed by densitometry using Image J (Figure 4.2G). The band also appears at the same molecular weight in both cell samples, suggesting that no significant truncation of the protein occurs. Loss of exon 3 (which has a length of 65 base pairs), would be expected to amount to a loss of 21 amino acids, causing a change in molecular weight of approximately 2.3kDa. This equates to approximately a 6% change, given PDSS1 has a predicted molecular weight of 46kDa. A change in molecular weight of this size may not be detectable by Western blotting.

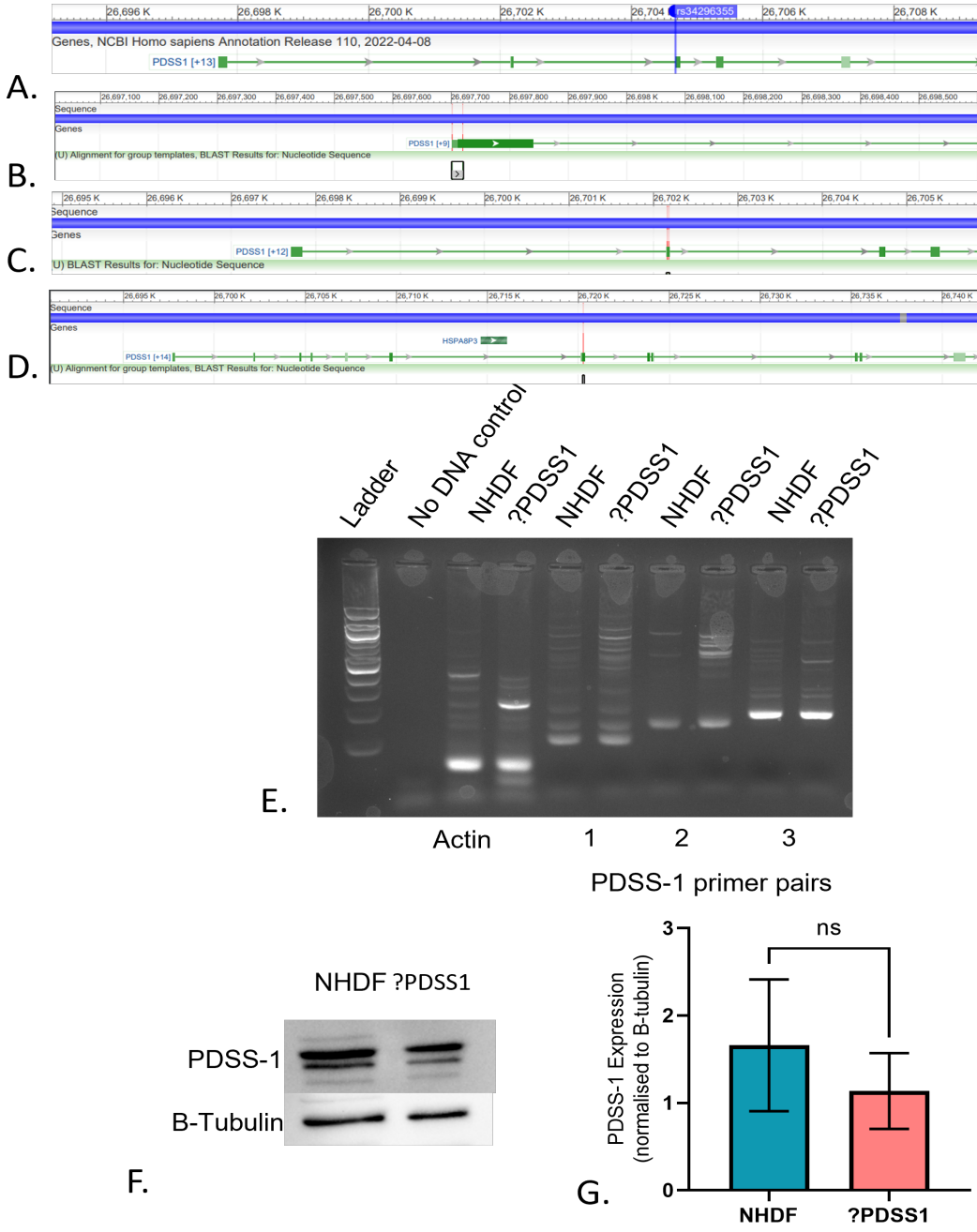

Figure 4.2: A. Diagram to show the location of T deletion on the PDSS1 gene, taken from NCBI B. Primer pair 1 target exon 1 of PDSS1. C. Primer pair 2 target exon 2 of PDSS1. D. Primer pair 3 target exon 6 for PDSS1. E. Electrophoresis gel showing PCR products from mRNA extraction from NHDF and ?PDSS1 fibroblasts. Lane 1 shows the ladder. Lane 2 is a no DNA control. Lanes 3 and 4 show actin as a loading control. Lanes 5-10 Show each of the PDSS-1 primer pairs in turn. F. Western blot to show expression of PDSS-1 in NHDF and ?PDSS1 cells, with B-tubulin as a loading control. G. Densitometry shows no significant difference in protein expression between the two cell types. (n=3)

4.2.2 Ubiquinone synthesis investigation by LCMS

LCMS analysis of the CoQ pool in normal and ?PDSS1 fibroblasts suggested a reduction in CoQ_{10} in the ?PDSS1 cells, which may suggest a dysfunctional synthesis pathway (Figure 4.3A). Less CoQ_9 was also observed (Figure 4.3B), confirming a potential problem with CoQ synthesis, which is independent of chain length. Notably, this is different from observations made in another study of a known PDSS1 mutation[214], which found that CoQ_9 levels were unaffected by PDSS1 loss. As PDSS1 catalyses the elongation of the prenyl side chain of CoQ, if the function was altered, it could be hypothesised that the synthesis of shorter chain CoQ forms might be favoured. As only CoQ_{10} and CoQ_9 could be measured here, a ratio was calculated of these, which shows no alteration (Figure 4.4).

The percentage of the CoQ_{10} pool which is reduced is significantly higher in the ?PDSS1 cells, although it is considerably more variable in this condition (Figure 4.3C), the percentage of CoQ_9 which is reduced also appears to be increased, but this did not reach significance (Figure 4.3D).

The amount of CoQ in the medium of these cells after 24 hours of incubation was measured in order to account for the potential uptake of CoQ in response to reduced synthesis. A control media sample was used to determine baseline amounts, from which the normalised media amounts were subtracted for each of the conditions. These values can then be used to determine net intake or uptake by cells from the medium. The data suggested a trend towards decreased extracellular CoQ_{10} in the ?PDSS1 cells, with several samples showing uptake, although again there is no significant difference between conditions (Figure 4.3E). There was also no significant change observed in CoQ_9 levels (Figure 4.3F).

Taken together, these data suggest that the CoQ pool is altered in ?PDSS1 fibroblasts, with a trend towards enhanced uptake reducing the magnitude of the effect of dysfunctional CoQ synthesis activity within the cells. In addition to a smaller CoQ_{10} pool, this pool is also more reduced. CoQ_9 levels are also lower, which suggests that any disruption to CoQ synthesis may be upstream of PDSS1.

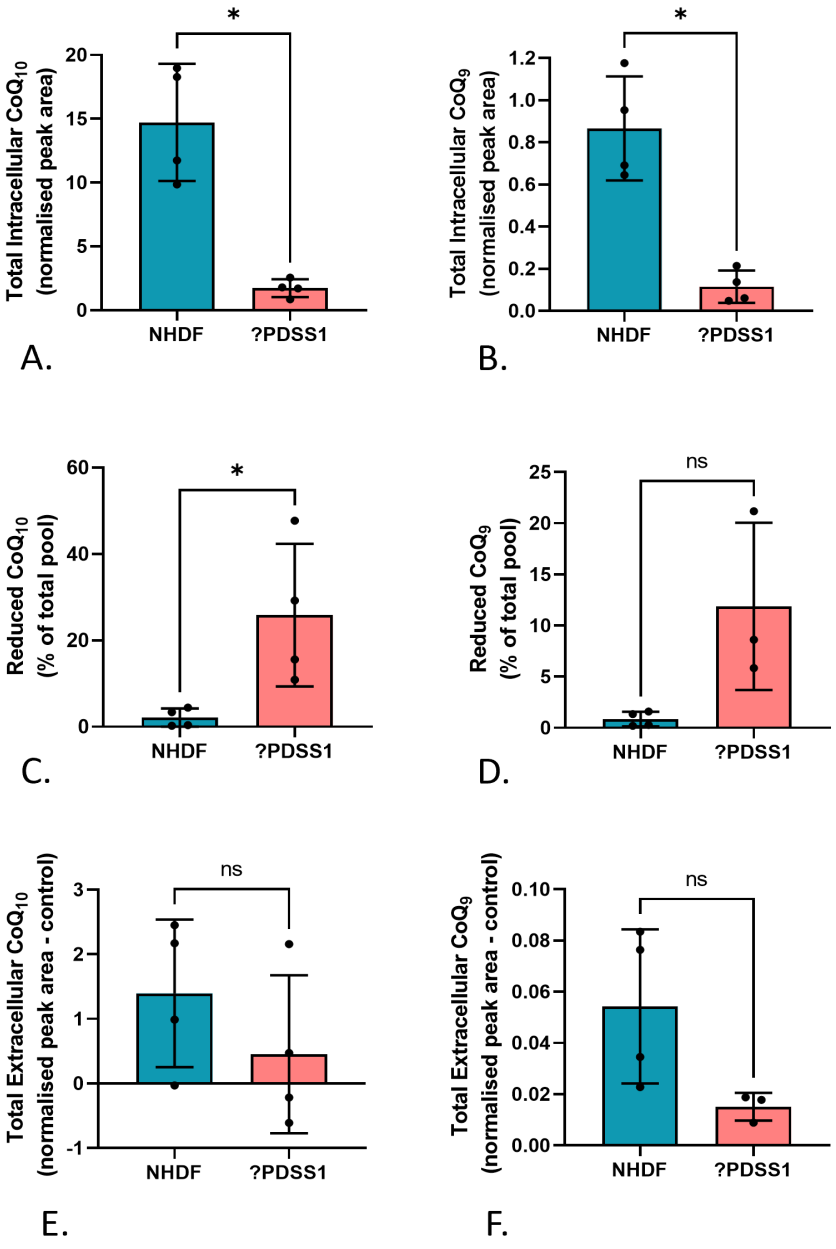

Figure 4.3: A. Total intracellular CoQ_{10} levels are lower in ?PDSS-1 cells. $*$, $p<0.05$. B. Total intracellular CoQ_9 levels are lower in ?PDSS-1 cells. $*$, $p<0.05$. C. The percentage of the CoQ_{10} pool which is reduced is higher in ?PDSS-1 cells. $*$, $p<0.05$. D. The percentage of the CoQ_9 pool which is reduced trends towards being higher in ?PDSS-1 cells, but does not reach significance. E. The total extracellular CoQ_{10} normalised peak area, corrected for amounts in control media sample, is not significantly different between conditions. F. The total extracellular CoQ_9 normalised peak area, corrected for amounts in control media sample, is not significantly different between conditions.(n=4 for all experiments)

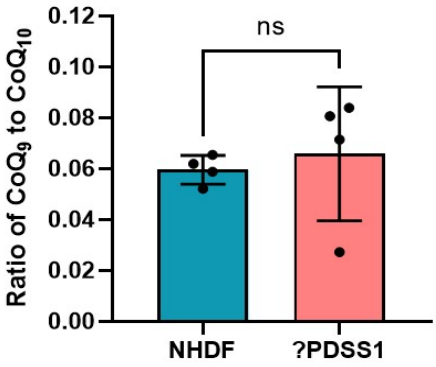

Figure 4.4: The ratio of CoQ_9 to CoQ_{10} in ?PDSS1 fibroblasts is not significantly different to that of the control cells. (n=4)

4.2.3 CoQ_{10} Supplementation

As the ?PDSS1 fibroblasts had a lower total amount of CoQ_{10} than the NHDF, it was hypothesised that they might respond to supplementation with CoQ_{10}. Plasma levels of CoQ_{10} range from 0.5μM-1.7μM, after supplementation therapy, levels as high as 10.7μM are reached[220]. For this reason, cells were treated with 10μM CoQ_{10} in culture medium. In standard FBS (that used routinely in cell culture), no change in cell number was seen at either 24, 48 or 72 hours (Figure 4.5A). The cell-free media sample taken for LCMS was seen to contain CoQ_{10} and to a lesser extent, CoQ_9, which was not a component of the medium. It was hypothesised that the likely source of this exogenous CoQ was the serum component, so to control for this charcoal-stripped FBS was used, which removes non-polar components. However, no difference was seen in proliferation rate when CoQ_{10} was supplemented in these conditions.

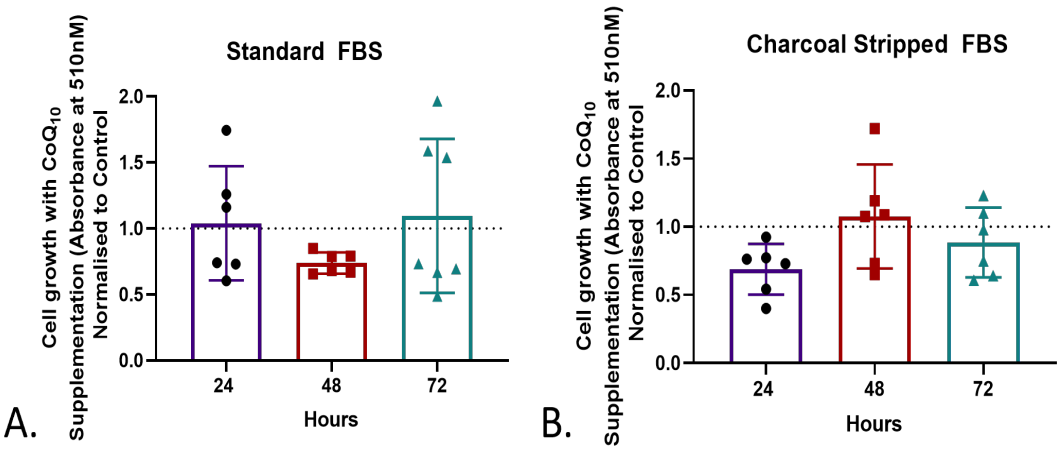

Figure 4.5: A.C Cell number as measured by SRB, normalised to time=0 and the control condition. CoQ_{10} supplementation has no effect on cell growth in normal FBS. (n=6 biological replicates) B. Cell number as measured by SRB, normalised to time=0 and the control condition. CoQ_{10} supplementation has no effect on cell growth in charcoal stripped FBS. (n=6 biological replicates)

4.2.4 Metabolic Implications

As alterations to both the total CoQ_{10} pool and the redox state of the pool are likely to impact the wider metabolic network, this was investigated using both [$U_{13}C$]-glucose and [$U_{13}C$]-glutamine tracing.

As read-outs of glucose metabolism, indicators of glycolytic flux - the m+3 isotopologues of pyruvate, lactate, and alanine were the most abundant, when using $U_{13}C$]-glucose as a tracer. In the ?PDSS1 cells, incorporation in to both pyruvate and lactate was reduced compared to the NHDF (Figures 4.6A and B), while incorporation into alanine was similar (Figure 4.6C). In citrate, the most abundant isotopologue was m+2 in both conditions, indicative of high levels of PDH activity. There is very little m+3 in either cell line, which mainly results from PC activity, although contribution from multiple TCA cycles can also increase this isotopologue. While the NHDF cells have some m+3, this isotopologue is near the limit of detection in the ?PDSS1 cells. Total label into citrate, and especially label into m+2 is reduced in ?PDSS1 cells (Figure 4.6D), suggesting reduced overall incorporation of glucose carbons into the TCA cycle, but particularly through pyruvate oxidation.

Incorporation of [$U_{13}C$]-glutamine carbons into glutamate is consistent between con-

ditions, suggesting conversion of glutamine to glutamate through glutaminase activity is unaffected (Figure 4.6E). However, incorporation into citrate, through the TCA cycle is altered (Figure 4.6F). In both cell types, the predominant isotopologue is m+4, which is the result of oxidative TCA cycle activity. In ?PDSS1 cells, this value is approximately halved, strongly suggestive of a reduced ability to oxidise NADH in the mitochondrion.

As the percentage of reduced CoQ_{10} is increased, the lactate to pyruvate ratio was measured as an indication of the redox state of the cytosol. In the ?PDSS-1 cells this was found to be significantly increased (Figure 4.6G). Furthermore, the ratio of m+4 to m+5 citrate, an indicator of the relative metabolism of glutamine by either oxidative or reductive pathways was decreased, confirming that oxidative TCA cycle activity is impaired in ?PDSS-1 cells (Figure 4.6H). Finally, the incorporation of glucose and glutamine carbons into citrate was compared to investigate changes in nutrient preference. Both cell types demonstrated higher rates of incorporation of glutamine compared to glucose under these conditions. However, the ?PDSS-1 cells showed less incorporation from both sources, with both reduced by approximately 50% (Figure 4.6I).

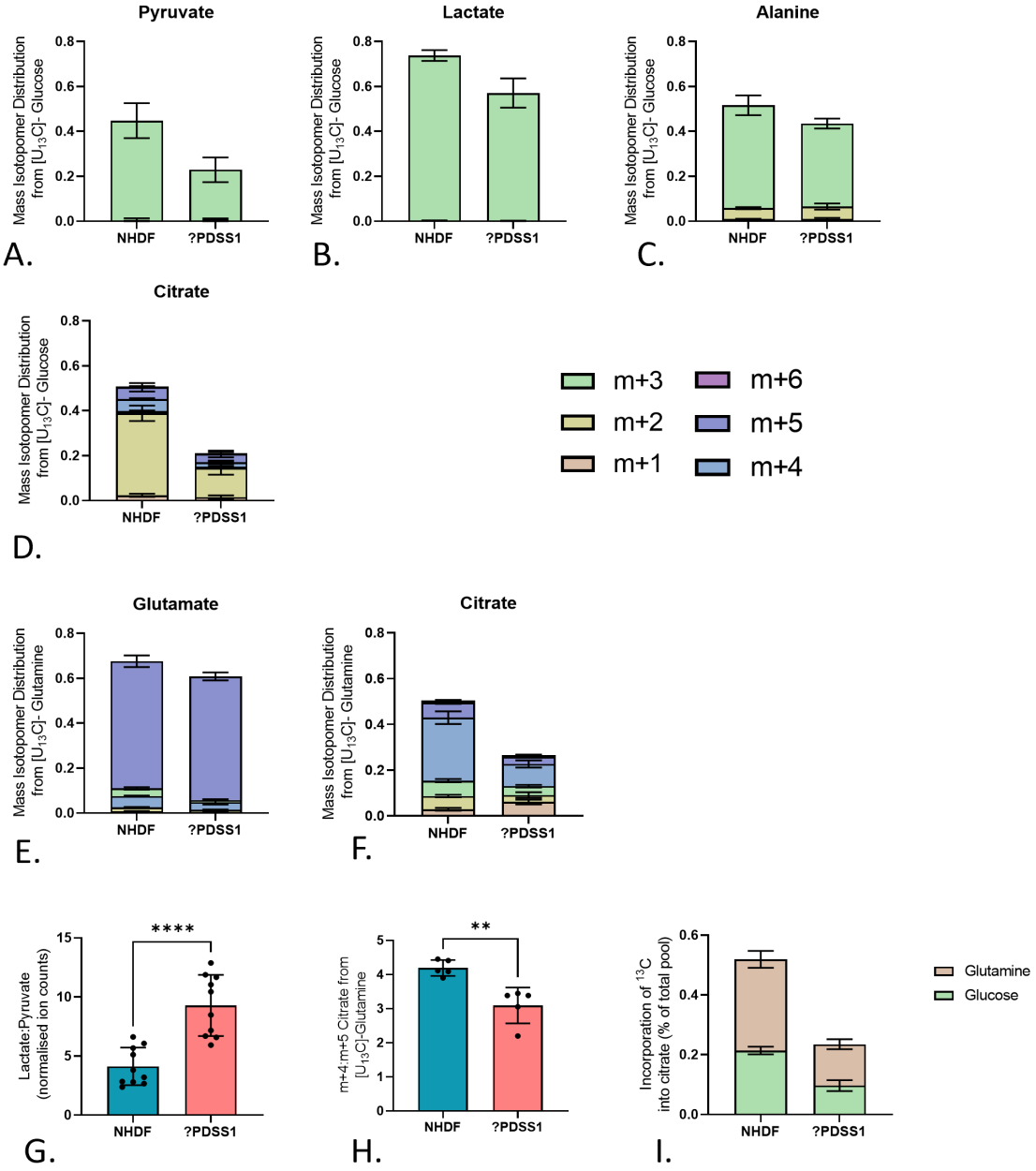

Figure 4.6: A.[U_{13}C]-glucose tracing into pyruvate, showing reduced incorporation in ?PDSS1 cells. (n=5 technical replicates, representative of 3 biological replicates) B. [U_{13}C]-glucose tracing into lactate, showing reduced incorporation in ?PDSS1 cells. C. [U_{13}C]-glucose tracing into alanine. (n=5 technical replicates, representative of 3 biological replicates) D. [U_{13}C]-glucose tracing into citrate, showing a reduction in ?PDSS1 cells. (n=5 technical replicates, representative of 3 biological replicates) E. [U_{13}C]-glutamine tracing into glutamate, showing similar incorporation in both conditions. (n=5 technical replicates, representative of 3 biological replicates) F. [U_{13}C]-glutamine tracing into citrate, showing reduced label in ?PDSS1 cells, particularly the m+4 isotopologue. (n=5 technical replicates, representative of 3 biological replicates)

Figure 4.6: G. The ratio of lactate to pyruvate normalised total ion counts is increased in ?PDSS1 cells. $***$, $p<0.001$. (n=10 technical replicates, from 2 biological replicates) H. The ratio of m+4 to m+5 citrate from [$U_{13}C$]-glutamine tracing is lower in the ?PDSS1 cells. $**$, $p<0.01$. (n=5 technical replicates, representative of 3 biological replicates) I. Total incorporation of carbons into citrate from glucose and glutamine. Incorporation from both sources is reduced in ?PDSS1 cells. (n=5 technical replicates, representative of 3 biological replicates)

4.3 Discussion

In order to explore whether the identified mutation in the PDSS1 gene contributes to the patient phenotype, the gene products were first investigated. Analysis of PDSS1 mRNA in the patient fibroblasts and the normal human dermal fibroblasts revealed no significant changes, in any of the three target regions. It was hypothesised that there may be total loss of the protein due to nonsense-mediated decay of the RNA, but this is not the case. This analysis still leaves the possibility of a mis-splicing event.

Analysis at the protein level by Western blotting also shows no significant changes between the two conditions. This implies that the mutation has no effect on the total expression of the protein. However, these data cannot assess whether this protein is structurally or functionally the same. Based on the type and location of the mutation, it was hypothesised that it could lead to mis-splicing and loss of exon 3. The change in molecular weight which would result from this would not be large enough to see by clearly Western blot. A conformational change in the protein, or a change in ability to form the COQ2 complex with PDSS2 cannot, therefore, be ruled out.

4.3.1 Alteration to the CoQ pool

In order to investigate the functionality of PDSS1 in these cells, the CoQ_{10} synthesis pathway was investigated using LCMS methods. This revealed reduced total CoQ_{10} levels in the patient fibroblasts, suggesting a defect in the synthesis pathway. The levels of CoQ_9 were also significantly lower in these cells. Loss or impaired function of PDSS1 would be expected to reduce the CoQ_{10} level, with minimal or no effect on CoQ_9, as seen in the literature[217]. It would be interesting to investigate the abundance of shorter chain lengths, as it is likely that reduced function of PDSS1 would favour the production of these.

4.3.2 Central carbon metabolism

The effect of a lower level of CoQ_{10} would be expected to include upregulation of genes associated with glycolysis and pyruvate metabolism[221], according to studies of CoQ_{10} deficiency. As CoQ_{10} is a central part of the ETC, these cells likely rely on glycolysis to compensate for the loss of ATP production through OXPHOS.

In this model, a decrease in the flux of glucose carbons into pyruvate was observed (Figure 4.6A), which suggests that these cells are in fact less efficient at metabolising glucose. This trend is also seen in labelling from glucose into lactate; this is also unexpected, based on previously published transcriptome analysis of CoQ_{10} deficient cells[219].

Entry of glucose-derived carbons into the TCA cycle through pyruvate is also decreased in ?PDSS1 cells. However, the percentage of alanine which is labeled from glucose is much less affected. This may suggest some degree of pool separation in pyruvate, with the pool available for alanine synthesis being unchanged in the patient fibroblasts, and therefore a highly reduced pool of pyruvate available for oxidation in the TCA cycle, or reduction to lactate.

The CoQ_{10} pool was also significantly more reduced in the patient fibroblasts, compared to controls (Figure 4.3C and D). A more reduced pool of CoQ_{10} would also be expected to reduce the efficiency of OXPHOS, again reducing ATP production via this mechanism. This is also likely to lead to an increase in the NADH:NAD^+ ratio, as the regeneration of NAD^+ by the ETC is slowed[222]. Conversely, a more reduced CoQ_{10} pool could be caused by an altered NADH:NAD^+ ratio. When more NADH is available, the flux of electrons to the ETC can increase, saturating the CoQ_{10} pool. It is not possible to establish from these data whether the more reduced pool of CoQ_{10} is a direct result of the mutation, or whether this is secondary to an altered NAD:NADH ratio.

In addition, the more reduced state of the CoQ_{10} pool in ?PDSS1 cells may mean that the NOX system at the plasma membrane is likely to be less efficient, as the CoQ_{10} is more likely to be saturated and unable to transfer the electrons across the membrane. This may further dysregulate the $NADP^+$:NADPH balance in the cytosol, which is likely to affect systems including the glutathione antioxidant system. This may make these cells more vulnerable to oxidative stress, compounding the loss of CoQ_{10} and its antioxidant protection.

The metabolic tracing data further supports a perturbed redox balance in these cells. The ratio of lactate to pyruvate is increased, which is indicative of a more reduced cytosolic NAD pool. Additionally, the ratio of m+4 to m+5 citrate is decreased, suggesting that the citrate pool is relatively more reliant on incorporation of glutamine carbons through reductive TCA cycle activity, than oxidative (Figure 4.6H). Several of the reactions which form the oxidative TCA cycle require NAD^+ as a cofactor (Figure 1.2. This is less favourable when the NAD^+:NADH ratio is lower, which in this case may also be due to reduced function of SDH, due to the smaller CoQ_{10} pool size, which is worthy of further investigation.

A more reduced CoQ_{10} pool may offer more protection against membrane lipid peroxidation, as in its reduced form CoQ_{10} can prevent the formation of lipid peroxyl radicals[199]. Again, this may be a direct consequence of the mutation, or it may be a protective response due to increased oxidative stress. The sensitivity of these cells to treatment with oxidative stress inducer, such as H_2O_2 would be interesting to investigate.

Supplementation of CoQ_{10} in the cell culture medium had no effect on the growth of these cells under the conditions used. Here, cells were treated for 72 hours. However, it may be that a longer period of treatment may be necessary, to reverse any epigenetic adaptations to low CoQ_{10}[219]. It is interesting to note that, the patient was started on CoQ_{10} supplementation in response to the genetic analysis. We understand that no changes were observed clinically in response to treatment, although, the patient's mother reported that he seemed more alert.

4.3.3 Relation to patient phenotype

IEMs often present as a diverse range of phenotypes in different individuals, and through developmental stages. There are, however, several common phenotypes (seen in at least 2 patients) associated with previously reported cases of PDSS1 mutations. These are: intellectual disability, deafness, optic atrophy, and increased plasma lactate levels[213,217]. Patient M has a much more metabolic phenotype, sharing only the increased plasma lactate levels. There may be other shared phenotypes, which have not been investigated in either the previously described cases or in Patient M, or which Patient M has not yet experienced due to their young age.

Several aspects of Patient M's phenotype are common with several inborn errors of fatty acid oxidation. These include, hypoglycaemia in the absence of insulin, faltering growth, fasting intolerance associated with a poor lipolytic and ketonic response, and hepatomegaly[223]. Changes seen in the CoQ pool of these cells could be hypothesised to interfere with fatty acid oxidation, as the overall pool is smaller and more reduced - meaning less is available to accept electrons from this pathway.

Metabolic tracing experiments in the patient fibroblasts in culture suggest a perturbed redox balance. Whether this is caused by, or itself results in alterations to the CoQ_{10} and CoQ_9 pools cannot be established from these data. It may be that the increased plasma lactate levels seen in this patient and in those with a known PDSS1 mutation are a result of a dysregulated NAD^+:NADH ratio under both conditions.

Further investigations are needed to establish whether the identified mutation is the cause of the patient's phenotype. Alterations to the CoQ pools are seen, but the cause of these cannot be determined. Based on previous studies of patients with PDSS1 mutations, and work in models of CoQ_{10} deficiency, the phenotype seen here does not appear to suggest total loss or severe loss of function of PDSS1. It may be that the mutation seen in PDSS1 occurs in conjunction with another mutation and compounds this phenotype.

4.3.4 Future directions

In order to establish whether the PDSS1 protein expressed in the patient cells was functional, it should be purified and investigated biochemically. Cell lines could also be generated which express the mutation, allowing continued continued experimentation. Use of this model would allow a direct comparison between a control cell line, and a cell line of the same origin expressing the mutation. This would act as a more relevant control than the NHDF cells used in this study, as the generated cell lines would have the same genetic background, reducing confounding variables. Additionally, a pool or bank of NHDF cells from a range of different donors would be useful to account for natural variation in PDSS1 activity, and potentially investigate any interacting genes.

Measurement of the patients plasma CoQ_{10} levels would also be important in determining whether the lower levels seen in cultured fibroblasts are clinically relevant.

If the alteration in the PDSS1 gene was found to affect the function of the protein, CoQ_{10} supplementation is the only treatment option suggested by the available literature[217,189], alongside symptom management. Supplementation has thus far shown no clinical benefit in this case, although the patients mother reported he was more alert. Supplementation should be implemented as early in life as possible, in order to support healthy development[224]. High doses are given orally in the case of a primary deficiency (5-50mg per kg per day)[224]. It may take longer than the current supplementation period for any clinical affects to be measurable.

Given the data suggesting an altered redox balance, this should be assessed directly. The whole cell ratio could be measured by LCMS. The effects of long-term treatment with CoQ_{10} could then be assessed. If this does rescue the NAD^+:NADH ratio then it would suggest that the CoQ_{10} level is the cause of the redox alteration, rather than a result of it.

It is likely that these cells will respond differently to certain stress conditions, compared to the control fibroblasts. Altered NAD^+:NADH and a more reduced CoQ pool may affect how effectively the cell can respond to oxidative or hypoxic stress. Investigating this, in conjunction with determining the mutational cause of the phenotype could shed light on cellular processes which extend beyond the model used here. Recently, the possibility of a role for PDSS1 in hypoxic cancer cells has been proposed[209]. If this mutation was determined to be functional, this research could inform studies into this relationship.

The metabolism of fatty acids should also be investigated, considering the likely effects of loss of CoQ reducing potential in the mitochondria for fatty acid oxidation, and the considerable overlap in phenotype with fatty acid oxidation disorders. It would also be important to investigate the substrates and products of the other mitochondrial reactions which require CoQ as an electron acceptor. For example, supplementation with pyrimidines.

In conclusion, further research is needed to establish the role of this PDSS1 mutation in the patient phenotype, with the aim of informing treatment strategies.

4.4 Materials and Methods

4.4.1 Cell Culture

Fibroblasts from the patient with a suspected inborn error of metabolism were received in culture from the Human Biomaterials Resource Centre at the University of Birmingham. Fibroblasts were released under the Research Tissue Bank ethical approval (NRES Committee North West Haydock 20/NW/0001), under project reference 19-346 Tennant. NHDFs (C-12302) were purchased from PromoCell. Both were maintained in RPMI with 10% FBS, and 1% Penicillin-streptomycin, at 37°C in 5% CO_2 and passaged when they reached 70-80% confluency. Cells were used for experiments until no later than passage 10.

4.4.2 RNA Extraction and PCR

Cells were plated 24 hours before, to be 80% confluent for processing. Cells were lysed in 350μl buffer RLT (Qiagen). Samples were then homogenised to maximise RNA yield using the QIAshredder kit (Qiagen, 79656). RNA was then extracted with the RNeasy mini kit (Qiagen, 74104), RNA concentration were checked using a NanoDrop (Thermo Scientific, ND-2000). RNA was then converted to cDNA using the Promega Reverse Transcription M-MLV system (Promega, A3500), according to the manufacturers protocol. The PCR reaction was carried out using the Q5 high-fidelity DNA polymerase kit from New England Biolabs (E0555S/L), again according to included instructions.

Primer number	Forward	Reverse
Pair 1	GACTCCGACCATGGCCTC	AGTCCCTTCCGCCTATGAAC
Pair 2	GTTCATAGGCGGAAGGGAC	CGAGTTTGAAAGGATCGGTGT
Pair 3	ACTGCTAGTCTGGTTCACGA	CACCACGCACCAAATCTTCA

Table 4.1: Primer Information

Samples were then run through a 2% agarose gel with Gel Red at 100V for 45 minutes. The gel was then imaged with a ChemiDoc-MP system (BioRad).

4.4.3 Western Blotting

Cells were plated in a 6 well plate, to be 70-80% confluent for protein collection after 24 hours. The media was first removed, and wells were washed with 1x PBS, before scraping into Laemmli buffer. Samples were then boiled for ten minutes, before vortexing and centrifuging. Samples were run through a 10% SDS-polyacrylamide gel at 120V for 1 hour. Proteins were then transferred to a nitrocellulose membrane via an iBlot 2 transfer system (Thermo Fisher). Membranes were then blocked in 5% bovine serum albumin (BSA) for 1 hour. The primary antibody was then incubated overnight, before washing with PBS-T and 1 hour incubation with the secondary antibody. Antibody details are including in Table 4.2. After more washing, ECL Western Blotting substate was added to the membrane before imaging with a ChemiDoc-MP system (BioRad).

Target Protein	Molecular Weight	Host	Dilution	Catalogue number
B-Tubulin	55kDa	Rabbit	1:5000	Cell Signalling 2146
PDSS1	46	Rabbit	1:100	Sigma-Aldrich HPA038032

Table 4.2: Antibody Information

4.4.4 Metabolite Extraction for GCMS

Cells were plated 24 hours prior to the addition of the tracing medium, to be 80% confluent at the time of extraction. The plating medium was removed and wells were washed with sterile PBS. DMEM with no glucose, no glutamine or phenol red was used as a base medium. To this, 5 or 10% (again, depending on the cell line) dialysed FBS was added, with 10mM glucose and 2mM glutamine, using fully heavy isotope labeled where required.

Metabolite extraction was carried out on ice throughout. Media was removed before washing twice with 0.9% saline. 500μl pre-chilled methanol was added, with 200μl pentanedioic-d6 acid (CDN isotopes, D-5227) in LCMS grade water. This was scraped and collected, before the addition of 500μl pre-cooled chloroform. Tubes were vortexed for 10 seconds and centrifuged at 13,000 rpm for 10 minutes. The top (polar) layer was transferred to a fresh tube and dried in a vacuum centrifuge.

Samples were derivatized by reconstitution in 40μl 2% methoxamine in pyridine, followed by vortexing and heating at 60°C for 1 hour, addition of 50μl N-tert-Butyldimethylsilyl-

N-methyltrifluoroacetamide with 1% tert-Butyldimethylchlorosilane, and another hour at 60°C. 80μl of each sample was then transferred to glass GCMC vials.

4.4.5 Gas Chromatography Mass Spectroscopy

1μl of sample was injected in splitless mode, using helium as a carrier gas at a rate of 1ml/minute. The GC oven temperature was 100°C for 1 minute, before ramping to 160°C at 10°C/minute, then to 200°C at 5°C/minute and finally to 320 °C at 10°C/minute and a 5 minute hold. Detection was carried out in scan mode. D^6-Glutaric acid was used as an internal standard. Data were analysed using a MatLab script, kindly shared by the Fendt Lab.

4.4.6 CoQ Extraction for Liquid Chromatography Mass Spectroscopy (LCMS)

Cells were plated in 6 well plates to be 80-90% confluent on the day of extraction. Media was removed and cells were washed with x1 PBS. All following steps were carried out on ice. 250μl acidified methanol (UHPLC (ultra high performance liquid chromatography)-grade methanol with 0.1% w/v hydrochloric acid and 1nM CoQ4-one) was added to the well before scraping and transfer to an eppendorf tube. 250μl ice cold UHPLC-grade water and 500μl hexane were added to the tube before vortexing for 10 second, 3 times. Samples were then centrifuged at 4C for 5 minutes. The top (hexane) layer was transferred to a glass tube and dried under nitrogen without heating. The dried extract was re-suspended in 100μl methanol and running buffer (methanol and 2mM ammonium formate). Samples were then transferred to glass vials and run immediately on the LCMS.

4.4.7 Liquid Chromatography Mass Spectroscopy

Samples were run on a Waters Xevo TQ-XS instrument by Dr Adam Boufersaoui. CoQ_4 was used as an internal standard, values were normalised to this and to cell number.

4.4.8 Sulforhodamine B assay

100μl 20% trichloracetic acid was added to the medium and incubated at 4°C for 30 minutes. This was then removed and wells were washed 3 x with tap water and left to dry. Once dry, wells were covered with 0.4% sulforhodamine B (Sigma, 230162) and incubated at 10°C at RT. This was removed and well were washed with 1% acetic acid and wells were allowed to dry again. The stain was dissolved using 50mM pH8.8 Tris, and samples were transferred to a 96 well plate, to be read on a platereader at 510nm.

Chapter Five

Conclusions

5.1 Introduction

The ways in which cells maintain their mitochondrial redox homeostasis are integral to continued proliferation and cell survival when this balance is challenged. This work aims to investigate mitochondrial redox in several contexts. Firstly, it sets out to address the hypothesis that proline synthesis is increased in hypoxia in order to regenerate NAD^+, thereby maintaining an NAD^+:NADH ratio which is more favourable for TCA cycle activity. The role of PYCR1 in this context is also investigated *in vivo* using core needle biopsy samples and machine learning driven analysis of spatially resolved protein expression. Finally, a potential inborn error of metabolism: suspected loss of function one of the enzymes involved in the synthesis of the redox-active compound, CoQ_{10}, is investigated.

5.2 Summary of Key Findings

The data presented in Chapter 2 support the hypothesis that PYCR1 activity is increased in hypoxic cells, and that this activity supports the continued activity of the TCA cycle under these conditions. Furthermore, this work shows that the proline produced through PYCR1 in hypoxia is in excess of cellular demands and is exported into the medium of cells in culture. The induction of loss of PYCR1 in established xenografts leads to significant cell death and necrosis, with an increase in hypoxia and hypoxic signalling. Taken together, these data suggest the PYCR1 activity is redox modulatory, and supports the survival of

cells in tumours, particularly in response to hypoxia.

Investigations using a set of core needle biopsy samples, detailed in Chapter 3, show the majority of tumour cells express PYCR1, while the majority of cells in the stroma do not. This work also find that CA9 and collagen are more likely to be expressed by tumour cells than by stromal cells. Furthermore, PYCR1 expression is more likely to be seen in hypoxic tumour regions than in tumour cells which do not express CA9. This supports the findings from Chapter 2, further suggesting that PYCR1 expression confers a survival advantage in hypoxic tumour cells.

Finally, Chapter 3 covers an investigation into the phenotype of fibroblasts from a patient with a suspected inborn error of CoQ_{10} synthesis, and the potential redox implications of this. From this data, is is still unclear whether the structure or function of PDSS1 are affected in this patient. However, alterations to the CoQ_{10} and CoQ_9 pools are detected, and metabolic tracing suggests a perturbed mitochondrial redox balance.

5.3 Discussion

The data presented in Chapters 2 and 3 add to the wealth of literature which presents a role for amino acid metabolism which goes beyond their use as a fuel source or as building blocks for protein synthesis.

The role of proline metabolism in cancer cell biology has been increasingly researched over the last few years, with associations made to anchorage independant growth[130], ECM interaction[127,133], signalling pathways[135,225] and redox[127,159]. Accordingly, this has lead to interest in targeting proline synthetic enzymes as a potential therapeutic strategy. Work presented here demonstrates a further role for proline biosynthesis through PYCR1 in redox regulation, which is particularly important in hypoxia. Additionally, the *in vivo* work shows that loss of PYCR1 in established xenografts leads to a significant increase in the necrotic tumour area of establish xenografts. This may suggest that inhibition of PYCR1 could be an option to reduce tumour volume in hypoxic tumours, perhaps in combination with current chemotherapy.

However, the regions which remain after PYCR1 knockdown in xenografts show an

increase in hypoxia and hypoxic signalling. This residual population of cells is therefore likely to exhibit the features of hypoxic tumour cells which are the reason they are such an important research focus, including increased metastatic potential and radio-resistance. This is an important consideration for any potential future studies investigating PYCR1 inhibition.

Furthermore, the additional burden of a large increase in necrotic area should be considered. In this study, after 24 hours of knockdown, the percentage of the xenograft which was necrotic was approximately doubled. Although small-molecule inhibition of PYCR1 is not likely to illicit such as large change, care should be taken to avoid potential toxicity from large-scale cell lysis.

Additionally, the lack of sufficient vascularisation which occurs in and contributes to tumour hypoxia, may hamper delivery of a small-molecule inhibitor of PYCR1 to the cells of the tumour which are most likely to be sensitive.

Notably, this work describes a role for PYCR1, but not PYCR2 in this system. Similarly, PYCR1 is implicated in the response to redox stress upon TGFβ stimulation[127], with PYCR2 not shown to affect this. Given the similarity in structure, function and cellular location of these two isozymes, the specificity of their roles is particularly interesting. Given that proline supplementation does not rescue the growth defect in PYCR1 KO cells, it may be that PYCR2 or PYCRL is the main isozyme responsible for proline synthesis for proteins. More research into the regulation of flux through either of these branches of the proline synthesis pathway is worth of further investigation. Additionally, this should be considered as inhibitors of PYCR1 are beginning to be developed and tested.

The regulation of proline export mechanisms in hypoxia is also highlighted here, as the majority of proline synthesised in hypoxia is exported to the media. Across most samples in most cell lines, an increase in intracellular proline is seen at 1% O_2, which drops off at 0.3%. In the medium, at 1% the proline level is often very variable, but consistently increased at 0.3%. This may suggest an export mechanism which is responsive, either to high levels of intracellular proline, or in fact to the oxygen tension. It would be interesting to assess proline levels in the mitochondria, the cytosol and the medium at differing oxygen tensions, with the hope of determining if either a mitochondrial or plasma membrane transported is responsive to oxygen tension. The plasma membrane proline transporter are known, however

there is as yet no established mitochondrial proline transporter.

The increased export of proline is likely to affect the microenvironment surrounding hypoxic cells. In Chapter 3, the expression of PYCR1 could not be correlated with collagen. However, we cannot infer anything about the activity of PYCR1 in these cells from this data. In light of recently published data which defines a role for PYCR1 in collagen production by CAFs[179], it would be interesting to assess the effect of hypoxia in this model. It also seems likely that increased proline availability in the ECM could be up-taken by CAFs and used to produce collagen. Co-culture experiments with tumour cells and CAFs in differing oxygen tensions, using fully labelled glutamine and monitoring labelling into collagen, could begin to explore this relationship.

Recently, the possibility of selectively removing amino acids from the diet as a therapeutic strategy has started to be explored. Serine starvation has been shown to reduce the growth of xenografts[90], and to sensitise them to radiotherapy[226]. Indeed, selective proline starvation has been found to impact tumourigenesis in one study[119]. Data presented in this thesis appears to suggest that a lack of dietary proline is unlikely to affect the redox regulatory effect of proline synthesis in hypoxia, where it appears that cells synthesise proline in excess of their requirements. It may be that the importance of systemic proline levels vary at different stages of tumour progression, depending on genetic and microenvironmental factors. Additionally, it is interesting to note that in patients with germline mutations in both PYCR1 and PYCR2 have blood proline levels which fall within the normal range, despite having lost a significant source of proline synthesis[124,148]. This may suggest that blood proline levels are kept under tighter regulation that we yet appreciate. PYCR1 loss leads to significant issue with the connective tissue, which is rich in collagen. Collagen is a source of proline, which may be available to compensate for a lack of synthesis, or potentially a lack of intake of proline. The long-term effects of proline starvation are yet to be investigated.

Finally, this work also uncovers a metabolic phenotype associated with a perturbed NAD^+:NADH ratio in fibroblasts from a patient with a potential inborn error of CoQ_{10} synthesis. Although this work was unable to conclude whether the identified mutation was the cause of Patient Ms symptoms, this dysregulated redox balance is a starting point for further investigations. This work predicts that there may be issues with fatty acid oxidation, which correspond with the patients symptoms. It is hoped that further investigations can inform the management of Patient Ms symptoms. If the PDSS1 mutation is shown to

affect the enzyme function, definitively, these cells will also be a useful model in further understanding the relationship between CoQ_{10}, redox regulation and fatty acid oxidation. This is a relationship which seems likely to be important in cancer cells.

5.4 Concluding Remarks

Work presented here further demonstrates the importance of redox regulation. Metabolites often considered as the main products of metabolic reactions may not, in some circumstances, be as important as the co-factors which the reaction generates. This is the case for proline synthesis in hypoxia, which produces proline at a level which exceeds the cellular demand.

This work contributes to the current understanding of proline metabolism, and how this is altered in response to different conditions. It also raises further questions about the impact of potentially increased extracellular proline levels in the hypoxic niche. Importantly, it also shows that hypoxia is increased in the residual cells after PYCR1 loss in xenografts, which is an important consideration for inhibitor development.

Finally, it is hoped that the data shown in Chapter 4 can be built on, to better understand Patients Ms disorder, with the aim of improving his quality of life.

References

[1] Archibald E. Garrod. "The Croonian Lectures ON INBORN ERRORS OF METABOLISM." In: *The Lancet* 172.4427 (July 1908), pp. 1–7. ISSN: 0140-6736. DOI: 10.1016/S0140-6736(01)78482-6.

[2] Barton Childs, David Valle, and Gerardo Jimenez-Sanchez. "The Inborn Error and Biochemical Individuality". In: *The Online Metabolic and Molecular Bases of Inherited Disease*. Ed. by David L Valle et al. New York, NY: McGraw-Hill Education, Aug. 2019. URL: http://ommbid.mhmedical.com/content.aspx?aid=1181400767.

[3] Ralph J. Deberardinis and Craig B. Thompson. "Cellular metabolism and disease: what do metabolic outliers teach us?" In: *Cell* 148.6 (Mar. 2012), p. 1132. ISSN: 10974172. DOI: 10.1016/J.CELL.2012.02.032. URL: /pmc/articles/PMC3337773/%20/pmc/articles/PMC3337773/?report=abstract%20https://www.ncbi.nlm.nih.gov/pmc/articles/PMC3337773/.

[4] Douglas Hanahan and Robert A. Weinberg. "Hallmarks of Cancer: The Next Generation". In: *Cell* 144.5 (Mar. 2011), pp. 646–674. ISSN: 0092-8674. DOI: 10.1016/J.CELL.2011.02.013.

[5] Willem H. Koppenol, Patricia L. Bounds, and Chi V. Dang. "Otto Warburg's contributions to current concepts of cancer metabolism". In: *Nature reviews. Cancer* 11.5 (May 2011), pp. 325–337. ISSN: 1474-1768. DOI: 10.1038/NRC3038. URL: https://pubmed.ncbi.nlm.nih.gov/21508971/.

[6] Otto Warburg. "On the origin of cancer cells". In: *Science (New York, N.Y.)* 123.3191 (1956), pp. 309–314. ISSN: 0036-8075. DOI: 10.1126/SCIENCE.123.3191.309. URL: https://pubmed.ncbi.nlm.nih.gov/13298683/.

[7] R. J. Deberardinis and T. Cheng. "Q's next: the diverse functions of glutamine in metabolism, cell biology and cancer". In: *Oncogene* 29.3 (Jan. 2010), pp. 313–324. ISSN: 1476-5594. DOI: 10.1038/ONC.2009.358. URL: https://pubmed.ncbi.nlm.nih.gov/19881548/.

[8] Johannes V. Swinnen, Koen Brusselmans, and Guido Verhoeven. "Increased lipogenesis in cancer cells: new players, novel targets". In: *Current opinion in clinical nutrition and metabolic care* 9.4 (July 2006), pp. 358–365. ISSN: 1363-1950. DOI: 10.1097/01.MCO.0000232894.28674.30. URL: https://pubmed.ncbi.nlm.nih.gov/16778563/.

[9] Russell G. Jones and Craig B. Thompson. "Tumor suppressors and cell metabolism: a recipe for cancer growth". In: *Genes & development* 23.5 (Mar. 2009), pp. 537–548. ISSN: 1549-5477. DOI: 10.1101/GAD.1756509. URL: https://pubmed.ncbi.nlm.nih.gov/19270154/.

[10] Fabiana Schwartzenberg-Bar-Yoseph, Michai Armoni, and Eddy Karnieli. "The Tumor Suppressor p53 Down-Regulates Glucose Transporters GLUT1 and GLUT4 Gene Expression". In: *Cancer Research* 64.7 (Apr. 2004), pp. 2627–2633. ISSN: 0008-5472. DOI: 10.1158/0008-5472.CAN-03-0846. URL: https://aacrjournals.org/cancerres/article/64/7/2627/512513/The-Tumor-Suppressor-p53-Down-Regulates-Glucose.

[11] Karen H. Vousden and Kevin M. Ryan. "p53 and metabolism". In: *Nature Reviews Cancer 2009 9:10* 9.10 (Sept. 2009), pp. 691–700. ISSN: 1474-1768. DOI: 10.1038/nrc2715. URL: https://www.nature.com/articles/nrc2715.

[12] Javier Garcia-Bermudez et al. "Aspartate is a limiting metabolite for cancer cell proliferation under hypoxia and in tumours". In: *Nature Cell Biology 2018 20:7* 20.7 (June 2018), pp. 775–781. ISSN: 1476-4679. DOI: 10.1038/s41556-018-0118-z. URL: https://www.nature.com/articles/s41556-018-0118-z.

[13] Lucas B. Sullivan et al. "Supporting Aspartate Biosynthesis Is an Essential Function of Respiration in Proliferating Cells". In: *Cell* 162.3 (Aug. 2015), pp. 552–563. ISSN: 10974172. DOI: 10.1016/J.CELL.2015.07.017/ATTACHMENT/4F109938-55F4-41B1-A625-0907134FE486/MMC1.PDF. URL: http://www.cell.com/article/S0092867415008545/fulltext%20http://www.cell.com/article/S0092867415008545/abstract%20https://www.cell.com/cell/abstract/S0092-8674(15)00854-5.

[14] Caroline R. Bartman et al. "Slow TCA flux and ATP production in primary solid tumours but not metastases". In: *Nature 2023* (Feb. 2023), pp. 1–9. ISSN: 1476-4687. DOI: 10.1038/s41586-022-05661-6. URL: https://www.nature.com/articles/s41586-022-05661-6.

[15] B E Baysal and E Baysal. "Clinical and molecular progress in hereditary paraganglioma". In: *Journal of Medical Genetics* 45.11 (Nov. 2008), pp. 689–694. ISSN: 0022-2593. DOI: 10.1136/JMG.2008.058560. URL: https://jmg.bmj.com/content/45/11/689%20https://jmg.bmj.com/content/45/11/689.abstract.

[16] Sungwoo Lee et al. "Neuronal apoptosis linked to EglN3 prolyl hydroxylase and familial pheochromocytoma genes: Developmental culling and cancer". In: *Cancer Cell* 8.2 (Aug. 2005), pp. 155–167. ISSN: 1535-6108. DOI: 10.1016/J.CCR.2005.06.015.

[17] Mary A. Selak et al. "Succinate links TCA cycle dysfunction to oncogenesis by inhibiting HIF-α prolyl hydroxylase". In: *Cancer Cell* 7.1 (Jan. 2005), pp. 77–85. ISSN: 1535-6108. DOI: 10.1016/J.CCR.2004.11.022.

[18] Hai Yan et al. "IDH1 and IDH2 Mutations in Gliomas ". In: *New England Journal of Medicine* 360.8 (Feb. 2009), pp. 765–773. ISSN: 0028-4793. DOI: 10.1056/NEJMOA0808710/SUPPL{_}FILE/NEJM{_}YAN{_}765SA1.PDF. URL: https://www.nejm.org/doi/full/10.1056/NEJMoa0808710.

[19] Lenny Dang et al. "Cancer-associated IDH1 mutations produce 2-hydroxyglutarate". In: *Nature* 462.7274 (Dec. 2009), pp. 739–744. ISSN: 1476-4687. DOI: 10.1038/NATURE08617. URL: https://pubmed.ncbi.nlm.nih.gov/19935646/.

[20] Tahira Batool et al. "A Comprehensive Review on l-Asparaginase and Its Applications". In: *Applied Biochemistry and Biotechnology* 178.5 (Mar. 2016), pp. 900–923. ISSN: 15590291. DOI: 10.1007/S12010-015-1917-3/FIGURES/2. URL: https://link.springer.com/article/10.1007/s12010-015-1917-3.

[21] Christian Frezza et al. "Haem oxygenase is synthetically lethal with the tumour suppressor fumarate hydratase". In: *Nature* 477.7363 (Sept. 2011), pp. 225–228. ISSN: 1476-4687. DOI: 10.1038/NATURE10363. URL: https://pubmed.ncbi.nlm.nih.gov/21849978/.

[22] Aaron M. Hosios and G. Vander Heiden Matthew. "The redox requirements of proliferating mammalian cells". In: *Journal of Biological Chemistry* 293.20 (May 2018), pp. 7490–7498. ISSN: 0021-9258. DOI: 10.1074/JBC.TM117.000239. URL: http:

//www.jbc.org/article/S0021925820369490/fulltext%20http://www.jbc.org/article/S0021925820369490/abstract%20https://www.jbc.org/article/S0021-9258(20)36949-0/abstract.

[23] Jonathan L. Coloff et al. "Differential Glutamate Metabolism in Proliferating and Quiescent Mammary Epithelial Cells". In: *Cell Metabolism* 23.5 (May 2016), pp. 867–880. ISSN: 19327420. DOI: 10.1016/J.CMET.2016.03.016/ATTACHMENT/DE6CD6FF-1B04-414C-8DC8-0039376446A5/MMC2.XLSX. URL: http://www.cell.com/article/S155041311630119X/fulltext%20http://www.cell.com/article/S155041311630119X/abstract%20https://www.cell.com/cell-metabolism/abstract/S1550-4131(16)30119-X.

[24] Xuegang Yuan et al. "NAD+/NADH redox alterations reconfigure metabolism and rejuvenate senescent human mesenchymal stem cells in vitro". In: *Communications Biology 2020 3:1* 3.1 (Dec. 2020), pp. 1–15. ISSN: 2399-3642. DOI: 10.1038/s42003-020-01514-y. URL: https://www.nature.com/articles/s42003-020-01514-y.

[25] Maria V. Liberti and Jason W. Locasale. "The Warburg Effect: How Does it Benefit Cancer Cells?" In: *Trends in biochemical sciences* 41.3 (Mar. 2016), p. 211. ISSN: 13624326. DOI: 10.1016/J.TIBS.2015.12.001. URL: /pmc/articles/PMC4783224/%20/pmc/articles/PMC4783224/?report=abstract%20https://www.ncbi.nlm.nih.gov/pmc/articles/PMC4783224/.

[26] Otto Warburg, Franz Wind, and Erwin Negelein. "THE METABOLISM OF TUMORS IN THE BODY". In: *The Journal of General Physiology* 8.6 (Mar. 1927), p. 519. ISSN: 15407748. DOI: 10.1085/JGP.8.6.519. URL: https://www.ncbi.nlm.nih.gov/pmc/articles/PMC2140820/.

[27] Riekelt H. Houtkooper et al. "The Secret Life of NAD+: An Old Metabolite Controlling New Metabolic Signaling Pathways". In: *Endocrine Reviews* 31.2 (Apr. 2010), pp. 194–223. ISSN: 0163-769X. DOI: 10.1210/ER.2009-0026. URL: https://academic.oup.com/edrv/article/31/2/194/2354747.

[28] Huai Qiang Ju et al. "NADPH homeostasis in cancer: functions, mechanisms and therapeutic implications". In: *Signal Transduction and Targeted Therapy 2020 5:1* 5.1 (Oct. 2020), pp. 1–12. ISSN: 2059-3635. DOI: 10.1038/s41392-020-00326-0. URL: https://www.nature.com/articles/s41392-020-00326-0.

[29] Amit V. Pandey and Christa E. Flück. "NADPH P450 oxidoreductase: Structure, function, and pathology of diseases". In: *Pharmacology & Therapeutics* 138.2 (May 2013), pp. 229–254. ISSN: 0163-7258. DOI: 10.1016/J.PHARMTHERA.2013.01.010.

[30] Claudia Rita Corso and Alexandra Acco. "Glutathione system in animal model of solid tumors: From regulation to therapeutic target". In: *Critical Reviews in Oncology/Hematology* 128 (Aug. 2018), pp. 43–57. ISSN: 1040-8428. DOI: 10.1016/J.CRITREVONC.2018.05.014.

[31] Jean Francois Collet and Joris Messens. "Structure, Function, and Mechanism of Thioredoxin Proteins". In: *https://home.liebertpub.com/ars* 13.8 (Aug. 2010), pp. 1205–1216. ISSN: 15230864. DOI: 10.1089/ARS.2010.3114. URL: https://www.liebertpub.com/doi/abs/10.1089/ars.2010.3114.

[32] H. N. Kirkman and G. F. Gaetani. "Catalase: a tetrameric enzyme with four tightly bound molecules of NADPH." In: *Proceedings of the National Academy of Sciences of the United States of America* 81.14 (1984), p. 4343. ISSN: 00278424. DOI: 10.1073/PNAS.81.14.4343. URL: /pmc/articles/PMC345585/?report=abstract%20https://www.ncbi.nlm.nih.gov/pmc/articles/PMC345585/.

[33] Peter C. Hinkle. "P/O ratios of mitochondrial oxidative phosphorylation". In: *Biochimica et biophysica acta* 1706.1-2 (Jan. 2005), pp. 1–11. ISSN: 0006-3002. DOI: 10.1016/J.BBABIO.2004.09.004. URL: https://pubmed.ncbi.nlm.nih.gov/15620362/.

[34] Hongying Yang et al. "Nutrient-Sensitive Mitochondrial NAD+ Levels Dictate Cell Survival". In: *Cell* 130.6 (Sept. 2007), pp. 1095–1107. ISSN: 0092-8674. DOI: 10.1016/J.CELL.2007.07.035.

[35] Yuzheng Zhao et al. "Genetically encoded fluorescent sensors for intracellular NADH detection". In: *Cell Metabolism* 14.4 (Oct. 2011), pp. 555–566. ISSN: 15504131. DOI: 10.1016/J.CMET.2011.09.004/ATTACHMENT/7D30CACF-3307-46BE-B327-EA6F0B0ED2C0/MMC1.PDF. URL: http://www.cell.com/article/S1550413111003500/fulltext%20http://www.cell.com/article/S1550413111003500/abstract%20https://www.cell.com/cell-metabolism/abstract/S1550-4131(11)00350-0.

[36] Lucas B. Sullivan et al. "Supporting Aspartate Biosynthesis Is an Essential Function of Respiration in Proliferating Cells". In: *Cell* 162.3 (July 2015), pp. 552–563. ISSN: 0092-8674. DOI: 10.1016/J.CELL.2015.07.017.

[37] Hai Yan et al. “IDH1 and IDH2 mutations in gliomas”. In: *The New England journal of medicine* 360.8 (Feb. 2009), pp. 765–773. ISSN: 1533-4406. DOI: 10.1056/NEJMOA0808710. URL: https://pubmed.ncbi.nlm.nih.gov/19228619/.

[38] Hai Yan et al. “IDH1 and IDH2 mutations in gliomas”. In: *The New England journal of medicine* 360.8 (Feb. 2009), pp. 765–773. ISSN: 1533-4406. DOI: 10.1056/NEJMOA0808710. URL: https://pubmed.ncbi.nlm.nih.gov/19228619/%20https://pubmed.ncbi.nlm.nih.gov/19228619/?dopt=Abstract.

[39] Sotirios Bisdas et al. “MR spectroscopy for in vivo assessment of the oncometabolite 2-hydroxyglutarate and its effects on cellular metabolism in human brain gliomas at 9.4T”. In: *Journal of magnetic resonance imaging : JMRI* 44.4 (Oct. 2016), pp. 823–833. ISSN: 1522-2586. DOI: 10.1002/JMRI.25221. URL: https://pubmed.ncbi.nlm.nih.gov/26970248/.

[40] Roberta Lugano, Mohanraj Ramachandran, and Anna Dimberg. “Tumor angiogenesis: causes, consequences, challenges and opportunities”. In: *Cellular and Molecular Life Sciences* 77.9 (May 2020), p. 1745. ISSN: 14209071. DOI: 10.1007/S00018-019-03351-7. URL: /pmc/articles/PMC7190605/%20/pmc/articles/PMC7190605/?report=abstract%20https://www.ncbi.nlm.nih.gov/pmc/articles/PMC7190605/.

[41] E. M. Hammond et al. “The Meaning, Measurement and Modification of Hypoxia in the Laboratory and the Clinic”. In: *Clinical Oncology* 26.5 (May 2014), pp. 277–288. ISSN: 0936-6555. DOI: 10.1016/J.CLON.2014.02.002. URL: http://www.clinicaloncologyonline.net/article/S0936655514000697/fulltext%20http://www.clinicaloncologyonline.net/article/S0936655514000697/abstract%20https://www.clinicaloncologyonline.net/article/S0936-6555(14)00069-7/abstract.

[42] Mahesh A. Varia et al. “Pimonidazole: a novel hypoxia marker for complementary study of tumor hypoxia and cell proliferation in cervical carcinoma”. In: *Gynecologic oncology* 71.2 (1998), pp. 270–277. ISSN: 0090-8258. DOI: 10.1006/GYNO.1998.5163. URL: https://pubmed.ncbi.nlm.nih.gov/9826471/.

[43] Rachel E. Airley et al. “GLUT-1 and CAIX as intrinsic markers of hypoxia in carcinoma of the cervix: relationship to pimonidazole binding”. In: *International journal of cancer* 104.1 (Mar. 2003), pp. 85–91. ISSN: 0020-7136. DOI: 10.1002/IJC.10904. URL: https://pubmed.ncbi.nlm.nih.gov/12532423/.

[44] R. K. Bruick and S. L. McKnight. "A conserved family of prolyl-4-hydroxylases that modify HIF". In: *Science* 294.5545 (Nov. 2001), pp. 1337–1340. ISSN: 00368075. DOI: 10.1126/SCIENCE.1066373/ASSET/C4259A48-5858-4C6D-8324-C080207838E7/ASSETS/GRAPHIC/SE4319914005.JPEG. URL: https://www.science.org/doi/full/10.1126/science.1066373.

[45] Andrew C.R. Epstein et al. "C. elegans EGL-9 and mammalian homologs define a family of dioxygenases that regulate HIF by prolyl hydroxylation". In: *Cell* 107.1 (Oct. 2001), pp. 43–54. ISSN: 0092-8674. DOI: 10.1016/S0092-8674(01)00507-4. URL: https://pubmed.ncbi.nlm.nih.gov/11595184/%20https://pubmed.ncbi.nlm.nih.gov/11595184/?dopt=Abstract.

[46] William G. Kaelin and Peter J. Ratcliffe. "Oxygen Sensing by Metazoans: The Central Role of the HIF Hydroxylase Pathway". In: *Molecular Cell* 30.4 (May 2008), pp. 393–402. ISSN: 1097-2765. DOI: 10.1016/J.MOLCEL.2008.04.009. URL: http://www.cell.com/article/S109727650800292X/fulltext%20http://www.cell.com/article/S109727650800292X/abstract%20https://www.cell.com/molecular-cell/abstract/S1097-2765(08)00292-X.

[47] Gregg L. Semenza. "Hypoxia-Inducible Factors in Physiology and Medicine". In: *Cell* 148.3 (Feb. 2012), p. 399. ISSN: 10974172. DOI: 10.1016/J.CELL.2012.01.021. URL: /pmc/articles/PMC3437543/%20/pmc/articles/PMC3437543/?report=abstract%20https://www.ncbi.nlm.nih.gov/pmc/articles/PMC3437543/.

[48] Gregg L. Semenza. "HIF-1: upstream and downstream of cancer metabolism". In: *Current opinion in genetics & development* 20.1 (Feb. 2010), p. 51. ISSN: 0959437X. DOI: 10.1016/J.GDE.2009.10.009. URL: /pmc/articles/PMC2822127/%20/pmc/articles/PMC2822127/?report=abstract%20https://www.ncbi.nlm.nih.gov/pmc/articles/PMC2822127/.

[49] Tariq Shah et al. "HIF isoforms have divergent effects on invasion, metastasis, metabolism and formation of lipid droplets". In: *Oncotarget* 6.29 (Sept. 2015), p. 28104. ISSN: 19492553. DOI: 10.18632/ONCOTARGET.4612. URL: /pmc/articles/PMC4695047/%20/pmc/articles/PMC4695047/?report=abstract%20https://www.ncbi.nlm.nih.gov/pmc/articles/PMC4695047/.

[50] Debbie Liao and Randall S. Johnson. "Hypoxia: a key regulator of angiogenesis in cancer". In: *Cancer metastasis reviews* 26.2 (June 2007), pp. 281–290. ISSN: 0167-

7659. DOI: 10.1007/S10555-007-9066-Y. URL: https://pubmed.ncbi.nlm.nih.gov/17603752/%20https://pubmed.ncbi.nlm.nih.gov/17603752/?dopt=Abstract.

[51] Liping Liu and M. C. Simon. "Regulation of transcription and translation by hypoxia". In: *Cancer biology & therapy* 3.6 (2004), pp. 492–497. ISSN: 1538-4047. DOI: 10.4161/CBT.3.6.1010. URL: https://pubmed.ncbi.nlm.nih.gov/15254394/.

[52] Laura A. Dada et al. "Hypoxia-induced endocytosis of Na,K-ATPase in alveolar epithelial cells is mediated by mitochondrial reactive oxygen species and PKC-zeta". In: *The Journal of clinical investigation* 111.7 (2003), pp. 1057–1064. ISSN: 0021-9738. DOI: 10.1172/JCI16826. URL: https://pubmed.ncbi.nlm.nih.gov/12671055/.

[53] Todd C. Carpenter et al. "Hypoxia reversibly inhibits epithelial sodium transport but does not inhibit lung ENaC or Na-K-ATPase expression". In: *American journal of physiology. Lung cellular and molecular physiology* 284.1 (Jan. 2003). ISSN: 1040-0605. DOI: 10.1152/AJPLUNG.00181.2002. URL: https://pubmed.ncbi.nlm.nih.gov/12388331/.

[54] Guy C. Brown and Chris E. Cooper. "Nanomolar concentrations of nitric oxide reversibly inhibit synaptosomal respiration by competing with oxygen at cytochrome oxidase". In: *FEBS letters* 356.2-3 (Dec. 1994), pp. 295–298. ISSN: 0014-5793. DOI: 10.1016/0014-5793(94)01290-3. URL: https://pubmed.ncbi.nlm.nih.gov/7805858/.

[55] Vivian Y. Lee et al. "Hypoxia sensitizes cells to nitric oxide-induced apoptosis". In: *The Journal of biological chemistry* 277.18 (May 2002), pp. 16067–16074. ISSN: 0021-9258. DOI: 10.1074/JBC.M111177200. URL: https://pubmed.ncbi.nlm.nih.gov/11861645/.

[56] Emilio Clementi et al. "On the mechanism by which vascular endothelial cells regulate their oxygen consumption". In: *Proceedings of the National Academy of Sciences of the United States of America* 96.4 (Feb. 1999), pp. 1559–1562. ISSN: 0027-8424. DOI: 10.1073/PNAS.96.4.1559. URL: https://pubmed.ncbi.nlm.nih.gov/9990063/.

[57] Ryo Fukuda et al. "HIF-1 Regulates Cytochrome Oxidase Subunits to Optimize Efficiency of Respiration in Hypoxic Cells". In: *Cell* 129.1 (Apr. 2007), pp. 111–122. ISSN: 0092-8674. DOI: 10.1016/J.CELL.2007.01.047.

[58] Dominik C. Fuhrmann and Bernhard Brüne. "Mitochondrial composition and function under the control of hypoxia". In: *Redox Biology* 12 (Aug. 2017), pp. 208–215. ISSN: 2213-2317. DOI: 10.1016/J.REDOX.2017.02.012.

[59] Joslyn K. Brunelle et al. "Oxygen sensing requires mitochondrial ROS but not oxidative phosphorylation". In: *Cell Metabolism* 1.6 (June 2005), pp. 409–414. ISSN: 1550-4131. DOI: 10.1016/J.CMET.2005.05.002.

[60] Robert D. Guzy et al. "Mitochondrial complex III is required for hypoxia-induced ROS production and cellular oxygen sensing". In: *Cell Metabolism* 1.6 (June 2005), pp. 401–408. ISSN: 15504131. DOI: 10.1016/j.cmet.2005.05.001. URL: http://www.cell.com/article/S1550413105001397/fulltext%20http://www.cell.com/article/S1550413105001397/abstract%20https://www.cell.com/cell-metabolism/abstract/S1550-4131(05)00139-7.

[61] K L Eales, K E R Hollinshead, and D A Tennant. "Hypoxia and metabolic adaptation of cancer cells". In: *Oncogenesis 2016 5:1* 5.1 (Jan. 2016), e190–e190. ISSN: 2157-9024. DOI: 10.1038/oncsis.2015.50. URL: https://www.nature.com/articles/oncsis201550.

[62] Mohammed S. Ullah, Andrew J. Davies, and Andrew P. Halestrap. "The plasma membrane lactate transporter MCT4, but not MCT1, is up-regulated by hypoxia through a HIF-1alpha-dependent mechanism". In: *The Journal of biological chemistry* 281.14 (Apr. 2006), pp. 9030–9037. ISSN: 0021-9258. DOI: 10.1074/JBC.M511397200. URL: https://pubmed.ncbi.nlm.nih.gov/16452478/%20https://pubmed.ncbi.nlm.nih.gov/16452478/?dopt=Abstract.

[63] Jessica B. Spinelli et al. "Fumarate is a terminal electron acceptor in the mammalian electron transport chain". In: *Science (New York, N.Y.)* 374.6572 (Dec. 2021), p. 1227. ISSN: 10959203. DOI: 10.1126/SCIENCE.ABI7495. URL: /pmc/articles/PMC8803114/%20/pmc/articles/PMC8803114/?report=abstract%20https://www.ncbi.nlm.nih.gov/pmc/articles/PMC8803114/.

[64] Zachary T. Schafer et al. "Antioxidant and oncogene rescue of metabolic defects caused by loss of matrix attachment". In: *Nature* 461.7260 (Sept. 2009), pp. 109–113. ISSN: 1476-4687. DOI: 10.1038/NATURE08268. URL: https://pubmed.ncbi.nlm.nih.gov/19693011/.

[65] Mark A. Hawk and Zachary T. Schafer. "Mechanisms of redox metabolism and cancer cell survival during extracellular matrix detachment". In: *The Journal of biological chemistry* 293.20 (May 2018), pp. 7531–7537. ISSN: 1083-351X. DOI: 10.1074/JBC.TM117.000260. URL: https://pubmed.ncbi.nlm.nih.gov/29339552/.

[66] Abraham Q. Kohrman and David Q. Matus. "Divide or Conquer: Cell Cycle Regulation of Invasive Behavior". In: *Trends in cell biology* 27.1 (Jan. 2017), pp. 12–25. ISSN: 1879-3088. DOI: 10.1016/J.TCB.2016.08.003. URL: https://pubmed.ncbi.nlm.nih.gov/27634432/.

[67] David Q. Matus et al. "Invasive Cell Fate Requires G1 Cell-Cycle Arrest and Histone Deacetylase-Mediated Changes in Gene Expression". In: *Developmental cell* 35.2 (Oct. 2015), pp. 162–174. ISSN: 1878-1551. DOI: 10.1016/J.DEVCEL.2015.10.002. URL: https://pubmed.ncbi.nlm.nih.gov/26506306/.

[68] Jessalyn M. Ubellacker et al. "Lymph protects metastasizing melanoma cells from ferroptosis". In: *Nature* 585.7823 (Sept. 2020), pp. 113–118. ISSN: 1476-4687. DOI: 10.1038/S41586-020-2623-Z. URL: https://pubmed.ncbi.nlm.nih.gov/32814895/.

[69] Yu Zheng et al. "Expression of β-globin by cancer cells promotes cell survival during blood-borne dissemination". In: *Nature communications* 8 (Feb. 2017). ISSN: 2041-1723. DOI: 10.1038/NCOMMS14344. URL: https://pubmed.ncbi.nlm.nih.gov/28181495/.

[70] Alpaslan Tasdogan, Jessalyn M. Ubellacker, and Sean J. Morrison. "Redox regulation in cancer cells during metastasis". In: *Cancer discovery* 11.11 (Nov. 2021), p. 2682. ISSN: 21598290. DOI: 10.1158/2159-8290.CD-21-0558. URL: /pmc/articles/PMC8563381/%20/pmc/articles/PMC8563381/?report=abstract%20https://www.ncbi.nlm.nih.gov/pmc/articles/PMC8563381/.

[71] Elena Piskounova et al. "Oxidative stress inhibits distant metastasis by human melanoma cells". In: *Nature 2015 527:7577* 527.7577 (Oct. 2015), pp. 186–191. ISSN: 1476-4687. DOI: 10.1038/nature15726. URL: https://www.nature.com/articles/nature15726.

[72] Mariana F. Rodrigues et al. "Enhanced OXPHOS, glutaminolysis and β-oxidation constitute the metastatic phenotype of melanoma cells". In: *Biochemical Journal* 473.6 (Mar. 2016), pp. 703–715. ISSN: 0264-6021. DOI: 10.1042/BJ20150645. URL: /biochemj/article/473/6/703/49376/Enhanced-OXPHOS-glutaminolysis-and-oxidation%20https://portlandpress.com/biochemj/article/473/6/703/49376/Enhanced-OXPHOS-glutaminolysis-and-oxidation.

[73] Brian J. Dillon et al. "Incidence and distribution of argininosuccinate synthetase deficiency in human cancers". In: *Cancer* 100.4 (Feb. 2004), pp. 826–833. ISSN: 1097-0142. DOI: 10.1002/CNCR.20057. URL: https://onlinelibrary.wiley.com/doi/full/10.1002/

cncr.20057%20https://onlinelibrary.wiley.com/doi/abs/10.1002/cncr.20057%20https://acsjournals.onlinelibrary.wiley.com/doi/10.1002/cncr.20057.

[74] Peter W. Szlosarek et al. "In vivo Loss of Expression of Argininosuccinate Synthetase in Malignant Pleural Mesothelioma Is a Biomarker for Susceptibility to Arginine Depletion". In: *Clinical Cancer Research* 12.23 (Dec. 2006), pp. 7126–7131. ISSN: 1078-0432. DOI: 10.1158/1078-0432.CCR-06-1101. URL: https://aacrjournals.org/clincancerres/article/12/23/7126/191717/In-vivo-Loss-of-Expression-of-Argininosuccinate.

[75] Nigel G.J. Richards and Michael S. Kilberg. "Asparagine Synthetase Chemotherapy". In: *Annual review of biochemistry* 75 (2006), p. 629. ISSN: 00664154. DOI: 10.1146/ANNUREV.BIOCHEM.75.103004.142520. URL: /pmc/articles/PMC3587692/%20/pmc/articles/PMC3587692/?report=abstract%20https://www.ncbi.nlm.nih.gov/pmc/articles/PMC3587692/.

[76] Martina Chiu et al. "Oligodendroglioma Cells Lack Glutamine Synthetase and Are Auxotrophic for Glutamine, but Do not Depend on Glutamine Anaplerosis for Growth". In: *International journal of molecular sciences* 19.4 (Apr. 2018). ISSN: 1422-0067. DOI: 10.3390/IJMS19041099. URL: https://pubmed.ncbi.nlm.nih.gov/29642388/.

[77] Marina Bolzoni et al. "Dependence on glutamine uptake and glutamine addiction characterize myeloma cells: a new attractive target". In: *Blood* 128.5 (2016), pp. 667–679. ISSN: 1528-0020. DOI: 10.1182/BLOOD-2016-01-690743. URL: https://pubmed.ncbi.nlm.nih.gov/27268090/.

[78] Caroline R. Bartman et al. "Slow TCA flux and ATP production in primary solid tumours but not metastases". In: *Nature 2023* (Feb. 2023), pp. 1–9. ISSN: 1476-4687. DOI: 10.1038/s41586-022-05661-6. URL: https://www.nature.com/articles/s41586-022-05661-6.

[79] Sarah Maria Fendt et al. "Reductive glutamine metabolism is a function of the α-ketoglutarate to citrate ratio in cells". In: *Nature communications* 4 (2013). ISSN: 2041-1723. DOI: 10.1038/NCOMMS3236. URL: https://pubmed.ncbi.nlm.nih.gov/23900562/.

[80] Christian M. Metallo et al. "Reductive glutamine metabolism by IDH1 mediates lipogenesis under hypoxia". In: *Nature* 481.7381 (Jan. 2011), pp. 380–384. ISSN: 1476-4687. DOI: 10.1038/NATURE10602. URL: https://pubmed.ncbi.nlm.nih.gov/22101433/.

[81] E. V. Kalinina and L. A. Gavriliuk. "Glutathione Synthesis in Cancer Cells". In: *Biochemistry. Biokhimiia* 85.8 (Aug. 2020), pp. 895–907. ISSN: 1608-3040. DOI: 10.1134/S0006297920080052. URL: https://pubmed.ncbi.nlm.nih.gov/33045950/.

[82] David R. Wise et al. "Myc regulates a transcriptional program that stimulates mitochondrial glutaminolysis and leads to glutamine addiction". In: *Proceedings of the National Academy of Sciences of the United States of America* 105.48 (Dec. 2008), pp. 18782–18787. ISSN: 1091-6490. DOI: 10.1073/PNAS.0810199105. URL: https://pubmed.ncbi.nlm.nih.gov/19033189/.

[83] Sawako Suzuki et al. "Phosphate-activated glutaminase (GLS2), a p53-inducible regulator of glutamine metabolism and reactive oxygen species". In: *Proceedings of the National Academy of Sciences of the United States of America* 107.16 (Apr. 2010), pp. 7461–7466. ISSN: 1091-6490. DOI: 10.1073/PNAS.1002459107. URL: https://pubmed.ncbi.nlm.nih.gov/20351271/.

[84] Amy C. Mandigo et al. "Rb/e2f1 as a master regulator of cancer cell metabolism in advanced disease". In: *Cancer Discovery* 11.9 (Sept. 2021), pp. 2334–2353. ISSN: 21598290. DOI: 10.1158/2159-8290.CD-20-1114/674143/AM/RB-E2F1-AS-A-MASTER-REGULATOR-OF-CANCER-CELL. URL: https://aacrjournals.org/cancerdiscovery/article/11/9/2334/666292/RB-E2F1-as-a-Master-Regulator-of-Cancer-Cell.

[85] Hai Feng Zhang et al. "Transsulfuration, minor player or crucial for cysteine homeostasis in cancer". In: *Trends in Cell Biology* 32.9 (Sept. 2022), pp. 800–814. ISSN: 0962-8924. DOI: 10.1016/J.TCB.2022.02.009. URL: http://www.cell.com/article/S0962892422000605/fulltext%20http://www.cell.com/article/S0962892422000605/abstract%20https://www.cell.com/trends/cell-biology/abstract/S0962-8924(22)00060-5.

[86] Mark R. Sullivan et al. "Quantification of microenvironmental metabolites in murine cancers reveals determinants of tumor nutrient availability". In: *eLife* 8 (Apr. 2019). ISSN: 2050084X. DOI: 10.7554/ELIFE.44235.

[87] Alexander Muir et al. "Environmental cystine drives glutamine anaplerosis and sensitizes cancer cells to glutaminase inhibition". In: *eLife* 6 (Aug. 2017). ISSN: 2050084X. DOI: 10.7554/ELIFE.27713.

[88] Chun Shik Shin et al. "The glutamate/cystine xCT antiporter antagonizes glutamine metabolism and reduces nutrient flexibility". In: *Nature communications* 8 (2017). ISSN: 2041-1723. DOI: 10.1038/NCOMMS15074. URL: https://pubmed.ncbi.nlm.nih.gov/28429737/.

[89] Zhen Wei et al. "Metabolism of Amino Acids in Cancer". In: *Frontiers in Cell and Developmental Biology* 8 (Jan. 2020), p. 603837. ISSN: 2296634X. DOI: 10.3389/FCELL.2020.603837. URL: /pmc/articles/PMC7835483/%20/pmc/articles/PMC7835483/?report=abstract%20https://www.ncbi.nlm.nih.gov/pmc/articles/PMC7835483/.

[90] Oliver D.K. Maddocks et al. "Serine starvation induces stress and p53-dependent metabolic remodelling in cancer cells". In: *Nature* 493.7433 (Jan. 2013), pp. 542–546. ISSN: 1476-4687. DOI: 10.1038/NATURE11743. URL: https://pubmed.ncbi.nlm.nih.gov/23242140/.

[91] Katherine R. Mattaini, Mark R. Sullivan, and Matthew G. Vander Heiden. "The importance of serine metabolism in cancer". In: *The Journal of Cell Biology* 214.3 (Aug. 2016), p. 249. ISSN: 15408140. DOI: 10.1083/JCB.201604085. URL: /pmc/articles/PMC4970329/%20/pmc/articles/PMC4970329/?report=abstract%20https://www.ncbi.nlm.nih.gov/pmc/articles/PMC4970329/.

[92] Richard Possemato et al. "Functional genomics reveal that the serine synthesis pathway is essential in breast cancer". In: *Nature* 476.7360 (Aug. 2011), pp. 346–350. ISSN: 1476-4687. DOI: 10.1038/NATURE10350. URL: https://pubmed.ncbi.nlm.nih.gov/21760589/.

[93] Gina M. DeNicola et al. "NRF2 regulates serine biosynthesis in non-small cell lung cancer". In: *Nature genetics* 47.12 (Dec. 2015), pp. 1475–1481. ISSN: 1546-1718. DOI: 10.1038/NG.3421. URL: https://pubmed.ncbi.nlm.nih.gov/26482881/.

[94] Michael E. Pacold et al. "A PHGDH inhibitor reveals coordination of serine synthesis and one-carbon unit fate". In: *Nature chemical biology* 12.6 (June 2016), pp. 452–458. ISSN: 1552-4469. DOI: 10.1038/NCHEMBIO.2070. URL: https://pubmed.ncbi.nlm.nih.gov/27110680/.

[95] Sijing Pan et al. "Serine, glycine and one-carbon metabolism in cancer (Review)". In: *International Journal of Oncology* 58.2 (Feb. 2021), p. 158. ISSN: 17912423. DOI: 10.3892/IJO.2020.5158. URL: /pmc/articles/PMC7864012/%20/pmc/articles/

PMC7864012/?report=abstract%20https://www.ncbi.nlm.nih.gov/pmc/articles/PMC7864012/.

[96] Alice C. Newman and Oliver D.K. Maddocks. "One-carbon metabolism in cancer". In: *British Journal of Cancer 2017 116:12* 116.12 (May 2017), pp. 1499–1504. ISSN: 1532-1827. DOI: 10.1038/bjc.2017.118. URL: https://www.nature.com/articles/bjc2017118.

[97] Caroline A. Lewis et al. "Tracing compartmentalized NADPH metabolism in the cytosol and mitochondria of mammalian cells". In: *Molecular cell* 55.2 (July 2014), pp. 253–263. ISSN: 1097-4164. DOI: 10.1016/J.MOLCEL.2014.05.008. URL: https://pubmed.ncbi.nlm.nih.gov/24882210/%20https://pubmed.ncbi.nlm.nih.gov/24882210/?dopt=Abstract.

[98] Wen Cai Zhang et al. "Glycine decarboxylase activity drives non-small cell lung cancer tumor-initiating cells and tumorigenesis". In: *Cell* 148.1-2 (Jan. 2012), pp. 259–272. ISSN: 1097-4172. DOI: 10.1016/J.CELL.2011.11.050. URL: https://pubmed.ncbi.nlm.nih.gov/22225612/%20https://pubmed.ncbi.nlm.nih.gov/22225612/?dopt=Abstract.

[99] Dohoon Kim et al. "SHMT2 drives glioma cell survival in ischaemia but imposes a dependence on glycine clearance". In: *Nature* 520.7547 (Apr. 2015), pp. 363–367. ISSN: 1476-4687. DOI: 10.1038/NATURE14363. URL: https://pubmed.ncbi.nlm.nih.gov/25855294/%20https://pubmed.ncbi.nlm.nih.gov/25855294/?dopt=Abstract.

[100] Christiaan F. Labuschagne et al. "Serine, but not glycine, supports one-carbon metabolism and proliferation of cancer cells". In: *Cell reports* 7.4 (May 2014), pp. 1248–1258. ISSN: 2211-1247. DOI: 10.1016/J.CELREP.2014.04.045. URL: https://pubmed.ncbi.nlm.nih.gov/24813884/%20https://pubmed.ncbi.nlm.nih.gov/24813884/?dopt=Abstract.

[101] Naama Kanarek et al. "Histidine catabolism is a major determinant of methotrexate sensitivity". In: *Nature* 559.7715 (July 2018), pp. 632–636. ISSN: 1476-4687. DOI: 10.1038/S41586-018-0316-7. URL: https://pubmed.ncbi.nlm.nih.gov/29995852/.

[102] Alice Clare Newman et al. "Immune-regulated IDO1-dependent tryptophan metabolism is source of one-carbon units for pancreatic cancer and stellate cells". In: *Molecular Cell* 81.11 (June 2021), p. 2290. ISSN: 10974164. DOI: 10.1016/J.MOLCEL.2021.03.019. URL: /pmc/articles/PMC8189438/%20/pmc/articles/PMC8189438/?report=abstract%20https://www.ncbi.nlm.nih.gov/pmc/articles/PMC8189438/.

[103] Lucas B. Sullivan et al. "Supporting Aspartate Biosynthesis Is an Essential Function of Respiration in Proliferating Cells". In: *Cell* 162.3 (July 2015), pp. 552–563. ISSN: 0092-8674. DOI: 10.1016/J.CELL.2015.07.017.

[104] Kivanç Birsoy et al. "An Essential Role of the Mitochondrial Electron Transport Chain in Cell Proliferation Is to Enable Aspartate Synthesis". In: *Cell* 162.3 (July 2015), pp. 540–551. ISSN: 0092-8674. DOI: 10.1016/J.CELL.2015.07.016.

[105] Lisa A. Vettore, Rebecca L. Westbrook, and Daniel A. Tennant. "Proline metabolism and redox; maintaining a balance in health and disease". In: *Amino Acids* 53.12 (Dec. 2021), p. 1779. ISSN: 14382199. DOI: 10.1007/S00726-021-03051-2. URL: /pmc/articles/PMC8651533/%20/pmc/articles/PMC8651533/?report=abstract%20https://www.ncbi.nlm.nih.gov/pmc/articles/PMC8651533/.

[106] Ewa Karna et al. "Proline-dependent regulation of collagen metabolism". In: *Cellular and Molecular Life Sciences* 77.10 (May 2020), p. 1911. ISSN: 14209071. DOI: 10.1007/S00018-019-03363-3. URL: /pmc/articles/PMC7228914/%20/pmc/articles/PMC7228914/?report=abstract%20https://www.ncbi.nlm.nih.gov/pmc/articles/PMC7228914/.

[107] Magda Chalecka et al. "P5C as an Interface of Proline Interconvertible Amino Acids and Its Role in Regulation of Cell Survival and Apoptosis". In: *International Journal of Molecular Sciences* 22.21 (Nov. 2021), p. 11763. ISSN: 14220067. DOI: 10.3390/IJMS222111763. URL: /pmc/articles/PMC8584052/%20/pmc/articles/PMC8584052/?report=abstract%20https://www.ncbi.nlm.nih.gov/pmc/articles/PMC8584052/.

[108] Jessica de Ingeniis et al. "Functional Specialization in Proline Biosynthesis of Melanoma". In: *PLOS ONE* 7.9 (Sept. 2012), e45190. ISSN: 1932-6203. DOI: 10.1371/JOURNAL.PONE.0045190. URL: https://journals.plos.org/plosone/article?id=10.1371/journal.pone.0045190.

[109] Jui Pandhare et al. "Regulation and function of proline oxidase under nutrient stress". In: *Journal of cellular biochemistry* 107.4 (July 2009), pp. 759–768. ISSN: 1097-4644. DOI: 10.1002/JCB.22174. URL: https://pubmed.ncbi.nlm.nih.gov/19415679/.

[110] James M. Phang. "Proline Metabolism in Cell Regulation and Cancer Biology: Recent Advances and Hypotheses". In: *Antioxidants & redox signaling* 30.4 (2019), pp. 635–649. ISSN: 1557-7716. DOI: 10.1089/ARS.2017.7350. URL: https://pubmed.ncbi.nlm.nih.gov/28990419/.

[111] Shamsul Hayat et al. "Role of proline under changing environments: A review". In: *Plant Signaling & Behavior* 7.11 (Nov. 2012), p. 1456. ISSN: 15592316. DOI: 10.4161/PSB.21949. URL: /pmc/articles/PMC3548871/%20/pmc/articles/PMC3548871/?report=abstract%20https://www.ncbi.nlm.nih.gov/pmc/articles/PMC3548871/.

[112] James Ming Phang et al. "The proline regulatory axis and cancer". In: *Frontiers in oncology* 2 (2012). ISSN: 2234-943X. DOI: 10.3389/FONC.2012.00060. URL: https://pubmed.ncbi.nlm.nih.gov/22737668/.

[113] S. Kaul, S. S. Sharma, and I. K. Mehta. "Free radical scavenging potential of L-proline: evidence from in vitro assays". In: *Amino acids* 34.2 (Feb. 2008), pp. 315–320. ISSN: 1438-2199. DOI: 10.1007/S00726-006-0407-X. URL: https://pubmed.ncbi.nlm.nih.gov/17086481/.

[114] Nicholas Smirnoff and Quinton J. Cumbes. "Hydroxyl radical scavenging activity of compatible solutes". In: *Phytochemistry* 28.4 (Jan. 1989), pp. 1057–1060. ISSN: 0031-9422. DOI: 10.1016/0031-9422(89)80182-7.

[115] Jiacheng Wang et al. "Proline improves cardiac remodeling following myocardial infarction and attenuates cardiomyocyte apoptosis via redox regulation". In: *Biochemical pharmacology* 178 (Aug. 2020). ISSN: 1873-2968. DOI: 10.1016/J.BCP.2020.114065. URL: https://pubmed.ncbi.nlm.nih.gov/32492448/.

[116] Sathish Kumar Natarajan et al. "Proline dehydrogenase is essential for proline protection against hydrogen peroxide-induced cell death". In: *Free radical biology & medicine* 53.5 (Sept. 2012), pp. 1181–1191. ISSN: 1873-4596. DOI: 10.1016/J.FREERADBIOMED.2012.07.002. URL: https://pubmed.ncbi.nlm.nih.gov/22796327/.

[117] Kornelia Polyak et al. "A model for p53-induced apoptosis". In: *Nature* 389.6648 (1997), pp. 300–305. ISSN: 0028-0836. DOI: 10.1038/38525. URL: https://pubmed.ncbi.nlm.nih.gov/9305847/.

[118] H. F. Horn and K. H. Vousden. "Coping with stress: multiple ways to activate p53". In: *Oncogene* 26.9 (Feb. 2007), pp. 1306–1316. ISSN: 0950-9232. DOI: 10.1038/SJ.ONC.1210263. URL: https://pubmed.ncbi.nlm.nih.gov/17322916/.

[119] Nisebita Sahu et al. "Proline Starvation Induces Unresolved ER Stress and Hinders mTORC1-Dependent Tumorigenesis". In: *Cell Metabolism* 24.5 (Nov. 2016), pp. 753–761. ISSN: 19327420. DOI: 10.1016/j.cmet.2016.08.008. URL: http://www.cell.com/article/S1550413116304247/fulltext%20http://www.cell.com/article/

S1550413116304247/abstract%20https://www.cell.com/cell-metabolism/abstract/S1550-4131(16)30424-7.

[120] Gergely Pallag et al. "Proline Oxidation Supports Mitochondrial ATP Production When Complex I Is Inhibited". In: *International journal of molecular sciences* 23.9 (May 2022). ISSN: 1422-0067. DOI: 10.3390/IJMS23095111. URL: https://pubmed.ncbi.nlm.nih.gov/35563503/.

[121] Mei Ling Kuo et al. "PYCR1 and PYCR2 Interact and Collaborate with RRM2B to Protect Cells from Overt Oxidative Stress". In: *Scientific reports* 6 (Jan. 2016). ISSN: 2045-2322. DOI: 10.1038/SREP18846. URL: https://pubmed.ncbi.nlm.nih.gov/26733354/.

[122] Iosifina P. Foskolou and Ester M. Hammond. "RRM2B: An oxygen-requiring protein with a role in hypoxia". In: *Molecular & cellular oncology* 4.5 (Sept. 2017). ISSN: 2372-3556. DOI: 10.1080/23723556.2017.1335272. URL: https://pubmed.ncbi.nlm.nih.gov/29057303/.

[123] Xiyong Liu, Lijun Xue, and Yun Yen. "Redox property of ribonucleotide reductase small subunit M2 and p53R2". In: *Methods in molecular biology (Clifton, N.J.)* 477 (2008), pp. 195–206. ISSN: 1064-3745. DOI: 10.1007/978-1-60327-517-0{_}15. URL: https://pubmed.ncbi.nlm.nih.gov/19082948/.

[124] Bruno Reversade et al. "Mutations in PYCR1 cause cutis laxa with progeroid features". In: *Nature Genetics 2009 41:9* 41.9 (Aug. 2009), pp. 1016–1021. ISSN: 1546-1718. DOI: 10.1038/ng.413. URL: https://www.nature.com/articles/ng.413.

[125] Diem H. Tran et al. "Mitochondrial NADP + is essential for proline biosynthesis during cell growth". In: *Nature metabolism* 3.4 (Apr. 2021), pp. 571–585. ISSN: 2522-5812. DOI: 10.1038/S42255-021-00374-Y. URL: https://pubmed.ncbi.nlm.nih.gov/33833463/.

[126] Kathryn E. Wellen and Craig B. Thompson. "Cellular metabolic stress: considering how cells respond to nutrient excess". In: *Molecular cell* 40.2 (Oct. 2010), pp. 323–332. ISSN: 1097-4164. DOI: 10.1016/J.MOLCEL.2010.10.004. URL: https://pubmed.ncbi.nlm.nih.gov/20965425/.

[127] Simon Schwörer et al. "Proline biosynthesis is a vent for TGFβ-induced mitochondrial redox stress". In: *The EMBO journal* 39.8 (Apr. 2020). ISSN: 1460-2075. DOI: 10.15252/EMBJ.2019103334. URL: https://pubmed.ncbi.nlm.nih.gov/32134147/.

[128] Miao Liu et al. "Inhibiting both proline biosynthesis and lipogenesis synergistically suppresses tumor growth". In: *Journal of Experimental Medicine* 217.3 (Mar. 2020). ISSN: 15409538. DOI: 10.1084/JEM.20191226/133620. URL: https://doi.org/10.1084/jem.20191226.

[129] Yao Zheng et al. "The proline cycle as an eukaryotic redox valve". In: *Journal of Experimental Botany* 72.20 (Oct. 2021), pp. 6856–6866. ISSN: 0022-0957. DOI: 10.1093/JXB/ERAB361. URL: https://academic.oup.com/jxb/article/72/20/6856/6333154.

[130] Ilaria Elia et al. "Proline metabolism supports metastasis formation and could be inhibited to selectively target metastasizing cancer cells". In: *Nature Communications 2017 8:1* 8.1 (May 2017), pp. 1–11. ISSN: 2041-1723. DOI: 10.1038/ncomms15267. URL: https://www.nature.com/articles/ncomms15267.

[131] Vance L. Albaugh, Kaushik Mukherjee, and Adrian Barbul. "Proline Precursors and Collagen Synthesis: Biochemical Challenges of Nutrient Supplementation and Wound Healing". In: *The Journal of Nutrition* 147.11 (Nov. 2017), pp. 2011–2017. ISSN: 0022-3166. DOI: 10.3945/JN.117.256404. URL: https://academic.oup.com/jn/article/147/11/2011/4743236.

[132] Orianne Olivares et al. "Collagen-derived proline promotes pancreatic ductal adenocarcinoma cell survival under nutrient limited conditions". In: *Nature communications* 8 (July 2017). ISSN: 2041-1723. DOI: 10.1038/NCOMMS16031. URL: https://pubmed.ncbi.nlm.nih.gov/28685754/%20https://pubmed.ncbi.nlm.nih.gov/28685754/?dopt=Abstract.

[133] Ling Guo et al. "Kindlin-2 links mechano-environment to proline synthesis and tumor growth". In: *Nature Communications* 10.1 (Dec. 2019). ISSN: 20411723. DOI: 10.1038/S41467-019-08772-3. URL: /pmc/articles/PMC6381112/%20/pmc/articles/PMC6381112/?report=abstract%20https://www.ncbi.nlm.nih.gov/pmc/articles/PMC6381112/.

[134] Fabricio Loayza-Puch et al. "Tumour-specific proline vulnerability uncovered by differential ribosome codon reading". In: *Nature* 530.7591 (Feb. 2016), pp. 490–494. ISSN: 1476-4687. DOI: 10.1038/NATURE16982. URL: https://pubmed.ncbi.nlm.nih.gov/26878238/.

[135] Shuangkuan Du et al. "PYCR1 promotes bladder cancer by affecting the Akt/Wnt/β-catenin signaling". In: *Journal of bioenergetics and biomembranes* 53.2 (Apr. 2021), pp. 247–258. ISSN: 1573-6881. DOI: 10.1007/S10863-021-09887-3. URL: https://pubmed.ncbi.nlm.nih.gov/33689096/.

[136] Kun Yan et al. "Knockdown of PYCR1 inhibits proliferation, drug resistance and EMT in colorectal cancer cells by regulating STAT3-Mediated p38 MAPK and NF-κB signalling pathway". In: *Biochemical and biophysical research communications* 520.2 (Dec. 2019), pp. 486–491. ISSN: 1090-2104. DOI: 10.1016/J.BBRC.2019.10.059. URL: https://pubmed.ncbi.nlm.nih.gov/31606203/.

[137] Shiyu Xiao et al. "Pyrroline-5-carboxylate reductase 1 (PYCR1) upregulation contributes to gastric cancer progression and indicates poor survival outcome". In: *Annals of translational medicine* 8.15 (Aug. 2020), pp. 937–937. ISSN: 2305-5839. DOI: 10.21037/ATM-19-4402. URL: https://pubmed.ncbi.nlm.nih.gov/32953737/.

[138] Dongchang Wang et al. "PYCR1 promotes the progression of non-small-cell lung cancer under the negative regulation of miR-488". In: *Biomedicine & pharmacotherapy = Biomedecine & pharmacotherapie* 111 (Mar. 2019), pp. 588–595. ISSN: 1950-6007. DOI: 10.1016/J.BIOPHA.2018.12.089. URL: https://pubmed.ncbi.nlm.nih.gov/30605882/.

[139] Juhua Zhuang et al. "PYCR1 interference inhibits cell growth and survival via c-Jun N-terminal kinase/insulin receptor substrate 1 (JNK/IRS1) pathway in hepatocellular cancer". In: *Journal of translational medicine* 17.1 (Oct. 2019). ISSN: 1479-5876. DOI: 10.1186/S12967-019-2091-0. URL: https://pubmed.ncbi.nlm.nih.gov/31619254/.

[140] Yawen Gao et al. "PYCR1 knockdown inhibits the proliferation, migration, and invasion by affecting JAK/STAT signaling pathway in lung adenocarcinoma". In: *Molecular carcinogenesis* 59.5 (May 2020), pp. 503–511. ISSN: 1098-2744. DOI: 10.1002/MC.23174. URL: https://pubmed.ncbi.nlm.nih.gov/32133692/.

[141] Jiefeng Ding et al. "Human mitochondrial pyrroline-5-carboxylate reductase 1 promotes invasiveness and impacts survival in breast cancers". In: *Carcinogenesis* 38.5 (May 2017), pp. 519–531. ISSN: 0143-3334. DOI: 10.1093/CARCIN/BGX022. URL: https://academic.oup.com/carcin/article/38/5/519/3098469.

[142] Shiyu Xiao et al. "Pyrroline-5-carboxylate reductase 1 (PYCR1) upregulation contributes to gastric cancer progression and indicates poor survival outcome". In: *Annals of translational medicine* 8.15 (Aug. 2020), pp. 937–937. ISSN: 2305-5839. DOI: 10.21037/ATM-19-4402. URL: https://pubmed.ncbi.nlm.nih.gov/32953737/.

[143] Kate E.R. Hollinshead et al. "Oncogenic IDH1 Mutations Promote Enhanced Proline Synthesis through PYCR1 to Support the Maintenance of Mitochondrial Redox Homeostasis". In: *Cell Reports* 22.12 (Mar. 2018), p. 3107. ISSN: 22111247. DOI: 10.1016/J.CELREP.2018.02.084. URL: /pmc/articles/PMC5883319/%20/pmc/articles/PMC5883319/?report=abstract%20https://www.ncbi.nlm.nih.gov/pmc/articles/PMC5883319/.

[144] Brendan Lanpher, Nicola Brunetti-Pierri, and Brendan Lee. "Inborn errors of metabolism: the flux from Mendelian to complex diseases". In: *Nature reviews. Genetics* 7.6 (June 2006), pp. 449–460. ISSN: 1471-0056. DOI: 10.1038/NRG1880. URL: https://pubmed.ncbi.nlm.nih.gov/16708072/.

[145] Jean Marie Saudubray and Fanny Mochel. "The phenotype of adult versus pediatric patients with inborn errors of metabolism". In: *Journal of inherited metabolic disease* 41.5 (Sept. 2018), pp. 753–756. ISSN: 1573-2665. DOI: 10.1007/S10545-018-0209-9. URL: https://pubmed.ncbi.nlm.nih.gov/29876767/.

[146] Pinar Akdemir Özişik et al. "Medulloblastoma in a child with the metabolic disease L-2-hydroxyglutaric aciduria". In: *Pediatric neurosurgery* 37.1 (2002), pp. 22–26. ISSN: 1016-2291. DOI: 10.1159/000065097. URL: https://pubmed.ncbi.nlm.nih.gov/12138215/.

[147] Ayelet Erez et al. "Insights into the Pathogenesis and Treatment of Cancer from Inborn Errors of Metabolism". In: *The American Journal of Human Genetics* 88.4 (Apr. 2011), pp. 402–421. ISSN: 0002-9297. DOI: 10.1016/J.AJHG.2011.03.005. URL: http://www.cell.com/article/S0002929711000978/fulltext%20http://www.cell.com/article/S0002929711000978/abstract%20https://www.cell.com/ajhg/abstract/S0002-9297(11)00097-8.

[148] Maha S. Zaki et al. "PYCR2 mutations cause a lethal syndrome of microcephaly and failure to thrive". In: *Annals of neurology* 80.1 (July 2016), p. 59. ISSN: 15318249. DOI: 10.1002/ANA.24678. URL: /pmc/articles/PMC4938747/%20/pmc/articles/PMC4938747/?report=abstract%20https://www.ncbi.nlm.nih.gov/pmc/articles/PMC4938747/.

[149] Andrew N. Lane, Teresa W.M. Fan, and Richard M. Higashi. "Stable isotope-assisted metabolomics in cancer research". In: *IUBMB life* 60.2 (2008), pp. 124–129. ISSN: 1521-6543. DOI: 10.1002/IUB.17. URL: https://pubmed.ncbi.nlm.nih.gov/18380001/.

[150] Cholsoon Jang, Li Chen, and Joshua D. Rabinowitz. "Metabolomics and Isotope Tracing". In: *Cell* 173.4 (May 2018), pp. 822–837. ISSN: 1097-4172. DOI: 10.1016/J.CELL.2018.03.055. URL: https://pubmed.ncbi.nlm.nih.gov/29727671/.

[151] Christian Potter and Adrian L. Harris. "Hypoxia inducible carbonic anhydrase IX, marker of tumour hypoxia, survival pathway and therapy target". In: *Cell cycle (Georgetown, Tex.)* 3.2 (2004), pp. 164–167. ISSN: 1538-4101. DOI: 10.4161/cc.3.2.618. URL: https://pubmed.ncbi.nlm.nih.gov/14712082/.

[152] Yoichi Shimizu. "[Accumulation Mechanism of 2-Nitroimidazole-based Hypoxia Imaging Probes Revealed by Imaging Mass Spectrometry]". In: *Yakugaku zasshi : Journal of the Pharmaceutical Society of Japan* 138.11 (2018), pp. 1345–1352. ISSN: 1347-5231. DOI: 10.1248/YAKUSHI.18-00146. URL: https://pubmed.ncbi.nlm.nih.gov/30381642/.

[153] Dirk Vordermark and Michael R. Horsman. "Hypoxia as a Biomarker and for Personalized Radiation Oncology". In: *Recent results in cancer research. Fortschritte der Krebsforschung. Progres dans les recherches sur le cancer* 198 (2016), pp. 123–142. ISSN: 0080-0015. DOI: 10.1007/978-3-662-49651-0{_}6. URL: https://pubmed.ncbi.nlm.nih.gov/27318684/.

[154] Brian J. Altman, Zachary E. Stine, and Chi V. Dang. "From Krebs to clinic: glutamine metabolism to cancer therapy". In: *Nature reviews. Cancer* 16.10 (Sept. 2016), pp. 619–634. ISSN: 1474-1768. DOI: 10.1038/NRC.2016.71. URL: https://pubmed.ncbi.nlm.nih.gov/27492215/.

[155] Bo Hyun Choi and Jonathan L. Coloff. "The Diverse Functions of Non-Essential Amino Acids in Cancer". In: *Cancers* 11.5 (May 2019). ISSN: 20726694. DOI: 10.3390/CANCERS11050675. URL: /pmc/articles/PMC6562791/%20/pmc/articles/PMC6562791/?report=abstract%20https://www.ncbi.nlm.nih.gov/pmc/articles/PMC6562791/.

[156] H. F. Dvorak et al. "Vascular permeability factor/vascular endothelial growth factor and the significance of microvascular hyperpermeability in angiogenesis". In: *Current topics in microbiology and immunology* 237 (1999), pp. 98–132. ISSN: 0070-217X. DOI:

10.1007/978-3-642-59953-8{_}6. URL: https://pubmed.ncbi.nlm.nih.gov/9893348/%20https://pubmed.ncbi.nlm.nih.gov/9893348/?dopt=Abstract.

[157] Avraham Mayevsky. "Brain NADH redox state monitored in vivo by fiber optic surface fluorometry". In: *Brain Research Reviews* 7.1 (Mar. 1984), pp. 49–68. ISSN: 0165-0173. DOI: 10.1016/0165-0173(84)90029-8.

[158] Barbara Muz et al. "The role of hypoxia in cancer progression, angiogenesis, metastasis, and resistance to therapy". In: *Hypoxia* 3 (Dec. 2015), p. 83. ISSN: 2324-1128. DOI: 10.2147/HP.S93413. URL: /pmc/articles/PMC5045092/%20/pmc/articles/PMC5045092/?report=abstract%20https://www.ncbi.nlm.nih.gov/pmc/articles/PMC5045092/.

[159] Rebecca L. Westbrook et al. "Proline synthesis through PYCR1 is required to support cancer cell proliferation and survival in oxygen-limiting conditions". In: *Cell Reports* 38.5 (Feb. 2022). ISSN: 22111247. DOI: 10.1016/j.celrep.2022.110320. URL: http://www.cell.com/article/S2211124722000316/fulltext%20http://www.cell.com/article/S2211124722000316/abstract%20https://www.cell.com/cell-reports/abstract/S2211-1247(22)00031-6.

[160] Stefano Donati, Timur Sander, and Hannes Link. "Crosstalk between transcription and metabolism: how much enzyme is enough for a cell?" In: *Wiley Interdisciplinary Reviews: Systems Biology and Medicine* 10.1 (Jan. 2018), e1396. ISSN: 1939-005X. DOI: 10.1002/WSBM.1396. URL: https://onlinelibrary.wiley.com/doi/full/10.1002/wsbm.1396%20https://onlinelibrary.wiley.com/doi/abs/10.1002/wsbm.1396%20https://wires.onlinelibrary.wiley.com/doi/10.1002/wsbm.1396.

[161] Anupam Patgiri et al. "An engineered enzyme that targets circulating lactate to alleviate intracellular NADH:NAD+ imbalance". In: *Nature Biotechnology 2020 38:3* 38.3 (Jan. 2020), pp. 309–313. ISSN: 1546-1696. DOI: 10.1038/s41587-019-0377-7. URL: https://www.nature.com/articles/s41587-019-0377-7.

[162] Cholsoon Jang, Li Chen, and Joshua D. Rabinowitz. "Metabolomics and Isotope Tracing". In: *Cell* 173.4 (May 2018), pp. 822–837. ISSN: 0092-8674. DOI: 10.1016/J.CELL.2018.03.055. URL: http://www.cell.com/article/S0092867418303878/fulltext%20http://www.cell.com/article/S0092867418303878/abstract%20https://www.cell.com/cell/abstract/S0092-8674(18)30387-8.

[163] Andrea Ivascu and Manfred Kubbies. "Rapid generation of single-tumor spheroids for high-throughput cell function and toxicity analysis". In: *Journal of biomolecular screening* 11.8 (Dec. 2006), pp. 922–932. ISSN: 1087-0571. DOI: 10.1177/1087057106292763. URL: https://pubmed.ncbi.nlm.nih.gov/16973921/.

[164] Panida Lertkiatmongkol et al. "Endothelial functions of platelet/endothelial cell adhesion molecule-1 (CD31)". In: *Current opinion in hematology* 23.3 (2016), pp. 253–259. ISSN: 1531-7048. DOI: 10.1097/MOH.0000000000000239. URL: https://pubmed.ncbi.nlm.nih.gov/27055047/.

[165] Linda A. Buss et al. "Effect of post-implant exercise on tumour growth rate, perfusion and hypoxia in mice". In: *PLoS ONE* 15.3 (2020). ISSN: 19326203. DOI: 10.1371/JOURNAL.PONE.0229290. URL: /pmc/articles/PMC7080225/%20/pmc/articles/PMC7080225/?report=abstract%20https://www.ncbi.nlm.nih.gov/pmc/articles/PMC7080225/.

[166] Thomas Scholzen and Johannes Gerdes. "The Ki-67 Protein: From the Known and the Unknown". In: (2000). DOI: 10.1002/(SICI)1097-4652(200003)182:3.

[167] David R. McIlwain, Thorsten Berger, and Tak W. Mak. "Caspase Functions in Cell Death and Disease". In: *Cold Spring Harbor Perspectives in Biology* 5.4 (Apr. 2013), pp. 1–28. ISSN: 19430264. DOI: 10.1101/CSHPERSPECT.A008656. URL: /pmc/articles/PMC3683896/%20/pmc/articles/PMC3683896/?report=abstract%20https://www.ncbi.nlm.nih.gov/pmc/articles/PMC3683896/.

[168] Nathalie Escande-Beillard et al. "Loss of PYCR2 Causes Neurodegeneration by Increasing Cerebral Glycine Levels via SHMT2". In: *Neuron* 107.1 (July 2020), pp. 82–94. ISSN: 10974199. DOI: 10.1016/j.neuron.2020.03.028. URL: http://www.cell.com/article/S089662732030235X/fulltext%20http://www.cell.com/article/S089662732030235X/abstract%20https://www.cell.com/neuron/abstract/S0896-6273(20)30235-X.

[169] Tojo Nakayama et al. "Mutations in PYCR2, Encoding Pyrroline-5-Carboxylate Reductase 2, Cause Microcephaly and Hypomyelination". In: *American Journal of Human Genetics* 96.5 (May 2015), p. 709. ISSN: 15376605. DOI: 10.1016/J.AJHG.2015.03.003. URL: /pmc/articles/PMC4570282/%20/pmc/articles/PMC4570282/?report=abstract%20https://www.ncbi.nlm.nih.gov/pmc/articles/PMC4570282/.

[170] Alexandra R. Grassian et al. "IDH1 Mutations Alter Citric Acid Cycle Metabolism and Increase Dependence on Oxidative Mitochondrial Metabolism". In: *Cancer research* 74.12 (June 2014), p. 3317. ISSN: 15387445. DOI: 10.1158/0008-5472.CAN-14-0772-T. URL: /pmc/articles/PMC4885639/%20/pmc/articles/PMC4885639/?report=abstract%20https://www.ncbi.nlm.nih.gov/pmc/articles/PMC4885639/.

[171] Philippe Marchetti et al. "Mitochondrial spare respiratory capacity: Mechanisms, regulation, and significance in non-transformed and cancer cells". In: *FASEB Journal* 34.10 (Oct. 2020), pp. 13106–13124. ISSN: 15306860. DOI: 10.1096/FJ.202000767R.

[172] Kirsty Milne et al. "A fragment-like approach to PYCR1 inhibition". In: *Bioorganic & medicinal chemistry letters* 29.18 (Sept. 2019), pp. 2626–2631. ISSN: 1464-3405. DOI: 10.1016/J.BMCL.2019.07.047. URL: https://pubmed.ncbi.nlm.nih.gov/31362921/.

[173] Inge Oudaert et al. "Pyrroline-5-Carboxylate Reductase 1: a novel target for sensitizing multiple myeloma cells to bortezomib by inhibition of PRAS40-mediated protein synthesis". In: *Journal of Experimental and Clinical Cancer Research* 41.1 (Dec. 2022), pp. 1–17. ISSN: 17569966. DOI: 10.1186/S13046-022-02250-3/FIGURES/8. URL: https://jeccr.biomedcentral.com/articles/10.1186/s13046-022-02250-3.

[174] Juhua Zhuang et al. "PYCR1 interference inhibits cell growth and survival via c-Jun N-terminal kinase/insulin receptor substrate 1 (JNK/IRS1) pathway in hepatocellular cancer". In: *Journal of translational medicine* 17.1 (Oct. 2019). ISSN: 1479-5876. DOI: 10.1186/S12967-019-2091-0. URL: https://pubmed.ncbi.nlm.nih.gov/31619254/.

[175] Vinayak Bhandari et al. "Molecular landmarks of tumor hypoxia across cancer types". In: *Nature Genetics 2019 51:2* 51.2 (Jan. 2019), pp. 308–318. ISSN: 1546-1718. DOI: 10.1038/s41588-018-0318-2. URL: https://www.nature.com/articles/s41588-018-0318-2.

[176] Thomas R. Cox. "The matrix in cancer". In: *Nature Reviews Cancer 2021 21:4* 21.4 (Feb. 2021), pp. 217–238. ISSN: 1474-1768. DOI: 10.1038/s41568-020-00329-7. URL: https://www.nature.com/articles/s41568-020-00329-7.

[177] Min Fang et al. "Collagen as a double-edged sword in tumor progression". In: *Tumour Biology* 35.4 (Apr. 2014), p. 2871. ISSN: 14230380. DOI: 10.1007/S13277-013-1511-7. URL: /pmc/articles/PMC3980040/%20/pmc/articles/PMC3980040/?report=abstract%20https://www.ncbi.nlm.nih.gov/pmc/articles/PMC3980040/.

[178] Pawel Swietach, Richard D. Vaughan-Jones, and Adrian L. Harris. "Regulation of tumor pH and the role of carbonic anhydrase 9". In: *Cancer and Metastasis Reviews 2007 26:2* 26.2 (Apr. 2007), pp. 299–310. ISSN: 1573-7233. DOI: 10.1007/S10555-007-9064-0. URL: https://link.springer.com/article/10.1007/s10555-007-9064-0.

[179] Emily J. Kay et al. "Cancer-associated fibroblasts require proline synthesis by PYCR1 for the deposition of pro-tumorigenic extracellular matrix". In: *Nature Metabolism 2022 4:6* 4.6 (June 2022), pp. 693–710. ISSN: 2522-5812. DOI: 10.1038/s42255-022-00582-0. URL: https://www.nature.com/articles/s42255-022-00582-0.

[180] Yanzhen Xu et al. "Deciphering the effects of PYCR1 on cell function and its associated mechanism in hepatocellular carcinoma". In: *International journal of biological sciences* 17.9 (2021), pp. 2223–2239. ISSN: 1449-2288. DOI: 10.7150/IJBS.58026. URL: https://pubmed.ncbi.nlm.nih.gov/34239351/.

[181] Sadiq M.I. Saleh et al. "Identification of interacting stromal axes in triple-negative breast cancer". In: *Cancer Research* 77.17 (Sept. 2017), pp. 4673–4683. ISSN: 15387445. DOI: 10.1158/0008-5472.CAN-16-3427.

[182] Patrick Micke et al. "The prognostic impact of the tumour stroma fraction: A machine learning-based analysis in 16 human solid tumour types". In: *EBioMedicine* 65 (Mar. 2021). ISSN: 23523964. DOI: 10.1016/j.ebiom.2021.103269. URL: http://www.thelancet.com/article/S2352396421000621/fulltext%20http://www.thelancet.com/article/S2352396421000621/abstract%20https://www.thelancet.com/journals/ebiom/article/PIIS2352-3964(21)00062-1/abstract.

[183] Valerie A. McCormack and Isabel Dos Santos Silva. "Breast density and parenchymal patterns as markers of breast cancer risk: a meta-analysis". In: *Cancer epidemiology, biomarkers & prevention : a publication of the American Association for Cancer Research, cosponsored by the American Society of Preventive Oncology* 15.6 (June 2006), pp. 1159–1169. ISSN: 1055-9965. DOI: 10.1158/1055-9965.EPI-06-0034. URL: https://pubmed.ncbi.nlm.nih.gov/16775176/.

[184] Wen Juan Huang, Wei Wei Chen, and Xia Zhang. "Glioblastoma multiforme: Effect of hypoxia and hypoxia inducible factors on therapeutic approaches". In: *Oncology Letters* 12.4 (Oct. 2016), p. 2283. ISSN: 17921082. DOI: 10.3892/OL.2016.4952. URL: /pmc/articles/PMC5038353/%20/pmc/articles/PMC5038353/?report=abstract%20https://www.ncbi.nlm.nih.gov/pmc/articles/PMC5038353/.

[185] Abramowicz Anna and Gos Monika. "Splicing mutations in human genetic disorders: examples, detection, and confirmation". In: *Journal of applied genetics* 59.3 (Aug. 2018), pp. 253–268. ISSN: 2190-3883. DOI: 10.1007/S13353-018-0444-7. URL: https://pubmed.ncbi.nlm.nih.gov/29680930/.

[186] Martin Mikl et al. "Dissecting splicing decisions and cell-to-cell variability with designed sequence libraries". In: *Nature Communications 2019 10:1* 10.1 (Oct. 2019), pp. 1–14. ISSN: 2041-1723. DOI: 10.1038/s41467-019-12642-3. URL: https://www.nature.com/articles/s41467-019-12642-3.

[187] N. S. Van de Water et al. "Factor IX polypyrimidine tract mutation analysis using mRNA from peripheral blood leukocytes". In: *Journal of thrombosis and haemostasis : JTH* 2.11 (Nov. 2004), pp. 2073–2075. ISSN: 1538-7933. DOI: 10.1111/J.1538-7836.2004.00989.X. URL: https://pubmed.ncbi.nlm.nih.gov/15550058/.

[188] Yuka Aoyama et al. "A novel mutation (c.121-13T>A) in the polypyrimidine tract of the splice acceptor site of intron 2 causes exon 3 skipping in Mitochondrial acetoacetyl-CoA thiolase gene". In: *Molecular Medicine Reports* 15.6 (June 2017), pp. 3879–3884. ISSN: 17913004. DOI: 10.3892/MMR.2017.6434/HTML. URL: http://www.spandidos-publications.com/10.3892/mmr.2017.6434/abstract%20https://www.spandidos-publications.com/10.3892/mmr.2017.6434.

[189] Maria Andrea Desbats et al. "Genetic bases and clinical manifestations of coenzyme Q10 (CoQ10) deficiency". In: *Journal of Inherited Metabolic Disease* 38.1 (Jan. 2015), pp. 145–156. ISSN: 1573-2665. DOI: 10.1007/S10545-014-9749-9. URL: https://onlinelibrary.wiley.com/doi/full/10.1007/s10545-014-9749-9%20https://onlinelibrary.wiley.com/doi/abs/10.1007/s10545-014-9749-9%20https://onlinelibrary.wiley.com/doi/10.1007/s10545-014-9749-9.

[190] C. M. Quinzii et al. "Human CoQ10 deficiencies". In: *BioFactors (Oxford, England)* 32.0 (2008), p. 113. ISSN: 09516433. DOI: 10.1002/BIOF.5520320113. URL: /pmc/articles/PMC3625975/%20/pmc/articles/PMC3625975/?report=abstract%20https://www.ncbi.nlm.nih.gov/pmc/articles/PMC3625975/.

[191] Cecilia Hägerhäll. "Succinate: quinone oxidoreductases. Variations on a conserved theme". In: *Biochimica et biophysica acta* 1320.2 (June 1997), pp. 107–141. ISSN: 0006-3002. DOI: 10.1016/S0005-2728(97)00019-4. URL: https://pubmed.ncbi.nlm.nih.gov/9210286/.

[192] Agustín Hidalgo-Gutiérrez et al. "Metabolic Targets of Coenzyme Q10 in Mitochondria". In: *Antioxidants* 10.4 (Apr. 2021). ISSN: 20763921. DOI: 10.3390/ANTIOX10040520. URL: /pmc/articles/PMC8066821/%20/pmc/articles/PMC8066821/?report=abstract%20https://www.ncbi.nlm.nih.gov/pmc/articles/PMC8066821/.

[193] Esther Lapuente-Brun et al. "Supercomplex assembly determines electron flux in the mitochondrial electron transport chain". In: *Science (New York, N.Y.)* 340.6140 (2013), pp. 1567–1570. ISSN: 1095-9203. DOI: 10.1126/SCIENCE.1230381. URL: https://pubmed.ncbi.nlm.nih.gov/23812712/.

[194] Hans Löw, Frederick L. Crane, and D. James Morré. "Putting together a plasma membrane NADH oxidase: A tale of three laboratories". In: *The International Journal of Biochemistry & Cell Biology* 44.11 (Nov. 2012), pp. 1834–1838. ISSN: 1357-2725. DOI: 10.1016/J.BIOCEL.2012.06.032.

[195] Jari A. Larm et al. "Up-regulation of the plasma membrane oxidoreductase as a prerequisite for the viability of human Namalwa rho 0 cells." In: *Journal of Biological Chemistry* 269.48 (Dec. 1994), pp. 30097–30100. ISSN: 0021-9258. DOI: 10.1016/S0021-9258(18)43779-9. URL: http://www.jbc.org/article/S0021925818437799/fulltext%20http://www.jbc.org/article/S0021925818437799/abstract%20https://www.jbc.org/article/S0021-9258(18)43779-9/abstract.

[196] A. Lawen et al. "The universality of bioenergetic disease: The role of mitochondrial mutation and the putative inter-relationship between mitochondria and plasma membrane NADH oxidoreductase". In: *Molecular Aspects of Medicine* 15.SUPPL. 1 (Jan. 1994), s13–s27. ISSN: 0098-2997. DOI: 10.1016/0098-2997(94)90009-4.

[197] Lars Gille and Hans Nohl. "The Existence of a Lysosomal Redox Chain and the Role of Ubiquinone". In: *Archives of Biochemistry and Biophysics* 375.2 (Mar. 2000), pp. 347–354. ISSN: 0003-9861. DOI: 10.1006/ABBI.1999.1649.

[198] Fredrik Åberg et al. "Distribution and redox state of ubiquinones in rat and human tissues". In: *Archives of Biochemistry and Biophysics* 295.2 (June 1992), pp. 230–234. ISSN: 0003-9861. DOI: 10.1016/0003-9861(92)90511-T.

[199] Balz Frei, Mike C. Kim, and Bruce N. Ames. "Ubiquinol-10 is an effective lipid-soluble antioxidant at physiological concentrations". In: *Proceedings of the National Academy of Sciences of the United States of America* 87.12 (1990), pp. 4879–4883. ISSN: 00278424. DOI: 10.1073/PNAS.87.12.4879. URL: https://www.pnas.org.

[200] Martin Klingenberg and Shu Gui Huang. "Structure and function of the uncoupling protein from brown adipose tissue". In: *Biochimica et Biophysica Acta (BBA) - Biomembranes* 1415.2 (Jan. 1999), pp. 271–296. ISSN: 0005-2736. DOI: 10.1016/S0005-2736(98)00232-6.

[201] Karim S. Echtay et al. "Uncoupling proteins 2 and 3 are highly active H+ transporters and highly nucleotide sensitive when activated by coenzyme Q (ubiquinone)". In: *Proceedings of the National Academy of Sciences of the United States of America* 98.4 (Feb. 2001), pp. 1416–1421. ISSN: 00278424. DOI: 10.1073/PNAS.98.4.1416. URL: www.pnas.org.

[202] N. Takeyama, N. Matsuo, and T. Tanaka. "Oxidative damage to mitochondria is mediated by the Ca2+-dependent inner-membrane permeability transition". In: *Biochemical Journal* 294.3 (Sept. 1993), pp. 719–725. ISSN: 0264-6021. DOI: 10.1042/BJ2940719. URL: /biochemj/article/294/3/719/29950/Oxidative-damage-to-mitochondria-is-mediated-by%20https://portlandpress.com/biochemj/article/294/3/719/29950/Oxidative-damage-to-mitochondria-is-mediated-by.

[203] Massimo Bonora and Paolo Pinton. "The mitochondrial permeability transition pore and cancer: Molecular mechanisms involved in cell death". In: *Frontiers in Oncology* 4.NOV (2014), p. 302. ISSN: 2234943X. DOI: 10.3389/FONC.2014.00302/BIBTEX.

[204] Sabzali Javadov and Morris Karmazyn. "Mitochondrial Permeability Transition Pore Opening as an Endpoint to Initiate Cell Death and as a Putative Target for Cardioprotection". In: *Cellular Physiology and Biochemistry* 20.1-4 (2007), pp. 1–22. ISSN: 1015-8987. DOI: 10.1159/000103747. URL: https://www.karger.com/Article/FullText/103747%20https://www.karger.com/Article/Abstract/103747.

[205] Mikael Turunen, Jerker Olsson, and Gustav Dallner. "Metabolism and function of coenzyme Q". In: *Biochimica et Biophysica Acta (BBA) - Biomembranes* 1660.1-2 (Jan. 2004), pp. 171–199. ISSN: 0005-2736. DOI: 10.1016/J.BBAMEM.2003.11.012.

[206] Yiyi Zhang et al. "The lipid compositions of different regions of rat brain during development and aging". In: *Neurobiology of Aging* 17.6 (Nov. 1996), pp. 869–875. ISSN: 0197-4580. DOI: 10.1016/S0197-4580(96)00076-0.

[207] Valerian E. Kagan et al. "Antioxidant action of ubiquinol homologues with different isoprenoid chain length in biomembranes". In: *Free Radical Biology and Medicine* 9.2 (Jan. 1990), pp. 117–126. ISSN: 0891-5849. DOI: 10.1016/0891-5849(90)90114-X.

[208] Justin G. Fedor et al. "Correlating kinetic and structural data on ubiquinone binding and reduction by respiratory complex I". In: *Proceedings of the National Academy of Sciences of the United States of America* 114.48 (Nov. 2017), pp. 12737–12742. ISSN: 10916490. DOI: 10.1073/PNAS.1714074114/-/DCSUPPLEMENTAL. URL: /pmc/articles/PMC5715780/%20/pmc/articles/PMC5715780/?report=abstract%20https://www.ncbi.nlm.nih.gov/pmc/articles/PMC5715780/.

[209] Yuping Yang et al. "Decaprenyl Diphosphate Synthase Subunit 1 (PDSS1): A Potential Prognostic Biomarker and Immunotherapy-Target for Hepatocellular Carcinoma". In: *Cancer management and research* 14 (2022), pp. 1627–1639. ISSN: 1179-1322. DOI: 10.2147/CMAR.S364346. URL: https://pubmed.ncbi.nlm.nih.gov/35535267/.

[210] Baohui Zhang et al. "A hypoxia-related signature for clinically predicting diagnosis, prognosis and immune microenvironment of hepatocellular carcinoma patients". In: *Journal of Translational Medicine* 18.1 (Sept. 2020). ISSN: 14795876. DOI: 10.1186/S12967-020-02492-9. URL: /pmc/articles/PMC7487492/%20/pmc/articles/PMC7487492/?report=abstract%20https://www.ncbi.nlm.nih.gov/pmc/articles/PMC7487492/.

[211] Irene Liparulo et al. "Coenzyme Q biosynthesis inhibition induces HIF-1α stabilization and metabolic switch toward glycolysis". In: *The FEBS journal* 288.6 (Mar. 2021), pp. 1956–1974. ISSN: 1742-4658. DOI: 10.1111/FEBS.15561. URL: https://pubmed.ncbi.nlm.nih.gov/32898935/.

[212] Tulin Dadali et al. "Elevated levels of mitochondrial CoQ 10 induce ROS-mediated apoptosis in pancreatic cancer". In: *Scientific reports* 11.1 (Dec. 2021). ISSN: 2045-2322. DOI: 10.1038/S41598-021-84852-Z. URL: https://pubmed.ncbi.nlm.nih.gov/33707480/.

[213] Francesca Nardecchia et al. "Missense PDSS1 mutations in CoenzymeQ10 synthesis cause optic atrophy and sensorineural deafness". In: *Annals of clinical and translational neurology* 8.1 (Jan. 2021), pp. 247–251. ISSN: 2328-9503. DOI: 10.1002/ACN3.51232. URL: https://pubmed.ncbi.nlm.nih.gov/33285023/.

[214] Julie Mollet et al. "Prenyldiphosphate synthase, subunit 1 (PDSS1) and OH-benzoate polyprenyltransferase (COQ2) mutations in ubiquinone deficiency and oxidative phosphorylation disorders". In: *The Journal of clinical investigation* 117.3 (Mar. 2007), pp. 765–772. ISSN: 0021-9738. DOI: 10.1172/JCI29089. URL: https://pubmed.ncbi.nlm.nih.gov/17332895/.

[215] "Mutations in COQ2 in familial and sporadic multiple-system atrophy". In: *The New England journal of medicine* 369.3 (July 2013), pp. 233–244. ISSN: 1533-4406. DOI: 10.1056/NEJMOA1212115. URL: https://pubmed.ncbi.nlm.nih.gov/23758206/.

[216] Agnès Rötig et al. "Quinone-responsive multiple respiratory-chain dysfunction due to widespread coenzyme Q10 deficiency". In: *Lancet (London, England)* 356.9227 (July 2000), pp. 391–395. ISSN: 0140-6736. DOI: 10.1016/S0140-6736(00)02531-9. URL: https://pubmed.ncbi.nlm.nih.gov/10972372/.

[217] Julie Mollet et al. "Prenyldiphosphate synthase, subunit 1 (PDSS1) and OH-benzoate polyprenyltransferase (COQ2) mutations in ubiquinone deficiency and oxidative phosphorylation disorders". In: *The Journal of Clinical Investigation* 117.3 (Mar. 2007), pp. 765–772. ISSN: 0021-9738. DOI: 10.1172/JCI29089. URL: http://www.jci.org.

[218] Iain Hargreaves, Robert A. Heaton, and David Mantle. "Disorders of Human Coenzyme Q10 Metabolism: An Overview". In: *International Journal of Molecular Sciences* 21.18 (Sept. 2020), pp. 1–13. ISSN: 14220067. DOI: 10.3390/IJMS21186695. URL: /pmc/articles/PMC7555759/%20/pmc/articles/PMC7555759/?report=abstract%20https://www.ncbi.nlm.nih.gov/pmc/articles/PMC7555759/.

[219] Daniel J M Fernández-Ayala et al. "Survival transcriptome in the coenzyme Q 10 deficiency syndrome is acquired by epigenetic modifications: a modelling study for human coenzyme Q 10 deficiencies". In: *BMJ Open* 3 (2013), p. 2524. DOI: 10.1136/bmjopen-2012. URL: http://dx.doi.org/10.1136/bmjopen-2012-002524.

[220] Delia Yubero et al. "Biochemical Diagnosis of Coenzyme Q10 Deficiency". In: *Molecular Syndromology* 5.3-4 (2014), p. 147. ISSN: 16618777. DOI: 10.1159/000362390. URL: /pmc/articles/PMC4112526/%20/pmc/articles/PMC4112526/?report=abstract%20https://www.ncbi.nlm.nih.gov/pmc/articles/PMC4112526/.

[221] Daniel J.M. Fernandez-Ayala et al. "Survival transcriptome in the coenzyme Q10 deficiency syndrome is acquired by epigenetic modifications: a modelling study for human coenzyme Q10 deficiencies". In: *BMJ Open* 3.3 (Jan. 2013), e002524. ISSN: 2044-6055. DOI: 10.1136/BMJOPEN-2012-002524. URL: https://bmjopen.bmj.com/content/3/3/e002524%20https://bmjopen.bmj.com/content/3/3/e002524.abstract.

[222] Alba Luengo et al. "Increased demand for NAD + relative to ATP drives aerobic glycolysis". In: *Molecular cell* 81.4 (Feb. 2021), pp. 691–707. ISSN: 1097-4164. DOI: 10.1016/J.MOLCEL.2020.12.012. URL: https://pubmed.ncbi.nlm.nih.gov/33382985/.

[223] Michael J. Bennett, Piero Rinaldo, and Arnold W. Strauss. "Inborn errors of mitochondrial fatty acid oxidation". In: *Critical reviews in clinical laboratory sciences* 37.1 (2000), pp. 1–44. ISSN: 1040-8363. DOI: 10.1080/10408360091174169. URL: https://pubmed.ncbi.nlm.nih.gov/10737439/.

[224] Leonardo Salviati et al. "Primary Coenzyme Q10 Deficiency". In: *GeneReviews®* (Jan. 2017). URL: https://www.ncbi.nlm.nih.gov/books/NBK410087/.

[225] Shuaiyi Chen et al. "SIRT3 regulates cancer cell proliferation through deacetylation of PYCR1 in proline metabolism". In: *Neoplasia (New York, N.Y.)* 21.7 (July 2019), pp. 665–675. ISSN: 1476-5586. DOI: 10.1016/J.NEO.2019.04.008. URL: https://pubmed.ncbi.nlm.nih.gov/31108370/.

[226] Mattia Falcone et al. "Sensitisation of cancer cells to radiotherapy by serine and glycine starvation". In: *British Journal of Cancer 2022 127:10* 127.10 (Sept. 2022), pp. 1773–1786. ISSN: 1532-1827. DOI: 10.1038/s41416-022-01965-6. URL: https://www.nature.com/articles/s41416-022-01965-6.

[227] Kivanç Birsoy et al. "An Essential Role of the Mitochondrial Electron Transport Chain in Cell Proliferation Is to Enable Aspartate Synthesis". In: *Cell* 162.3 (Aug. 2015), pp. 540–551. ISSN: 1097-4172. DOI: 10.1016/J.CELL.2015.07.016. URL: https://pubmed.ncbi.nlm.nih.gov/26232224/.

[228] Kivanç Birsoy et al. "An Essential Role of the Mitochondrial Electron Transport Chain in Cell Proliferation Is to Enable Aspartate Synthesis". In: *Cell* 162.3 (July 2015), pp. 540–551. ISSN: 0092-8674. DOI: 10.1016/J.CELL.2015.07.016.

[229] Zhaoqi Li et al. "Cancer cells depend on environmental lipids for proliferation when electron acceptors are limited". In: *Nature Metabolism 2022 4:6* 4.6 (June 2022), pp. 711–723. ISSN: 2522-5812. DOI: 10.1038/s42255-022-00588-8. URL: https://www.nature.com/articles/s42255-022-00588-8.

[230] Chad N. Hancock et al. "Co-regulation of mitochondrial respiration by proline dehydrogenase/oxidase and succinate". In: *Amino acids* 48.3 (Mar. 2016), pp. 859–872. ISSN: 1438-2199. DOI: 10.1007/S00726-015-2134-7. URL: https://pubmed.ncbi.nlm.nih.gov/26660760/.

[231] Matthew D. Shoulders and Ronald T. Raines. "COLLAGEN STRUCTURE AND STABILITY". In: *Annual review of biochemistry* 78 (2009), p. 929. ISSN: 00664154. DOI: 10.1146/ANNUREV.BIOCHEM.77.032207.120833. URL: /pmc/articles/

PMC2846778/%20/pmc/articles/PMC2846778/?report=abstract%20https://www.ncbi.nlm.nih.gov/pmc/articles/PMC2846778/.

[232] Bing Hua Jiang et al. "Dimerization, DNA Binding, and Transactivation Properties of Hypoxia-inducible Factor 1 *". In: *Journal of Biological Chemistry* 271.30 (July 1996), pp. 17771–17778. ISSN: 0021-9258. DOI: 10.1074/JBC.271.30.17771. URL: http://www.jbc.org/article/S0021925819869806/fulltext%20http://www.jbc.org/article/S0021925819869806/abstract%20https://www.jbc.org/article/S0021-9258(19)86980-6/abstract.

[233] Dylan G. Ryan et al. "Disruption of the TCA cycle reveals an ATF4-dependent integration of redox and amino acid metabolism". In: *eLife* 10 (Dec. 2021). ISSN: 2050084X. DOI: 10.7554/ELIFE.72593. URL: /pmc/articles/PMC8735863/%20/pmc/articles/PMC8735863/?report=abstract%20https://www.ncbi.nlm.nih.gov/pmc/articles/PMC8735863/.

[234] Fredrik Åberg et al. "Distribution and redox state of ubiquinones in rat and human tissues". In: *Archives of Biochemistry and Biophysics* 295.2 (June 1992), pp. 230–234. ISSN: 0003-9861. DOI: 10.1016/0003-9861(92)90511-T.

[235] S. Kaul, S. S. Sharma, and I. K. Mehta. "Free radical scavenging potential of L-proline: Evidence from in vitro assays". In: *Amino Acids* 34.2 (Feb. 2008), pp. 315–320. ISSN: 09394451. DOI: 10.1007/S00726-006-0407-X/METRICS. URL: https://link.springer.com/article/10.1007/s00726-006-0407-x.

[236] Rachel E. Airley et al. "GLUT-1 and CAIX as intrinsic markers of hypoxia in carcinoma of the cervix: relationship to pimonidazole binding". In: *International journal of cancer* 104.1 (Mar. 2003), pp. 85–91. ISSN: 0020-7136. DOI: 10.1002/IJC.10904. URL: https://pubmed.ncbi.nlm.nih.gov/12532423/.

[237] Todd C. Carpenter et al. "Hypoxia reversibly inhibits epithelial sodium transport but does not inhibit lung ENaC or Na-K-ATPase expression". In: *American journal of physiology. Lung cellular and molecular physiology* 284.1 (Jan. 2003). ISSN: 1040-0605. DOI: 10.1152/AJPLUNG.00181.2002. URL: https://pubmed.ncbi.nlm.nih.gov/12388331/.

[238] Emily M. Christensen et al. "In crystallo screening for proline analog inhibitors of the proline cycle enzyme PYCR1". In: *Journal of Biological Chemistry* 295.52 (Dec. 2020), pp. 18316–18327. ISSN: 0021-9258. DOI: 10.1074/JBC.RA120.016106. URL:

http://www.jbc.org/article/S0021925817507012/fulltext%20http://www.jbc.org/article/S0021925817507012/abstract%20https://www.jbc.org/article/S0021-9258(17)50701-2/abstract.

[239] Tomer Meirson, Hava Gil-Henn, and Abraham O. Samson. "Invasion and metastasis: the elusive hallmark of cancer". In: *Oncogene 2019 39:9* 39.9 (Nov. 2019), pp. 2024–2026. ISSN: 1476-5594. DOI: 10.1038/s41388-019-1110-1. URL: https://www.nature.com/articles/s41388-019-1110-1.

[240] Daniel J.M. Fernández-Ayala et al. "Invertebrate Models for Coenzyme Q10 Deficiency". In: *Molecular Syndromology* 5.3-4 (2014), pp. 170–179. ISSN: 1661-8769. DOI: 10.1159/000362751. URL: https://www.karger.com/Article/FullText/362751%20https://www.karger.com/Article/Abstract/362751.

[241] Ralph J. DeBerardinis. "Is cancer a disease of abnormal cellular metabolism? New angles on an old idea". In: *Genetics in medicine : official journal of the American College of Medical Genetics* 10.11 (Nov. 2008), pp. 767–777. ISSN: 1530-0366. DOI: 10.1097/GIM.0B013E31818B0D9B. URL: https://pubmed.ncbi.nlm.nih.gov/18941420/.

[242] *l-Asparagine Requirement and the Effect of l-Asparaginase on the Normal and Leukemic Human Bone Marrow1 | Cancer Research | American Association for Cancer Research.* URL: https://aacrjournals.org/cancerres/article/30/2/466/477756/l-Asparagine-Requirement-and-the-Effect-of-l.

[243] Diem H. Tran et al. "Mitochondrial NADP+ is essential for proline biosynthesis during cell growth". In: *Nature metabolism* 3.4 (Apr. 2021), p. 571. ISSN: 25225812. DOI: 10.1038/S42255-021-00374-Y. URL: /pmc/articles/PMC9210447/%20/pmc/articles/PMC9210447/?report=abstract%20https://www.ncbi.nlm.nih.gov/pmc/articles/PMC9210447/.

[244] Philippe Marchetti et al. "Mitochondrial spare respiratory capacity: Mechanisms, regulation, and significance in non-transformed and cancer cells". In: *FASEB Journal* 34.10 (Oct. 2020), pp. 13106–13124. ISSN: 15306860. DOI: 10.1096/FJ.202000767R.

[245] Yongmin Liu et al. "MnSOD inhibits proline oxidase-induced apoptosis in colorectal cancer cells". In: *Carcinogenesis* 26.8 (Aug. 2005), pp. 1335–1342. ISSN: 0143-3334. DOI: 10.1093/CARCIN/BGI083. URL: https://pubmed.ncbi.nlm.nih.gov/15817612/.

[246] Sotirios Bisdas et al. "MR spectroscopy for in vivo assessment of the oncometabolite 2-hydroxyglutarate and its effects on cellular metabolism in human brain gliomas at 9.4T". In: *Journal of magnetic resonance imaging : JMRI* 44.4 (Oct. 2016), pp. 823–833. ISSN: 1522-2586. DOI: 10.1002/JMRI.25221. URL: https://pubmed.ncbi.nlm.nih.gov/26970248/.

[247] Rub En Zapata-P Erez et al. "NAD+ homeostasis in human health and disease". In: *EMBO Molecular Medicine* 13.7 (July 2021), e13943. ISSN: 1757-4684. DOI: 10.15252/EMMM.202113943. URL: https://onlinelibrary.wiley.com/doi/full/10.15252/emmm.202113943%20https://onlinelibrary.wiley.com/doi/abs/10.15252/emmm.202113943%20https://www.embopress.org/doi/abs/10.15252/emmm.202113943.

[248] Weihai Ying. "NAD+/NADH and NADP+/NADPH in Cellular Functions and Cell Death: Regulation and Biological Consequences". In: *https://home.liebertpub.com/ars* 10.2 (Dec. 2007), pp. 179–206. ISSN: 15230864. DOI: 10.1089/ARS.2007.1672. URL: https://www.liebertpub.com/doi/abs/10.1089/ars.2007.1672.

[249] Chien An Hu et al. "Overexpression of proline oxidase induces proline-dependent and mitochondria-mediated apoptosis". In: *Molecular and cellular biochemistry* 295.1-2 (Jan. 2007), pp. 85–92. ISSN: 0300-8177. DOI: 10.1007/S11010-006-9276-6. URL: https://pubmed.ncbi.nlm.nih.gov/16874462/.

[250] Jui Pandhare, Sandra K. Cooper, and James M. Phang. "Proline oxidase, a proapoptotic gene, is induced by troglitazone: evidence for both peroxisome proliferator-activated receptor gamma-dependent and -independent mechanisms". In: *The Journal of biological chemistry* 281.4 (Jan. 2006), pp. 2044–2052. ISSN: 0021-9258. DOI: 10.1074/JBC.M507867200. URL: https://pubmed.ncbi.nlm.nih.gov/16303758/.

[251] Shuangkuan Du et al. "PYCR1 promotes bladder cancer by affecting the Akt/Wnt/β-catenin signaling". In: *Journal of bioenergetics and biomembranes* 53.2 (Apr. 2021), pp. 247–258. ISSN: 1573-6881. DOI: 10.1007/S10863-021-09887-3. URL: https://pubmed.ncbi.nlm.nih.gov/33689096/.

[252] Inge Oudaert et al. "Pyrroline-5-Carboxylate Reductase 1: a novel target for sensitizing multiple myeloma cells to bortezomib by inhibition of PRAS40-mediated protein synthesis". In: *Journal of experimental & clinical cancer research : CR* 41.1 (Dec. 2022). ISSN: 1756-9966. DOI: 10.1186/S13046-022-02250-3. URL: https://pubmed.ncbi.nlm.nih.gov/35105345/.

[253] Shuaiyi Chen et al. "SIRT3 regulates cancer cell proliferation through deacetylation of PYCR1 in proline metabolism". In: *Neoplasia (New York, N.Y.)* 21.7 (July 2019), pp. 665–675. ISSN: 1476-5586. DOI: 10.1016/J.NEO.2019.04.008. URL: https://pubmed.ncbi.nlm.nih.gov/31108370/.

[254] Tommi A. White et al. "Structure and kinetics of monofunctional proline dehydrogenase from Thermus thermophilus". In: *The Journal of biological chemistry* 282.19 (May 2007), pp. 14316–14327. ISSN: 0021-9258. DOI: 10.1074/JBC.M700912200. URL: https://pubmed.ncbi.nlm.nih.gov/17344208/.

[255] Lucas B. Sullivan et al. "Supporting Aspartate Biosynthesis Is an Essential Function of Respiration in Proliferating Cells". In: *Cell* 162.3 (Aug. 2015), pp. 552–563. ISSN: 1097-4172. DOI: 10.1016/J.CELL.2015.07.017. URL: https://pubmed.ncbi.nlm.nih.gov/26232225/.

[256] Frederick L. Crane and Plácido Navas. "The diversity of coenzyme Q function". In: *Molecular aspects of medicine* 18 Suppl.SUPPL. (1997), pp. 1–6. ISSN: 0098-2997. DOI: 10.1016/S0098-2997(97)00016-2. URL: https://pubmed.ncbi.nlm.nih.gov/9266500/.

[257] *The Ki-67 protein: From the known and the unknown.* URL: https://onlinelibrary.wiley.com/doi/epdf/10.1002/%28SICI%291097-4652%28200003%29182%3A3%3C311%3A%3AAID-JCP1%3E3.0.CO%3B2-9?saml_referrer.

.1 Proline synthesis through PYCR1 is required to support cancer cell proliferation and survival in oxygen-limiting conditions

Article

Cell Reports

Proline synthesis through PYCR1 is required to support cancer cell proliferation and survival in oxygen-limiting conditions

Graphical abstract

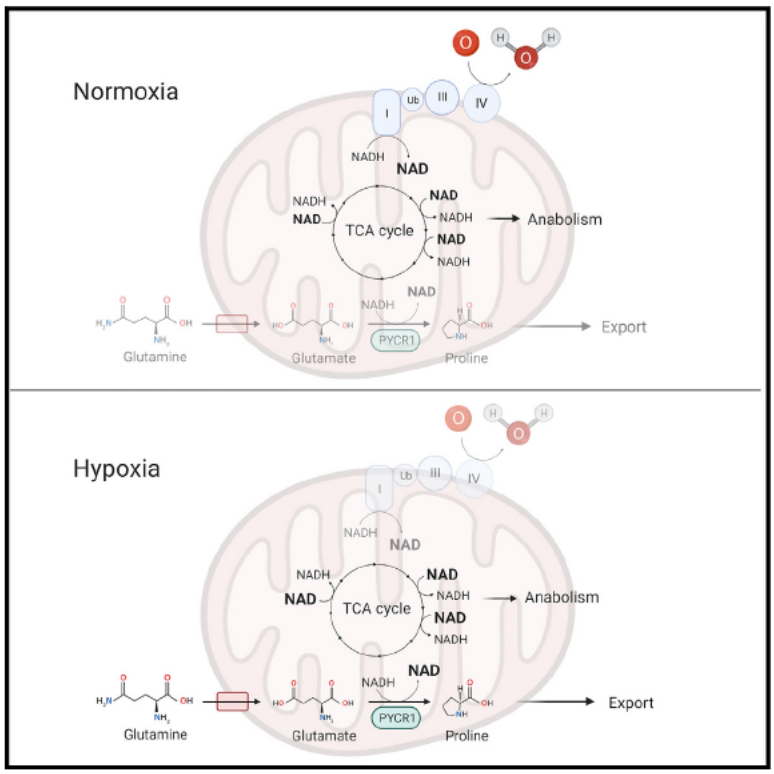

Highlights

- Proline synthesis through PYCR1 is increased in low-oxygen conditions
- PYCR1 activity in hypoxia supports TCA cycle function through NADH oxidation
- PYCR1 is required for maintenance of hypoxic tumor regions

Authors

Rebecca L. Westbrook, Esther Bridges, Jennie Roberts, ..., David J. Hodson, Adrian L. Harris, Daniel A. Tennant

Correspondence

In brief

Westbrook et al. show that proline synthesis from glutamine through PYCR1 supports NADH oxidation when oxygen is limited. PYCR1 therefore represents an oxygen-independent means of regenerating NAD^+ in hypoxia, supporting continued oxidative TCA cycle activity. Loss of PYCR1 in tumors results in increased hypoxia, reduced cell viability, and necrosis.

Westbrook et al., 2022, Cell Reports *38*, 110320
February 1, 2022
https://doi.org/10.1016/j.celrep.2022.110320

CellPress

Cell Reports

CellPress
OPEN ACCESS

Article

Proline synthesis through PYCR1 is required to support cancer cell proliferation and survival in oxygen-limiting conditions

Rebecca L. Westbrook,[1] Esther Bridges,[2,3] Jennie Roberts,[1] Cristina Escribano-Gonzalez,[1] Katherine L. Eales,[1] Lisa A. Vettore,[1] Paul D. Walker,[1] Elias Vera-Siguenza,[1] Himani Rana,[1] Federica Cuozzo,[1] Kattri-Liis Eskla,[4,5] Hans Vellama,[4,5] Abeer Shaaban,[6] Colin Nixon,[7] Hendrik Luuk,[4,5] Gareth G. Lavery,[1,8] David J. Hodson,[1] Adrian L. Harris,[2] and Daniel A. Tennant[1,9,10,*]

[1]Institute of Metabolism and Systems Research, College of Medical and Dental Sciences, University of Birmingham, Birmingham B15 2TT, UK
[2]Hypoxia and Angiogenesis Group, Cancer Research UK Molecular Oncology Laboratories, Weatherall Institute of Molecular Medicine, Department of Oncology, University of Oxford, Oxford OX3 9DS, UK
[3]MRC Human Immunology Unit, MRC Weatherall Institute of Molecular Medicine, Department of Oncology, University of Oxford, Oxford OX3 9DS, UK
[4]Institute of Biomedicine and Translational Medicine, Department of Physiology, University of Tartu, Tartu, Estonia
[5]Centre of Excellence for Genomics and Translational Medicine, University of Tartu, Tartu, Estonia
[6]University Hospital Birmingham NHS Foundation Trust and Institute of Cancer and Genomic Sciences, College of Medical and Dental Sciences, University of Birmingham, Birmingham B15 2TT, UK
[7]Beatson Institute for Cancer Research, University of Glasgow, Switchback Road, Glasgow G61 1BD, UK
[8]Present address: Department of Biosciences, School of Science and Technology, Nottingham Trent University, Clifton Campus, Nottingham, UK
[9]Twitter: @tennantlab
[10]Lead contact
*Correspondence: d.tennant@bham.ac.uk
https://doi.org/10.1016/j.celrep.2022.110320

SUMMARY

The demands of cancer cell proliferation alongside an inadequate angiogenic response lead to insufficient oxygen availability in the tumor microenvironment. Within the mitochondria, oxygen is the major electron acceptor for NADH, with the result that the reducing potential produced through tricarboxylic acid (TCA) cycle activity and mitochondrial respiration are functionally linked. As the oxidizing activity of the TCA cycle is required for efficient synthesis of anabolic precursors, tumoral hypoxia could lead to a cessation of proliferation without another means of correcting the redox imbalance. We show that in hypoxic conditions, mitochondrial pyrroline 5-carboxylate reductase 1 (PYCR1) activity is increased, oxidizing NADH with the synthesis of proline as a by-product. We further show that PYCR1 activity is required for the successful maintenance of hypoxic regions by permitting continued TCA cycle activity, and that its loss leads to significantly increased hypoxia *in vivo* and in 3D culture, resulting in widespread cell death.

INTRODUCTION

Proline is a unique non-essential amino acid with critical roles in both protein structure and the cellular stress response (Phang et al., 2008). Although its function in the appropriate folding of polypeptides has long been understood, evidence over the past few years has suggested that it may play a central role in maintaining redox homeostasis in mammalian systems (Krishnan et al., 2008; Phang, 2019; Phang et al., 2008; Vettore et al., 2021).

Much of the balance of oxidizing and reducing potential within cells is achieved by two pyridine nucleotide couples: NAD^+:NADH and $NADP^+$:NADPH. The NAD^+:NADH redox couple are of particular importance in linking central carbon metabolism with ATP generation. One of the best defined cytosolic examples of this is the activity of lactate dehydrogenase (LDH), which balances the cytosolic NAD^+/NADH ratio through reduction of pyruvate (or oxidation of lactate) (Markert, 1984). However, the mitochondria are major contributors to the overall cellular NAD^+/NADH ratio, with the oxidizing activity of the tricarboxylic acid (TCA) cycle driving significant reduction of the mitochondrial NAD^+ pool. Under normal conditions, the high energy electrons from resulting NADH are used to generate the proton gradient across the inner mitochondrial membrane, which generates ATP through oxidative phosphorylation. However, NADH oxidation by the electron transport chain requires sufficient oxygen to act as the terminal electron acceptor. In conditions of low oxygen (hypoxia) the mitochondrial NADH/NAD^+ ratio increases, resulting in fragmentation of the TCA cycle and the need to shuttle reducing potential into the cytosol through the malate-aspartate shuttle (Frezza et al., 2011; LaNoue et al., 1973). The resulting shift in the cytosolic NAD^+/NADH ratio

results in an increase in lactate production (Eales et al., 2016). Importantly, hypoxia is a particularly prevalent factor in cancer growth, during which the rate of cell proliferation is often in excess of the delivery of oxygen via the dysfunctional tumor vasculature (Harris, 2002). In such conditions, the NAD^+/NADH ratio can become limiting for cell proliferation (Luengo et al., 2021), which may increase the activity of other redox-active pathways as a means of regenerating NAD^+.

The metabolism of proline is significantly linked to cellular redox state (Phang et al., 2008). Proline degradation is catalyzed by proline oxidase (also known as proline dehydrogenase [PRODH]), which reduces ubiquinone in the mitochondrial inner membrane via $FADH_2$ (Phang et al., 2010). This facilitates proton pumping and ATP synthesis, and can also generate reactive oxygen species through electron leakage. Synthesis of proline utilizes the reducing potential of either NADH or NADPH (De Ingeniis et al., 2012). This reaction is a two-step process, the first of these generating the intermediate glutamate 5-semialdehyde (GSA), which spontaneously cyclizes to form pyrroline 5-carboxylate (P5C). GSA can be formed either from glutamate by the action of P5C synthase (P5CS/ALDH18A1) coupled to the oxidation of NADPH, or from ornithine, which is coupled instead to the transamination of α-ketoglutarate (Burke et al., 2020). The second reaction is catalyzed by one of three isozymes with pyrroline 5-carboxylate reductase activity, known as PYCR1, PYCR2, and PYCR3/L. Importantly, while PYCR1 and PYCR2 are in the mitochondrial matrix, PYCR3 is known to be cytosolic, compartmentalizing aspects of this metabolic network (De Ingeniis et al., 2012). Previous studies have suggested that the activity of PRODH and PYCR enzymes might act together as a cycle, which could move proline, intermediates, and, therefore, redox equivalents between the mitochondria and the cytosol (Phang et al., 2012). However, it is likely that the activity of each of these enzymes is dependent on the cellular context and microenvironment. As an example, while metastatic cells have been shown to have an overall proline catabolic activity utilizing the energy generated via proline degradation to support the invasive process (Elia et al., 2017; Scott et al., 2019), fibroblasts stimulated with transforming growth factor β demonstrate increased proline synthesis (Schworer et al., 2020).

We and others recently suggested that proline biosynthesis through PYCR1 could be an alternative means by which mitochondria could continue to support TCA cycle oxidative activity while bypassing the need to pass the resulting electrons into the electron transport chain (Hollinshead et al., 2018; Schworer et al., 2020). There is some evidence that this could be true in conditions where oxygen is limiting due to reduction of the electron transport chain and increase in NADH/NAD^+ ratio in the mitochondrial matrix (Liu et al., 2020). In this study, we show that mitochondrial proline synthesis, specifically through PYCR1 activity, is essential to support hypoxic metabolism and viability. Loss of PYCR1 *in vivo* results in an unsustainable compensatory increase in respiration, cell death, and decreased tumor growth. We therefore propose that inhibition of PYCR1 is a viable target for killing cancer cells in hypoxic tumor regions, which are refractory to many conventional treatment approaches.

RESULTS

Hypoxia increases PYCR1-dependent proline synthesis and export from glutamine

Our previous research, and that of others, suggested that proline synthesis is increased in cells when cellular redox homeostasis is perturbed or when enhanced oxidation of mitochondrial NADH is required (Hollinshead et al., 2018; McGregor et al., 2020; Schworer et al., 2020). We previously hypothesized that this phenotype is likely to occur under conditions where the NADH/NAD^+ ratio becomes limiting for oxidizing TCA cycle activity, such as in hypoxia (Hollinshead et al., 2018). We therefore investigated whether this was the case by incubating human cells in either normoxia (21% O_2) or increasing severity of hypoxia (1% and 0.3% O_2). We found that in a number of cell models representing triple-negative breast cancer (SUM159PT, HCC1806), medulloblastoma (ONS), and bone marrow stromal cells (HS-5), hypoxia enhanced proline synthesis and efflux into the medium (Figures 1A and S1A). Importantly, this appeared to occur without a consistent change in expression of either of the key biosynthetic enzymes, PYCR1 or PYCR2 (Figures 1B, 1C, and S1B), suggesting that the normoxic expression of these enzymes is capable of supporting flux through the pathway in excess of that observed under normoxic conditions.

We previously showed that PYCR1 is responsible for enhanced proline biosynthesis from glutamine in cells expressing the oncogenic IDH1 R132H mutation (Hollinshead et al., 2018). We therefore first examined whether glutamine-derived proline synthesis also underpinned the hypoxia-driven response. SUM159PT cells were incubated with [U-^{13}C]glutamine in normoxia or hypoxia (1% and 0.3% O_2) and demonstrated the expected hypoxia-induced reductions in glutamine oxidation (M + 4 isotopomer of aspartate and citrate; Figures S1C and S1D) as well as a relative increase in the contribution of reductive carboxylation of glutamine to the citrate pool (M + 5 isotopomer; Figure S1D). Under the same conditions, we noted that glutamine-derived proline exported into the medium increased significantly with increasing severity of hypoxia (Figure 1D), indicative of increased mitochondrial synthesis. We consider the ratio of fully labeled glutamate to proline a surrogate of the overall activity of this pathway (Figure 1B). Although this ratio was significantly increased in 1% O_2, it returned to normoxic levels in 0.3% O_2 (Figure 1E). Given that export of proline into the medium was significantly enhanced in these conditions (Figure 1D), we concluded that this likely reflected a further adaptation to increased proline synthesis under severe hypoxia to relieve the product inhibition on PYCR enzymes that may otherwise be suboptimal for continued cell viability (De Ingeniis et al., 2012).

Two constitutively expressed mitochondrial isozymes, PYCR1 and PYCR2, are responsible for the second step in the synthesis of proline from glutamate (Figure 1B). To elucidate which of these might demonstrate a hypoxia-mediated induction of activity, we knocked down PYCR1 or PYCR2 (Figure S1E) and examined the synthesis of proline in normoxia and hypoxia. We observed that knockdown of PYCR1 resulted in a significant decrease of intracellular proline in normoxia and an inability to respond to hypoxia (Figure 1F). Conversely, knockdown of PYCR2 had little effect (Figure 1F). In light of our previous data suggesting that PYCR1

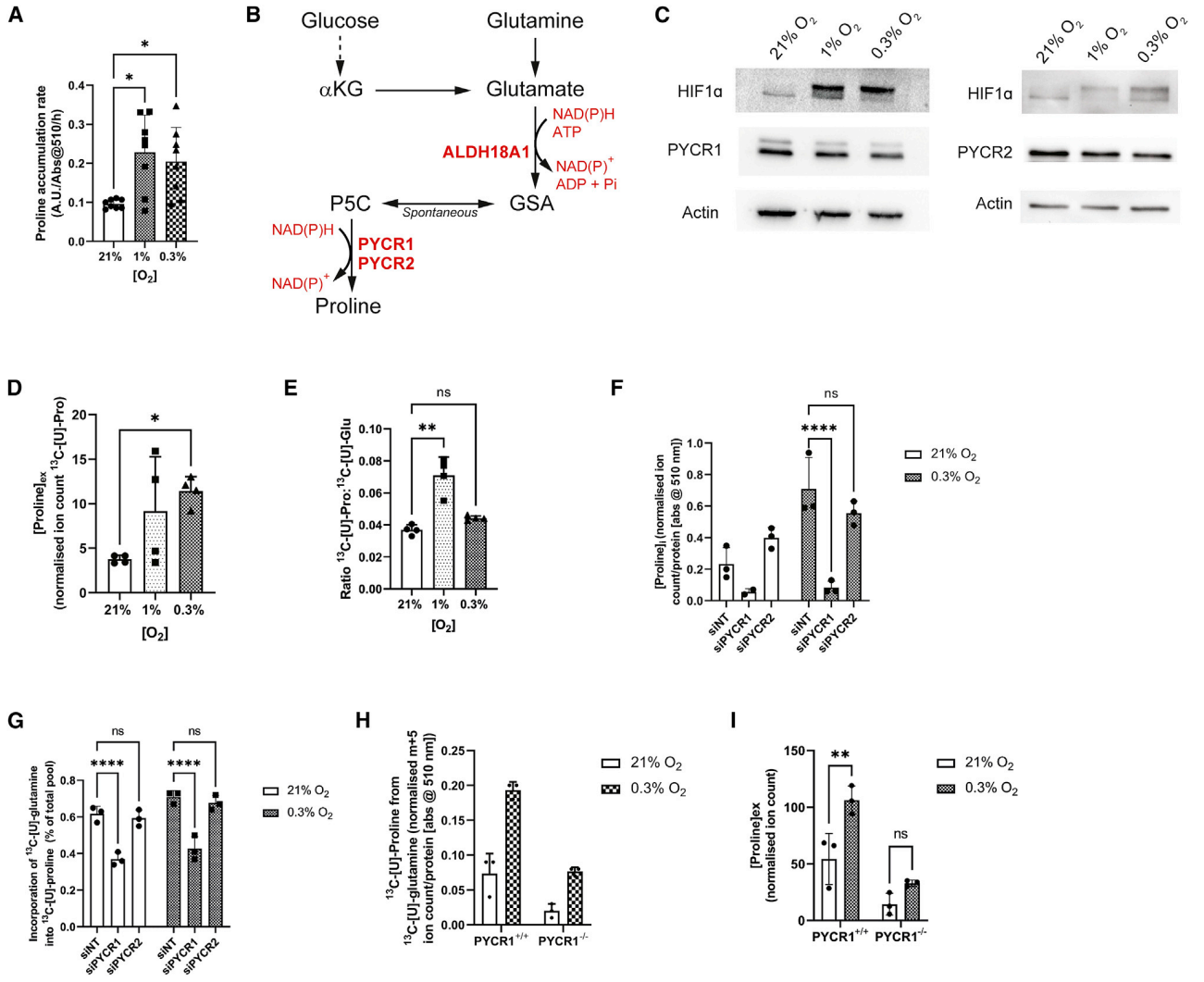

Figure 1. Hypoxia increases PYCR1 dependent proline synthesis and export from glutamine

(A) Intracellular proline abundance in SUM159PT cells is increased with hypoxia (n = 8, presented as mean ± SD). *, $p < 0.05$

(B) Diagram of proline synthesis from glucose and glutamine. αKG, α ketoglutarate; ALDH18A1, aldehyde dehydrogenase 18 family member A1 (pyrroline 5 carboxylate synthase [P5CS]); PYCR1, pyrroline 5 carboxylate reductase 1; PYCR2, pyrroline 5 carboxylate reductase 2.

(C) Protein expression of proline synthetic enzymes does not change with decreasing oxygen tension in SUM159PT cells.

(D) Extracellular proline abundance is significantly increased in 0.3% O_2 in SUM15PT cells (n = 4, presented as mean ± SD). *, $p < 0.05$

(E) The ratio of [U ^{13}C]proline to [U ^{13}C]glutamate from [U ^{13}C]glutamine tracing is significantly increased in 1% O_2 (n = 4, presented as mean ± SD). **, $p < 0.01$

(F) Extracellular proline concentration in SUM159PT cells transfected with siPYCR1 is significantly decreased in hypoxia (0.3%) compared with siNT. siPYCR2 does not significantly alter the proline concentration (n = 3, presented as mean ± SD). ****, $p < 0.0001$

(G) The contribution of glutamine to the total proline pool (%) is significantly reduced with siPYCR1 and not with siPYCR2 (n = 3, presented as mean ± SD). ****, $p < 0.0001$

(H) In hypoxia (0.3% O_2), abundance of [U ^{13}C]proline from [U ^{13}C]glutamine is increased in SUM159PT PYCR1$^{+/+}$ cells. This increase is not seen in PYCR1 $^{/}$ cells (n = 3, presented as mean ± SD).

(I) Total extracellular proline is increased in hypoxia (0.3%) in PYCR1$^{+/+}$ cells. This increase is not seen in PYCR1 $^{/}$ cells (n = 3, presented as mean ± SD). **, $p < 0.01$. αKG, α ketoglutarate; ALDH18A1, aldehyde dehydrogenase 18 family member A1; GSA, glutamate semialdehyde; P5C, pyrroline 5 carboxylate; PYCR1, P5C reductase 1; PYCR2, P5C reductase 2.

was the major determinant of IDH1^{R132H}-driven increased proline synthesis from glutamine in glioma (Hollinshead et al., 2018), we also assessed glutamine-derived proline and noted that knockdown of PYCR1 but not PYCR2 led to a decrease in the proportion of proline derived from glutamine in both normoxia and hypoxia (Figure 1G). To extend these findings to an alternative cell model, we utilized a previously described CRISPR-engineered *PYCR1*$^{-/-}$ SUM159PT cell line (Figure S1F) with $^{13}C_5$-glutamine (Loayza-Puch et al., 2016). In the absence of PYCR1, intracellular proline synthesis from glutamine was

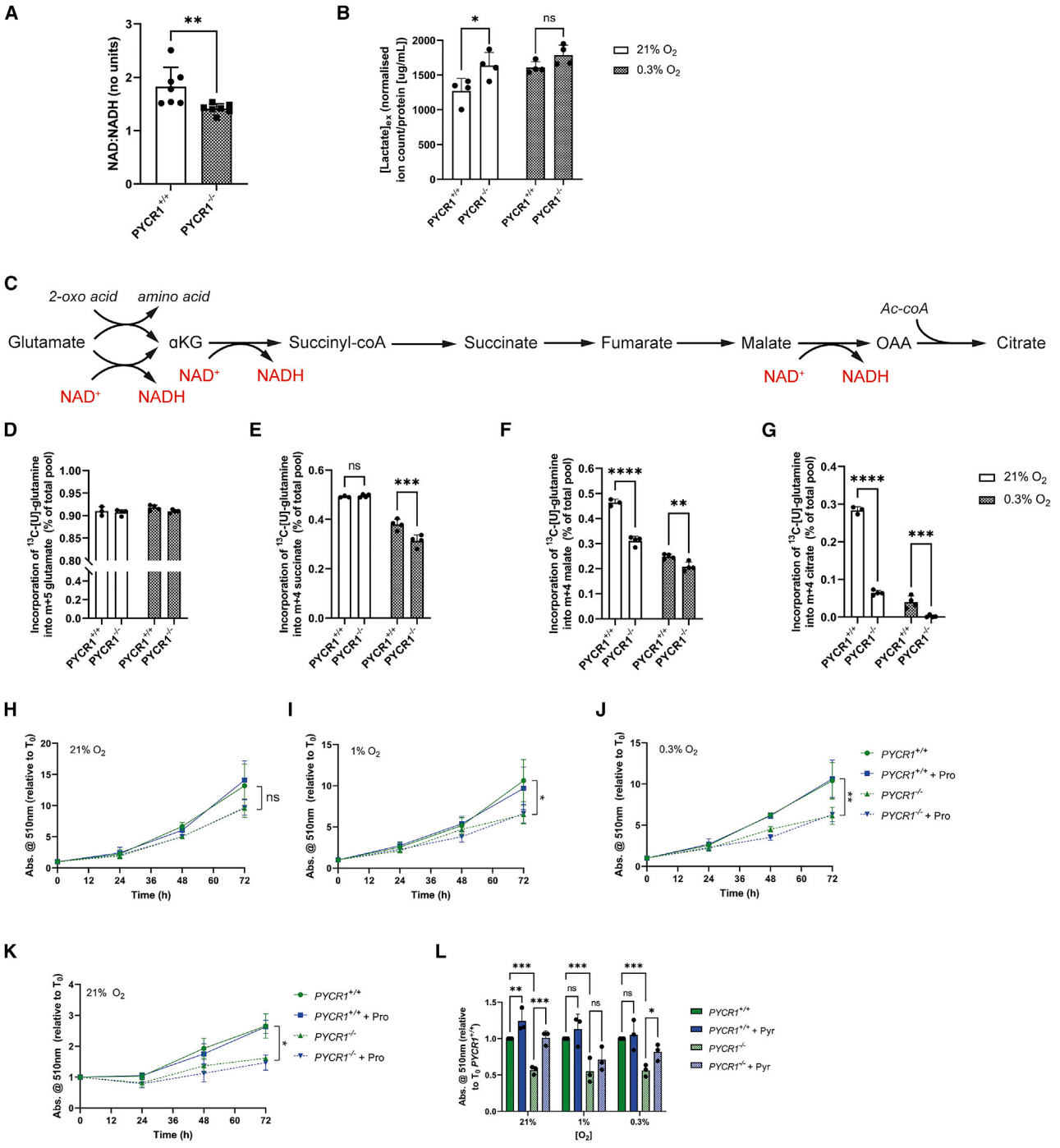

Figure 2. PYCR1 activity supports normal TCA cycle activity and proliferation

(A) The NAD/NADH ratio is significantly reduced in PYCR1 $^{-/-}$ cells (n = 7, presented as mean ± SD). **, $p < 0.01$

(B) Total extracellular lactate (ion count/protein) is increased in PYCR1 $^{-/-}$ cells compared with PYCR1$^{+/+}$. In hypoxia (0.3%) there is no significant change (n = 4, presented as mean ± SD). *, $p < 0.05$

(C) Diagram showing glutamate entry into the TCA cycle, highlighting NAD requiring steps.

(D) Percentage incorporation of [U ^{13}C]glutamine into M + 5 glutamate is unchanged between conditions (n = 4, presented as mean ± SD).

(E) Percentage incorporation of [U ^{13}C]glutamine into M + 4 succinate is decreased in the PYCR1 $^{-/-}$ cells in hypoxia (n = 4, presented as mean ± SD). ***, $p < 0.001$

(F) Percentage incorporation of [U ^{13}C]glutamine into M + 4 malate is reduced in both oxygen tensions in the PYCR1 $^{-/-}$ cells (n = 4, presented as mean ± SD). **, $p < 0.01$; ****, $p < 0.0001$

(legend continued on next page)

significantly reduced but, importantly, the response to hypoxia was also blunted (Figures 1H and S1G). This was also observed in the medium, in which loss of PYCR1 ameliorated the hypoxia-induced efflux of proline (Figure 1I). Our data therefore shows that hypoxia leads to an increase in proline synthesis and export, which is mainly derived from glutamine and is dependent on PYCR1.

PYCR1 activity supports normal TCA cycle activity and proliferation

We and others have suggested that mitochondrial proline synthesis may be an important mechanism to buffer changes in the mitochondrial NAD^+/NADH ratio (Hollinshead et al., 2018; Schworer et al., 2020). We therefore investigated whether loss of PYCR1 led to a change in the NAD^+/NADH ratio in this model, and found that this was indeed the case (Figure 2A), supporting a role for PYCR1 as part of an obligate mitochondrial NAD^+ regeneration system. We also tested whether loss of PYCR1 activity might affect the $NADP^+$/NADPH ratio, as these enzymes are also capable of oxidizing this pyridine nucleotide. To this end, we measured the reduced/oxidized glutathione (GSH/GSSG) ratio—a surrogate of the $NADP^+$/NADPH ratio due to the tight coupling of these systems—and found that it was unchanged in either the small interfering RNA or knockout cell model (Figures S2A and S2B). Due to the specific effect of loss of PYCR1 activity on the NAD^+/NADH ratio, we hypothesized that this may elicit a compensatory increase in respiration or perturbation of the malate-aspartate shuttle, the latter of which could be observed by increased lactate production and export due to enhanced cytosolic NAD^+ regeneration. We found that while respiration was not significantly affected (Figures S2C and S2D), lactate synthesis and efflux was increased in cells deficient for PYCR1 activity in normoxia (Figure 2B). Due to this incomplete compensation, we further examined whether the loss of PYCR1-mediated NADH-oxidizing activity may reduce oxidative TCA cycle flux (Figure 2C). We incubated cells with [U-^{13}C]glutamine and observed reduced incorporation into TCA cycle metabolites in hypoxia after the first NADH-generating steps (synthesis of succinate; Figures 2D, 2E, S2E, and S2F), which was further decreased in subsequent steps (Figures 2F, 2G, S2G, and S2H). Of note, the synthesis of citrate from glutamine, which is downstream of a further NAD^+-dependent step (malate dehydrogenase), was reduced in normoxia and almost entirely absent in hypoxia (Figures 2G and S2H). The reduction in TCA cycle activity after loss of PYCR1 activity could be expected to reduce cell proliferation (Loayza-Puch et al., 2016), as TCA cycle activity (and the synthesis of aspartate) is critical for cellular anabolism (Birsoy et al., 2015; Sullivan et al., 2015). We monitored proliferation in PYCR1$^{-/-}$ cells and noted reduced proliferation in both normoxia and hypoxia (Figures 2H–2J), consistent with other recent data (Milne et al., 2019). As reduced proliferation could be a result of either perturbed redox homeostasis or deficiency in intracellular proline (Sahu et al., 2016), we tested both of these hypotheses. First, we cultured the cells in the presence of exogenous proline and found that despite efficient uptake (Figure S2I), the proliferative defect remained (Figures 2H–2J). However, the fact that the PYCR1$^{-/-}$ cells remained capable of proliferation suggested that the proline normally present in the medium (150 μM) and/or the activities of PYCR2/3 were sufficient to support proliferation. To test this, we cultured cells in an alternative medium without proline and found that the relative proliferative defect between PYCR1$^{+/+}$ and PYCR1$^{-/-}$ cells was still observed, and the phenotype was still not rescued with additional proline (Figure 2K). These data therefore suggested that the remaining PYCR enzymes were capable of synthesizing sufficient proline to support this reduced proliferative rate. To test whether further metabolic support of cellular redox homeostasis might rescue the proliferative defect, we cultured the cells in medium containing additional exogenous pyruvate, which could support increased rates of NADH oxidation. We found that in contrast to proline supplementation, exogenous pyruvate did at least partially rescue proliferation in both normoxia and hypoxia (Figure 2L). Overall, these data strongly support the hypothesis that PYCR1 supports proliferation through maintaining efficient oxidative TCA cycle activity, but in conditions where redox cannot be buffered, such as when oxygen is diffusion limited, PYCR1 may become essential.

Loss of PYCR1 in 3D culture leads to redox imbalance and excessive oxygen consumption

To more accurately recapitulate the multiple metabolite diffusion gradients present *in vivo*, most importantly that of oxygen, we extended our investigation to a three-dimensional (3D) spheroid model. When these were grown using the soft-agar approach, we found that loss of PYCR1 led to a substantial reduction in spheroid size (Figures 3A and 3B). However, due to the duration of this experiment (10 days), the previously described effect on cell proliferation (Figures 2H–2J; Loayza-Puch et al., 2016; Sahu et al., 2016) made it difficult to appropriately interpret the results. We therefore used an alternative method to generate the spheroids, which allows them to rapidly form from a pre-plated number of cells, rather than proliferating to reach the desired cell number (Ivascu and Kubbies, 2006). While spheroids formed efficiently, they remained significantly smaller (Figures 3C and 3D). Importantly, the spheroids did reach a size at which oxygen diffusion was limiting, resulting in hypoxia (pimonidazole staining;

(G) Percentage incorporation of [U ^{13}C]glutamine into M + 4 citrate is reduced in both oxygen tensions in the PYCR1 $^{/}$ cells and is almost undetectable in 0.3% oxygen (n = 4, presented as mean ± SD). ***, $p < 0.001$; ****, $p < 0.0001$

(H J) Cell growth with PYCR1 loss. Statistical analysis shown compares PYCR1$^{+/+}$ and PYCR1 $^{/}$ cells without proline. Comparison of growth of either cell type with or without proline was not significant in 21% O_2 (H), $p < 0.05$ in 1% O_2 (I), and $p < 0.01$ in 0.3% O_2 (J) in DMEM/Nutrient Mixture F 12 Ham. Growth was not altered by the addition of 2 mM exogenous proline in any oxygen tension (n = 3, presented as mean ± SEM).

(K) Cell growth of PYCR1 $^{/}$ cells is maintained in DMEM flux medium without proline and is not rescued with the addition of exogenous proline (n = 3, presented as mean ± SEM). Statistical analysis shown compares PYCR1$^{+/+}$ and PYCR1 $^{/}$ cells without proline. *, $p < 0.05$. Comparison of growth of either cell type with or without proline was not significant.

(L) Cell growth of PYCR1 $^{/}$ cells can be rescued with the addition of 2 mM sodium pyruvate (n = 3, presented as mean ± SD).*, $p < 0.05$; **, $p < 0.01$; ***, $p < 0.0001$

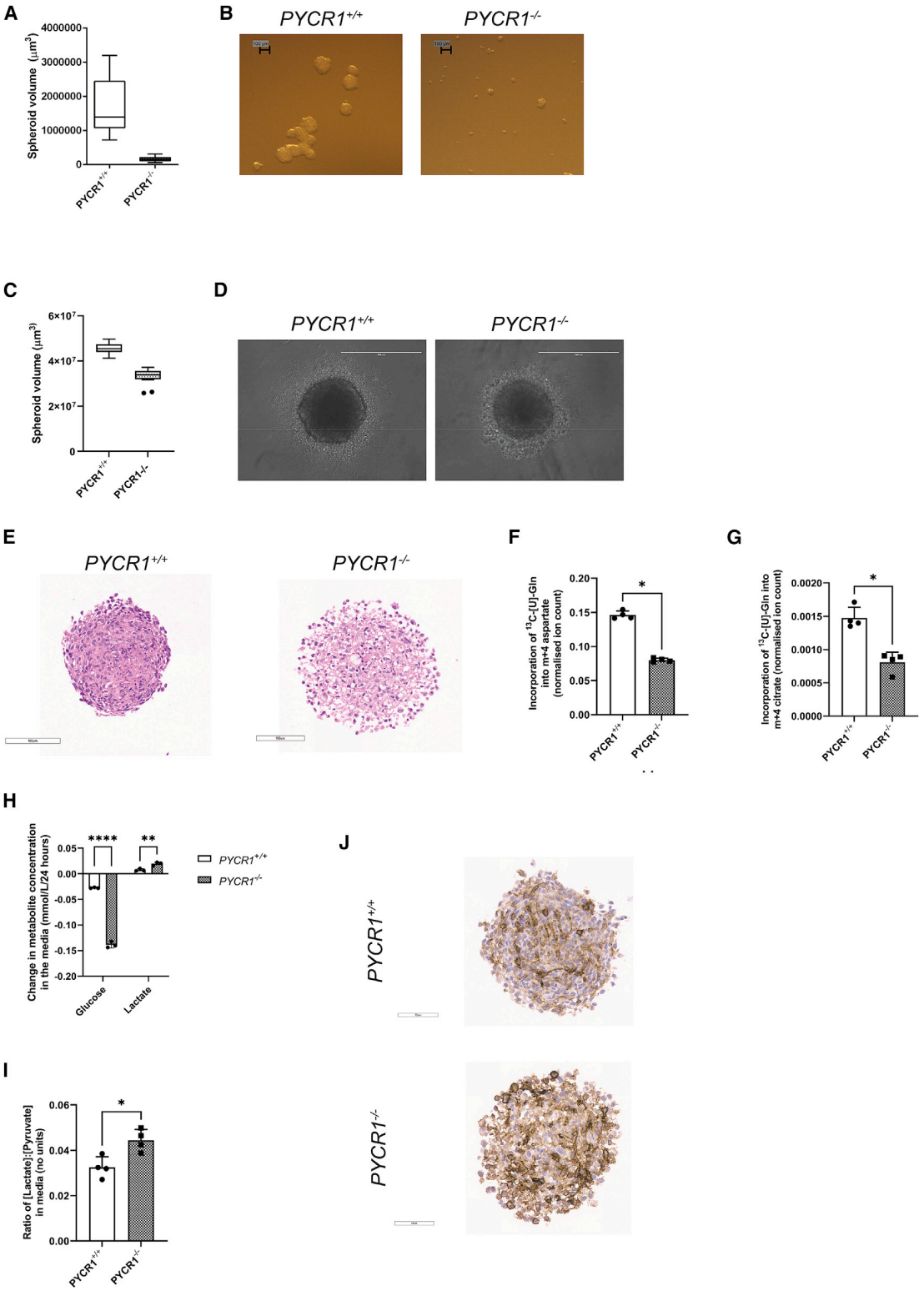

Figure 3. Loss of PYCR1 in 3D culture leads to redox imbalance and excessive oxygen consumption

(A) Volume of PYCR1 $^{/}$ and PYCR1$^{+/+}$ spheroids grown on agarose coated plates (n = 3, presented with Tukey whiskers).

(B) Representative images of spheroids from (A). Scale bars, 100 μm.

(legend continued on next page)

Figure S3A) and increased expression of the hypoxia-inducible enzymes GLUT1 and carbonic anhydrase 9 (CA9; Figures S3B and 3J). We performed further histological analysis of similarly sized spheroids and found that the PYCR1$^{-/-}$ spheroids had an altered morphology, characterized by a less compact center containing significant numbers of clear inclusions (Figure 3E). We first investigated whether loss of PYCR1 in spheroids also led to decreased proline synthesis and export, as observed in two-dimensional (2D) culture. We incubated spheroids with [U-^{13}C]glutamine and found that the incorporation of glutamine into proline was decreased both in the spheroids and the medium (Figures S3C and S3D). In light of this, we also tested whether exogenous proline could rescue spheroid growth but, in line with our 2D results, there was little effect (Figure S3E). We subsequently investigated the metabolic activity of PYCR1-deficient spheroids and found that, consistent with the previously observed defect in TCA cycle oxidative activity, PYCR1-deficient spheroids contained less glutamine-derived aspartate and citrate (Figures 3F and 3G). We therefore also investigated whether glycolysis may be increased as a result of the mitochondrial dysfunction in response to loss of PYCR1 and found that glucose consumption and lactate export increased (Figure 3H). Finally, as we showed in 2D that loss of PYCR1 activity altered the NAD$^+$/NADH ratio, we examined the lactate/pyruvate ratio, a well-described surrogate for the cytosolic NAD$^+$/NADH ratio, in the medium. Consistent with the reduced oxidative TCA cycle activity, we noted an increase in the ratio in the medium from spheroids, indicative of an increased need of PYCR1$^{-/-}$ cells to regenerate NAD$^+$ in the cytosol (Figure 3I). Given the significant changes in oxidative metabolism observed, we hypothesized that mitochondrial respiration may be increased as an attempt to compensate, leading to a steeper oxygen gradient across the spheroid and greater area of hypoxia. We therefore stained the spheroids for CA9, a well-characterized hypoxia-responsive protein (Wykoff et al., 2001). While CA9 was present in the wild-type spheroids as expected, levels were significantly higher and in greater cell numbers when PYCR1 was absent (Figure 3J). These results suggested that PYCR1 is a critical component of the hypoxic response in the metabolic network and that its loss leads to widespread dysfunction.

PYCR1 is essential for maintenance of viable hypoxic regions and tumor growth

To investigate the role of PYCR1 in the hypoxic regions of tumors, we engineered a cell model in which PYCR1 could be inducibly knocked down, thereby minimizing the effect of PYCR1 on other cell processes during tumor initiation and initial growth. We found that in our model, PYCR1 expression could be rapidly reduced after induction of the short hairpin RNA construct with doxycycline (DOX), with no effect on the control cell model either *in vitro* or *in vivo* (shNT; Figures S4A–S4D). Using this cell model, we first investigated the effect of short-term PYCR1 knockdown on hypoxia and hypoxic signaling in tumors after a single dose of DOX. We found that the extent of hypoxia increased significantly across the tumor in response to knockdown of PYCR1 (Figures 4A and 4E). This was accompanied by significant changes in hypoxia signaling, indicated by increased expression of the HIF1 target genes, CA9 and GLUT1 (Figures 4B, 4C, 4F, 4G, and S4E). Finally, we assessed the effect of enhanced hypoxic signaling on tumor angiogenesis (measured by CD31-positive cells) and observed a surprising relative decrease in CD31-positive cells, suggesting reduced angiogenic signaling (Figures 4D and 4H). However, this latter marker was not accompanied by a reduction in apparent blood flow (Figure S4F), suggesting that this time point may be insufficient to elicit an angiogenic response of magnitude sufficient to reduce perfusion. As we had observed a significant increase in tumoral hypoxia over a relatively short time frame, we investigated whether this may affect tumor phenotype. We found again that a single dose of DOX resulted in reduced tumor cell proliferation (Ki67 staining; Figures 5A and 5D) only in the shPYCR1 tumors, which also demonstrated increased apoptotic cell death (cleaved caspase-3; Figures 5B, 5E, and S5A). These significant changes in cell phenotype were mirrored by extensive areas of histological necrosis indicative of substantial cell death (Figures 5C and 5F). Given these data, we examined the effect of chronic dosing of mice with DOX to provide long-term knockdown of PYCR1 on established tumor growth. We found that, in agreement with the acute dosing study, only the shPYCR1 + DOX-treated tumors showed a significant change in growth, increasing the time taken to reach an average of 500 mm^3 by over 30% (Figures 5G, 5H, and S5B–S5I).

Overall, our studies show that PYCR1 supports normal mitochondrial metabolism by contributing to redox homeostasis. In hypoxia, PYCR1 becomes an essential oxygen-sparing enzyme, permitting continued TCA cycle activity and reducing lactate production. Loss of PYCR1 in cells results in significant metabolic rewiring, and loss of PYCR1 in tumors results in cell death and reduced tumor growth.

DISCUSSION

There is increasing evidence supporting the hypothesis that activity of the proline synthesis and degradation pathways is

(C) Volume of PYCR1 $^{/}$ and PYCR1$^{+/+}$ spheroids at 72 h grown in U bottomed plates (n = 3, presented with Tukey whiskers).
(D) Representative images of spheroids from (C). Scale bars, 400 μm.
(E) Hematoxylin and eosin (H&E) staining of sectioned spheroids showing that PYCR1 $^{/}$ spheroids have an altered morphology, with less densely packed cells and more rounded nuclei. Scale bars, 100 μm.
(F) The percentage incorporation of [U ^{13}C]glutamine into M + 4 aspartate is lower in PYCR1 $^{/}$ spheroids, presented as mean ± SD. *, $p < 0.05$
(G) The percentage incorporation of [U ^{13}C]glutamine into M + 4 citrate is lower in PYCR1 $^{/}$ spheroids (n = 4 [× 24 spheroids], presented as mean ± SD). *, $p < 0.05$
(H) Glucose consumption is increased in the PYCR1 $^{/}$ spheroids while lactate export into the medium is increased (n = 3 [× 24 spheroids], presented as mean ± SD). **, $p < 0.01$; ****, $p < 0.0001$
(I) The ratio extracellular lactate to extracellular pyruvate is higher in PYCR1 $^{/}$ spheroids (n = 4 [× 24 spheroids], presented as mean ± SD). *, $p < 0.05$
(J) PYCR1$^{+/+}$ and PYCR1 $^{/}$ spheroids stained for carbonic anhydrase IX expression, as a marker of hypoxic cells. More intense and diffuse staining is seen in the PYCR1 $^{/}$ spheroids. Scale bars, 70 μm.

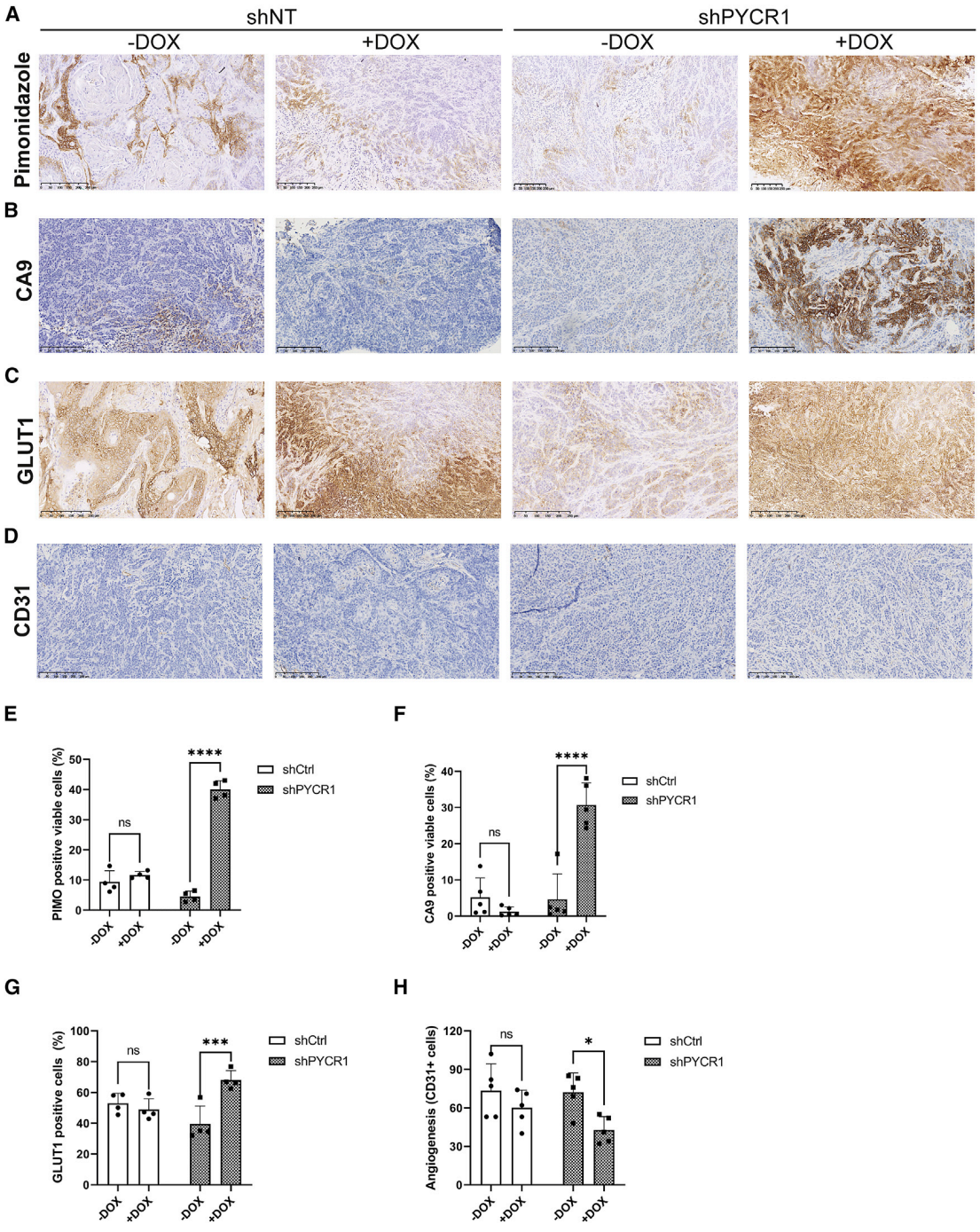

Figure 4. PYCR1 loss leads to increased tumor hypoxia

(A) Representative images showing pimonidazole staining in xenografts.

(B) Representative images showing CA9 staining in xenografts.

(C) Representative images showing GLUT1 staining in xenografts.

(D) Representative images showing CD31 staining in xenografts.

(E) Quantification of pimonidazole staining as percentage of positive cells, presented as mean ± SD. ****, $p < 0.0001$. Doxycycline (DOX) induced shPYCR1 xenografts have significantly higher staining positivity, indicating that PYCR1 loss increases hypoxia.

(F) Quantification of CA9 staining as percentage of positive cells, presented as mean ± SD. ****, $p < 0.0001$. . Doxycycline induced shPYCR1 xenografts have significantly higher staining positivity.

(legend continued on next page)

important in certain cellular and environmental conditions to modulate the redox state in mammalian cells. PYCR1 activity in particular has been shown to be responsive to the mitochondrial NAD/NADH ratio (Hollinshead et al., 2018; Schworer et al., 2020).

Our data suggest that PYCR1 represents a critical component of an obligate mitochondrial NADH-oxidizing pathway, which under limiting oxygen conditions becomes essential. We also show that despite being expressed constitutively alongside PYCR2, these enzymes are non-redundant (Figures 1F and 1G). Although both of these isozymes catalyze the same reaction and are localized to the mitochondria, it is thought that PYCR2 has a higher affinity for NADPH as a co-factor (De Ingeniis et al., 2012). However, more work is needed to understand the regulation and distinct roles of these two isozymes. It should also be noted that the synthesis of proline through PYCR1 is still dependent on the availability of NADP for reduction of glutamate, as cells lacking NADK2 have sufficiently impaired proline synthesis to become proline auxotrophic (Tran et al., 2021; Zhu et al., 2021). Importantly, expression of PYCR1 was not increased in hypoxia (Figure 1C). This suggests that PYCR1 is constitutively expressed at a level that allows it to respond very rapidly to acute changes in mitochondrial redox homeostasis, providing the ability to maintain a functional mitochondrial network in the short term while a longer-term transcriptional framework is put in place through hypoxia-activated signaling mechanisms (such as hypoxia-inducible factor 1).

Proline synthesized through the reduction of glutamate appears in our models to be in excess of cellular anabolic requirements and is exported into the medium, much like the reduction of pyruvate to lactate in the cytosol. PYCR1 activity therefore appears to functionally uncouple the TCA cycle from ATP synthesis, a concept previously suggested to be permissive to enhanced proliferation (Luengo et al., 2021) and which our data support. In line with this, we find that PYCR1$^{-/-}$ cells produce increased extracellular lactate in normoxia, suggesting that PYCR1 supports the normal function of mitochondrial redox shuttles such as the malate-aspartate shuttle, which is also important for cellular anabolism. However, our data also suggest that under conditions of severe hypoxia, further mechanisms to maintain PYCR1 activity by avoiding previously described product inhibition may be in place (De Ingeniis et al., 2012), which could include the upregulation of an as yet unidentified mitochondrial transporter for this amino acid (Figures 1D and 1E).

In 3D culture, which is more representative of the oxygen and nutrient gradients observed in the tumor microenvironment, we also found that PYCR1 loss reduced proline export. The knockout also affected spheroid morphology, increased hypoxia, and resulted in a metabolic phenotype indicative of significant metabolic dysfunction. Finally, we showed *in vivo* that loss of PYCR1 significantly decreased growth in a mouse xenograft model. We found that proliferation was reduced while hypoxia and cell death were increased. This further suggests that proline synthesis through PYCR1 is conditionally essential when cellular redox state is reduced, such as in a hypoxic microenvironment.

In summary, in parallel with the original hypothesis supporting the use of anti-angiogenic drugs in tumors, our data suggest that inhibition of PYCR1 may push hypoxic tumor regions into a non-viable state, making the overall tumor more amenable to conventional therapies whose efficacy suffers in hypoxia. However, further work is needed to define the roles of other PYCR isozymes in both normoxia and hypoxia, as our data and that of others clearly show that the metabolic network surrounding proline is complex and remains poorly understood.

Limitations of the study

While we showed much of the downstream biochemical effects of reduced PYCR1 activity in normoxia and hypoxia *in vitro*, we were only able to show some of these markers in the subsequent *in vivo* study due to the cross-species, multicellular nature of the orthotopic xenograft model used. The role of PYCR1 specifically in redox homeostasis could therefore not be confirmed *in vivo*. In terms of translation of these findings, the implications of pharmacological inhibition of PYCR1 are not yet entirely clear, as studies did not address this. Although PYCR1 deficiency led to a necrotic phenotype, it also increased tumoral hypoxia that itself could increase hypoxia-induced phenotypes such as therapy resistance. Further studies are therefore needed to clarify how PYCR1 inhibition could contribute to future therapeutic interventions.

STAR★METHODS

Detailed methods are provided in the online version of this paper and include the following:

- KEY RESOURCES TABLE
- RESOURCE AVAILABILITY
  - Lead contact
  - Materials availability
  - Data and code availability
- EXPERIMENTAL MODEL AND SUBJECT DETAILS
  - Cell culture
  - *In vivo* model
- METHOD DETAILS
  - Spheroids
  - Metabolic tracing
  - Glucose and lactate consumption
  - Bicinchoninic acid (BCA) protein assay
  - Derivatization and GCMS
  - Western blotting
  - Cell number and GCMS data normalization values
  - Oxygen consumption
  - GSH:GSSG assay
  - NAD^+:NADH assay
  - Immunohistochemistry
- QUANTIFICATION AND STATISTICAL ANALYSIS

(G) Quantification of GLUT1 staining, as percentage of positive cell, presented as mean ± SD. ***, $p < 0.001$. s. Doxycycline induced shPYCR1 xenografts have significantly higher staining positivity.
(H) Quantification of CD31 staining, presented as mean ± SD. *, $p < 0.05$. . Doxycycline induced shPYCR1 xenografts show a small but statistically significant decrease in staining positivity, suggesting that angiogenesis is impaired by PYCR1 loss.
All scale bars represent 250 μm. All experiments: n = 5.

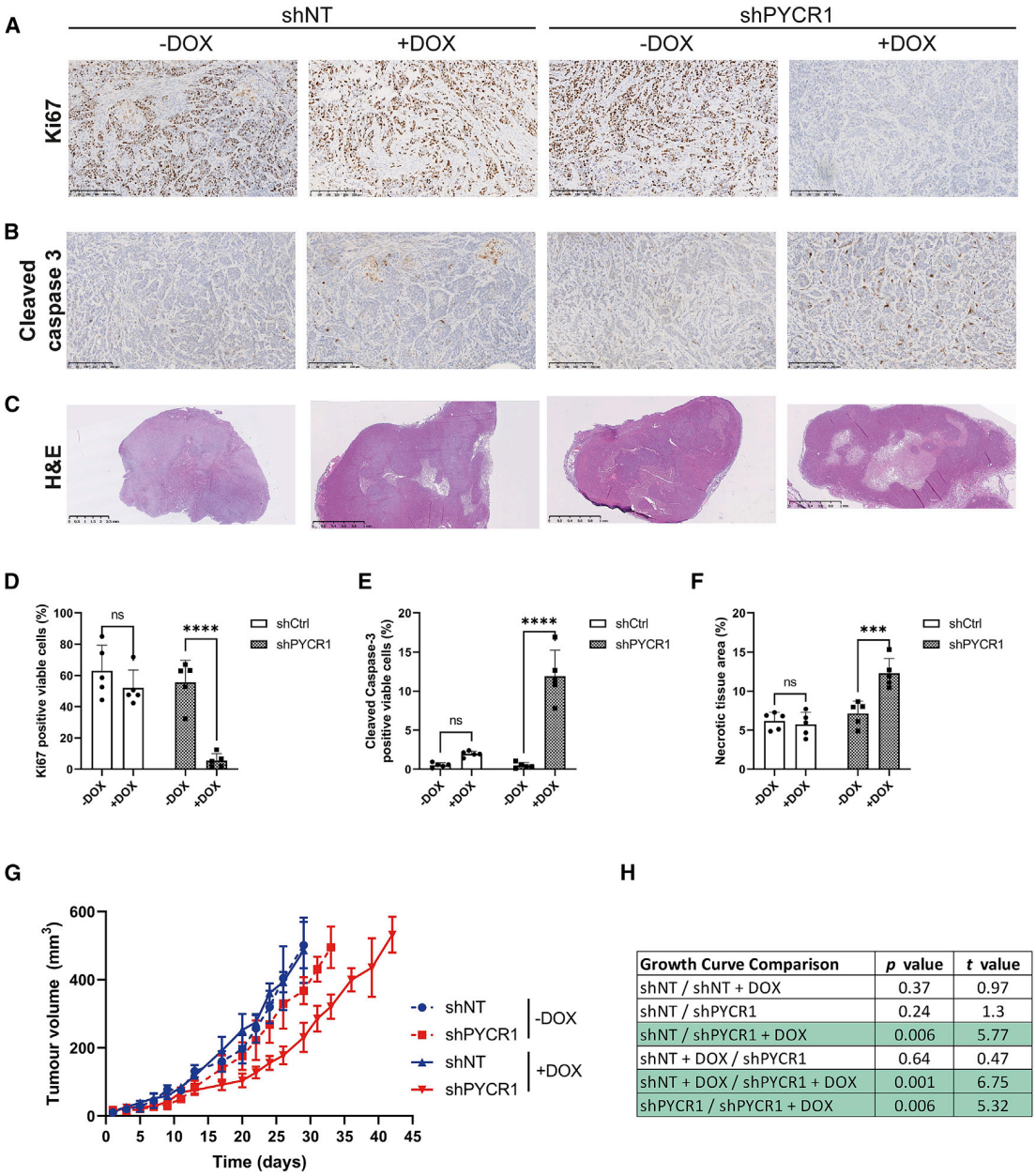

Growth Curve Comparison	*p* value	*t* value
shNT / shNT + DOX	0.37	0.97
shNT / shPYCR1	0.24	1.3
shNT / shPYCR1 + DOX	0.006	5.77
shNT + DOX / shPYCR1	0.64	0.47
shNT + DOX / shPYCR1 + DOX	0.001	6.75
shPYCR1 / shPYCR1 + DOX	0.006	5.32

Figure 5. PYCR1 is essential for maintenance of viable hypoxic tumor regions

(A C) Representative images showing (A) Ki67, (B) cleaved caspase 3, and (C) H&E staining in xenografts (n = 5 for all conditions).

(D) Quantification of Ki67 positive cells as percentage of viable cells, presented as mean ± SD. ****, $p < 0.0001$.

(E) Quantification of cleaved caspase 3 positive cells as percentage of viable cells, presented as mean ± SD. ****, $p < 0.0001$. Doxycycline induced shPYCR1 xenografts have significantly higher staining positivity, indicating that PYCR1 loss increases apoptosis.

(F) Quantification of necrotic area as percentage of total xenograft tumor area, presented as mean ± SD. ***, $p < 0.001$. Doxcycline induced shPYCR1 xenografts have significantly higher percentage necrotic area.

(G) Tumor volume over time; shows doxycycline induced shPYCR1 xenografts take more days to reach endpoint (500mm3) (n = 7, presented as mean ± SD).

(H) Significance values for tumor growth curve. p values reach significance for doxycycline induced shPYCR1 comparison with shNT, doxycycline induced shNT and shPYCR1. Scale bar = 250 μM (A), 1 mm (C; shPYCR1 + DOX) or 2.5 mm (C; shNT ±DOX & shPYCR1 DOX).

SUPPLEMENTAL INFORMATION

Supplemental information can be found online at https://doi.org/10.1016/j.celrep.2022.110320.

ACKNOWLEDGMENTS

The authors would like to acknowledge funding from Cancer Research UK to R.L.W., C.E.G., K.L.E., E.V. S., L.A.V., and P.D.W. (C42109/A26982 and

C42109/A24747). We would also like to acknowledge Professor Reuven Agami, who kindly gifted the PYCR1 / line and control. The graphical ab stract was created with BioRender.com. Finally, we would like to acknowledge the support and resources of the Birmingham Metabolic Tracer Analysis Core.

AUTHOR CONTRIBUTIONS

R.L.W., E.B., A.S., H.L., A.L.H., and D.A.T. conceptualized the study and de signed the methodology. R.L.W., E.B., C.E.G., J.R., H.R., K.L.E., K. L.E., H.V., E.V. S., L.A.V., P.D.W., F.C., and C.N. performed investigations. E.V. S., E.B., R.L.W., K. L.E., H.V., C.N., and D.A.T. performed formal analysis and data visualization. G.G.L., D.J.H., A.S., H.L., C.N., A.L.H., and D.A.T. pro vided resources. R.L.W., E.B., J.B., C.N., and D.A.T. wrote the original manu script draft, while all authors contributed to reviewing and editing of the manuscript.

DECLARATION OF INTERESTS

The authors declare no competing interests.

Received: July 2, 2021
Revised: November 12, 2021
Accepted: January 10, 2022
Published: February 1, 2022

REFERENCES

Birsoy, K., Wang, T., Chen, W.W., Freinkman, E., Abu Remaileh, M., and Sa batini, D.M. (2015). An essential role of the mitochondrial electron transport chain in cell proliferation is to enable aspartate synthesis. Cell *162*, 540 551.

Burke, L., Guterman, I., Palacios Gallego, R., Britton, R.G., Burschowsky, D., Tufarelli, C., and Rufini, A. (2020). The Janus like role of proline metabolism in cancer. Cell Death Discov. *6*, 104.

De Ingeniis, J., Ratnikov, B., Richardson, A.D., Scott, D.A., Aza Blanc, P., De, S.K., Kazanov, M., Pellecchia, M., Ronai, Z., Osterman, A.L., et al. (2012). Functional specialization in proline biosynthesis of melanoma. PLoS One *7*, e45190.

Eales, K.L., Hollinshead, K.E., and Tennant, D.A. (2016). Hypoxia and meta bolic adaptation of cancer cells. Oncogenesis *5*, e190.

Elia, I., Broekaert, D., Christen, S., Boon, R., Radaelli, E., Orth, M.F., Verfaillie, C., Grunewald, T.G.P., and Fendt, S.M. (2017). Proline metabolism supports metastasis formation and could be inhibited to selectively target metastasizing cancer cells. Nat. Commun. *8*, 15267.

Frezza, C., Zheng, L., Tennant, D.A., Papkovsky, D.B., Hedley, B.A., Kalna, G., Watson, D.G., and Gottlieb, E. (2011). Metabolic profiling of hypoxic cells re vealed a catabolic signature required for cell survival. PLoS One *6*, e24411.

Harris, A.L. (2002). Hypoxia a key regulatory factor in tumour growth. Nat. Rev. Cancer *2*, 38 47.

Hollinshead, K.E.R., Munford, H., Eales, K.L., Bardella, C., Li, C., Escribano Gonzalez, C., Thakker, A., Nonnenmacher, Y., Kluckova, K., Jeeves, M., et al. (2018). Oncogenic IDH1 mutations promote enhanced proline synthesis through PYCR1 to support the maintenance of mitochondrial redox homeosta sis. Cell Rep. *22*, 3107 3114.

Ivascu, A., and Kubbies, M. (2006). Rapid generation of single tumor spher oids for high throughput cell function and toxicity analysis. J. Biomol. Screen *11*, 922 932.

Krishnan, N., Dickman, M.B., and Becker, D.F. (2008). Proline modulates the intracellular redox environment and protects mammalian cells against oxida tive stress. Free Radic. Biol. Med. *44*, 671 681.

LaNoue, K.F., Walajtys, E.I., and Williamson, J.R. (1973). Regulation of gluta mate metabolism and interactions with the citric acid cycle in rat heart mito chondria. J. Biol. Chem. *248*, 7171 7183.

Liu, M., Wang, Y., Yang, C., Ruan, Y., Bai, C., Chu, Q., Cui, Y., Chen, C., Ying, G., and Li, B. (2020). Inhibiting both proline biosynthesis and lipogenesis syn ergistically suppresses tumor growth. J. Exp. Med. *217*, e20191226.

Loayza Puch, F., Rooijers, K., Buil, L.C., Zijlstra, J., Oude Vrielink, J.F., Lopes, R., Ugalde, A.P., van Breugel, P., Hofland, I., Wesseling, J., et al. (2016). Tumour specific proline vulnerability uncovered by differential ribosome codon reading. Nature *530*, 490 494.

Luengo, A., Li, Z., Gui, D.Y., Sullivan, L.B., Zagorulya, M., Do, B.T., Ferreira, R., Naamati, A., Ali, A., Lewis, C.A., et al. (2021). Increased demand for NAD(+) relative to ATP drives aerobic glycolysis. Mol. Cell *81*, 691 707.e696.

Markert, C.L. (1984). Lactate dehydrogenase. Biochemistry and function of lactate dehydrogenase. Cell Biochem. Funct. *2*, 131 134.

McGregor, G.H., Campbell, A.D., Fey, S.K., Tumanov, S., Sumpton, D., Blanco, G.R., Mackay, G., Nixon, C., Vazquez, A., Sansom, O.J., et al. (2020). Targeting the metabolic response to statin mediated oxidative stress produces a synergistic antitumor response. Cancer Res. *80*, 175 188.

Milne, K., Sun, J., Zaal, E.A., Mowat, J., Celie, P.H.N., Fish, A., Berkers, C.R., Forlani, G., Loayza Puch, F., Jamieson, C., et al. (2019). A fragment like approach to PYCR1 inhibition. Bioorg. Med. Chem. Lett. *29*, 2626 2631.

Phang, J.M. (2019). Proline metabolism in cell regulation and cancer biology: recent advances and hypotheses. Antioxid. Redox Signal. *30*, 635 649.

Phang, J.M., Liu, W., Hancock, C., and Christian, K.J. (2012). The proline reg ulatory axis and cancer. Front. Oncol. *2*, 60.

Phang, J.M., Liu, W., and Zabirnyk, O. (2010). Proline metabolism and micro environmental stress. Annu. Rev. Nutr. *30*, 441 463.

Phang, J.M., Pandhare, J., and Liu, Y. (2008). The metabolism of proline as microenvironmental stress substrate. J. Nutr. *138*, 2008S 2015S.

Sahu, N., Dela Cruz, D., Gao, M., Sandoval, W., Haverty, P.M., Liu, J., Stephan, J.P., Haley, B., Classon, M., Hatzivassiliou, G., et al. (2016). Proline starvation induces unresolved ER stress and hinders mTORC1 dependent tumorigen esis. Cell Metab. *24*, 753 761.

Schworer, S., Berisa, M., Violante, S., Qin, W., Zhu, J., Hendrickson, R.C., Cross, J.R., and Thompson, C.B. (2020). Proline biosynthesis is a vent for TGFbeta induced mitochondrial redox stress. EMBO J. *39*, e103334.

Scott, G.K., Yau, C., Becker, B.C., Khateeb, S., Mahoney, S., Jensen, M.B., Hann, B., Cowen, B.J., Pegan, S.D., and Benz, C.C. (2019). Targeting mito chondrial proline dehydrogenase with a suicide inhibitor to exploit synthetic le thal interactions with p53 upregulation and glutaminase inhibition. Mol. Cancer Ther. *18*, 1374 1385.

Sullivan, L.B., Gui, D.Y., Hosios, A.M., Bush, L.N., Freinkman, E., and Vander Heiden, M.G. (2015). Supporting aspartate biosynthesis is an essential func tion of respiration in proliferating cells. Cell *162*, 552 563.

Tran, D.H., Kesavan, R., Rion, H., Hoseini Soflaee, M., Solmonson, A., Bez wada, D., Vu, H.S., Cai, F., Phillips, J.A., DeBerardinis, R.J., et al. (2021). Mito chondrial $NADP^+$ is essential for proline biosynthesis during cell growth. Nat. Med. *3*, 571 585.

Vettore, L.A., Westbrook, R.L., and Tennant, D.A. (2021). Proline metabolism and redox; maintaining a balance in health and disease. Amino Acids *53*, 1779 1788.

Wykoff, C.C., Beasley, N., Watson, P.H., Campo, L., Chia, S.K., English, R., Pastorek, J., Sly, W.S., Ratcliffe, P., and Harris, A.L. (2001). Expression of the hypoxia inducible and tumor associated carbonic anhydrases in ductal carcinoma in situ of the breast. Am. J. Pathol. *158*, 1011 1019.

Zhu, J., Schworer, S., Berisa, M., Kyung, Y.J., Ryu, K.W., Yi, J., Jiang, X., Cross, J.R., and Thompson, C.B. (2021). Mitochondrial NADP(H) generation is essential for proline biosynthesis. Science *372*, 968 972.

STAR★METHODS

KEY RESOURCES TABLE

REAGENT or RESOURCE	SOURCE	IDENTIFIER
Antibodies		
Carbonic Anhydrase IX	Novus Biologicals	Cat#NB100 417; RRID:AB 10003398
Ki67	Cell Signaling	Cat#12202; RRID:AB 2620142
Actin	Sigma	Cat#A4700; RRID:AB 476730
PYCR1	Proteintech	Cat#13108 1 AP; RRID:AB 2174878
PYCR2	Proteintech	Cat#17146 1 AP; RRID:AB 2253344
HIF1α	BD Biosciences	Cat#610959; RRID:AB 398272
Anti Rabbit HRP	Cell Signalling	Cat#7074S; RRID:AB 2099233
Anti Mouse HRP	Cell Signalling	Cat#7076S; RRID:AB 330924
PYCR1	Cell Signalling	Cat#37635; RRID:AB 2904491
Ki67	Agilent	Cat#M7240; RRID:AB 2142367
CD31	Agilent	Cat#M082301 2; RRID:AB 2904492
Carbonic Anhydrase 9	Absolute Antibody	Cat#M75; RRID:AB 2904493
GLUT1	Abcam	Cat#ab652; RRID:AB 305540
Critical commercial assays		
NAD^+:NADH assay kit	Biovision	Cat#K337
GSH:GSSG assay kit	Promega	Cat#V6612
Experimental models: Cell lines		
HCC1806	ATCC	CRL 2335; RRID:CVCL 1258
SUM159PT	BioIVT	HUMANSUM 0003006
SUM159PT PYCR1$^{-/-}$	Professor Reuven Agami	N/A
MDA MB 231	ATCC	HTB 26; RRID:CVCL 0062
HS5	ATCC	CRL 11882; RRID:CVCL 3720
ONS 76	Accegen	ABC TC0875
Doxycycline inducible shPYCR1 HCC1806	This paper	N/A
Oligonucleotides		
PYCR1 siRNA	Dharmacon	Cat#J 012349 06 0005
PYCR2 siRNA	Dharmacon	Cat#J 016646 06 0005
Non targeting siRNA	Dharmacon	Cat#D 001810 10 05
shERWOOD UltraMiR Lentiviral inducible pZip target gene set for PYCR1	Transomic	Cat# TLHSU2300 5831
Software and algorithms		
MATLAB	Mathworks	N/A
GraphPad Prism	GraphPad Software	N/A
Adobe Illustrator	Adobe	N/A
Deposited data		
Metabolic data	N/A	Mendeley Data: https://doi.org/10.17632/vbjp8xs9k6.1

RESOURCE AVAILABILITY

Lead contact

Further information and requests for resources and/or reagents should be directed to and will be fulfilled by Professor Daniel A Tennant (D.Tennant@bham.ac.uk)

Materials availability

Materials generated in this study are available from the lead contact.

Data and code availability

- Metabolic tracing data have been deposited at Mendeley and are publicly available as of the date of publication. DOIs are listed in the key resources table.
- This paper does not report any original code
- Any additional information required to reanalyze the data reporting in this paper is available from the lead author on request.

EXPERIMENTAL MODEL AND SUBJECT DETAILS

Cell culture

HCC1806, MDA-MB-231 and HS5 cell lines were purchased from ATCC, SUM159-PT from BioIVT and ONS-76 from Accegen. The SUM159PT PYCR1$^{-/-}$ and paired control were previously reported (Loayza-Puch et al., 2016). All cell lines were passaged when they reached 70%–80% confluence, using 0.05% Trypsin (Gibco, 15400-054) for dissociation and 1x phosphate buffered saline (PBS) for washing. MDA-MB-231, HCC1806 and HS5 cells were maintained in RPMI (Sigma-Aldrich, R8758) with 10% FBS. SUM159-PT cells were growth in Dulbecco's Modified Eagle's Medium (DMEM) Nutrient Mixture F-12 Ham (Sigma, D8062), with 5% FBS, 5 mg/ml insulin (Sigma, I6634) and 1 μg/ml hydrocortisone (Sigma, H0888). ONS-76 cell lines were grown in DMEM Nutrient Mixture F-12 Ham (Sigma, D8062), with 10% FBS. Doxycycline-inducible shPYCR1 expressing HCC1806 cell line was established using shERWOOD UltraMiR Lentiviral inducible pZip target gene set for PYCR1 (Transomic, TLHSU2300-5831).

In vivo model

Fresh and sterile doxycycline was used in these experiments. 100 μl of matrigel containing 2 × 10^6 HCC-1806 doxycycline –shControl (shC) or -inducible shPYCR1 cells were established into the mammary fat pad of CD1 nude female mice aged 5–6 weeks. Where shown, mice were given doxycycline when tumor growth reached average tumor volume 50 mm^3 (single dose study) or 75 mm^3 (chronic dosing study). Single dose: mice (7 mice per group of shNT or shPYCR1) were administered one dose of oral gavage of doxycycline (25 mg/kg). Adverse effects on animal welfare was observed in the shPYCR1 group only, with one mortality and remaining six mice displayed moderate changes in welfare, including significantly reduced mobility and decreased body temperature. Chronic dosing: mice were administered oral gavage of doxycycline (10 mg/kg) every two days rota (one day treat and one day rest) until endpoint. No changes in animal welfare was observed in either group (of shC or shPYCR1). Endpoint procedures: Single dose: animals were culled the day after dosing, and tumors sectioned for both flash-freezing and fixation for downstream analysis. Chronic dosing: when tumors attained endpoint size permitted mice were injected with $^{13}C_5$-glutamine (3 × 200 μl [7.2 mg] each 36.2 mg/ml stock solution at 15 min intervals [total = 142 μmol] 45 minutes before cull. Pimonidazole (2 mg/kg) and a 647-Tomato lectin (1 mg/kg)/Hoescht (2 mg/kg) mix was given intravenous 5 min before visualization on IVIS system for fluorescence imaging of perfused tumors and mice culled. Tumors were excised, sectioned, and samples flash-frozen and fixed for downstream analysis. Blood samples were also collected by cardiac puncture when culling mice.

METHOD DETAILS

Spheroids

Cells were trypsinized, counted, and either plated in 6 well plates coated with 0.5% agarose in DMEM or on low adherence U-bottomed 96 well plates (Thermo, 174925) and then centrifuged for 5 minutes at 500 × g. For proline supplementation experiments, spheroids were seeded in DMEM flux media (without phenol red, glutamine, and glucose) ((Gibco, A14430), with or without 1mM proline. For all other experiments spheroids were left to form for at least 72 hours before investigation. For staining, spheroids were grown for 7 days before fixing in neutral buffered formalin overnight, and transfer to 70% ethanol for storage. The solution containing spheroids was transferred onto the center of a sheet of biopsy paper (CellPath, UK) before processing for histology. All staining was performed on 4 μm formalin fixed paraffin embedded (FFPE) sections. Sections for Haematoxylin & Eosin staining were stained using a Leica ST5020 autostainer. Carbonic Anhydrase XI (NB100-417, Novus Biologicals), Caspase 3 (9661, Cell Signaling) and Ki67 (12202, Cell Signaling) antibodies were stained on a Leica Bond Rx autostainer. FFPE sections were loaded onto the autostainer and underwent dewaxing (Leica, AR9222) and epitope retrieval on board. Carbonic Anhydrase XI, Caspase 3 and Ki67 was retrieved using ER2 buffer (Leica, AR9640). All sections were retrieved at 95°C for 20 minutes. After retrieval sections were rinsed with wash buffer (Leica, AR9590) before peroxidase block was performed for 5 minutes using an Intense R kit (Leica, DS9263). Sections were rinsed with wash buffer. After rinsing with wash buffer the antibodies were applied at previously optimized dilutions (Carbonic Anhydrase XI, 1/250; Caspase 3, 1/500; Ki67, 1/1000) for 30 minutes before washing with buffer and then application of appropriate secondary antibody (Carbonic Anhydrase XI and Ki67 – Rabbit EnVision, Agilent, K4003) for 30 minutes. Sections were rinsed with wash buffer before being visualized using DAB in the Intense R kit. The sections were counterstained with Haematoxylin in the Intense R kit

before coverslipping the sections with DPX mountant (CellPath, SEA-1300-00A). Images were captured from the stained sections using a Leica Aperio AT2 slide scanner.

Metabolic tracing

For tracing experiments, cells were plated to be 70% confluent after 24 hours. Media was then changed to flux media (without phenol red, glutamine, and glucose) ((Gibco, A14430)), depending on cell line, with 10 mM glucose and 2 mM glutamine (either one universally labelled, depending on experiment). Cells were transferred into hypoxic conditions (Don Whitley H35 Hypoxystation). After 24 hours, 100 μl of media was removed for extraction. The rest of the media was removed and wells were washed twice with ice cold saline, 500 μl MeOH was added, with 200 μl D_6-glutaric acid (2.5 mg/ml) (CDN isotopes, D-5227). Cells were scraped and transferred to a cold Eppendorf with 500 μl ice-cold H_2O and the same volume of chloroform (pre-chilled to −20°C). After shaking on ice for 15 minutes and centrifugation, the polar phase was transferred to another tube for derivatization, which was dried with centrifugation at 45°C. Spheroids grown in U-bottom 96 well plates were collected and washed with PBS before transfer to flux media with ^{13}C-[U]-glutamine in agarose-coated 12 well plates and incubated for 48 hours. Spheroids were collected and washed in ice cold saline, transferred to ice cold MeOH and homogenized (2 × 30 seconds) using a Precellys 24 tissue homogenizer (Bertin Instruments). Metabolite extraction was performed as previously described in cells. Data were normalized to total ion abundance.

Glucose and lactate consumption

Media was changed to flux DMEM (without phenol red, glutamine, and glucose) (Gibco, A14430) with 10 mM glucose and 2 mM glutamine added. Glucose and lactate measurements were taking using a Nova Biomedical Stat Profile Prime CCS Analyzer and normalized to total protein.

Bicinchoninic acid (BCA) protein assay

Spheroids were collected and washed with PBS, before sonication for 10 minutes in 0.2 M NaOH, and boiling. The Pierce BCA Protein Assay Kit (Thermo Scientific, 23225) was used according to the manufacturers protocol.

Derivatization and GCMS

Dried down extracts are derivatized using a two-step protocol. Samples are first treated with 2% methoxamine in pyridine (40 μl, 1 h at 60°C), followed by addition of N-(tert-butyldimethylsilyl)-N-methyl-trifluoroacetamide, with 1% tert-butyldimethylchlorosilan (50 μl, 1 h at 60°C). Samples are transferred to glass vials for GC-MS analysis using an Agilent 8890 GC and 5977B MSD system. 1 μL of sample was injected in splitless mode with helium carrier gas at a rate of 1.0 mL.min^{-1}. Initial GC oven temperature was held at 100°C for 1 minute before ramping to 160°C at a rate of 10°C.min^{-1}, followed by a ramp to 200°C at a rate of 5°C.min^{-1} and a final ramp to 320°C at a rate of 10°C.min^{-1} with a 5 minute hold. Compound detection was carried out in scan mode. Total ion counts of each metabolite were normalized to the internal standard D^6-Glutaric acid.

Western blotting

Cells were washed once with 1 x PBS and scraped into 1x Laemmli buffer (Sigma, 2301-1VL). Samples were heated for 10 minutes at 100°C and briefly centrifuged, then vortexed. Samples were run at 150V through a 10% polyacrylamide gel. Protein was transferred to a nitrocellulose membrane using an Invitrogen iBlot. Membranes were blocked with 5% milk (Marvel) in PBS for 1 hour, before overnight incubation at 4°C with the primary antibody in 1% milk; actin (1:4000 dilution, Sigma, A4700), PYCR1 (1:5000 dilution, Proteintech, 13108-1-AP), PYCR2 (1:2000 dilution, Proteintech, 17146-1-AP), HIF1α (1:500 dilution, BD Biosciences, 610959). PBS-Tween was used for membrane washing before incubation with the secondary antibody at room temperature for 1 hour: Anti-Rabbit-HRP (Cell Signalling, 7074S) or Anti-Mouse-HRP (Cell Signalling, 7076S). After another washing step, EZ-ECL (Biological Industries, 20-500-120) was added to the membrane before imaging using a BioRed ChemiDoc Imaging System. Densitometry was performed using ImageJ-Fiji, values were normalized to loading controls. For siRNA blots, values were also normalized to the non-target.

Cell number and GCMS data normalization values

To assess cell number, a Sulforhodamine B (SRB) assay was used as previously described. 100 μL of 20% trichloracetic acid was added to each well and incubated at 4°C for 30 minutes. Wells were washed with tap water three times and allowed to dry. 0.4% Sulforhodamine B (Sigma, 230162) was added to cover the surface of the wells and incubated for 10 minutes at room temperature. Wells were washed with 1% acetic acid four times and again allowed to dry. The stain was dissolved in 50 mM tris at pH8.8 and absorbance was measured at 510 nm.

Oxygen consumption

Trypsinized cells were resuspended in media as above and loaded in an Oxygraph-2k (Oroboros instruments) chamber. After closing the chambers and recording routine respiration, oligomycin (2.5 μM) was added to inhibit ATP synthase. Measurements of the non-phosphorylating electron transfer system (ETS) capacity were obtained through stepwise (0.5 μM) titration of the uncoupler, carbonyl cyanide 4-(trifluoromethoxy)phenylhydrazone (FCCP). Respiration was inhibited by addition of rotenone (0.5 μM) and antimycin A (2.5 μM) at the end of the experiment.

GSH:GSSG assay

Cells were plated in 6 well plates to be 70% confluent for transfection. Transfection with siRNA at 50nM, either: siNT (Dharmacon, D-001810-10-05), siPYCR1 (Dharmacon, J-012349-06-0005) or siPYCR2 (Dharmacon, J-016646-06-0005) using Dharmafect 1 (Dharmacon, T-2001-03). After 24 hours, transfected cells were re-plated in white, clear bottom 96 well plates (Corning, 3903), and transferred to hypoxia. After 24 hours GSH:GSSH was measured using the Promega GSH:GSSG-Glo assay kit (Promega, V6612) according to manufacturer's protocol.

NAD^+:NADH assay

Cells were plated to be 70% confluent for assay. Cells were harvested and the assay was carried out according to the manufacturer's protocol (Biovision kit K337).

Immunohistochemistry

To summarize staining method the slides were firstly dewaxed in histoclear, rehydrated using decreasing concentrations of ethanol to tap water. A standard haematoxylin and eosin protocol was followed to assess the morphology and the amount of necrosis on xenografts. For immunohistochemistry staining antigen retrieval performed in pH 6 for all antibodies and, slides were stained using the FLEX staining protocol and reagents (Agilent). Endogenous peroxidase activity was blocked before slides were stained with primary antibodies: proliferation marker Ki67 (mouse, MIBI, 1:50 M7240 Agilent), endothelial marker CD31 (rabbit, JC70, Agilent), hypoxia marker CA9 (mouse, M75, Absolute antibody, 1:100), PYCR1 (rabbit, E7P3I, cell signaling), GLUT1 (rabbit, ab652, Abcam, 1:100). Slides incubated for 2h at room temperature. Slides were washed in Flex buffer before then being incubated with the Flex anti-rabbit/mouse secondary antibody for 30 minutes at room temperature and washed in Flex buffer. 3,3′-Diaminobenzidine (Flex-DAB) was applied to the sections for 10 minutes. The slides were counterstained by immersing in Flex-hematoxylin solution for 5 min, washed, and air-dried before mounted with mounting medium (Sigma). Secondary-only control staining was done routinely, these were negative. Expression of markers and viable/necrotic areas was quantified on whole sections quantitatively by using the Visiopharm Integrator System. HDAB-DAB color deconvolution band is used to detect positively stained cells. Threshold classification is used to identified necrosis and living regions and thus identify number of positive staining within these regions. Appropriate thresholds levels are checked against control xenografts staining before being set and the xenografts from all groups are then analyzed. Quantification based on intensity of staining (value calculated from pixilation of DAB, corresponding to stain intensity from no staining, weak to strong staining) and percentage of coverage (value calculated from DAB positive total area expressed relative to the total area of tissue).

QUANTIFICATION AND STATISTICAL ANALYSIS

GCMS data were analyzed using Agilent Mass Hunter software for real time analysis of data quality, before conversion to .CDF format and analysis with in-house MATLAB scripts. Graphs and statistical analysis were performed using GraphPad Prism 9. Where a 2-sample analysis is shown, results are from a Mann-Whitney test, while with >2 samples, results of a Kruskal-Wallis test are shown with Dunn's multiple comparison post hoc. Sample numbers are included in figure legends. To perform a statistical comparison of the xenograft growth curves was performed through first fitting a single exponential curve (Figures S5B–S5E), the integral of which was used to generate a linear regression for each xenograft (Figures S5F–S5I). These equations were then used to apply a Mann-Whitney test.

Cell Reports, Volume *38*

Supplemental information

Proline synthesis through PYCR1 is required to support cancer cell proliferation and survival in oxygen-limiting conditions

Rebecca L. Westbrook, Esther Bridges, Jennie Roberts, Cristina Escribano-Gonzalez, Katherine L. Eales, Lisa A. Vettore, Paul D. Walker, Elias Vera-Siguenza, Himani Rana, Federica Cuozzo, Kattri-Liis Eskla, Hans Vellama, Abeer Shaaban, Colin Nixon, Hendrik Luuk, Gareth G. Lavery, David J. Hodson, Adrian L. Harris, and Daniel A. Tennant

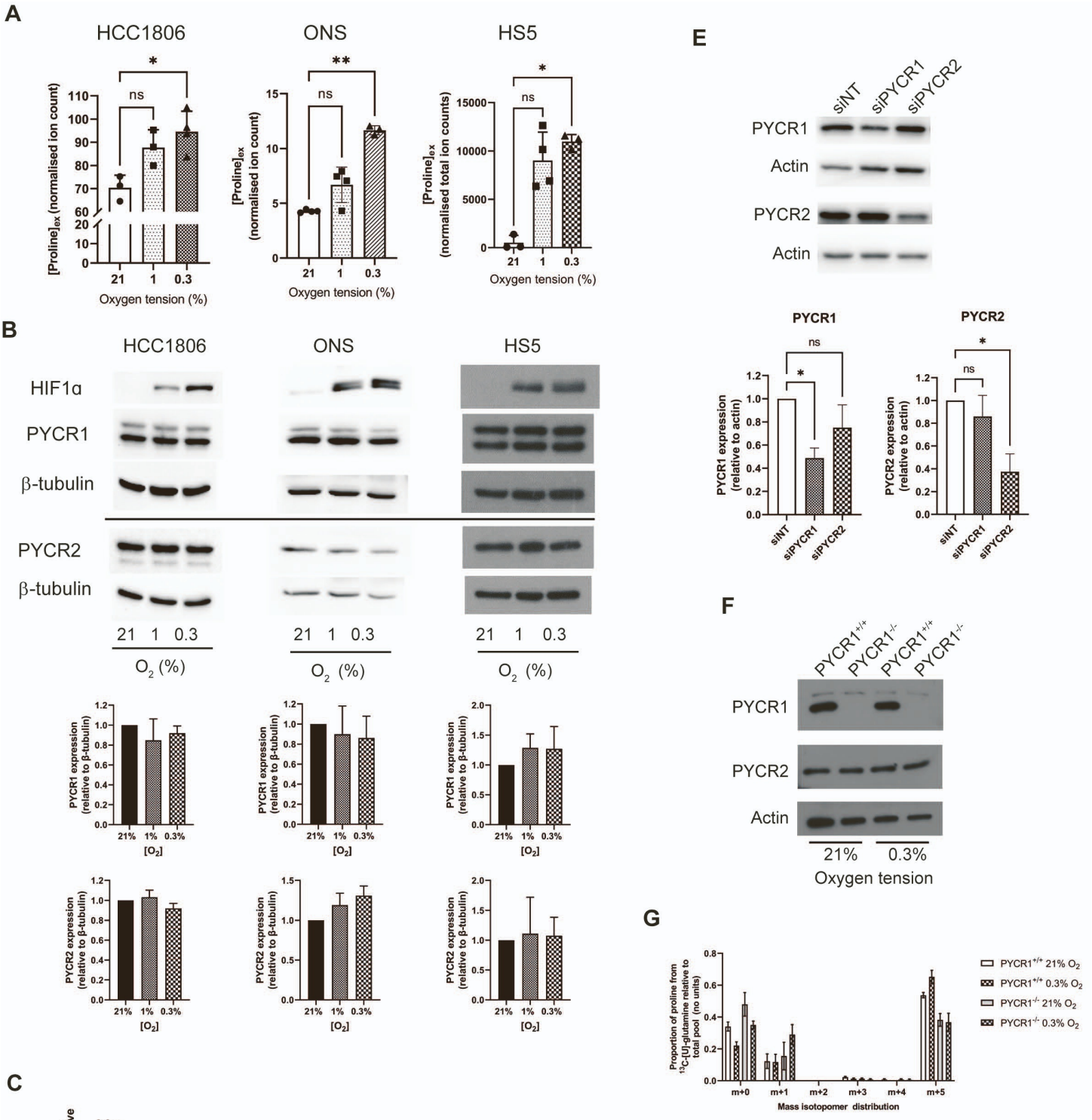

Supplementary Figure 1. Glutamine-derived proline export is increased in hypoxia without increased expression PYCR1 or PYCR2. Related to Figure 1. A: Extracellular proline is significantly increased in hypoxia (0.3% O_2) compared to normoxia (21% O_2) in the HCC1806, ONS and HS5 cell lines. *, $p<0.05$; **, $p<0.01$. **B:** Expression of PYCR1 and PYCR2 does not change with oxygen tension in HCC1806, ONS or HS5 cell lines. Densitometry shown is PYCR1 or 2 normalised to b-tubulin, SD of three independent blots shown. **C** and **D**: As oxygen decreases, the expected decrease in TCA cycle activity (m+4 aspartate [**C**] and citrate [**D**]) and relative increase in reductive carboxylation (m+5 citrate [**D**] and m+3 aspartate [**C**]) is observed in SUM159PT cells. **E:** Protein expression of PYCR1 and PYCR2 with siRNA knockdown of each isoform in SUM159PT cells. Actin as loading control. Densitometry shown below blots for PYCR1 and PYCR2 showing significant knockdown of the relevant isozyme. Statistical analysis shown is result of Kruskal-Wallis ANOVA with Dunn's post hoc test. *, $p<0.05$. **F:** Expression of PYCR1 and PYCR2 in the SUM159PT $PYCR1^{-/-}$ cell line in 21% and 0.3% oxygen. **G:** Mass isotopomer distribution of ^{13}C-[U]-glutamine incorporation into intracellular proline relative to the total pool in SUM159PT $PYCR1^{+/+}$ and $PYCR1^{-/-}$ cells. All metabolic data presented is mean of n=3 ± SD.

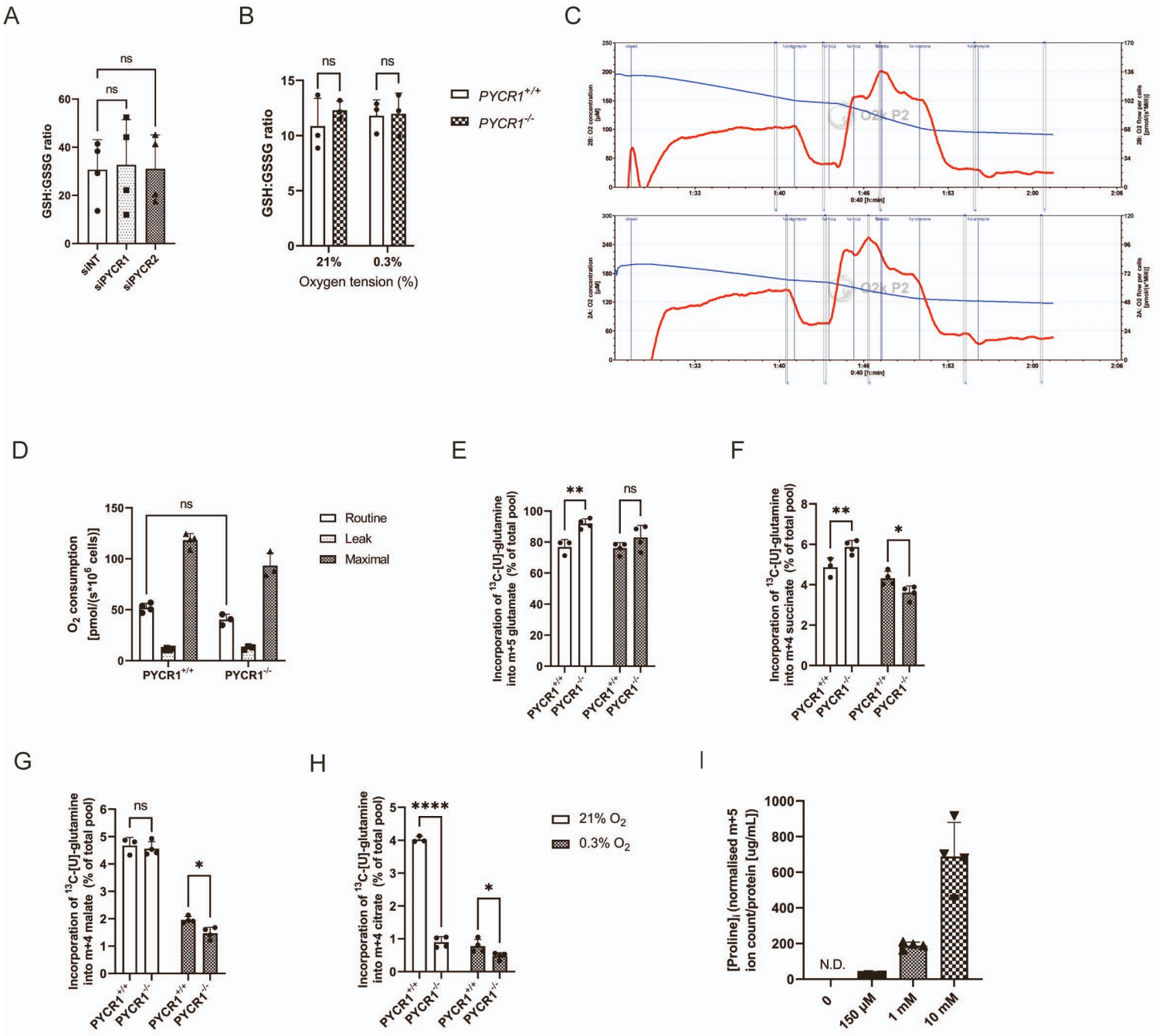

Supplementary Figure 2. Loss of PYCR1 in 2D cell culture. A: siPYCR1 or 2 does not change GSH:GSSG ratio in the SUM159PT cell line. Related to Figure 2. B: PYCR1$^{-/-}$ cells do not exhibit an alteration in the GSH:GSSG ratio in normoxia or hypoxia. **C:** Representative oxygraph traces of PYCR1$^{+/+}$ (top) and PYCR1$^{-/-}$ (bottom) cells. **D:** There is no significant difference in oxygen consumption in PYCR1$^{-/-}$ cells compared to PYCR1$^{+/+}$. Steady-state levels of glutamate (**E**), succinate (**F**), malate (**G**) and citrate (**H**). *, p<0.05; **, p<0.01; ****, p<0.0001. **I:** Abundance of intracellular ^{13}C-[U]-proline in SUM159PT cells incubated with increasing concentrations. All data presented as mean ± SD

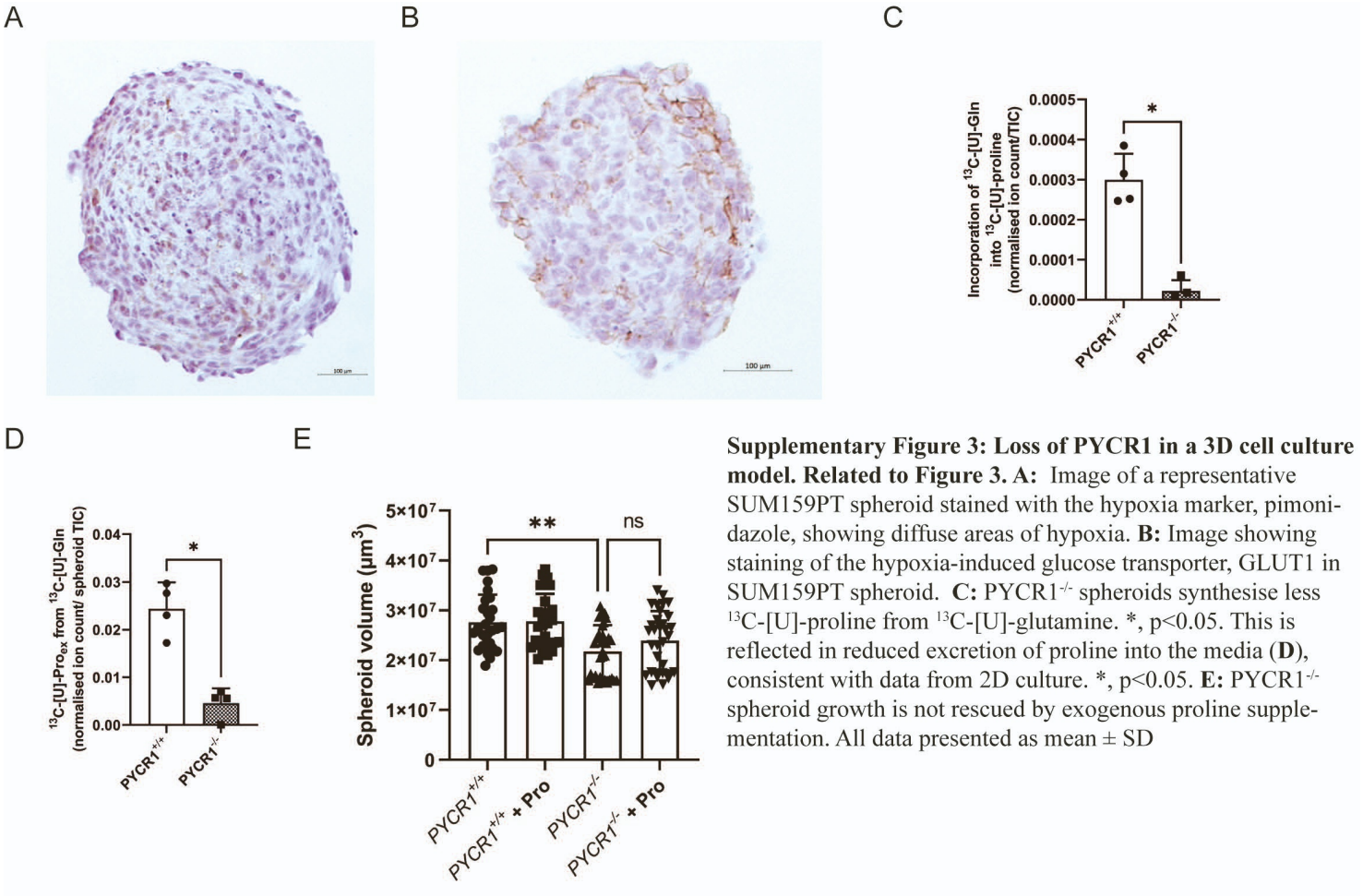

Supplementary Figure 3: Loss of PYCR1 in a 3D cell culture model. Related to Figure 3. A: Image of a representative SUM159PT spheroid stained with the hypoxia marker, pimonidazole, showing diffuse areas of hypoxia. **B:** Image showing staining of the hypoxia-induced glucose transporter, GLUT1 in SUM159PT spheroid. **C:** PYCR1$^{-/-}$ spheroids synthesise less ^{13}C-[U]-proline from ^{13}C-[U]-glutamine. *, $p<0.05$. This is reflected in reduced excretion of proline into the media (**D**), consistent with data from 2D culture. *, $p<0.05$. **E:** PYCR1$^{-/-}$ spheroid growth is not rescued by exogenous proline supplementation. All data presented as mean ± SD

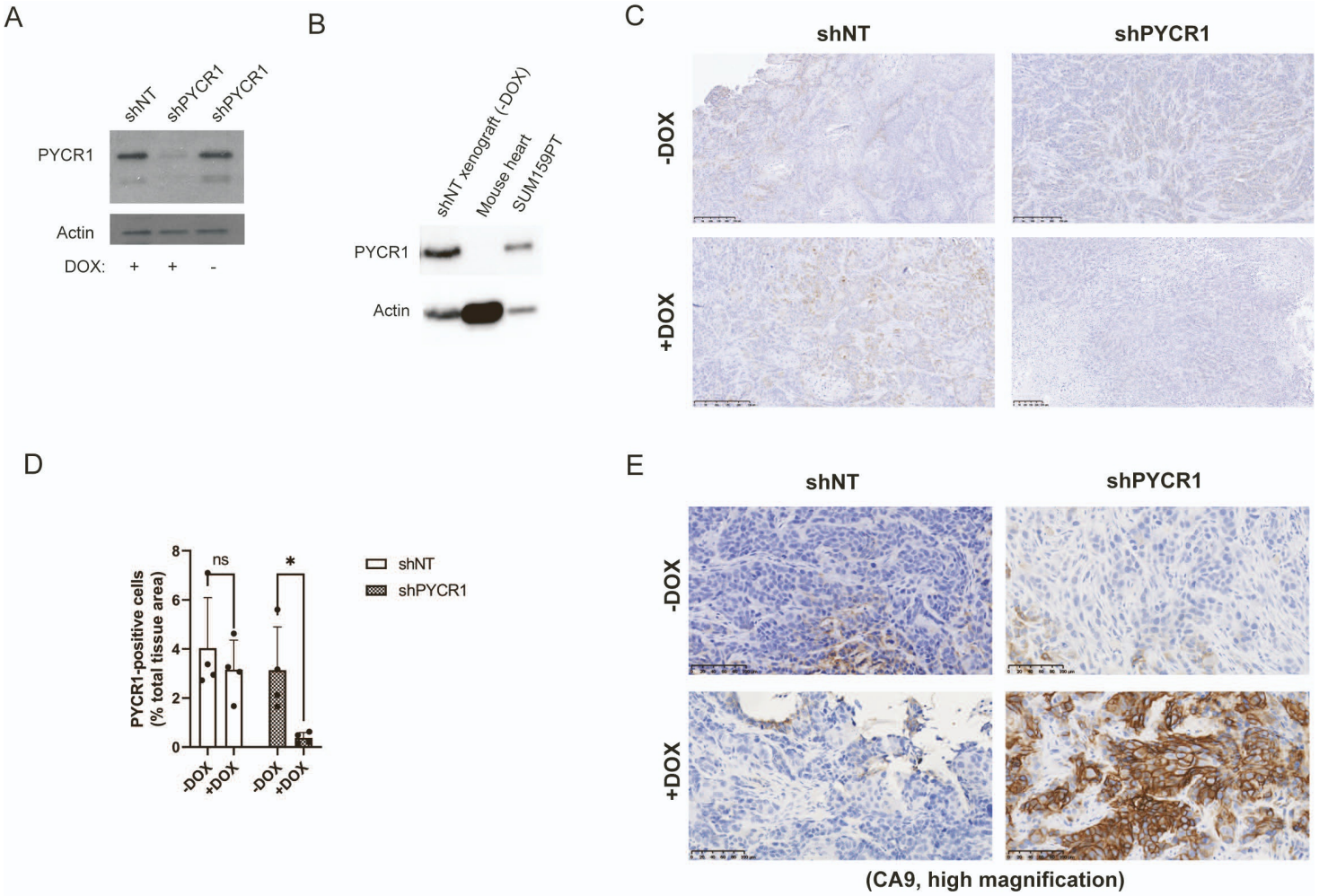

Supplementary Figure 4: Acute inducible PYCR1 knockdown in vivo xenografts. Related to Figure 4. A: Doxycycline elicits knockdown of PYCR1 in shPYCR1 cell model. **B:** Antibody against PYCR1 used to stain xenograft tissue (C) is specific for human protein. **C:** Representative images showing that PYCR1 expression in the tumour cells of the xenograft is reduced after DOX treatment. **D:** Quantification of PYCR1 staining in all tumours showing a reduction in PYCR1 expression after DOX treatment. *, $p<0.05$. **E:** Representative images at high magnification of CA9 staining in xenografts from the groups indicated, showing significantly increased hypoxia only in those tumours with shPYCR1+DOX. **F:** No significant differences in vascularity (measured through total radiant efficiency) were observed between groups (Figure 4). All quantitative data presented as mean ± SD

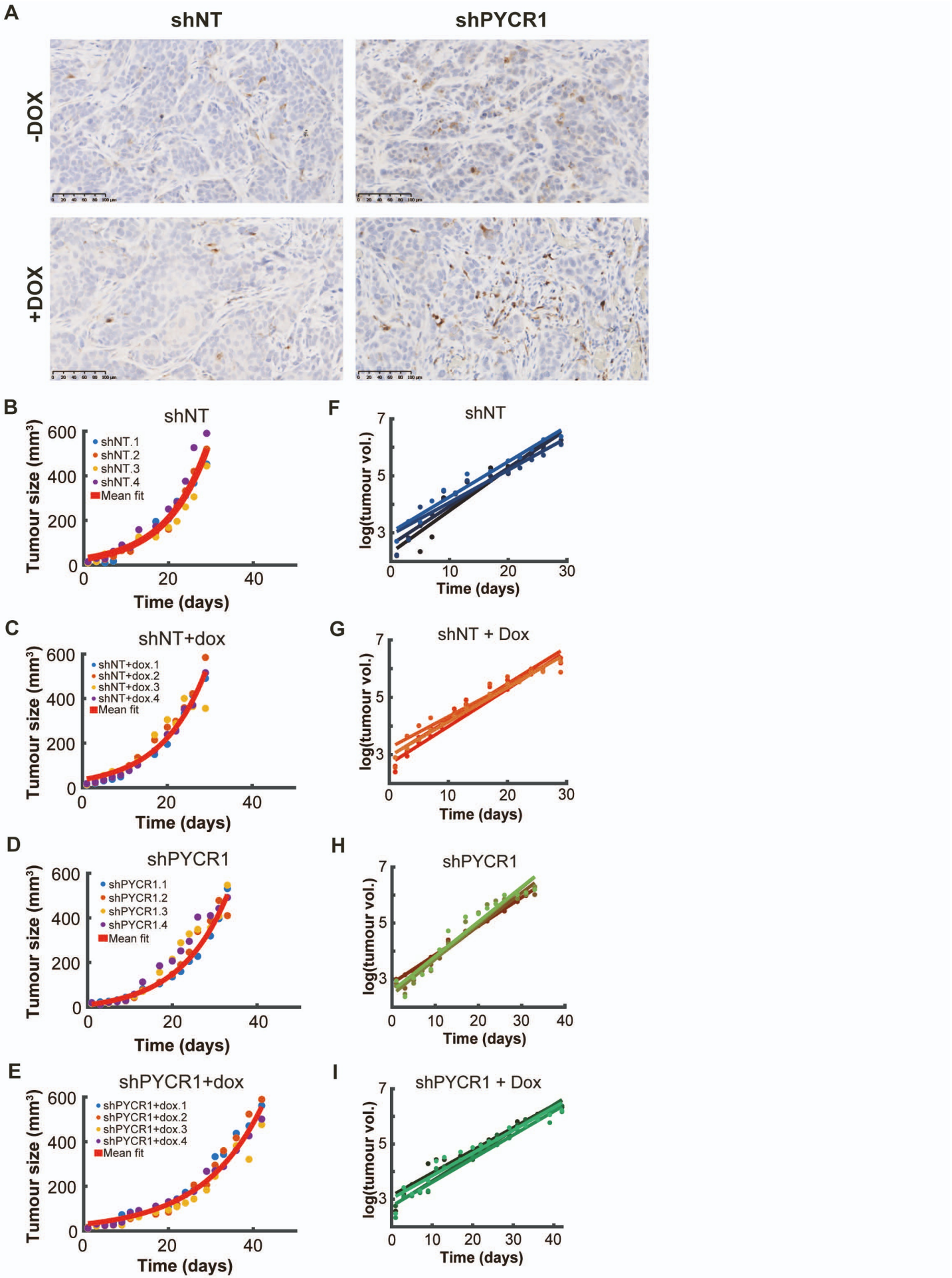

Supplementary Figure 5: Xenograft phenotype and xenograft growth curve fitting. Related to Figure 5. A: Representative higher magnification image of xenograft tumours stained for cleaved caspase-3. Scale bar = 100 mm. **B-E:** Exponential model fit of xenograft growth curves. **F-I:** Linear regression of log-transformed fitted curves B-E, allowing for appropriate statistical analysis (results shown in Figure 5F).